Coastal Protection and Restoration Authority
450 Laurel Street, Baton Rouge, LA 70804 | coastal@la.gov | www.coastal.la.gov

2017 Coastal Master Plan

Appendix C – Modeling

Attachment C3-25

Storm Surge and Risk Assessment

Report: DRAFT Version 1

Date: July 2015

Prepared By: RAND Corporation (Jordan R. Fischbach, David R. Johnson, Kenneth Kuhn, Michael Pollard, Chuck Stelzner, Rachel Costello, Edmundo Molina, and Ricardo Sanchez); ARCADIS (Hugh Roberts and Zachary Cobell)

Coastal Protection and Restoration Authority

This document was prepared in support of the 2017 Coastal Master Plan being prepared by the Coastal Protection and Restoration Authority (CPRA). The CPRA was established by the Louisiana Legislature in response to Hurricanes Katrina and Rita through Act 8 of the First Extraordinary Session of 2005. Act 8 of the First Extraordinary Session of 2005 expanded the membership, duties and responsibilities of the CPRA and charged the new Authority to develop and implement a comprehensive coastal protection plan, consisting of a Master Plan (revised every 5 years) and annual plans. The Coastal Protection and Restoration Authority's mandate is to develop, implement and enforce a comprehensive coastal protection and restoration Master Plan.

Suggested Citation:

Fischbach, J.R., Johnson, D.R., Kuhn, K., Pollard, M., Stelzner, C., Costello, R., Molina, E., Sanchez, R., Roberts, H., & Cobell, Z. (2015). *2017 Coastal Master Plan Modeling: Attachment C3-25 – Storm Surge and Risk Assessment.* Version 1. (pp. 1-210). Baton Rouge, Louisiana: Coastal Protection and Restoration Authority.

Acknowledgements

This document was developed as part of a broader Model Improvement Plan in support of the 2017 Coastal Master Plan under the guidance of the Modeling Decision Team (MDT):

- The Water Institute of the Gulf - Ehab Meselhe, Alaina Grace, and Denise Reed
- Coastal Protection and Restoration Authority (CPRA) of Louisiana - Mandy Green, Angelina Freeman, and David Lindquist.

The authors gratefully acknowledge feedback and support we have received during the model development process. We would like to thank Scott Hagen (Louisiana State University) and other members of the CPRA Predictive Model Technical Advisory Committee (PM-TAC) for their feedback and comments on key methodology questions. Keith Crane, Director of RAND's Environment, Energy, and Economic Development program, provided constructive comments on this draft. We would also like to thank two anonymous reviewers who provided timely in-progress feedback on the report draft in late 2014 and early 2015.

This effort was funded by the Coastal Protection and Restoration Authority (CPRA) of Louisiana under Cooperative Endeavor Agreement Number 2503-12-58, Task Order No. 03.

Executive Summary

The Coastal Louisiana Risk Assessment (CLARA) model is a quantitative simulation model of storm surge flood risk developed by researchers at the RAND Corporation. To support the development of its 2017 Coastal Master Plan update, CPRA contracted RAND (via The Water Institute of the Gulf) to make a series of improvements to the CLARA model to better address emerging coastal policy questions. In this technical report, improvements made to CLARA for the forthcoming master plan are described, including relevant background, new methods applied, and revised storm surge flood depth and damage estimates incorporating these new methods. A series of key improvements made to the CLARA model are discussed, including:

1. expanding the model domain to account for a growing floodplain;
2. creating a high resolution spatial unit designed to inform local planning in coastal communities;
3. updating and improving the inventory of coastal assets at risk;
4. developing new scenarios of levee fragility to capture the wide range of uncertainty; and
5. incorporating parametric uncertainty into estimates of flood depths and damage.

This draft report focuses on background and detailed methodology, but also describes selected model testing results. In addition, the document also describes a series of preliminary investigations conducted using the new version of the CLARA model. Specifically, the report includes a comparison of modeled results with observed data from Hurricane Isaac in 2012, additional analysis of nonstructural project performance intended to support preliminary identification and refinement of project areas, and a new framework to develop population and asset growth scenarios for the 2017 Coastal Master Plan.

Table of Contents

Coastal Protection and Restoration Authority 2
Acknowledgements 1
Executive Summary 2
Illustration 7
List of Tables 7
List of Figures 8
List of Abbreviations 12
Glossary of Relevant Statistical Terms 14
1.0 Introduction 15
1.1 Summary of the CLARA Model 16
1.2 Modeling Needs Identified During the 2012 Coastal Master Plan Analysis 17
1.3 Preliminary Analysis for the Flood Risk and Resilience Program 20
1.4 Purpose and Organization of This Report 21
2.0 Geospatial Updates to the CLARA Model 22
2.1 Revised Coastal Domain for CLARA v2.0 22
2.2 New Geospatial Unit of Analysis 26
3.0 Improved Asset and Valuation Data for Damage Estimation 31
3.1 Asset Inventory Module Data Updates 31
3.1.1 Structure Inventory 31
3.1.2 Transportation Infrastructure 34
3.1.3 Agricultural Crops 35
3.1.4 Critical Infrastructure 36
3.2 Asset Valuation Module Data Updates 38
3.3 Converting Data to CLARA v2.0 Grid Point Resolution 39
3.4 Results: Assets at Risk in the New CLARA Coastal Domain 42
3.4.1 Assets at Risk by Grid Point 43
3.4.2 Changes from the 2012 Analysis 46
3.4.3 Critical Infrastructure 48
4.0 Updates to Levee Fragility and Breaching Approach 50
4.1 Background 50
4.2 Volume-Based Breaching 51

4.3 Modified Fragility Scenarios for Enclosed Areas 53
5.0 Parametric Uncertainty Assessment in CLARA 58
5.1 Overview and Motivation 58
5.2 Flood Depth Uncertainty 59
5.2.1 Joint Probability Assessment and Flood Recurrence Statistics 61
5.2.2 Flood Depths in Unenclosed Areas 63
5.2.3 Flooding in Enclosed Areas 68
5.2.4 Integrated Flood Depth Uncertainty Calculations 74
5.2.5 Sources of Flood Depth Uncertainty Not Considered 75
5.3 Damage Estimation Uncertainty 76
5.3.1 Present-Day Structure Inventory 77
5.3.2 Asset Valuation 78
5.3.3 Depth-Damage Functions 78
5.4 Storm Frequency Modifications 80
6.0 Preliminary Analysis to Support Model Improvement 84
6.1 Data Sources 84
6.2 ADCIRC Raised-Feature Interpolation Methods 85
6.2.1 ARCADIS Bias Investigation 85
6.2.2 Surge and Wave Uncertainty 85
6.3 Contributions to Parametric Uncertainty in Unenclosed Areas 87
6.3.1 Approach and Experimental Design 87
6.3.2 Sensitivity Testing Results 88
6.4 Testing Sample Sizes in Enclosed Areas 91
6.4.1 Screening Analysis Experimental Design and Results 92
6.4.2 Detailed Analysis in the New Orleans HSDRRS 95
6.5 Storm Selection Analysis 97
6.5.1 Experimental Design 98
6.5.2 Results 99
6.5.3 Discussion 109
6.6 CLARA v2.0 Test Results with Uncertainty 111
6.6.1 Flood Depth in Unenclosed Areas with Parametric Uncertainty 111
6.6.2 Flood Depths in Enclosed Areas with Parametric Uncertainty 117
6.6.3 Flood Damage with Parametric Uncertainty 120
6.7 Summary 125

7.0 Model Comparisons: Hurricane Isaac 126
7.1 Overview 126
7.2 Hurricane Isaac Storm Data 127
7.3 Comparison Results 131
7.3.1 Comparison of Residential Structure Inventories 131
7.3.2 Comparison of Flood Depths in Unenclosed Areas 133
7.3.3 Comparison of Flood Depths in Enclosed Areas 141
7.3.4 Comparison of Damage to Residential Assets 148
7.4 Discussion 152
8.0 Nonstructural Vulnerability Analysis 154
8.1 Overview and Background 154
8.2 Cost-Effectiveness Analysis 155
8.2.1 Changes and Additions in CLARA v2.0 156
8.2.2 Derivation of Maximally Cost-Effective Mitigation Standards 157
8.2.3 Results 158
8.3 Defining Nonstructural Project Areas 171
8.3.1 Identifying Grid Points Eligible for Nonstructural Investment 172
8.3.2 Spatial Clustering Analysis 172
8.3.3 Defining Nonstructural Project Areas 174
9.0 Scenarios of Future Population and Asset Growth for the 2017 Coastal Master Plan 179
9.1 Introduction 179
9.2 Literature Review 181
9.2.1 Environmental Impacts on Migration 181
9.2.2 Environmental Impacts on Migration in Coastal Louisiana 182
9.2.3 Social Vulnerability 183
9.3 Scenario Development Methods 184
9.3.1 Overview of Approach 184
9.3.2 Constructing a Composite Index 185
9.3.3 Population Change Based on Index Categorization 187
9.3.4 Initial Parameter Assumptions 189
9.4 Sensitivity Testing Results 189
9.4.1 Block Group Composite Index Development and Bin Thresholds 189
9.4.2 Population Change with Different Parameter Assumptions 191
9.5 A Case Study: Terrebonne Parish 195

9.6 Discussion 197
10.0 Conclusion 198
10.1 Summary 198
10.2 Current Limitations 198
11.0 References 201
Appendices 207

Illustration

List of Tables

Table 2-1: Statistics for the Updated Coastal Domain and Geospatial Units. 29
Table 3-1: Crosswalk between Parcel Dataset Occupation Type and GBS Codes. 33
Table 3-2: Comparison of Road Mileage From NAVTEQ and Hazus Datasets. 35
Table 3-3: Counts of Critical Infrastructure in the CLARA v2.0 Database by Data Source. 37
Table 3-4: Data Elements for the Asset Inventory Module. 38
Table 3-5: Data Elements for the Asset Valuation Module 39
Table 3-6: Special Cases from Conversion of Assets at Risk Inventory. 40
Table 3-7: Comparison of Structure Counts by Parish. 42
Table 3-8: Counts by Parish of Critical Infrastructure in the CLARA v2.0 Database (Louisiana Only) .49
Table 4-1: Empirical Frequency of Failure Due to Overtopping and Scour as Observed During Hurricane Katrina 51
Table 5-1: Sources of Flood Depth Uncertainty Addressed by CLARA. 59
Table 5-2: Summary of Modeled Storm Parameters 61
Table 5-3: Summary of Calculation Steps and Uncertainties in Unenclosed Areas. 63
Table 5-4: CLARA v2.0 Response Surface Model Fit Priorities 66
Table 5-5: Summary of Calculation Steps and Flood Depth Uncertainties in Enclosed Areas. 69
Table 5-6: Sources of Damage Estimation Uncertainty. 76
Table 6-1: Simulation Cases Run for Specification Testing (Screening Analysis). 93
Table 6-2: Characteristics of Storm Sets Selected for Detailed Investigation. 99
Table 6-3: Number of Critical Infrastructure Assets Inundated by Type and Parish (1% AEP; Year 50 FWOA, Less Optimistic Scenario, MTTG Low Fragility Assumption). 124
Table 6-4: Number of Critical Infrastructure Assets Inundated by Type and Return Period 125
Table 7-1: Measured Peak Inundation Levels from Hurricane Isaac, by Selected Parish. 128
Table 7-2: Comparison of Plaquemines Housing Units to CLARA Residential Inventory 133
Table 7-3: Homes Damaged by Hurricane Isaac, Observed (Left Column) Versus Modeled. 148
Table 7-4: Observed and Simulated Count of Damaged Residences by Area and Housing Type, Plaquemines Parish (CLARA, 90th Percentile). 150
Table 7-5: Estimated Average Structural Damage Per Home in Plaquemines Parish, by Estimation Method 151

Table 8-1: Number of CLARA Grid Points by Most Cost-Effective Nonstructural Measure, Including Total Cost Under High Participation (2065 Basis Year, Residential Floodproofing Offered). 161

Table 8-2: Distribution of Costs by Asset Type and Mitigation Measure, $10.2 Billion Program. 170

Table 8-3: Number of Assets Mitigated by Measure and Nonstructural Strategy, $10.2 Billion Program.....171

Table 8-4: Number of Assets Mitigated by Measure and Nonstructural Strategy, $5 Billion Program.171

Table 9-1: Counts of Block Groups and Starting Population by Bin Using Alternate Definitions. ...190

Table 9-2: 2065 Population Projections by Bin Using Initial Scenario Parameters (Thousands of Persons). 194

Table 9-3: Population Projections for Selected Parishes, Three Scenarios. 194

Table 9-4: Bin Assignment and Population Change in Terrebonne Parish Example. 196

List of Figures

Figure 1-1: CLARA Model Structure.....17

Figure 2-1: CLARA v1.0 Geospatial Domain.....22

Figure 2-2: ADCIRC Analysis Boundary and Maximum Extent of Water. 23

Figure 2-3: Maximum Extent of Water with 2010 Census Urban Areas.....24

Figure 2-4: Geospatial Domains: CLARA 1.0 (red) and new CLARA v2.0 (blue). 26

Figure 2-5: CLARA v1.0 2000 US Census Block Centroids. 26

Figure 2-6. CLARA v2.0 2010 US Census Block Centroids. 28

Figure 2-7: CLARA v2.0 Final Grid Points. 30

Figure 3-1. CLARA Grid Points Updated with Parcel-Level Structure Inventories, by Data Source .32

Figure 3-2: Count of Single Family Homes by Grid Point, Current Conditions (2015). 44

Figure 3-3: Histogram Summarizing Count of Single Family Homes per Grid Point, Current Conditions (2015). 45

Figure 3-4: Single Family Homes by Grid Point in Greater New Orleans, Current Conditions (2015).45

Figure 3-5: Assets at Risk by Asset Class, Current (2015) and Future (2065) Conditions. 47

Figure 3-6: Critical Infrastructure Counts by Point (Louisiana Only). 48

Figure 4-1: Fragility Curve from MTTG Study 54

Figure 4-2: CLARA v2.0 2-D Erosion and Scour Fragility Curves by Fragility Scenario. 57

Figure 5-1: Illustration of Storm Wind Fields by Quadrant and Azimuthal Landfall Angle. 64

Figure 5-2: CLARA v2.0 Watershed Boundaries. 65

Figure 5-3: Greater New Orleans HSDRRS, as Divided into Segments. 71

Figure 5-4: Van der Meer Overtopping Equations and Random Coefficients Used by LACPR. 73

Figure 5-5. Structural Damage as a Function of Flood Depth for Single-Family Residences (One Story, Pier Foundation). 80

Figure 6-1: Maximum Surge Deviation by Grid Point Across Three Interpolation Methods. 86

Figure 6-2: Relative Contribution to Standard Deviation by Sampling Step in Unenclosed Areas. 88

Figure 6-3: Relative Contribution to Standard Deviation by Grid Point at three AEP Intervals. 90

Figure 6-4: Monte Carlo and Bootstrap Standard Deviation by Grid Point, 500-year AEP Interval. 91

Figure 6-5: Average Flood Elevation Variation from All Sample Sizes Versus Largest Sample Size Tested, by Enclosed Area Location. 94

Figure 6-6: Distributions of Standard Deviations of Adjusted Flood Elevation Observations Obtained when Varying the Number of Monte Carlo Replicates, New Orleans HSDRRS (500-year AEP). 96

Figure 6-7: Distributions of the Standard Deviations of Flood Depths Obtained by Different Numbers of Monte Carlo Replicates, 500-year AEP. 97

Figure 6-8: Average Coast Wide Bias and Variation by Number of Storms, 100-Year Flood Depths. 100

Figure 6-9: Average Bias and Variation by Exceedance. 101

Figure 6-10: Map of Bias by Grid Point for Sets 2, 3, and 11, 100-Year Flood Depths. 103

Figure 6-11: Average Bias and Variation, 500-Year Flood Depths (All Points, Split by Location). ..105

Figure 6-12: EAD Bias (50th Percentile, All Points, Split by Location). 107

Figure 6-13: Bias in Expected Annual Damage by Parish (percent), 50th percentile. 108

Figure 6-14: Coast Wide Bias in Terms of Expected Annual Damage (billions of 2010 dollars). 109

Figure 6-15: 10-Year Flood Depths by Grid Point, Year 50 FWOA Less Optimistic Scenario. 112

Figure 6-16: 90th Percentile Flood Depths by Exceedance, Current Conditions. 113

Figure 6-17: 90th Percentile Flood Depths by Exceedance, Year 50 FWOA Less Optimistic Scenario. 114

Figure 6-18: Change in 90th Percentile Flood Depths by Exceedance (FWOA-Current Conditions). 115

Figure 6-19: Difference in Flood Depth between CLARA v2.0 (50th Percentile) and CLARA v1.0, Year 50 FWOA Less Optimistic Scenario. 116

Figure 6-20: Flood Depth Annual Exceedance Probability Curve at a Sample Point Near Houma. 117

Figure 6-21: 500-Year Flood Depths, MTTG Low Fragility, Year 50 FWOA Less Optimistic Scenario. 119

Figure 6-22: 500-Year Flood Depths by Fragility Scenario in Greater New Orleans, Year 50 FWOA Less Optimistic Scenario. 120

Figure 6-23: Sum of Coast Wide Damage by AEP Interval, Current and Future Conditions. 121

Figure 6-24: Current, Future, and Change in EAD over Time. 122

Figure 6-25: Coast Wide EAD in Two Fragility Scenarios, All Percentiles, Current and Future Conditions (billions of 2010 constant dollars). 123

Figure 7-1: Hurricane Isaac Maximum Flood Depths (m), Compiled from Various Data Sources.128

Figure 7-2: Flood Depths Produced by ADCIRC Simulation of Hurricane Isaac (0.9 Wind Multiplier).130

Figure 7-3: Difference between ADCIRC Simulation of Isaac and Observed HWMs (0.9 Wind Multiplier).....130

Figure 7-4: Boundaries of Named Locations in Plaquemines Parish.....132

Figure 7-5: Map of Hurricane Isaac's Track. 135

Figure 7-6: Flood Depths from an "Isaac-Like" Synthetic Storm (CLARA v2.0, 10th Percentile). 136

Figure 7-7: Flood Depths from an "Isaac-Like" Synthetic Storm (CLARA v2.0, 50th Percentile). 137

Figure 7-8: Flood Depths from an "Isaac-Like" Synthetic Storm (CLARA v2.0, 90th Percentile). 137

Figure 7-9: Flood Depths from the CLARA "Isaac-Like" Synthetic Storm, Less Flood Depths from Observed High-Water Marks (10th Percentile).....138

Figure 7-10: Flood Depths from the CLARA "Isaac-Like" Synthetic Storm, Less Flood Depths from Observed High-Water Marks (50th Percentile).....138

Figure 7-11: Flood Depths from the CLARA "Isaac-Like" Synthetic Storm, Less Flood Depths from Observed High-Water Marks (90th Percentile).....139

Figure 7-12: Flood Depths in St. John the Baptist Parish (CLARA, 50th Percentile). 140

Figure 7-13: Flood Depths in St. Tammany Parish (CLARA, 50th Percentile). 140

Figure 7-14: CLARA Flood Depths (50th Percentile) in St. Tammany Parish, Less Flood Depths from Observed High-Water Marks.....141

Figure 7-15: Flood Depths in Plaquemines Parish, Unenclosed and Enclosed Areas (CLARA, 90th Percentile). 143

Figure 7-16: Detail of Plaquemines Federal and Non-Federal Levee System. 144

Figure 7-17: HSDRRS, Plaquemines, and Larose to Golden Meadow Protection System Reach Heights.....145

Figure 7-18: Calculated Overtopping Volumes from an Isaac-Like Synthetic Storm (CLARA, Median Values). 146

Figure 7-19: Probability of System Failure from an Isaac-Like Synthetic Storm, Normalized as the Probability per Characteristic Reach Length (Median Values).....147

Figure 7-20: Homes Damaged by Grid Point (CLARA, 90th Percentile). 149

Figure 8-1: Most Cost-Effective Mitigation Measure by Grid Point (Single-Family Residences, 2065 Basis Year; FWOA). 160

Figure 8-2: Cost-effectiveness of Nonstructural Mitigation, by Grid Point (Residential Floodproofing Allowed; 2065 Basis Year; FWOA).....160

Figure 8-3: Cumulative Damage Reduction as a Function of Program Cost. 161

Figure 8-4: Cumulative Damage Reduction as a Function of Program Cost (Comparison to 2012 Coastal Master Plan Structural Projects).....162

Figure 8-5: Points Included in a $10.2B Nonstructural Mitigation Program Based on Cost-Effectiveness....164

Figure 8-6: Proportional Damage Reduction from a $10.2B Nonstructural Mitigation Program....164

Figure 8-7: Distribution of Funds and EAD Reduction by Parish Based on Cost-Effectiveness (Residential Floodproofing Excluded; 2065 Basis Year; Medium-High Participation; FWOA).....165

Figure 8-8:. Unprotected Areas Included in a $10.2 Billion Program (Areas with Structural Protection under the 2012 Master Plan Included in (Top) or Excluded from (Bottom) the Program.166

Figure 8-9: Distribution of Funds and EAD Reduction by Parish, Points with Structural Protection Included or Excluded from Nonstructural Program(No Residential Floodproofing; 2065 Basis Year; Medium-High Participation).....167

Figure 8-10: EAD in Future Without Action, and Reduction in EAD by Asset Class and Scenario. 168

Figure 8-11: Reduction in EAD by Asset Class and Parish (FWOA; 2065 Basis Year, High Participation, Residential Floodproofing Excluded; $10.2 Billion Budget).....169

Figure 8-12: K-means Clusters Produced Using Geospatial Location and Proportional Damage Reduction. 176

Figure 8-13: K-means Clusters Produced Using Geospatial Location and Absolute Damage Reduction. 176

Figure 8-14: K-means Clusters Produced Using Geospatial Location and Nonstructural Cost-effectiveness. 177

Figure 8-15: K-means Clusters Produced Using Geospatial Location and Repetitive Loss Events.177

Figure 8-16: Proposed Rough Nonstructural Project Area Definitions. 178

Figure 8-17: Proposed Smoothed Nonstructural Project Area Definitions. 178

Figure 9-1: Flowchart Summary of the Population and Asset Scenario Methodology.....185

Figure 9-2: Average Annual Population Growth Rate by Census Tract, 2000-2010. 188

Figure 9-3: Initial Block Group Bin Assignment, Coast Wide.....190

Figure 9-4: Initial Block Group Bin Assignment, Greater New Orleans. 191

Figure 9-5: Average Annual Population Growth Rate by Bin Under Alternate Scenario Parameter Assumptions, 2010-2011.....192

Figure 9-6: Population Change 2010-2065 by Grid Point Under a Higher-Growth Scenario. 193

Figure 9-7: Population Change 2010-2065 by Grid Point Under a Lower-Growth Scenario. 193

Figure 9-8. Change in Residential Structures, 2015-2065 (0.67% Annual Growth Rate, 0.5% Bin Separation).....195

Figure 9-9: Map of Bin Assignment in Terrebonne Parish in 2010 and 2065, With and Without Project Implemented. 196

Figure 9-10: Population Change in Terrebonne Without and With Project Implemented.....197

List of Abbreviations

ACS	American Community Survey
ACV	Actual Cash Value
ADCIRC	Advanced Circulation Model
AEP	Annual Exceedance Probability
BHU	Base Hydrologic Unit
CBP	U.S. Census Bureau County Business Patterns
CLARA	Coastal Louisiana Risk Assessment Model
CPARLWR	Conditional Parametric Locally-Weighted Regression
CPRA	Coastal Protection and Restoration Authority
DEM	Digital Elevation Model
DMC	Disaster Monitoring Constellation
EAD	Expected Annual Damage
FEMA	Federal Emergency Management Agency
FIMA	Federal Insurance and Mitigation Administration
FVL	FEMA Verified Loss
FWOA	Future Without Action
GBS	General Building Stock
GNOCDC	Greater New Orleans Community Data Center
HAZUS	FEMA Hazards-US Multi-Hazard Model
HEC-FDA	U.S. Army Corps of Engineers Flood Damage Reduction Analysis Model
HSDRRS	Greater New Orleans Hurricane and Storm Damage Risk Reduction System
HSIP	Homeland Security Infrastructure Program
HURDAT	North Atlantic Hurricane Database
ICM	Integrated Compartment Model

IPET	Interagency Performance Evaluation Taskforce
IWR	US Army Corps of Engineers Institute for Water Resources
JPM-OS	Joint Probability Method with Optimal Sampling
LACPR	Louisiana Coastal Protection and Restoration
LONI	Louisiana Optical Network Initiative
LWR	Locally-Weighted Regression
MARIS	Mississippi Automated Resource Information System
MDT	Modeling Decision Team
MIP	Modeling Improvement Plan
MsCIP	Mississippi Coastal Improvement Program
MTTG	Morganza to the Gulf Reformulation Study
NFIP	National Flood Insurance Program
NOAA	National Oceanic and Atmospheric Administration
PM-TAC	CPRA Predictive Model Technical Advisory Committee
RGSPI	RAND Gulf States Policy Institute
RMSE	Root Mean Square Error
RSP	Regularly-Spaced Point
SBA	U.S. Small Business Administration
SEB	Science and Engineering Board
SWC	Southwest Coastal Louisiana
UnSWAN	Simulating Waves Nearshore Model - Unstructured
USACE	U.S. Army Corps of Engineers
Water Institute	Water Institute of the Gulf

Glossary of Relevant Statistical Terms

Aleatory uncertainty (in simulation) - diversity or heterogeneity that can be well understood, but is unavoidable (Oberkampf, DeLand, Rutherford, Diegert, & Alvin, 2002). This refers to the inherent randomness of some systems or natural processes. Gathering additional data and refining models can reduce epistemic uncertainty, but not aleatory uncertainty (Der Kiureghian & Ditlevsen, 2009). The term variability is often used to describe aleatory uncertainty.

Bootstrap - a family of methods used to calculate statistics describing the variance, bias, or, more generally, distributions of test statistics based on their derivation from a small sample of data (Efron, 1979). The most common bootstrap method involves repeated sampling with replacement from a sample of data to create multiple *bootstrap samples* of the same size as the original sample**.** All sample data points are considered equally likely to be chosen when selecting a data point for a bootstrap sample. The test statistic of interest is then estimated separately using each bootstrap sample. These parameter estimates are known as *bootstrap replications*. The set of bootstrap replications is then used to estimate a distribution function for the parameter of interest. The method outlined above is non-parametric.

Deep uncertainty - uncertainty for which it is difficult or impossible to gather empirical data or otherwise assign distributions in a defensible way. See Lempert, Popper, and Bankes (2003). It is important to identify deep uncertainty and to describe it, to the extent possible. Scenario analysis is often useful for considering deep uncertainties during decision making.

Epistemic uncertainty (in simulation) - a lack of knowledge regarding the function of systems being modeled. Much of this type of uncertainty stems from limitations in modelers' conceptual understanding, or from a lack of observed data describing the system or its relationships. Epistemic uncertainty and error can also be introduced during the translation of conceptual models into computer code and during the creation and analysis of simulation model outputs.

Parametric bootstrap - repeated resampling from a given, assumed distribution function to obtain bootstrap samples and bootstrap replications for use in describing sampling uncertainty (see **bootstrap**).

Sampling from the empirical distribution (in simulation) - collecting empirical observations of parameter values and inputing them into a simulation. A developer iteratively chooses sets of parameter values from the collection of observed data, with all observed sets equally likely to be selected. If random variables (or subsets of random variables) are assumed to be independent, it becomes possible to separately sample from the empirical distributions of each variable (subset of variables). The result will be a collection of sets of parameter values that actually have been observed or are reasonable to assume could have been observed.

Scenario analysis (in simulation) - running simulations for each of several "scenarios" which involve distinct simulation model assumptions, parameter values, mathematical formulae, etc., followed by interpretation and comparison of obtained results alongside scenario descriptions. Model developers often use scenario analysis to investigate or characterize the effect of aleatory uncertainty.

Sensitivity analysis (in simulation) - re-running simulations numerous times with different sets of parameter values. Sensitivity analysis can be a form of scenario analysis.

1.0 Introduction

The Coastal Louisiana Risk Assessment (CLARA) model is a quantitative simulation model of storm surge flood risk developed by a team of researchers at the RAND Corporation in 2011-2012 under contract to the Coastal Protection and Restoration Authority of Louisiana (CPRA). The original purpose of CLARA was to better understand how future coastal changes could lead to increased risk from storm surge flooding to residents and assets on the Louisiana coast and assess the degree to which projects proposed for Louisiana's 2012 *Comprehensive Master Plan for a Sustainable Coast* (2012 Coastal Master Plan)(CPRA, 2012a) could reduce this risk. CLARA allowed CPRA to systematically evaluate potential projects for inclusion in the 2012 Coastal Master Plan by estimating their risk reduction benefits. The methods and data used in CLARA, as well as the analysis conducted to support master plan development, are well-described in previously published literature (CPRA, 2012b; Fischbach, 2010; Fischbach et al., 2012a; Johnson, Fischbach, & Ortiz, 2013).

CPRA is mandated by the Louisiana State Legislature to update the state's coastal master plan every five years. To support the development of the next master plan in 2017, CPRA and The Water Institute of the Gulf (Water Institute) developed a Model Improvement Plan (MIP) designed to improve the coastal systems modeling applied to support the planning process and better represent current and future coastal systems. As part of the 2017 MIP, the state contracted (via the Water Institute of the Gulf) RAND to make a series of improvements to the CLARA model to better address emerging coastal policy questions.

This report describes the improvements made to the CLARA model to support the 2017 Coastal Master Plan. The most significant advance is a new approach to estimate the parametric and model uncertainty surrounding CLARA's estimates of coastal flood depths, which is in turn carried through the flood damage and damage reduction calculations. This uncertainty was not previously estimated. The new approach allows CLARA to produce probabilistic uncertainty ranges around flood depths and damage. Critically, it also allows the CLARA model to directly incorporate parametric uncertainty surrounding other key model inputs, such as landscape ground elevations and storm surge and wave estimates.

This technical report also describes new estimates of the increased value of assets at risk in the coastal floodplain, taking into account an expanded geographic area, updated population and structure inventories, and new classes of coastal assets not previously considered. These updates were requested both to support the 2017 Master Plan analysis and to provide preliminary planning analysis for Louisiana's Flood Risk and Resilience Program, which is charged with "implementing nonstructural projects, increasing flood risk awareness, and supporting state-level policies that promote greater resilience across the coast."[1]

The updated model and new asset inventory were then used to support a series of initial investigations to support both the 2017 plan and resilience program. These included a comparison of CLARA model results for an "Isaac-like" synthetic storm with observed flood and damage data from Hurricane Isaac in 2012, an updated evaluation of the cost-effectiveness of nonstructural risk reduction projects proposed in the 2012 Coastal Master Plan, and a new framework and approach to develop future population and asset growth scenarios for the 2017 Coastal Master Plan. In each case, this technical report describes the relevant background, new

[1] http://coastal.la.gov/project-content/ccrp/, accessed 12 January 2015.

methods applied, revised storm surge flood depth and damage estimates produced by CLARA, and relevant analysis results for coastal Louisiana.

1.1 Summary of the CLARA Model

CLARA's structure is based on the principles of quantitative risk analysis, which describe risk as the product of the *probability* or *likelihood* of a given event occurring—in this case, the annual probability of storm surge flooding at different depths—and the *consequences* of that event—the damage that results from the flooding. In CLARA, references to flood risk are best understood as flood risk to structures, physical infrastructure, and other local economic assets.

CLARA uses several types of information to estimate flood depths and resulting damage. First are estimated peak storm surge and wave heights. Second are data that characterize the landscape, hurricane protection systems, and assets at risk along the Louisiana coastline. Along the coast, CLARA labels different areas as *unenclosed*, with no levees, floodwalls, or other barriers or with structures that do not fully enclose the population at risk; or *enclosed*, with hurricane protection that fully encloses the area in a ring and creates a "polder."

The structure of the CLARA model is illustrated in Figure 1-1. In the **input preprocessing module**, CLARA uses information about the study region and generates flood depth estimates in unenclosed areas and storm hazard conditions for a sample of hypothetical storms. It also records surge and wave conditions along protection structures. In the **flood depth module**, CLARA estimates flood depths for enclosed areas, with a particular focus on storm surge and wave overtopping and system fragility. CLARA also calculates equilibrium flood depths by distributing water among adjacent enclosed areas. The depth of the flood directly determines the amount of damage that occurs, so flood depths are inputs to the **economic module**. In this step, CLARA values the assets at risk from flooding and estimates the damage in dollars (Fischbach et al., 2012a). **Model outputs** include summaries of flood depth and damage exceedance values, at a selected set of annual exceedance probabilities (AEP), and expected annual damage (EAD) from storm surge-based flooding events. These metrics are generated at each grid point in the model's spatial domain, as defined in Section 2.2, but may be aggregated to larger spatial units (census tract, parish, etc.) as necessary.

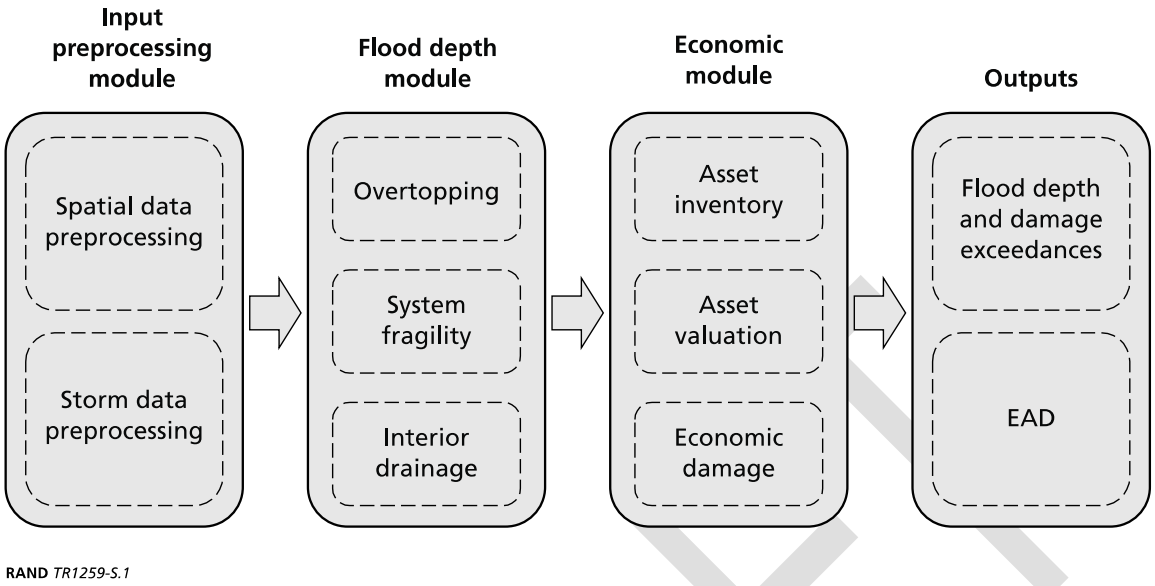

Figure 1-1: CLARA Model Structure.

1.2 Modeling Needs Identified During the 2012 Coastal Master Plan Analysis

CPRA and the Water Institute convened a workshop in October 2012 to develop the MIP. The modeling teams discussed high-priority improvements to the coastal systems models, with a focus on those improvements that directly address issues identified after the 2012 analysis. During this discussion, the RAND Gulf States Policy Institute (RGSPI) team provided a number of suggested improvements for CLARA, drawn from recommendations in RAND's final report summarizing the CLARA development and analysis process for the 2012 Coastal Master Plan (Fischbach et al., 2012a). After the workshop and subsequent iteration, RAND and CPRA identified several high-priority improvements to implement in preparation for the 2017 Coastal Master Plan analysis, and began the model improvement process in October 2013. The high-priority needs related to coastal flood risk and damage analysis identified for this effort are summarized below, and elaborated on in the subsequent sections. These needs guided the process of evolving CLARA from its original 2012 iteration, hereafter referred to as "CLARA v1.0," to a new version to be applied in for the 2017 Coastal Master Plan (hereafter "CLARA v2.0").

Expand the study region to account for a growing floodplain

The study region for the 2012 Coastal Master Plan effort was adopted from the 0.1 percent annual exceedance probability (AEP; or 1-in-1000 annual chance) floodplain estimated by the U.S. Army Corps of Engineers (USACE) in its 2009 Louisiana Coastal Protection and Restoration (LACPR) report (USACE, 2009a). Results from the ADCIRC storm surge analysis for the 2012 Coastal Master Plan, however, showed that the risk of flooding could extend further inland from coastal storms in some future conditions. Accordingly, a key step for 2017 is to expand CLARA's geographic boundaries northward to capture the growing floodplain, including towns such as Gueydan and Kaplan that were partially or completely excluded in the previous iteration.

Develop a new spatial grid to support higher resolution analysis for coastal communities

CLARA v1.0 was first applied to consider proposed risk reduction infrastructure investments, including protection structures such as levees, floodwalls, gates, and pumps, in addition to flood hazard mitigation projects such as elevating or floodproofing individual buildings. The latter project types, sometimes referred to as "nonstructural" risk reduction, were evaluated in a simplified, high-level way in the 2012 Coastal Master Plan analysis. These projects were defined using a handful of representative policy options, including structure elevations, floodproofing, or structure acquisitions. A simple set of decision rules was used to evaluate these project types uniformly in 56 different communities identified in the coastal region.

This high-level approach was useful for comparing the potential benefits of nonstructural investments with the benefits from structural risk reduction projects in a fair and consistent manner. However, the nonstructural projects themselves were ultimately defined too broadly to support specific investment or programmatic decisions at the local level. CPRA and its partners used the 2012 Coastal Master Plan analysis results to propose an overall level of investment in nonstructural risk reduction—$10.2 billion of the $50-billion plan—but otherwise determined that flood risk and benefits analysis at a higher level of spatial resolution would be helpful in refining nonstructural project strategies.

To support these planning needs, as part of the model improvement process, a new spatial unit of analysis for the flood depth and damage calculations was developed, and all aspects of the model were converted, including the database of assets at risk, to utilize this new grid. A preliminary analysis of nonstructural benefits and costs also was conducted using initial output at these grid points, with the goal of identifying specific areas with a substantial potential for risk reduction using building elevation, floodproofing, or acquisitions.

Improve the inventory of coastal assets at risk

The inventory of assets at risk in CLARA v1.0 was based largely on data collected by USACE to support its planning in Louisiana subsequent to the devastating 2005 hurricane season. Much of the data describing the coastal population or assets at risk in the floodplain can be dated to the period immediately preceding Hurricanes Katrina and Rita, or is drawn from earlier iterations of the FEMA Hazards-US (Hazus) Multi-hazard model (FEMA, 2011) or the 2000 U.S. Census. In addition, the 2012 Coastal Master Plan analysis did not include data on some key classes of coastal assets, such as power plants, refineries, ports, or other types of critical infrastructure. For 2017, the RAND Team updated the database of assets at risk with additional and more recent data identified subsequent to 2012. These updates draw from parcel-level building inventories developed for recent studies and made available by USACE, as well as from a federal infrastructure dataset made available to the state to support its long-term disaster resilience planning.

Review and incorporate recent research on levee systems into scenarios of system fragility

For the 2012 Coastal Master Plan analysis, CLARA used a simplified model to estimate the probability that levees, floodwalls, and other protection structures might fail when faced with increasingly severe storm surge and waves. The approach to fragility in CLARA v1.0 was based on work done by USACE for the Interagency Performance Evaluation Taskforce (IPET) Risk and Reliability study (IPET Vol. VIII, 2009). Soil boring samples were only available for the Greater New Orleans Hurricane and Storm Damage Risk Reduction System (HSDRRS), with assumptions made about the characteristics of other existing systems and future projects.

Since that time, additional studies have been completed on other protection systems or structures in the Louisiana coastal area, including Larose to Golden Meadow (USACE, 2013d), Morganza to the Gulf (USACE, 2013b), and the New Orleans HSDRRS armoring study (USACE Task Force Hope, 2013), all of which applied different assumptions and approaches to account for the additional risk introduced by potential structure failures. In this effort, CLARA's assumptions about protection system characteristics and the probability of failure in light of the recent literature on this topic were reviewed. Based on this review, the approach to estimating failure probabilities in CLARA v2.0 was revised, adding scenario uncertainty related to structure fragility to account for the continued lack of scientific consensus on this topic.

Incorporate parametric uncertainty in flood depth estimates

The first version of CLARA was designed with a balanced level of resolution, intended to provide spatially-detailed estimates of future flood depths, damage, and with-project damage reduction, but run across many proposed projects and in different scenarios reflecting plausible future coastal conditions. CLARA v1.0 was developed in such a way that it could address uncertainty from key external drivers looking out 50 years into the future, including sea level rise, coastal land subsidence rates, and future coastal economic growth, none of which could or can be reasonably assigned likelihoods. CLARA v1.0 used scenario analysis to capture the range of plausible outcomes from these drivers, but for any given scenario, the results calculated by the model were deterministic (with the exception of a simulation of breaching due to failure of protection system features).

However, given the number of steps, volume of input data, and overall complexity of the flood depth and damage calculations in CLARA, there are a variety of additional model uncertainties that were not captured and that may not be best addressed via a scenario approach alone. As a result, during the 2012 Coastal Master Plan analysis the RAND team identified the need to conduct a more thorough investigation of these potential parametric and model uncertainties. The goal was to explore the use of CLARA to generate estimates of this probabilistic uncertainty—captured using estimates of model variance and reported using statistical confidence intervals—and be able to compare the estimated uncertainty range to the outputs associated with scenario uncertainty ranges and spread of damage reduction benefits across different projects.

The need for an expanded uncertainty approach was originally identified by the Science and Engineering Board (SEB), which was organized to provide technical oversight to the 2012 Coastal Master Plan process. Because the simulation models were developed for use as a system, with one model's outputs serving as inputs to the next, in 2012 the SEB recommended that future iterations of the models include methods to estimate how parametric uncertainty propagates and expands throughout the modeling steps. This was especially significant for the flood risk assessment because CLARA uses outputs from most of the other systems models, particularly those describing the state of the landscape and hydrodynamics of extreme events.

To address CPRA's goal of incorporating parametric uncertainty into estimates of flood depth and damage, a primary focal point of the methods and analysis described in this report is a new approach for quantifying parametric uncertainty surrounding flood risk estimates implemented

in a revised version of the CLARA model. The new parametric uncertainty methods for CLARA v2.0 were designed first and foremost to directly incorporate "upstream" estimates of noise and uncertainty in the final flood depth estimates, as well as incorporate other sources of flood hazard and flood depth uncertainty. As discussed in Section 5, however, parametric uncertainty related specifically to asset exposure and damage are not yet incorporated into CLARA v2.0.

Compare CLARA estimates to flood depths and damage observed during Hurricane Isaac

Many parts of the CLARA risk estimation approach cannot be separately calibrated or validated using observed historical data because the model produces statistical projections of flood depth and damage risk spanning a wide range of plausible events. Some portions of the model—for instance, flood depth estimates from a single simulated storm—can be compared with observed results, but the original development of the CLARA model did not include such a validation of the model using a historically observed storm. The lack of relevant, available data and the development timeline for the 2012 Coastal Master Plan precluded such an analysis.

Hurricane Isaac, which made landfall in Louisiana in August 2012, presented an opportunity to compare results from the CLARA model to an observed storm surge flood event, as it impacted protection systems in New Orleans and Plaquemines Parish that were nearly identical to how they are currently represented in the model. This portion of the report therefore describes a comparison between data gathered during and after Hurricane Isaac and CLARA's economic asset database, response surface model, interior flood model, and damage calculations.

1.3 Preliminary Analysis for the Flood Risk and Resilience Program

CPRA and the Flood Risk and Resilience Program also sought to investigate additional policy analysis questions that were not fully resolved during the 2012 Coastal Master Plan analysis, particularly related to nonstructural risk reduction projects. In addition, a new approach for developing 50-year economic scenarios for coastal Louisiana was sought in order to better understand how future flood damage and risk reduction project performance might vary as population and asset patterns along the coast continue to change in the coming decades.

Focused investigation of proposed nonstructural risk reduction projects

The 2012 Coastal Master Plan analysis suggested that applying nonstructural mitigation to all structures vulnerable to storm surge flood damage would be prohibitively expensive. In addition, the cost-effectiveness of nonstructural measures varies widely across different coastal communities. To address this challenge and support future resilience planning in coastal Louisiana, a new analysis was conducted to identify areas of the coast that are most vulnerable to flood damage—with and without the structural measures included in the 2012 Coastal Master Plan—and where nonstructural measures could be applied to cost-effectively reduce current and projected future flood damage. This analysis will be applied to support project planning and investment decisions made by Louisiana's Flood Risk and Resilience Program, and will also help CPRA define a revised set of nonstructural projects for the 2017 Coastal Master Plan.

Future population and asset growth scenarios for the 2017 Master Plan

In the 2012 Coastal Master Plan, the flood risk analysis considered uncertainty related to the future growth and distribution of assets at risk in the coastal floodplain using scenario analysis. CLARA v1.0 implemented a simplified scenario approach that projected plausible population growth and geographic distribution over the 50-year period of analysis. The scenario approach utilized two scenario parameters: a coast wide growth rate for the population of all parishes in the study area, and a growth dispersion parameter that represented the proportion of the

population living in urban versus rural census blocks. This scenario approach assumed that asset growth and distribution would track population change.

For the 2017 Coastal Master Plan, CPRA asked RAND to revisit and update this scenario approach. A key goal of this update was to ensure that long-term drivers of coastal flood risk—including land loss rates, anticipated flood recurrence, and changes to anticipated flooding from new or upgraded structural protection alignments—could be represented in the long-term scenario approach.

This report describes a proposed new method for developing population and asset growth scenarios for use in the 2017 Coastal Master Plan analysis. The discussion includes a literature review of relevant studies examining the linkages between population vulnerability, coastal disasters, and population migration. A new framework and methods for scenario development are described, drawing on the literature review. The report also includes preliminary population growth and distribution results using the new framework, providing a range of results to support CPRA's subsequent selection of a small number of growth scenarios for economic assets in the 2017 Coastal Master Plan. However, the initial parameters and assumptions selected for this analysis remain preliminary as of this writing

1.4 Purpose and Organization of This Report

This technical report is intended to summarize and describe the improvements made to CLARA for the 2017 Coastal Master Plan, including methodological background, motivation for the data sources and methods chosen, results from initial sensitivity testing, and a discussion of current limitations. The report also describes several follow-on analyses conducted for CPRA and the Flood Risk and Resilience Program to better support near-term planning decisions. A future iteration of this report will be included as a technical appendix to the 2017 Coastal Master Plan.

The report is divided into nine sections. Section 2 describes the geospatial updates to the model, including the new coastal domain and new spatial units of analysis. Section 3 discusses the data sources and methods applied to update the CLARA v2.0 database of assets at risk, and presents figures and tables summarizing the revised asset distribution. Section 4 summarizes a literature review of recent research on levee fragility and describes a revised scenario approach for fragility assessment in CLARA based on these recent updates. Changes to the model implemented after the 2012 Coastal Master Plan analysis and before the current effort, not previously documented in a formal report, are also briefly discussed. Section 5 provides the statistical underpinnings of the parametric uncertainty methods through a review of the recent and relevant literature, and then describes in detail the methods applied to incorporate parametric uncertainty into the CLARA model. Section 6 summarizes the preliminary parametric uncertainty analysis and sensitivity testing results conducted to support CLARA v2.0 development. Section 7 summarizes the comparison of CLARA v2.0 results with observed Hurricane Isaac data. Section 8 describes the results of a preliminary reinvestigation of nonstructural project performance, building on the 2012 Coastal Master Plan analysis. Section 9 describes a new approach to develop population and asset growth scenarios for consideration in the 2017 Coastal Master Plan analysis. Finally, Section 10 provides a brief summary and describes current model limitations.

2.0 Geospatial Updates to the CLARA Model

2.1 Revised Coastal Domain for CLARA v2.0

The geospatial domain of the analysis in CLARA v1.0 was adopted directly from USACE's LACPR analysis (Fischbach et al., 2012a; USACE, 2009b). The original domain was a bounded area consisting entirely of whole year 2000 US census blocks, as shown in blue in Figure 2-1, which USACE derived by roughly bounding the coastal domain at Interstates 10 and 12.

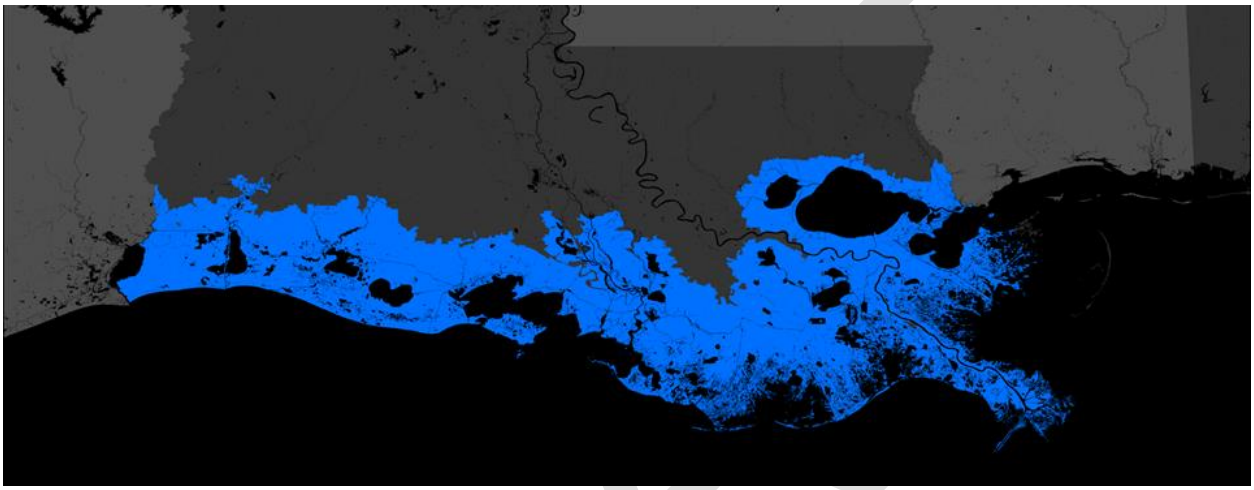

Figure 2-1: CLARA v1.0 Geospatial Domain.

During the 2012 analysis, the storm surge and risk teams noted that flooding that occurred during certain storms run with ADCIRC, particularly in future conditions when sea level rise and coastal land subsidence were included, was occurring beyond this initial northern boundary. In addition, the initial domain at times divided coastal communities in unexpected ways. For instance, the town of Gueydan, located in the west-central portion of the state and right along the northern boundary, was partially excluded from the original domain. This made it difficult to assess the potential risk reduction from a proposed ring levee surrounding this community.

To address these issues, the spatial domain has been updated for the 2017 Coastal Master Plan analysis. The revised geospatial domain for the analyses detailed in this report is a contiguous[2] bounded area consisting entirely of whole 2010 US census blocks. An explanation of its creation follows.

ARCADIS performs the storm surge and wave analysis using ADCIRC and UnSWAN within a broad bounded area. The upper boundary of this area, referred to as the ADCIRC analysis boundary, is shown in Figure 2-2. The ADCIRC analysis boundary provided initial guidance on the potential furthest extent of the CLARA model. Working with the surge and wave team it was decided that the latest CLARA geospatial domain would consist of 2010 US census blocks that fall at least partly inside this boundary.

[2] Contiguity was maintained as much as possible. The major portion of the geospatial domain which itself fell on the contiguous "mainland" is entirely contiguous. Where the geospatial domain covers many islands, however, contiguity was not possible.

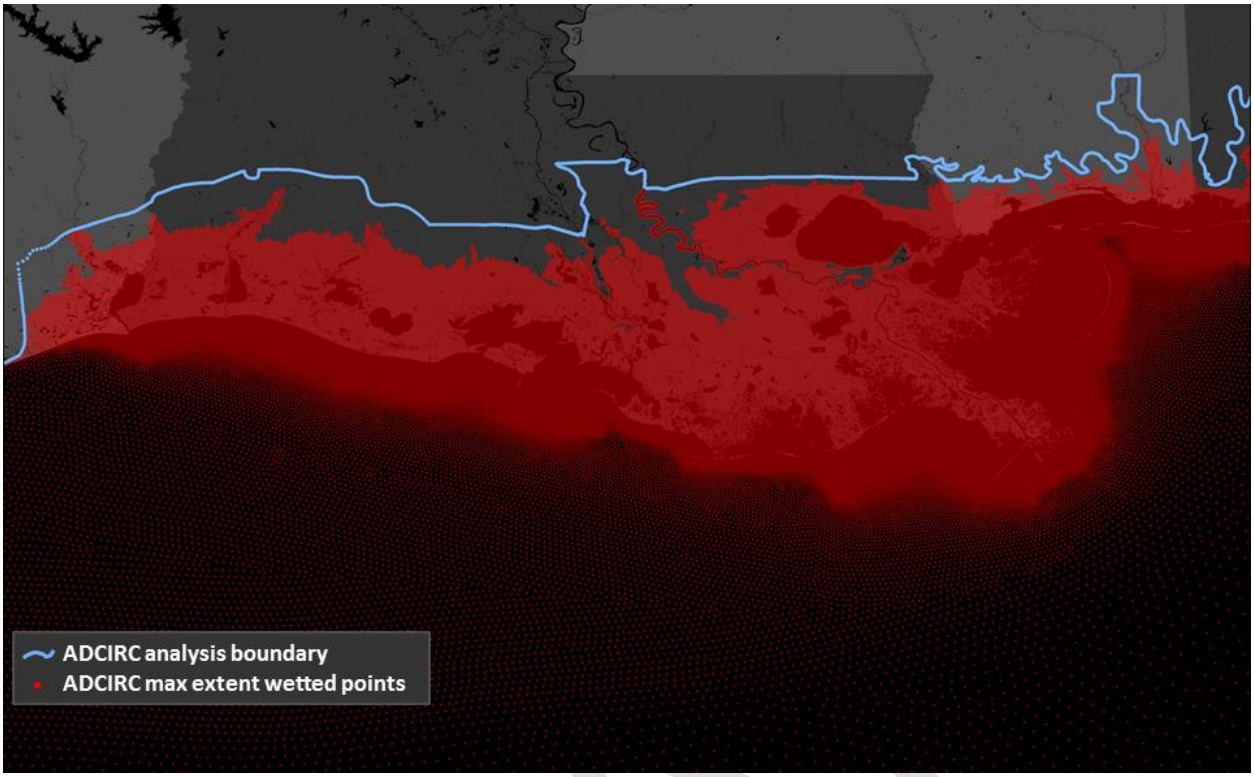

Figure 2-2: ADCIRC Analysis Boundary and Maximum Extent of Water.

The first analytic step in this process was to identify a new maximum extent of flooding that could occur in future conditions when sea level rise and subsidence are included. ARCADIS ran a subset of storms in a year 50 condition using CPRA's "Less Optimistic" landscape scenario and assuming that no 2012 Coastal Master Plan projects have been constructed (future without action, or "FWOA"). ARCADIS used expert judgment to identify the largest and most intense storms to help develop this new maximum extent. The maximum surge and wave heights for grid points that wetted at least once during the simulations were extracted and stitched together into a single dataset (Figure 2-2, red area).

As no locations outside of the red area shown would be flooded by coastal storms even under the most extreme storms identified by ARCADIS in the Less Optimistic scenario, the initial geospatial domain was created to include all wetted ADCIRC points from this dataset on land in Louisiana, Mississippi,[3] and portions of Texas.[4] Any "holes" in the geospatial domain at this

[3] Mississippi coastal counties were included in the boundary expansion to support a separate analysis currently underway for CPRA. CPRA asked RAND to use CLARA to evaluate the potential benefits of damage reduction from different proposed barrier alignments across Lake Pontchartrain, including the potential costs (induced damage) if storm surge were diverted to populated areas in coastal Mississippi. This analysis necessitated the inclusion of portions of Mississippi into CLARA. In Mississippi, the northern extent of the geospatial domain was either the boundaries of the county boundaries or the ADCIRC analysis boundary, whichever was southernmost at any given location.

[4] The RAND Team also decided to include a small portion of eastern Texas, in case the 2017 Coastal Master Plan were to evaluate barrier alignments that could affect coastal communities across the state boundary. These areas were included in the model boundary, but are not

stage—areas fully surrounded by wetted points yet containing none—were removed, and the formerly-empty areas were filled in as part of the geospatial domain.[5] Next, any whole 2010 US census blocks that touched at least part of the existing geospatial domain were combined to create a new geospatial domain. Where this left any holes (again, census blocks fully surrounded by the domain yet themselves not included), the relevant census blocks were also included in the domain.[6]

The next step was to account for municipal boundaries in the coastal domain. The goal was to ensure that contiguous communities were included as a whole rather than split, or were split along sensible municipal boundaries (e.g., major highways or roads). To identify recent updates to urban boundaries, 2010 US census urban area definitions were used. As shown in Figure 2-3, several urban areas fall only partially inside the area of the wetted ADCIRC points.

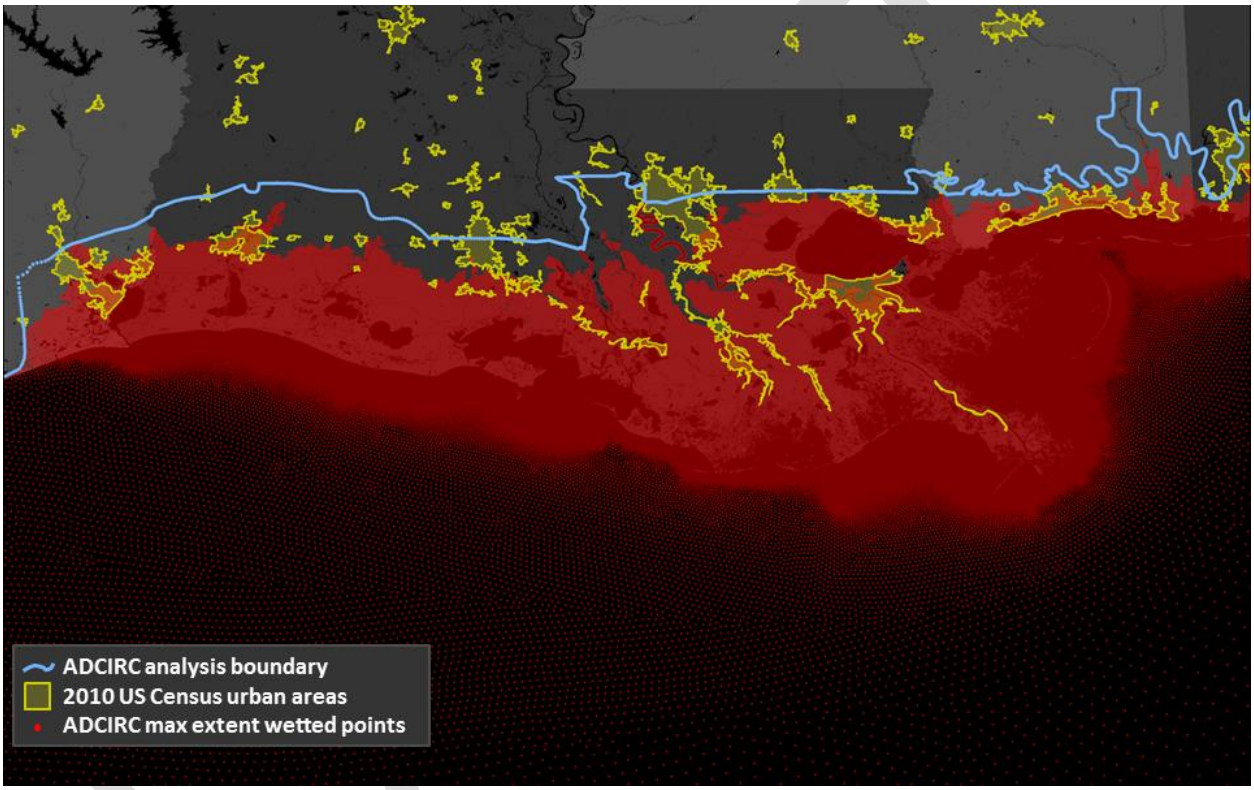

Figure 2-3: Maximum Extent of Water with 2010 Census Urban Areas.

otherwise active or used in any analysis described in this report. In Texas, the domain was restricted to Orange and Jefferson counties, as only a very small number of wetted points fell in adjacent counties.

[5] Unless stated otherwise, all geospatial work to create the updated geospatial domain was performed in ArcGIS Desktop.

[6] The blocks that appeared as holes in the extent in Mississippi fall entirely outside of the ADCIRC analysis boundary. However they were included in order to eliminate all holes and thereby simplify the extent for use elsewhere in the CLARA model.

Using these overlays and expert judgment built largely on the extent to which the urban areas overlapped the wetted ADCIRC points, the geospatial domain was then further expanded to include all census blocks inside selected urban areas.[7]

As a final step, this analysis was checked against a more detailed population dataset to help identify smaller areas with populations and assets that might not otherwise have been counted as part of an urban area in the 2010 census. The LandScan global population dataset, updated in July 2012, was used (U.S. Department of Energy Oak Ridge National Laboratory, 2011). LandScan contains estimates of both daytime and nighttime populations at a very high resolution (approximately 90 meters),[8] and in this case the daytime and nighttime datasets were combined to produce a dataset reflecting the maximum population at any time during the day at a given location. This maximum population dataset was then aggregated by a factor of ten in both the X and Y directions, producing a dataset with roughly 900 m resolution.

The aggregated population dataset was overlaid with the significant urban areas to identify any instances where sufficient population in LandScan was adjacent to the 2010 urban areas but otherwise outside of the geospatial domain—that is, locations where the urban area could be considered to have population growth or expansion which may have occurred since the 2010 census (Bureau of the Census, 2011).[9] In these cases, the census blocks in these adjacent populated areas were also added to the spatial domain.

After these population adjustments were made, a final assessment and simplification of the domain was conducted. Areas within the Atchafalaya and Mississippi Rivers, for example, are by definition always wet and were removed. Additionally, a low population area in the southwestern corner of Jefferson County, Texas was removed. Alternately, several natural or artificial levees without wetted ADCIRC points immediately adjacent to the Mississippi River can be seen in Figure 2-3 above. The shape of these regions was such that they were very nearly

[7]Sometimes, a single significant urban area will extend over several distinct populated areas, such as the population sprawl around two nearby cities. In several cases, such urban areas covered one populated area that overlapped the wetted ADCIRC points and one that did not. In these cases, the urban areas were split along sensible municipal boundaries, and only the relevant populated area was added to the geospatial domain. In some cases, this splitting was performed in order to remove urban coverage of a populated area that extended outside of the ADCIRC analysis area. In one instance, Mandeville-Covington on the northshore of Lake Pontchartrain, the populated areas involved overlapped the ADCIRC analysis boundary and were unable to be split in this fashion. As Mandeville-Covington is one of the fastest-growing areas in Louisiana, and owing to the flooding caused in the area by Hurricane Isaac in 2012, it was decided to include the entirety of the Mandeville-Covington urban area in the new geospatial domain.

[8] Oak Ridge National Laboratory, the producer of LandScan datasets, combines "socio-economic data including places of work, journey to work, and other mobility factors" to yield separate day and night population estimates. More information can be found at http://computing.ornl.gov/cse_home/about/LandScan%20long.pdf, as of September 3, 2014.

[9] Specifically, the 900m X 900m cells were filtered with a threshold density of 84 people per cell, which is roughly equivalent to a density of 250 people/sq mi. This threshold is one-half of the 500 people/sq mi threshold applied by the to identify and incorporate some census blocks into urban area definitions (Bureau of the Census, 2011), and was selected to help ensure the study boundary was as inclusive as possible of populated areas that fell just outside of the formal Census definitions.

holes in the area of wetted points, and as such they were added to the geospatial domain. The final domain is shown in Figure 2-4.

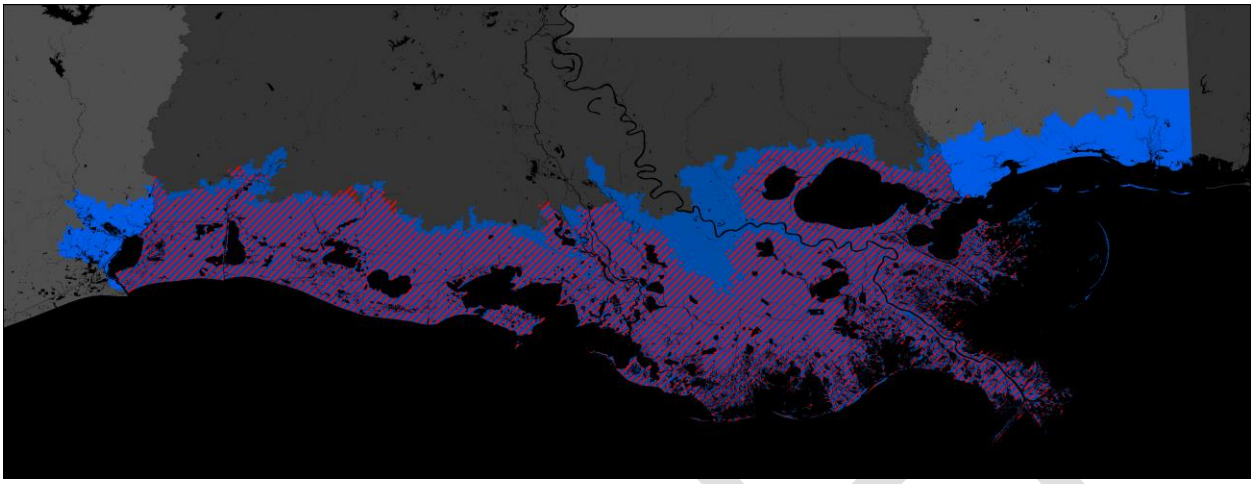

Figure 2-4: Geospatial Domains: CLARA 1.0 (red) and new CLARA v2.0 (blue).

2.2 New Geospatial Unit of Analysis

In CLARA v1.0, the primary geospatial units of analysis were 2000 US census blocks. Once again, these were adopted directly from the LACPR analysis, which in turn allowed for the direct application of USACE's post-Katrina asset and damage datasets. Flood depth calculations in the original version of the model are made at the centroid of each block (Figure 2-5); counts of assets at risk, structure characteristics, and damage estimates are subsequently made for each whole block. These results were useful to support lower-resolution analysis for the 2012 Coastal Master Plan—with results summarized by the 56 coastal communities identified across the coast—but were not sufficiently high-resolution to allow for detailed analysis of vulnerability or nonstructural risk reduction within these broadly-defined communities. This is particularly true in rural areas along the coast, where homes, businesses, and other economics assets are more dispersed and less likely to be located together near a census block centroid.

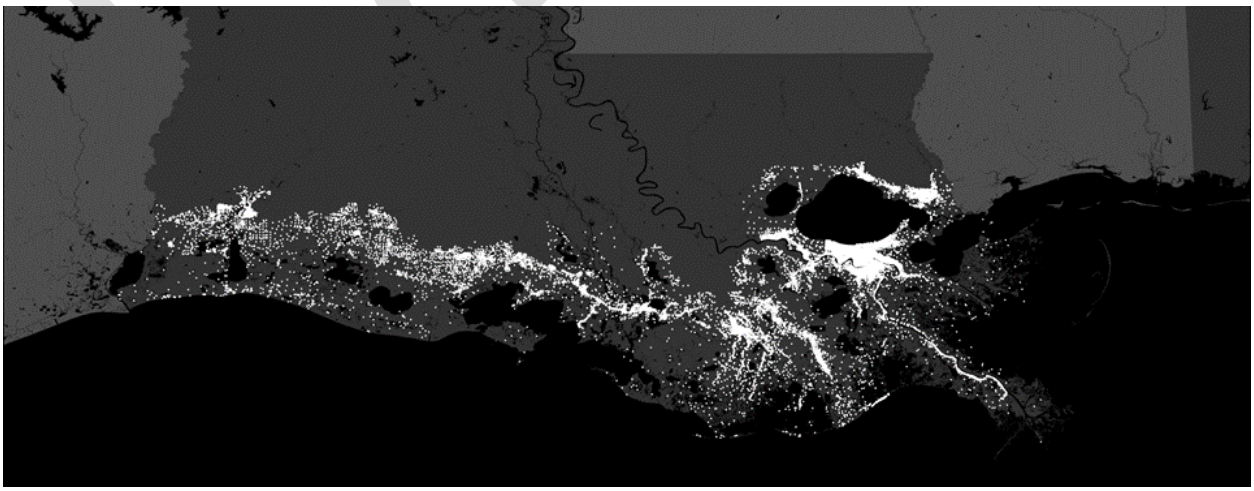

Figure 2-5: CLARA v1.0 2000 US Census Block Centroids.

To better facilitate vulnerability estimates and nonstructural project comparisons within communities, as well as to provide greater spatial fidelity to flood depth estimates, a new spatial analysis unit for CLARA v2.0 was created. This process, described in detail below, entailed first updating the economic units from 2000 to 2010 US census blocks, which allows census data from 2010 and onwards to be used in the analysis.[10] Then, a new set of grid points were created by combining the 2010 block centroids with a new grid of regularly-spaced points (RSPs) to ensure a minimum spatial resolution for the entire coast.

Specifically, to facilitate point-based geographic analysis using CLARA v2.0, a set of points, referred to as grid points, were created within the updated, finalized geospatial domain.

The overall requirements for the new set of grid points were as follows:

- The point set must consist of both RSPs and representative points created from census 2010 US census block centroids.
- The spatial resolution of the overall dataset in any location must be equal to or higher than the resolution of the RSPs.
- There must be at least one point inside each census block in the geospatial domain.

To determine the optimal RSP spacing—balancing the level of resolution for robust analysis with the need for reasonable analytic processing time throughout the CLARA depth and damage calculations—several regular spacings of RSPs were tested. The original CLARA geospatial domain was filled with RSPs at spacings of 1/10 km (2.5 million points), ¼ km (400,000 points), ½ km (100,000 points), and 1 km (25,000 points).[11] Testing suggested that the total number of grid points—RSPs and census block centroids combined—should be maintained on the order of 100,000 to keep model runtimes manageable. As a result, the 1 km spacing for RSPs, when summed with approximately 75,000 census block centroids, was selected to provide the appropriate balance.

To create points representative of the census blocks in the updated geospatial domain (representative points), a single point was first created at the centroid of each of the domain's constituent 2010 census blocks, as shown in Figure 2-6.[12]

[10] Results using new census blocks are still comparable to those from the earlier analysis when aggregated by parish or other summary units.

[11] This rough order of magnitude spacing testing was performed prior to the creation of the updated geospatial domain, with the assumption that the updated domain would be larger than the existing domain.

[12] Each census block is represented geographically by a single polygon, which need not be contiguous. By design, some census blocks contain multiple bounded, non-contiguous areas. Because a centroid is the geographically weighted center of a polygon, in some unusual cases a census block may not contain its centroid. When this occurred, the centroid was replaced with a single representative point created inside the census block.

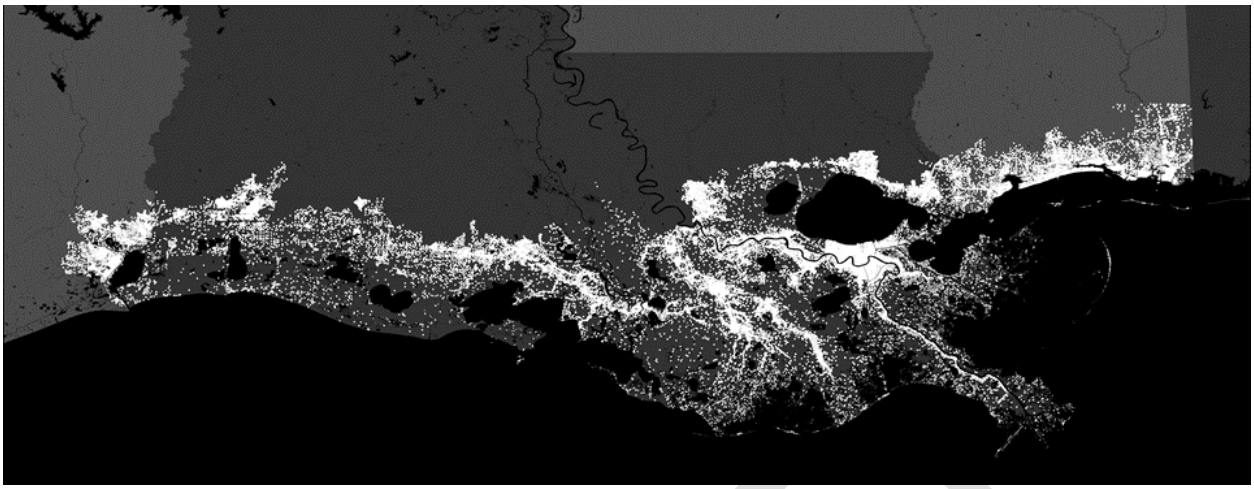

Figure 2-6. CLARA v2.0 2010 US Census Block Centroids.

Next, a scripted process was used to replace lower-resolution census blocks with RSPs where necessary. The specific steps were as follows.

- The areas of the 2010 census blocks were calculated in square kilometers (sq km).
- From this master point set, each point representing a block with an area equal to or greater than 1 sq km was removed.
- RSPs were generated at 1 km resolution, inside a rectangular box with its limits as the minimum and maximum latitude and longitude of the geospatial domain.[13]
- RSPs were then filtered to include only the points inside the new geospatial domain. Additionally, RSPs in areas of point spacing less than 1km were redundant to the grid points, and any RSPs found to be less than 1 km from a representative census block point were removed.
- The remaining RSPs and representative census block points were then combined in a single dataset of grid points.

Testing with this initial set revealed that some census blocks contained no grid points. These census blocks all had areas of at least 1 sq km, and their representative points had been removed earlier in the process due to odd configurations of nearby census blocks, or an unusual shape of the block itself. To remedy this issue, the representative points for the census blocks containing no intermediate grid points were added back in, yielding the final grid point set.

Table 2-1 provides a summary of this process, and shows the number of points included at key stages of the process and in the final grid. There are 90,373 grid points in Louisiana used for analysis in CLARA v2.0, an approximately 154 percent increase over the 35,556 census block centroids evaluated in CLARA v1.0.

The final grid points for the new CLARA v2.0 coastal domain are shown in Figure 2-7.

[13]As the spacing of RSPs within rows was created using a loxodromic (rhumb) distance of exactly 1 kilometer, there is no detectable error in the horizontal spacing. The vertical spacing between rows of RSPs has a maximum error of 0.286 percent.

Table 2-1: Statistics for the Updated Coastal Domain and Geospatial Units.

State	2010 Census Blocks	Grid Points			
		RSPs	Census Block Representative Points		Final CLARA v2.0 Points
			Initial	Re-added	
Louisiana	76,047	16,743	71,374	2,256	90,373
Mississippi	13,066	1,028	12,328	447	13,803
Texas	9,401	176	9,138	203	9,517
Total	98,514	17,947	92,840	2,906	113,693

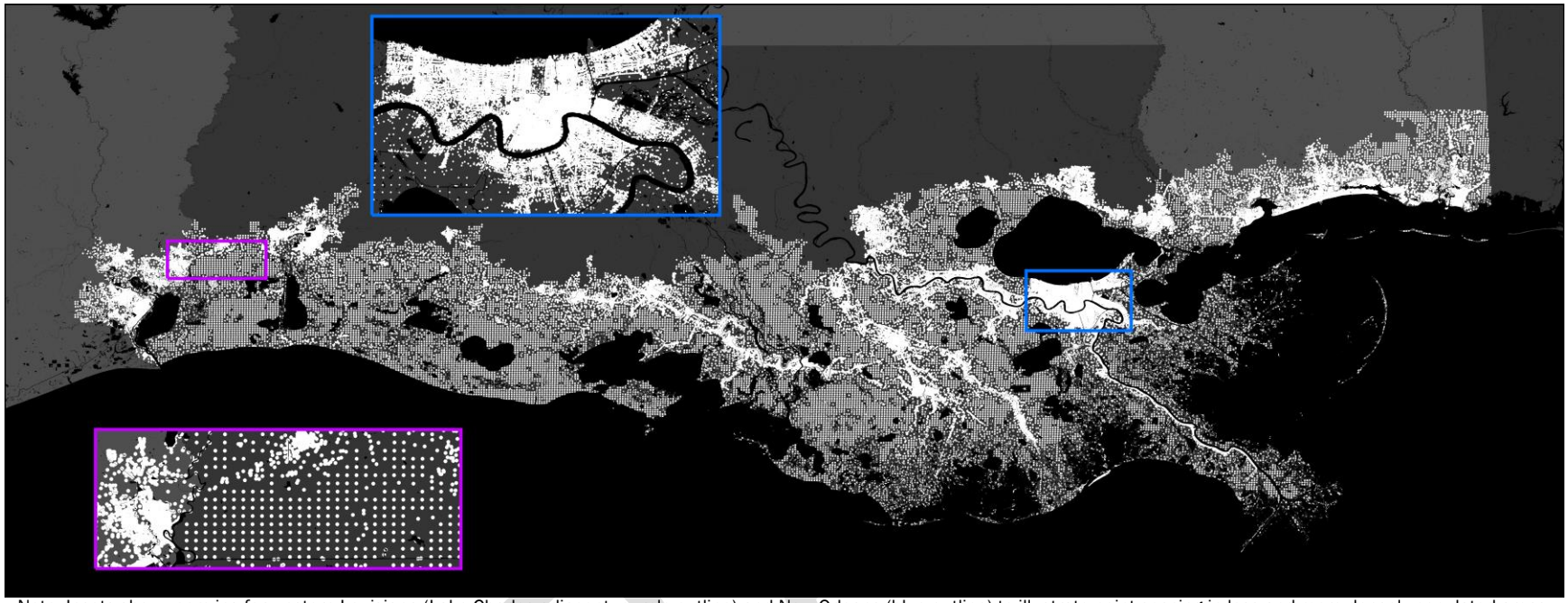

Note: Insets show zoom ins for western Louisiana (Lake Charles adjacent; purple outline) and New Orleans (blue outline) to illustrate point spacing in less and more densely populated areas.

Figure 2-7: CLARA v2.0 Final Grid Points.

3.0 Improved Asset and Valuation Data for Damage Estimation

In this section, data sources used and methods applied to update and improve the database of assets at risk in coastal Louisiana are described. Several types of improvements were required to expand the geographic scope, update older asset inventory and valuation data, and update the unit of analysis from 2000 census blocks to CLARA v2.0 grid points. Specifically, the following tasks were conducted, which are elaborated on in the subsections below:

- The RAND Team updated the inventory of assets at risk to include additional parishes in Louisiana and portions of coastal Mississippi. The team also sought to incorporate more recent data, as well as develop a framework to allow for new data sources to be incorporated into the model as they become available.
- Much of the data describing the coastal assets at risk in CLARA v1.0 dates to the period immediately preceding Hurricanes Katrina and Rita, drawn from earlier iterations of the FEMA Hazards-US (Hazus) Multi-hazard model, the USACE LACPR analysis, or 2000 US census data. CLARA v2.0 improves on this initial dataset by incorporating updated road, crop, and, for some areas, structure data.
- The CLARA v2.0 geospatial grid requires a higher level of geospatial fidelity than the previous analysis, motivating a move away from data sources based upon census blocks to those containing geospatial point, line, or polygon data.
- Finally, CLARA v2.0 includes data on new classes of coastal assets, such as power plants, refineries, ports, and other types of critical infrastructure.

3.1 Asset Inventory Module Data Updates

Below, the data sources used to describe assets at risk in the current CLARA v2.0 model are summarized, as well as ongoing work to update and improve this inventory. The data sources are summarized in Table 3-4.

3.1.1 Structure Inventory

Residential structure counts for Louisiana are adopted from several sources. The baseline inventory data was taken initially from the LACPR economics database used in CLARA v1.0 (USACE, 2009b). The LAPCR database contains Hazus-MH MR2 (Federal Emergency Management Agency, 2005) structural data, updated by Calthorpe Associates to reflect pre-Katrina (second-quarter 2005) economic conditions (Calthorpe Associates & USACE, 2008). Non-residential (i.e., commercial, industrial, agricultural, governmental, educational, and religious) structure counts for Louisiana are taken from the General Building Stock (GBS) inventory in the FEMA Hazus-MH MR4 model developed by Dun and Bradstreet and adjusted at the parish level by applying the percentage growth from 2005 to 2008 as reported by the Census Bureau's County Business Patterns (CBP) database to non-residential structures (FEMA, 2005). For seven parishes in and around New Orleans, the LACPR structure counts were adjusted using a Greater

New Orleans Community Data Center (GNOCDC) database of residences receiving mail (Ortiz & Plyer, 2011) and ACS estimates of current household unit and population counts (ACS, 2014).[14]

In CLARA v2.0, the original structure inventory has been partially replaced with more recent inventory estimates made available by the U.S. Army Corps of Engineers New Orleans District. These datasets describe individual structures (tax parcels) in the coastal floodplain, but only for portions of the state.

The new tax parcel-level data was derived from three separate USACE investigations, including: :

- Morganza to the Gulf (MTTG) Reformulation study (USACE, 2013b),
- Southwest Coastal Louisiana (SWC) Feasibility Study (USACE, 2013a), and
- West Shore Lake Pontchartrain Feasibility Study database (USACE, 2013e).

This new dataset includes part or all of the following Louisiana Parishes: Calcasieu, Cameron, Iberia, Jefferson Davis, Lafourche, St. Charles, St. James, St. John and Terrebonne. Grid points where parcel-level data were used to update the CLARA economic inventory are shown in Figure 3-1.

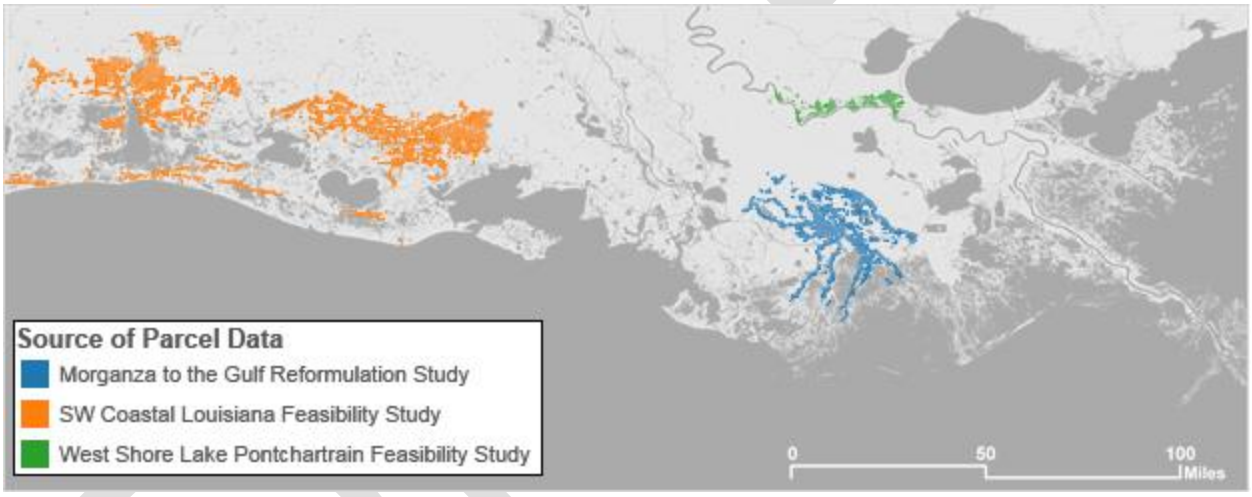

Figure 3-1. CLARA Grid Points Updated with Parcel-Level Structure Inventories, by Data Source

These data were integrated into a single parcel database for incorporation in CLARA V2.0. The structures in each parcel are described through the following characteristics: location (longitude and latitude coordinates), number of units, occupation type, damage category, square footage, and foundation type.

[14] Projections from LACPR with estimates from GNOCDC and ACS for the post-Katrina period were compared. For most parishes, the estimates of replacement value of structures were similar (i.e., within 10 percent). The discrepancies among the data sets are due largely to assumptions regarding population changes; model users may run different baseline population scenarios based on the values reported in the different databases. Moreover, because the ACS and GNOCDC estimates are similar for parishes where both data sets are available, the ACS could be used to develop alternative scenarios for parishes not included in GNOCDC.

The codes describing these characteristics in the parcel-level dataset were not equivalent to the GBS codes used in CLARA V2.0. As a result, it was necessary to map the parcel level data codes into the appropriate GBS codes. Table 3-1 lists the equivalent GBS code for a subset of the combinations of Occupation Type and Damage Category codes in the parcel level database. Using this crosswalk it was possible to map the structures contained in the integrated parcel level database into the standard GBS codes used in CLARA V2.0.

Table 3-1: Crosswalk between Parcel Dataset Occupation Type and GBS Codes.

Parcel Data Occupation Type Code	Parcel Data Damage Category Code	Equivalent GBS Code
1STY	Residential	RES1
2STY	Residential	RES1
MOBHOME	Mobile Home	RES2
MULTI-UNIT	Multi-unit	RES3
COM	Commercial	COM
IND	Industrial	IND
PROF	Commercial	COM
WARE	Industrial	IND
GROC	Commercial	COM
EAT	Commercial	COM
PUBL	Government	GOV
REPA	Commercial	COM
RETA	Commercial	COM

To support a separate evaluation of a potential barrier alignment across the mouth of Lake Pontchartrain, the structural asset inventory has also been expanded to include data for the coastal Mississippi counties in the expanded study region. Both residential and commercial structure counts for Mississippi are taken from the socio-economic database of the Mississippi Coastal Improvement Program (MsCIP) study (USACE, 2009d), in combination with the geodatabases of the Mississippi Automated Resource Information System (MARIS Technical Center, 2014). The resulting database contains information for over 200,000 tax parcels in Hancock, Harrison and Jackson counties.

Vehicle count estimates follow the same methodology as previous work. Vehicle counts are based on an average number of privately owned vehicles per household from 2010 US census

data. Commercial vehicle counts are based on the number of commercial licenses reported by the Louisiana Department of Motor Vehicles in October 2006 (USACE, 2009b).[15]

3.1.2 Transportation Infrastructure

The inventory of roads and bridges used in the analysis described later in this report comes from the NAVTEQ navigation data included in the Homeland Security Infrastructure Program (HSIP) Gold database (HSIP, 2014). This dataset provides more detailed road data for the entire study region; data for the State of Mississippi is excluded from the analysis in later sections.

A new inventory of roads, represented as a series of road lines in GIS format, was assembled for CLARA v2.0 using the NAVTEQ database. Each of the road lines from this inventory was split up and assigned to different grid points considered in the study region. Road types included in this database include highways, main roads, streets, and bridges. For each road type, the updated inventory includes the length of road (in road miles) that falls within the vicinity of each grid point.[16]

As part of the quality assurance process, the road miles estimated in the study region using the NAVTEQ database were compared against the total road miles previously estimated using the Hazus roads database. Table 3.2 compares estimated road miles across both databases, summarized by parish. This comparison is made considering only the area of each parish that falls inside the study region.

Because it was derived from GIS line files, the NAVTEQ roads data is summarized by point and assigned to grid points across the study region. The Hazus inventory, alternately, was initially provided as a summary by census block. Nevertheless, the table shows that, when estimated road mileage is aggregated by parish, the results from both the NAVTEQ database and Hazus database are largely similar. The slight differences that exist are likely due to differences in the geographical detail considered in each database, as well as methodological differences for portioning roads across the geographical unit of analysis.

[15] Commercial vehicle data from 2006 may underestimate the vehicle inventory due to the close proximity to Hurricanes Katrina and Rita. However, commercial vehicles represent a very small proportion of the total assets at risk, so any underestimate is unlikely to meaningfully affect CLARA damage estimates.

[16] Data on road elevations was also sought, but ultimately no dataset was identified for use in the initial assets database. NAVTEQ does not provide quantitative information on road elevations (categorical only). Data provided by the Louisiana Department of Transportation and Development was also considered, but included only a small number of areas (New Orleans, Lafayette, Lake Charles, Baton Rouge, and Hammond) and was not provided in a format that could be readily matched to the CLARA roads database. As a result, at present the model does not consider damage reduction from elevated roads.

Table 3-2: Comparison of Road Mileage From NAVTEQ and Hazus Datasets.

PARISH NAME	HSIP/NAVTEQ [road miles]	Hazus-MH [road miles]
Acadia	153.36	179.23
Ascension	935.37	975.70
Assumption	435.29	447.24
Calcasieu	1,887.54	2,047.04
Cameron	532.00	619.04
Iberia	822.05	1,116.37
Iberville	72.60	58.62
Jefferson	2,037.12	2,070.32
Jefferson Davis	421.65	472.97
Lafayette	32.18	35.75
Lafourche	1,145.49	1,239.23
Livingston	297.51	289.99
Orleans	2,069.58	2,065.17
Plaquemines	575.92	577.85
St. Bernard	323.26	404.26
St. Charles	532.33	545.06
St. James	477.06	468.98
St. John	404.28	409.15
St. Martin	76.88	121.06
St. Mary	883.50	1,033.47
St. Tammany	1,826.46	1,921.71
Tangipahoa	224.14	245.83
Terrebonne	1,021.75	1,280.93
Vermilion	1,351.22	1,459.51

3.1.3 Agricultural Crops

Acreage of agricultural crops was originally estimated from the same sources of data used in CLARA v1.0, including FEMA's Hazus-MH model, 2010 US census data, and Louisiana-specific economic updates provided by LACPR. A draft inventory of agricultural crops for the study was developed, based on data from the HSIP Gold database (HSIP, 2014). The area coverage of different crops for each grid point in the study area was estimated. As part of the quality assurance process, the grid point estimations using the HSIP Gold database were compared to

the census block acreage estimates in CLARA v1.0. The conclusion of this comparison was that the grid point crop data in the HSIP Gold database is biased low and should be replaced with more comprehensive crop data.

For this update, more recent and comprehensive crop data was taken from a crop-specific land cover data layer published by the US Department of Agriculture and National Agricultural Statistics Service in 2013 (U.S. Department of Agriculture, 2013). The area coverage of different crops for each grid point was estimated for the entire study area. The crop data layer in this dataset is produced using satellite imagery from the Landsat 8 OLI/TIRS sensor, Landsat 7 ETM+ sensor, and the Disaster Monitoring Constellation (DMC) DEIMOS-1 and UK2 sensors, and has a resolution of 30 meters.

Per-acre dollar values for different crops were estimated for the entire study area using Louisiana State University AgCenter data gathered by the LSU AgCenter's Louisiana Cooperative Extension Services and other agencies for 2013 (LSU AgCenter, 2013). Pasture, sugarcane, rice, aquaculture, and soybeans contributed 99 percent of the value in agricultural land for the study region, so only these five agricultural categories were included.

3.1.4 Critical Infrastructure

To improve overall estimates of risk and allow for more detailed consideration of nonstructural risk reduction as part of Louisiana's Flood Risk and Resilience Program, the RAND Team has added critical infrastructure assets to the inventory not previously considered in CLARA v1.0.[17] For this version of the model, the RAND Team identified newly-available datasets from the HSIP Gold database (HSIP, 2014) to incorporate electrical power plants, power substations, oil refineries, and petroleum pumping stations into the assets at risk inventory. These critical infrastructure asset classes are included because FEMA considers them vulnerable to flood damage and the FEMA Hazus model provides both depth-damage curves and valuation estimates (FEMA, 2011).

The HSIP database contains other critical infrastructure assets of potential interest, but which were not initially included in the damage assessment because the FEMA methodology considers them to have low to no risk of damage from flooding. For instance, Hazus assumes oil and natural gas pipelines and platforms will suffer no damage during a storm surge flood. Other critical infrastructure asset classes of interest included in HSIP Gold lacked detailed data to support damage assessment (e.g., port facilities), or the damage from flooding was difficult to determine. These assets were included in the CLARA v2.0 database for consideration in the non-structural analysis.

The critical infrastructure inventory was augmented by an inventory of strategic assets identified by the State of Louisiana and provided by CPRA in late 2014. The strategic assets identified by state agencies include the following categories: airports, gas processing, government/military, liquid natural gas (LNG), manufacturing/chemical, ports, power plants, oil refineries, the Louisiana Offshore Oil Port (LOOP), and the strategic petroleum reserve. The HSIP Gold dataset was merged with the Louisiana strategic asset list and duplicates were identified and removed, creating a single set for CLARA v2.0. For selected categories, however, only assets from the state's list were retained. In particular, there were a large number of manufacturing/chemical

[17] Critical infrastructure was not incorporated in time to be incorporated into the testing analysis described in Chapter 4. Instead, separate estimates of damage and functionality loss from critical infrastructure are intended to be produced after this writing to support the forthcoming coastal vulnerability assessment task.

facilities in the HSIP Gold dataset that appeared largely duplicative with CLARA's existing commercial assets data, so for this category only the Louisiana-provided inventory was included.

A summary of critical infrastructure from each data source is shown in Table 3-3. Some assets appeared in both sources. The table also indicates the asset classes for which depth-damage and valuation data are available are included in the damage calculations, as well as others that are considered for exposure to flooding only.

Table 3-3: Counts of Critical Infrastructure in the CLARA v2.0 Database by Data Source.

Critical Infrastructure Class	Louisiana Strategic Asset List	HSIP Gold	Both Sources (Duplicates)	Included in Analysis
Airport	5	212	4	Exposure only
Gas Processing	70	15	15	Damage and exposure
Government/Military	5	-	-	Exposure only*
Liquid Natural Gas	3	-	-	Exposure only
Louisiana Offshore Oil Port	2	-	-	Exposure only
Manufacturing/Chemical	54	-	-	Exposure only*
Port	16	-	-	Exposure only
Power Generation	11	105	2	Damage and exposure
Refinery	11	12	6	Damage and exposure
Strategic Petroleum Reserve	1	-	-	Exposure only

*Additional government, military, manufacturing, and chemical structures were included in the damage calculation as part of the public and industrial asset classes.

Table 3-4 provides an overall summary of the updated asset inventory data elements in CLARA v2.0, including asset class and data source or sources.

Table 3-4: Data Elements for the Asset Inventory Module.

Data Element	Asset Class	Source (by order of precedence)
Number of structures	All residential classes	SWC Feasibility Study, West Shore Lake Pontchartrain Feasibility Study, MTTG Reformulation Study, GNOCDC, ACS, LACPR, Hazus-MH
Number of structures	All nonresidential classes	LACPR, Hazus-MH, Census CBP
Acreage of agricultural crops	Agricultural crops	U.S. Department of Agriculture National Agricultural Statistics Service, LACPR
Number of vehicles	All vehicle classes	LACPR (adjusted by ACS)
Inventory of roads, railroads, bridges	Infrastructure	NAVTEQ, from HSIP Gold Infrastructure, LACPR
Square footage	All structural classes	LACPR, Hazus-MH
Critical infrastructure	Airports, heliports, gas processing, government/military, LNG, LOOP, manufacturing/chemical, ports, electrical power plants, power substations, oil refineries, petroleum pumping stations, water and sewer, strategic petroleum reserve	State of Louisiana; Platts, Ventyx, and Dun & Bradstreet from HSIP Gold

3.2 Asset Valuation Module Data Updates

As in CLARA v1.0, structural characteristics for many asset classes come from Hazus-MH. For single family residences, CLARA estimates replacement costs per square foot based on construction class, number of stories, the existence of a garage and estimates of average square footage per home based on the median household income of residences in each census block as reported in the 2013 ACS. For nonresidential structures, the replacement value is based on the total square footage of structures and the asset class. The value of inventory per square foot is estimated following the Hazus-MH methodology, which assumes an average value per square foot and only includes inventory in stock at the time of the flood event. Lost sales during recovery are estimated separately. New critical infrastructure (electrical power plants, substations, oil refineries, oil pump stations) valuations are taken from Hazus-MH estimates (FEMA, 2011).

Repair cost per mile for roads and bridges are based on the Economic Data Survey for the Mississippi River and Tributaries Protected Area and the Louisiana Department of Transportation and Development's Engineering Division (USACE, 2009b). The vehicle values are based on an average retail replacement value across all vehicle types and classes (FEMA, 2011).

Table 3-5: Data Elements for the Asset Valuation Module.

Data Element	Asset Class	Source (by order of precedence)
Structural characteristics for each asset class	All structural classes	SWC Feasibility Study, West Shore Lake Pontchartrain Feasibility Study, MTTG Reformulation Study, Hazus-MH,
Replacement cost per square foot	All structural classes	Hazus-MH
Proportion of structures by construction class (economy, average, custom, luxury)	All residential classes	Hazus-MH
Contents to Structure Value Ratio	All structural classes	Hazus-MH
Value of inventory per square foot	Commercial, industrial	Hazus-MH
Depreciation curves by structural age	All structural classes	Hazus-MH, economics literature
Repair cost per mile of road	Infrastructure	LACPR, Hazus-MH
Agricultural valuations	Agricultural crops	LSU AgCenter
Value of vehicles	All vehicle classes	Hazus-MH
Proportion of structures by construction method (e.g., wood frame, masonry)	All structural classes	Hazus-MH
Critical infrastructure	Power plants, power substations, oil refineries, petroleum pumping stations, water and sewer	Hazus-MH 2.0

3.3 Converting Data to CLARA v2.0 Grid Point Resolution

To develop the new CLARA v2.0 database of assets at risk, all economic asset data were converted, regardless of the original source resolution, to the level of resolution for the model's new grid points (at least 1 km). All asset inventories were either aggregated or decomposed and assigned to the nearest grid point using the procedure specified below. Assigning geospatial data stored as points, lines, or areas to grid points is relatively straightforward; disaggregating census block level data to grid points, however, requires additional assumptions.

In order to match geospatial point data to the nearest grid point, the study region was divided into a set of Thiessen polygons, where each polygon defines an area of influence around a given grid point, so that any location inside the polygon is closer to that grid point than any of the other grid points. The resulting polygons do not overlap, and fill the study region. Assets stored as geospatial points (e.g., electric power generating plants) are assigned to the grid point that corresponds to the polygon containing the asset.

A similar method was used for geospatial lines and polygons. The length of each road, railroad, and bridge within a polygon is assigned to the corresponding grid point. If a road crosses several Thiessen polygons, the length of the road within each Thiessen polygon is summed and assigned to the corresponding grid point. Similarly, the acreage of crops within a Thiessen polygon is assigned to the corresponding grid point.

Data aggregated at census block or lower resolution, such as residential and commercial structure inventories for coastal Louisiana, were disaggregated to the grid points within each census block. Structure counts are assigned to RSPs proportionally to the population at each grid point as estimated in the LandScan dataset (U.S. Department of Energy Oak Ridge National Laboratory, 2011).

The disaggregation process included several steps. First, LandScan population counts were assigned to grid points using the Thiessen polygons described above. Next, structure counts were assigned to the grid points within the census block in proportion to the LandScan population at each grid point. Population was determined by either the nighttime or daytime LandScan population, depending on the structure class. It is assumed that most coastal residents spend the day at work or school, while they spend the night at home. Commercial, industrial, agricultural, governmental, and educational structures in a census block are correspondingly divided amongst grid points proportional to their daytime population. Residential and religious structures in a census block are assigned to grid points using the nighttime population.[18]

This process led to a few special cases where the structure inventory and LandScan populations did not align. A small number of census blocks with nonzero structure counts in the CLARA database, for example, contain only unpopulated grid points for the daytime and/or nightime LandScan dataset. Rather than assigning these structures to unpopulated grid points, the structures were divided evenly among all populated grid points in the parish. Grid points without daytime population were not assigned commercial, industrial, agricultural, governmental, or educational structures. Grid points without nighttime populations were not assigned residential or religious structures. Conversely, grid points with a nonzero LandScan population contained in a census block with no structures were not assigned "new" structures, to avoid potential biasing. As a result, a small number of populated grid points do not contain structures. The special cases described here are summarized in Table 3-6.

Table 3-6: Special Cases from Conversion of Assets at Risk Inventory.

Structure Class	Total Count (2015)	Structures located in unpopulated census blocks (count)	Structures located in unpopulated census blocks (percent of total)
Single-family residences	700,779	14,705	2
All other residential structures	77,271	7,176	4
Non-residential structures	47,933	3,060	6

[18] Religious buildings were assigned in the same way as residential structures under the assumption that most people worship close to home.

As discussed above, the structure inventory used in CLARA v2.0 was updated using new tax parcel-level data provided by USACE. The parcel-level data was composed of different data sets, which were integrated into a single parcel database for CLARA v2.0.

The parcel-level dataset included a higher level of geospatial resolution than the CLARA grid points. To convert the parcel data to grid points, the parcels contained in this integrated database were linked to their nearest corresponding grid points in the study region using the Thiessen polygons. Then, the structures counts were aggregated for each grid point overlapping the geographic extent of the parcel level database.

The parcel-level data did not include the same level of detail regarding structure type as the initial structure dataset. For multifamily dwellings (RES3), as well as commercial (COM), industrial (IND), and government (GOV) buildings, it was not possible to classify structures at the same level of resolution as in CLARA v1.0. For these structure types, an additional iteration was carried out to classify them at the same resolution level as in CLARA v1.0. First, using the original database, the proportion of structures was estimated for each parish according to the more detailed occupancy codes. Then, the estimated aggregated counts of structures per grid point were multiplied by the estimated proportion of structures to approximate the more detailed breakdown. For example, for structures identified as multifamily (RES3), the proportion of structures types classified as RES3A, RES3B, RES3C, RES3D, RES3E and RES3F was estimated by parish from the CLARA v1.0 database, and were then multiplied by the estimated RES3 counts derived from the parcel-level dataset.

Table 3.6 compares the estimated structure counts from the CLARA v1.0 dataset, based on data from the LACPR analysis, and the updated estimates based on parcel-level data. The table shows that for each parish, the estimated structures using the parcel level data and using the LACPR data are largely similar. The differences that exist are likely the result of the higher spatial resolution and more recent date of last update for the parcel-level data.

Table 3-7: Comparison of Structure Counts by Parish.

Parish Name	Structure Type	Parcel Data Count	LACPR Count
Calcasieu	COM	1,374	1,651
Calcasieu	IND	595	370
Calcasieu	RES1	26,117	28,492
Calcasieu	RES2	5,027	5,862
Cameron	COM	156	144
Cameron	IND	267	45
Cameron	RES1	2,010	2,952
Cameron	RES2	965	1,212
Lafourche	COM	330	396
Lafourche	IND	781	122
Lafourche	RES1	7,194	8,112
Lafourche	RES2	2,631	1,902
St. Charles	COM	6	7
St. Charles	IND	4	4
St. Charles	RES1	557	370
St. Charles	RES2	167	106
St. James	COM	118	145
St. James	IND	80	46
St. James	RES1	4,093	3,088
St. James	RES2	435	754
St. John the Baptist	COM	726	510
St. John the Baptist	IND	458	128
St. John the Baptist	RES1	13,677	12,475
St. John the Baptist	RES2	967	1,428
Terrebonne	COM	2,014	1,904
Terrebonne	IND	2,172	561
Terrebonne	RES1	28,754	28,833
Terrebonne	RES2	7,793	5,384

3.4 Results: Assets at Risk in the New CLARA Coastal Domain

This section provides a snapshot of the database of assets at risk in CLARA as of December 2014. The underlying economic data will be refined as new data becomes available until model production begins in June 2015. As a result, the data summarized here are subject to change in future updates to this report. The database updates shown below reflect four significant updates: 1) the conversion of the economic unit of analysis from 2000 US census blocks in CLARA

v1.0 to the CLARA v2.0 grid points, 2) the incorporation of parcel-level inventory data for some portions of the coast, 3) the inclusion of critical infrastructure, and 4) a new simulation base year for the economic analysis (2015), adopted for the new 50-year simulation period 2015-2065.[19]

3.4.1 Assets at Risk by Grid Point

The change of the spatial unit of analysis to CLARA v2.0's grid points represents the greatest change in model data format. As described in Section 3.3, the LandScan data set was used to distribute assets, originally measured at the census block level, among the grid point(s) contained with each block. In rural areas, this provides a more precise image of where coastal assets are located at a resolution of at least 1 km.

Figure 3-2 and Figure 3-4 show the number of single-family residences by grid point coast wide and in Greater New Orleans, respectively. They demonstrate the benefit of the new spatial unit. In some cases, coastal census blocks, such as those in Cameron Parish, have been divided into hundreds of grid points; there is now a much clearer picture of where populations are concentrated. Unpopulated areas within the Greater New Orleans HSDRRS are also more readily apparent.

Figure 3-3 indicates that across the coast, approximately 55 percent of grid points include single-family homes. Note, however, that there are still areas of non-uniform point density in urban localities with census block areas less than 1 square km. The new grid points, together with the development of visualization packages in Tableau, enable quick inspections of development patterns and damage outcomes across the coast, which can better support CPRA's nonstructural risk reduction planning and future communication with coastal residents.

Single family residences are used as an example to show how the geographic distribution of assets at risk are visualized and studied. Similar patterns to those shown in the figures below hold across the coast for other asset types, the natural exception being the distribution of agricultural crops, which are spread throughout rural areas.

[19] Note that the landscape, storm surge, and wave data used in the test analysis (Section 6) use the original 2012 Coastal Master Plan base year (2010), and are not yet updated for the new modeling base year. The damage portion of the testing and sensitivity analysis therefore makes a simplifying assumption of no landscape change during the interim period.

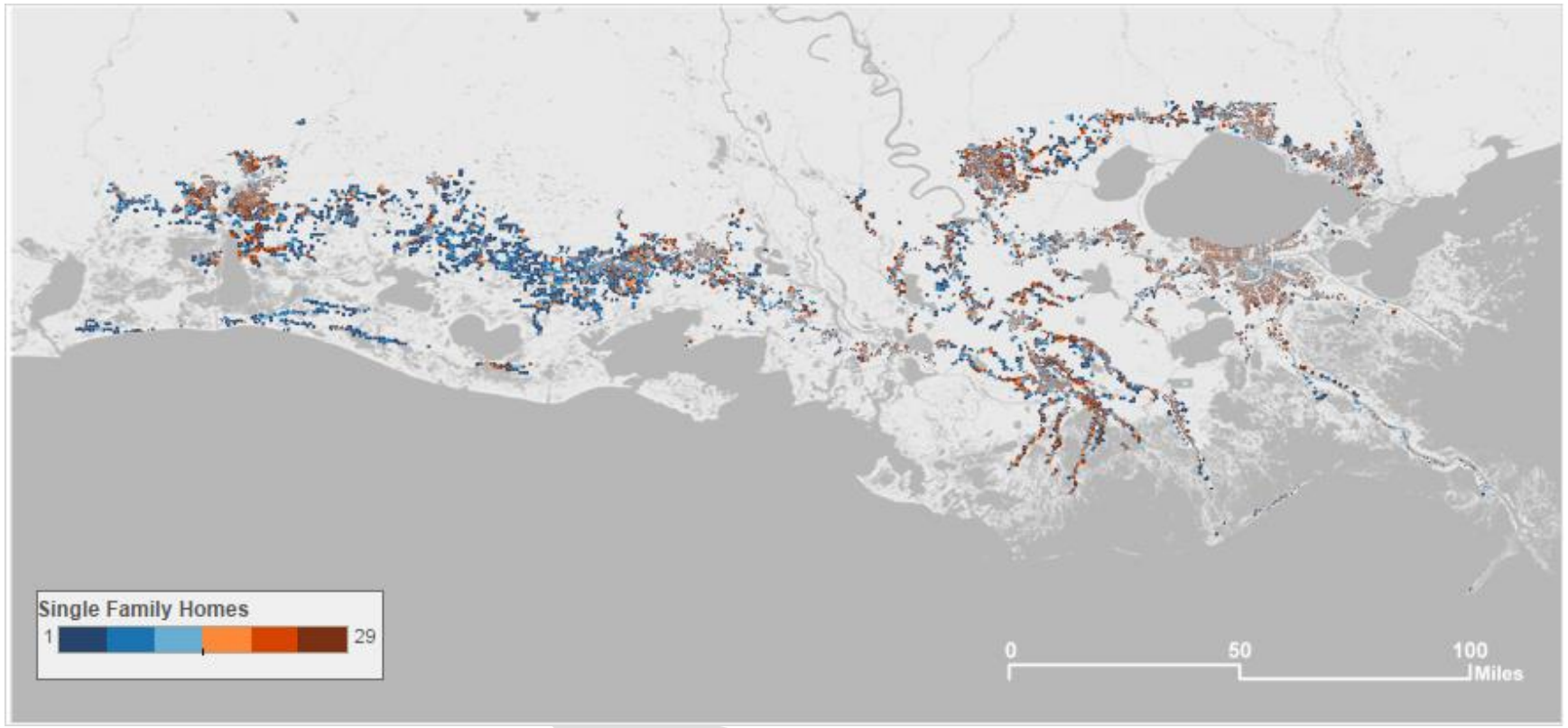

Note: figure only includes points with at least one structure.

Figure 3-2: Count of Single Family Homes by Grid Point, Current Conditions (2015).

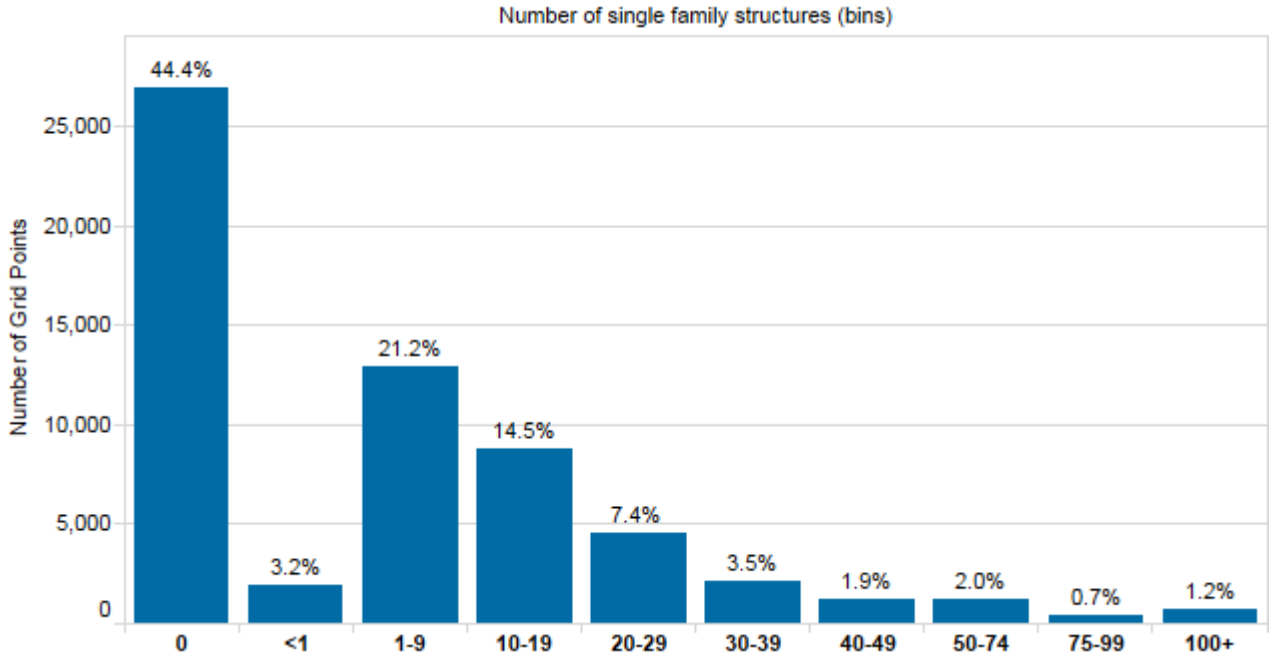

Figure 3-3: Histogram Summarizing Count of Single Family Homes per Grid Point, Current Conditions (2015).

Figure 3-4: Single Family Homes by Grid Point in Greater New Orleans, Current Conditions (2015).

3.4.2 Changes from the 2012 Analysis

Figure 3-5 summarizes the value of assets at risk across each major asset category, comparing them between the asset databases used by CLARA v1.0 and v2.0. Data shown here are restricted to grid points in Louisiana, and do not include the expansion of CLARA v2.0's study region into portions of Texas and Mississippi.

The significant increase in the value of assets at risk, 20 to 65 percent more than in CLARA v1.0, is due to several factors:

- Within Louisiana, CLARA v2.0 incorporates an expanded study region compared to CLARA v1.0 that encompasses several urban areas not previously considered.
- CLARA v2.0 models five years of additional growth in the baseline inventory.
- CLARA v2.0 incorporates more recent economic data, including new parcel-level inventories, which more accurately capture the recovery and long-term redevelopment after the 2005 hurricane season. The parameters used to estimate recovery in CLARA v1.0's economic database may have led to underestimates of the actual assets present in 2010.

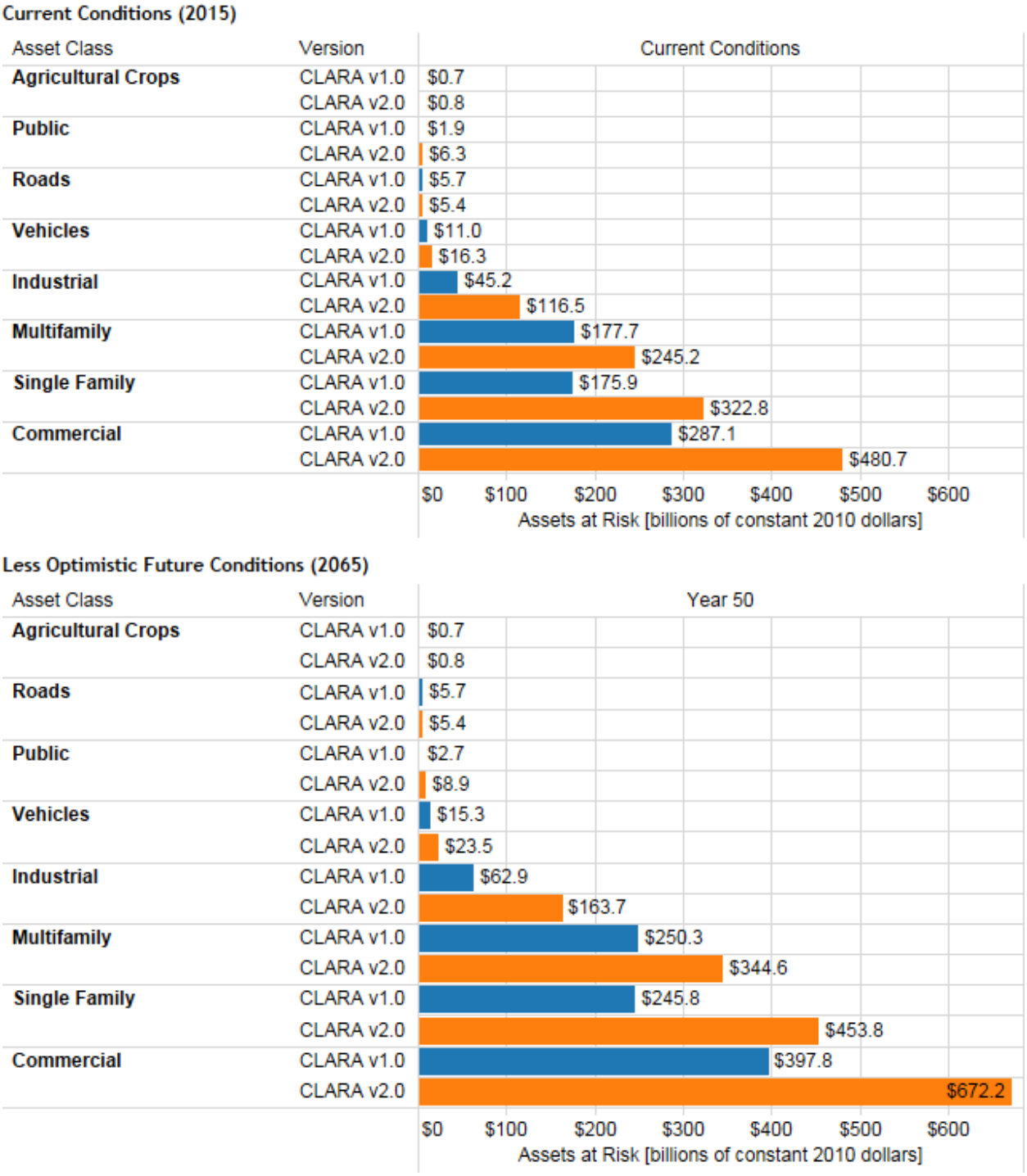

Figure 3-5: Assets at Risk by Asset Class, Current (2015) and Future (2065) Conditions.

It should also be noted that the commercial sector represents the single largest category of assets at risk, with nearly $500 billion at risk in 2015. In the 2012 Coastal Master Plan analysis, options for nonstructural risk reduction for these assets were very limited, including only structure floodproofing up to 3 feet of flood depth. Given the prominence of commercial assets in the CLARA assets at risk calculations, this suggests a gap that could be addressed through new options identified through Louisiana's new Flood Risk and Resilience Program.

3.4.3 Critical Infrastructure

One of CLARA v2.0's new features is the addition of critical infrastructure to the database of economic assets. Specifically, the locations and quantities of all asset types listed in Table 3-3 have been incorporated by grid point. As expected, many of these assets are concentrated in New Orleans and Lake Charles, though a substantial number of airports, gas processing facilities, and power plants are also distributed in other parts of the coast (see Figure 3-6). The critical infrastructure inventory also shows the large number of facilities that support oil and gas extraction, processing, and transport that are located in the coastal floodplain.

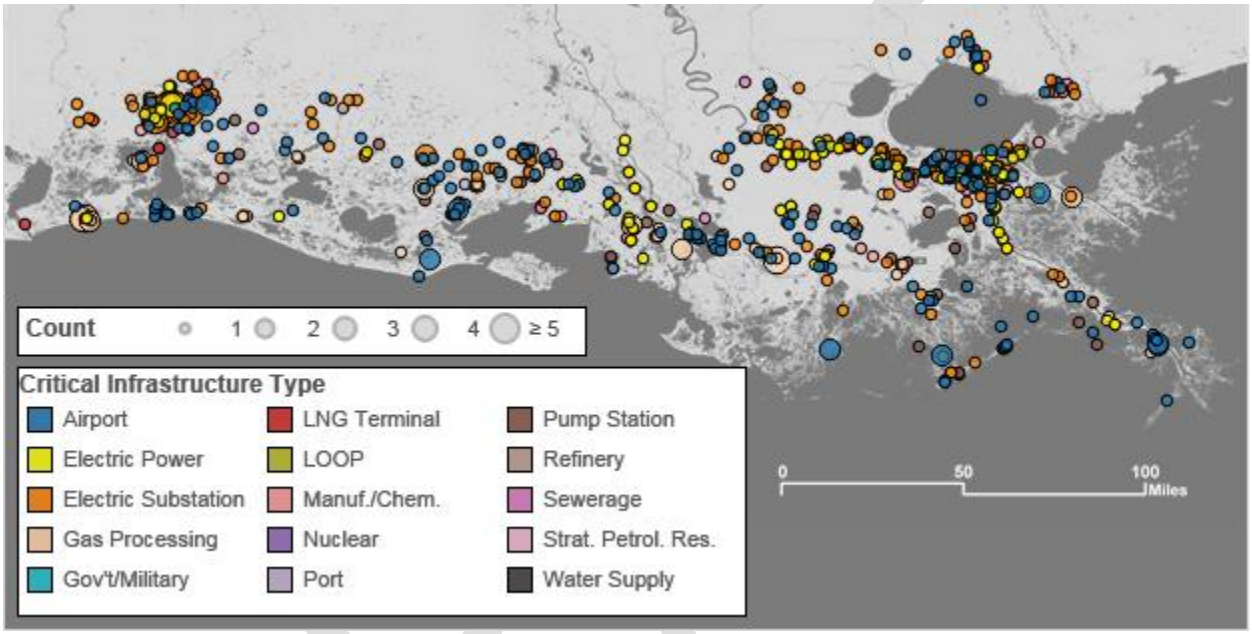

Figure 3-6: Critical Infrastructure Counts by Point (Louisiana Only).

Flood risk exposure of most critical infrastructure assets is excluded from the model's expected annual damage results discussed in Section 5.3.3 (see Table 3-3 for exceptions). Because of their specialized function and small number, critical infrastructure are treated separately in CLARA v2.0; critical facilities may also have site-specific hardening measures that reduce their vulnerability to given flood levels. The associated valuation methods and damage metrics are focused on loss of operational capacity in additional to structural damage. These risk measures are being implemented to support Louisiana's Flood Risk and Resilience Program and are subject to change based on the needs of that program.

Counts of critical infrastructure by parish are reported in Table 3-8 for initial planning purposes and to provide a general impression of exposure to augment the flood depth and damage data presented in Section 6.6.3. Note that in cases where parishes are only partially included in the CLARA v2.0 study region, these counts only represent facilities located in the portion of the parish inside the study region.

Table 3-8: Counts by Parish of Critical Infrastructure in the CLARA v2.0 Database (Louisiana Only).

Parish	Airport	Electric Power Plant	Electric Substation	Gas Proc.	Gov't/ Military	LOOP	LNG	Manuf./ Chem.	Nuclear Power	Port	Petrol. Pump Station	Refinery	Sewerage	Strat. Petrol. Reserve	Water Supply
Acadia			2								1				
Ascension	5		6								1		1		1
Assumption	2		2	3				2							
Calcasieu	18	10	89	4			1	16			6	6	8		
Cameron	17	2	7	19			2	1		1	3		1	1	
Iberia	12	3	10	3				2		2	3		2		
Jefferson	18	7	28	1				5			3	1	7		
Jeff. Davis	4		3									1			
Lafayette	1														
Lafourche	13	2	9	3		2		3		1	10		2		
Livingston			1												
Orleans	9	9	28		4			3		3			3		2
Plaquemines	21	8	9	3	1			3		1	3	3			
St. Bernard	3	7	12	5						1		3	1		
St. Charles	5	9	23	2				9	1		1	4	1		
St. James	2	12	16								1	1			
St. John The Baptist	2	3	9	1				6				2			
St. Martin		3	2								1		1		
St. Mary	16	11	9	13				4		1	3		1		
St. Tammany	8	1	9										4		2
Tangipahoa	1		1												
Terrebonne	12	2	7	9							1				
Vermilion	23	1	13	16						1	3				
Grand Total	**192**	**90**	**295**	**82**	**5**	**2**	**3**	**54**	**1**	**11**	**40**	**21**	**32**	**1**	**5**

4.0 Updates to Levee Fragility and Breaching Approach

4.1 Background

In the 2012 Coastal Master Plan analysis, the RAND Team observed that uncertainty related to the performance of hurricane protection structures, including levees, floodwalls, gates, and pumps, during storm surge and wave events can be a key driver of future flood damage and flood risk in Louisiana's coastal communities (Fischbach et al., 2012a). To support model improvement for the 2017 Coastal Master Plan analysis, recent literature describing methods for simulating the performance of hurricane protection structures was reviewed, and used to revise the CLARA approach to protection structure fragility.

The most common cause of levee and floodwall failure during Hurricane Katrina was erosion on the protected/inland side of floodwalls and scour on the top or back side of levees caused by water overtopping the structures (IPET Vol. V, 2007). Failures were also caused by seepage: water infiltrating the ground at the base of flood defenses. Seepage is more of a concern for levees built using uncompacted hydraulic fill as opposed to clay. Transitions between distinct sections of levees and floodwalls were particularly vulnerable during Katrina (IPET Vol. V, 2007) Finally, some floodwalls in New Orleans also failed catastrophically—before overtopping occurred—in some cases due to the use of poorly-designed I-wall structures (Andersen et al., 2007; Seed et al., 2006; van Heerden et al., 2006).

CLARA v1.0 was developed with multiple fragility scenarios that vary the factor of safety achieved by protection features, which in turn changes the calculated level of stress that would produce a given probability of geotechnical failure. Testing indicated that the variation across these scenarios had little effect on overall risk. For the 2017 analysis, a single model of geotechnical fragility is used instead, and CLARA v2.0 fragility scenarios are focused on variation in the probabilities of failure from overtopping and scour.

The primary tool used for modeling the fragility of protection system features is the fragility curve, a relationship that estimates the probability of failure for a particular type of levee, floodwall, or transition element as a function of external forcing from storm surge water elevations, waves, or overtopping rates.

The United States Army Corps of Engineers (USACE) established the Interagency Performance Evaluation Task Force (IPET) to develop and summarize lessons learned as a result of the devastation caused by Hurricane Katrina. IPET developed fragility curves based on empirical observations of levee and floodwall failure during Hurricane Katrina, as summarized in Table 4-1. As the table indicates, the fragility curves take as input the depth of overtopping during a storm. IPET's fragility curves are step functions, with thresholds of depth of overtopping separating regions with distinct probabilities of levee or floodwall failure. The IPET analysis also broke long sections of a levee or floodwall into sub-sections of length roughly equal to a parameter defined to be the "characteristic length" for analysis purposes. The resulting sub-sections are assumed to be independent in terms of whether or not they fail when faced with a common storm surge. The probability of failure of each subsection is found using the data shown in Table 4-1. Essentially, the table reflects fragility curves for sections of levees and floodwalls with length equal to the characteristic length. (In the cited study, these are referred to as the "2-D" probabilities of failure.)

Table 4-1: Empirical Frequency of Failure Due to Overtopping and Scour as Observed During Hurricane Katrina.

		Depth of Overtopping		
Structure	**Material**	**<= 0.3m (1 ft)**	**<= 0.6m (2 ft)**	**0.9m (3 ft)**
Levee	Hydraulic Fill	0	1	1
Levee	Clay	0	0.25	0.5
Levee	Protected	0	0	0.1
Floodwall	Hydraulic Fill	0	0.5	1
Floodwall	Clay	0	0.25	0.5
Floodwall	Protected	0	0	0.1

Source: (IPET Vol. V, 2007).

The IPET-provided fragility curves described above contrast markedly with those from the Morganza to the Gulf (MTTG) Reformulation Study (USACE, 2013b). In the MTTG study, levees may face substantial risk of failure even when the depth of overtopping is less than one foot. This is due in part to fragility being expressed as a function of the overtopping rate, rather than its depth. While overtopping rates are an increasing function of surge elevations and wave heights, the relationship is complex and also influenced by levee geometry, the wave period, the presence of floodwalls, and other factors; in some cases, levees may experience overtopping rates sufficient to cause a high probability of failure from wave overtopping alone.

The MTTG study considers two failure modes, "foundation failure" and scour caused by overtopping. The MTTG approach is described as appropriate when storm surge height is relatively close to levee height. Based in part on recent research performed at Colorado State University (Thornton, van der Meer, Scholl, Hughes, & Abt, 2011), the MTTG study assumed that federal levees have 0.45, 0.85, and 0.95 probabilities of failure when facing overtopping rates of 0.09, 0.14, and 0.19 cubic meters per second per linear meter (m^3s^{-1}/m), respectively. This corresponds to rates of 1, 1.5, and 2 cfs/ft. Similarly MTTG assumes that there is a 5 percent chance of local (non-federal) levees[20] failing when overtopping rates reach 0.009 m^3s^{-1}/m (0.1 cfs/ft), and a 95 percent chance when they reach 0.09 m^3s^{-1}/m (1 cfs/ft). It is unclear what interpolation was used for points in between the points at which the 5 and 95 percent failure probabilities occur. MTTG also does not reference a characteristic length parameter, and it appears the length of a levee was not considered when modeling the fragility of the levee.

This report describes scenario analysis investigating the impact of uncertainty in levee and floodwall fragility modeling. It also includes work done updating models of the consequences of floodwall and levee failures.

4.2 Volume-Based Breaching

When modeling the consequences of levee failure, one relatively simple approach previously applied is to assume that the interior water elevation in an enclosed system equalizes to the peak surge exterior to the system. This approach, referred to as "elevation-based breaching," was adopted by CLARA v1.0 and used in the 2012 Coastal Master Plan analysis. IPET used this elevation-based approach for their main study results, although the peak surge elevation was converted to a polder volume before running the interflow analysis. During an overtopping event, "all breach depths were assumed to be full levee height" and "maximum basin water elevations caused by the breach were set to the maximum surge elevation experienced

[20] Local (non-federal) levees are levee systems that have not been certified by the U.S. Army of Corps of Engineers as meeting minimum standards in terms of their design, operation, and maintenance (see Title 44 of the Code of Federal Regulations, Section 65.10).

adjacent to the breach" (IPET Vol. VIII, 2009). For failure due to a breach without overtopping, "breaches were considered to be a result of a structural or foundation failure" and the "maximum basin water elevations caused by the breach were set to the maximum surge elevation experienced adjacent to the breach."

IPET's alternative volume-based approach assumed certain breach depths and lengths, and used a different weir equation than that used for overtopping calculations in order to estimate breach flow. Each characteristic length was still treated independently when calculating breach volumes; no feedback was introduced to impact surge levels at adjacent reaches, or to redirect water from other spatial regions through the breach.

Elevation-based breaching is an aggressive assumption that likely overestimates the consequences of failure (flood depths and damage) in most circumstances. As a result, the fragility model was modified when developing CLARA v1.1[21] to include a more realistic fragility mode, referred to as "volume-based breaching," which is similar to IPET's alternative approach and estimates the volume of water spilling into the interior from a breach based on the modeled surge hydrograph (the levels of surge over time) at the location of the breach. Consistent with IPET, breaches are assumed to occur at the time of peak surge. The volume of water entering through the breach is calculated using the same weir equations used for overtopping, but under the assumption that the levee crest height is effectively reduced to zero from this time onward. This breach volume is added to rainfall, along with overtopping volumes elsewhere in the system, and then distributed throughout the enclosed area using CLARA's interior drainage module.

Under these assumptions, the volume-based breaching procedure is summed up as follows:

- Identify reaches where breaches occur under the Monte Carlo simulation, in accordance with the reach-specific probabilities of failure
- For breached reaches, calculate overtopping volumes as normal for each time period in the surge hydrograph that occurs before the time of peak surge
- For points in the surge hydrograph after the time of peak surge, reduce the protection feature's crest elevation to mean sea level to simulate a "full-depth" breach
    - Recalculate levee geometries, surf similarity coefficients, and other relevant parameters that impact overtopping rates
    - Calculate overtopping volumes for time periods after peak surge using the same overtopping equations but with the altered levee conditions

Another significant advantage of the volume-based breaching approach is that it allows differentiation between the case of a single point of failure and a case where many breaches occur in a particular region. Under elevation-based breaching, the final elevation in each case is set equal to the maximum surge causing a breach, regardless of whether one breach occurs or many. Under volume-based breaching, different numbers of breaches result in different volumes of water entering the system.

[21] CLARA v1.0 is the version that was used in the 2012 Coastal Master Plan analysis. CLARA v1.1 is a version subsequently developed which has been used in follow-on analyses and other post-2012 task orders. The primary distinction between the two versions is the addition of the volume-based breaching algorithm described here.

4.3 Modified Fragility Scenarios for Enclosed Areas

The differences between the fragility curves developed and applied in the IPET (IPET Vol. V, 2007) and MTTG (USACE, 2013b) studies highlight the high level of epistemic uncertainty associated with levee and floodwall fragility. As previously discussed, this gap in the scientific knowledge regarding levee fragility when overtopping occurs should be considered a deep uncertainty, and the range of outcomes possible from adopting different fragility curves is best evaluated using scenario analysis. As a result, in CLARA v2.0 the approaches taken by IPET and MTTG, respectively, have been adopted and used to develop a discrete set of levee fragility scenarios, replacing the approach described during the 2012 Coastal Master Plan analysis.

To develop these new scenarios, the IPET and MTTG fragility curves were first placed into common units to enable comparison. The translated fragility curves are each expressed as a function of overtopping rates, in units of cubic meters per second per linear meter of protection feature (m^3s^{-1}/m). Following the IPET approach, "2-D" fragility curves are first developed, representing the probability of failure of a section of levee or floodwall of one characteristic length. Fragility curves are assumed to have a sigmoid or "S" shape, with parameters set based on data from the cited studies.

The fragility curves from the IPET (2009) study, originally based on peak exterior water elevations relative to the top-of-wall, are modified here so that they instead translate overtopping rates into probabilities of failure. Basic free-flow weir calculations are used, neglecting wave overtopping when storm surge is above levee or floodwall height. The overtopping rate which would result from surge at the specified elevation relative to a protection feature's crest height is calculated. A sigmoid curve is then fit to pass through the resulting combinations of overtopping rate and failure probability, which is consistent with the MTTG Study (USACE, 2013a) and avoids the use of a step function with thresholds at seemingly arbitrary overtopping rates. An example is shown in Equation 4-1 and the supporting text:

$$y = \frac{p_{max}}{1 + e^{-k(x - x_c)}} \quad (4\text{-}1)$$

where the function variables and parameters are defined as follows:

- y: probability of failure
- x: overtopping rate, in m^3s^{-1}/m
- p_{max}: maximum probability of failure caused by overtopping, a model parameter equal to 0.5 for a clay floodwall
- k: sensitivity to changes in flow rate, a model parameter equal 3.595 for a clay floodwall
- x_c: critical overtopping rate where probability of failure is half of maximum, a model parameter equal to 1.129 for a clay floodwall).

Note that when there is no overtopping, x will be 0 and y will be $p_{max}/(1+\exp(kx_c))$, which will be greater than 0. This is a somewhat counterintuitive result arising from the use of the sigmoid curve. In practice, these probabilities of failure without overtopping are relatively small.

This approach was repeated across each structure type (levee or floodwall) and fill material (hydrofill, clay, or armored) specified by IPET, and the resulting set of 2-D fragility curves were used as "IPET-like" fragility scenarios for the CLARA analysis.

The MTTG study, alternatively, includes a plot of probability of failure of a federally certified levee as a function of overtopping flow, measured in cubic feet per second per linear foot (cfs/ft),

Figure 22 in USACE (2013b). Four points are explicitly labeled on the figure: an overtopping rate of 0.5 cfs/ft yields a 6 percent probability of failure, 1 cfs/ft yields a 45 percent probability, 1.5 cfs/ft yields a 85 percent probability, and 2 cfs/ft yields a 95 percent probability. A sigmoid curve runs through the labeled points. Figure 4-1 shows the relationship between overtopping flow and probability of failure in the cited work.

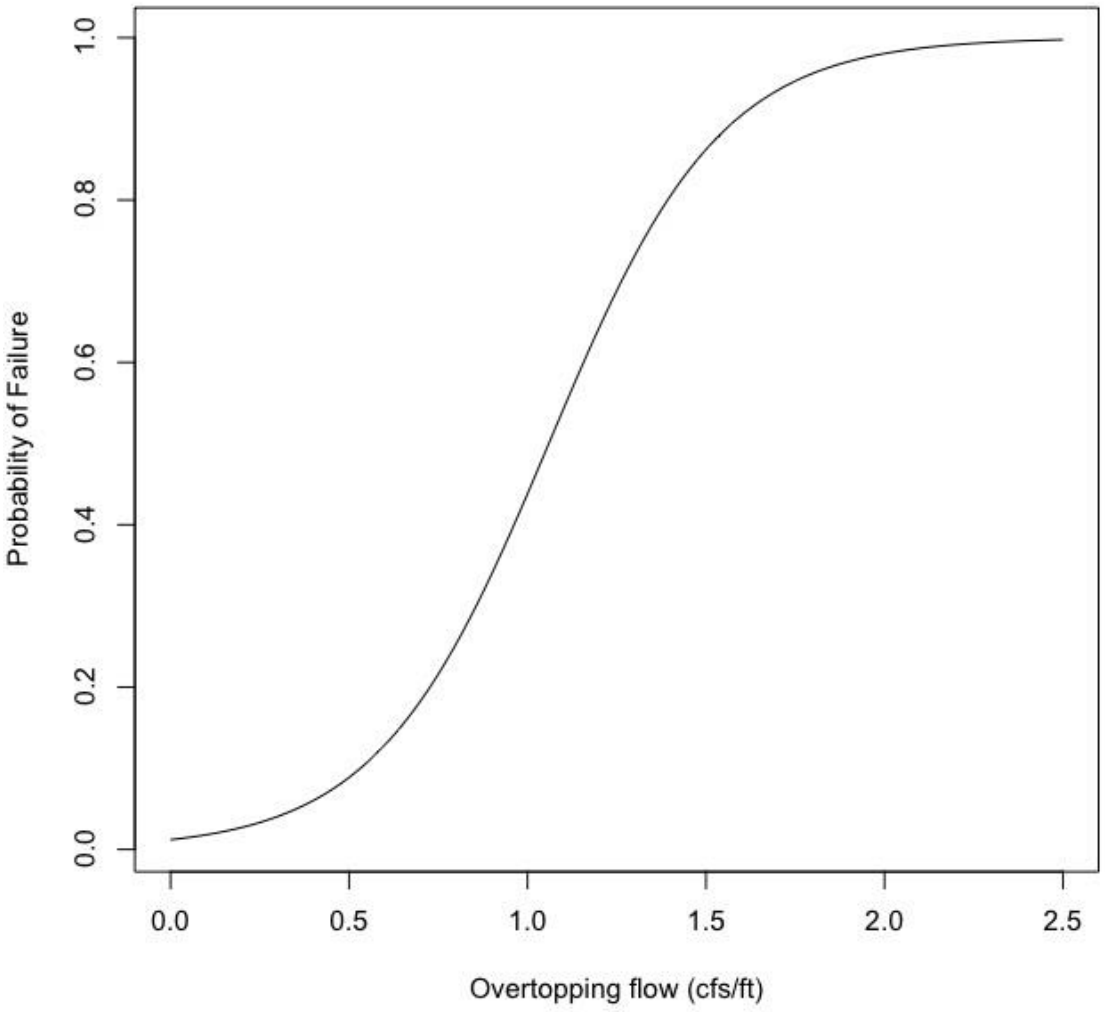

Figure 4-1: Fragility Curve from MTTG Study

Source: Adapted from USACE (2013b).

Fitting a curve to the data points listed in the preceding paragraph and translating to SI units reveals a closed-form equation. The parameter values in Equation 4-1 are defined as follows:

- The maximum probability of failure, p_{max}, is 1.
- The sensitivity, k, is 44.8.
- The critical overtopping rate, x_c, is 0.0985.

The MTTG study indicates that the probabilities of failure listed above were associated with overtopping rates half as severe as fragility curves for local (non-federal) levees. In this case, the defining parameter values are as follows:

- The maximum probability of failure, p_{max}, is 1.
- The sensitivity, k, is 89.6.
- The critical overtopping rate, x_c, is 0.0492.

Together, these equations are used to define a new "MTTG High" scenario for levee and floodwall fragility, with the functions above applied directly to each reach.

The MTTG study does not reference the length of levees or floodwalls. The equations were applied to "subreaches" that ranged from 993 to 25,243 meters. In contrast, the IPET 2-D probabilities of failure are associated with sections of levee or floodwall with equal, fixed characteristic lengths assumed to be 152, 305, or 610 meters (500, 1,000, or 2,000 feet). This value was varied as one component of IPET's uncertainty analysis. There is thus a need to adjust the equations listed above in order to enable a more accurate comparison to the IPET approach.

To perform this comparison, the Morganza subreaches were split into sections of roughly 305-meter (1,000-foot) lengths that were assumed to be homogeneous and independent (reflecting the IPET approach). The fragility curve equations given above were applied to each subreach, so that there was a 95 percent probability of failure for any subreach of a Federal levee subject to 0.186 m^3s^{-1}/m (2 cfs/ft) in overtopping rate. It was assumed that the fragility curve for any subreach could be found by aggregating results from fragility curves for the 305-meter length sections that comprise the subreach. Thus, each subreach's fragility curve implied a specific fragility curve for the (assumed homogeneous) 305-meter (1,000-foot) sections that comprise the subreach.

For example, a 3,050-meter (10,000-foot) subreach includes 10 characteristic reaches of length 305 meter (1,000 feet). Assume that each 305-meter section has a 26 percent probability of failure when subject to a an overtopping rate of 0.186 m^3s^{-1}/m (2 cfs/ft). The probability that none of the ten characteristic lengths will fail when the subreach is subject to an overtopping rate of 0.186 m^3s^{-1}/m is 5 percent. Thus, a subreach of this length that has a 95 percent probability of failure when subject to 0.186 m^3s^{-1}/m is consistent with 305-meter (1,000-foot) "characteristic length" sections that have a 26 percent probability of failure when subject to 0.186 m^3s^{-1}/m (2 cfs/ft).

Note that the fragility curves for the 305-meter (1,000-foot) sections have lower probabilities of failure than those for the subreaches, because aggregation of many of the former yields the latter.

The fragility curves of each 305-meter (1,000-foot) section were used as an estimate of a "2-D" fragility curve, in the language of the IPET study. Results from each MTTG subreach were calculated separately and then averaged to develop a single implied 2-D fragility curve for each structure type. The average of these across the subreaches was compared to the IPET fragility curve. The result was labelled the "MTTG Low" scenario for levee and floodwall fragility.

For federal levees, the resulting parameter values that define a 2-D fragility curve are as follows:

- The maximum probability of failure, p_{max}, is 0.604.
- The sensitivity, k, is 17.2.

- The critical overtopping rate, x_c, is 0.221.

For local levees, the 2-D relationship is defined by the following parameter values:

- The maximum probability of failure, p_{max}, is 0.604.
- The sensitivity, k, is 34.4.
- The critical overtopping rate, x_c, is 0.111.

These 2-D curves were then applied to the CLARA v2.0 reaches using the same approach as in IPET, assuming a 305-meter (1,000-foot) characteristic length. These equations yield lower probabilities of failure when compared to those that make up the MTTG High scenario, and are here used to define the "MTTG Low" fragility scenario.

Figure 4-2 summarizes the distinct curves derived from the available literature and applied as different scenarios in this analysis, by structure and fill type. Results are presented in terms of cfs/ft to enable comparison to results from prior studies. There is deep uncertainty regarding which of the classes of curves is the most representative of actual fragility. In addition, while the MTTG Low fragility curves were calculated assuming a 305-meter (1,000-foot) characteristic length, it is not clear what characteristic length should be associated with the other curves.

CLARA v2.0 implements four new fragility scenarios, each with a different fragility curve. The MTTG Low scenario uses the curves from the MTTG study, introduced previously, to describe the fragility of each 305-meter (1,000-foot) long section of levee. The MTTG High scenario applies the unadjusted MTTG fragility curves with an assumed characteristic length of 305 meters (1,000 feet), consistent with the MTTG Low scenario. (As Figure 4-2 makes clear, this scenario still has higher probabilities of failure for equivalent flood rates.)

The IPET Low and IPET High scenarios use the same IPET-derived 2-D fragility curves with different assumed characteristic lengths of 305 and 152 meters (1,000 and 500 feet), respectively. Note that a shorter characteristic length subdivides levee reaches into a greater number of independent units, leading to a greater chance of failure for each reach. Comparison of results from the IPET Low and IPET High scenarios can help us better understand the sensitivity of the flood risk model to alternate assumptions about appropriate characteristic length given their uncertain and varying geotechnical characteristics.

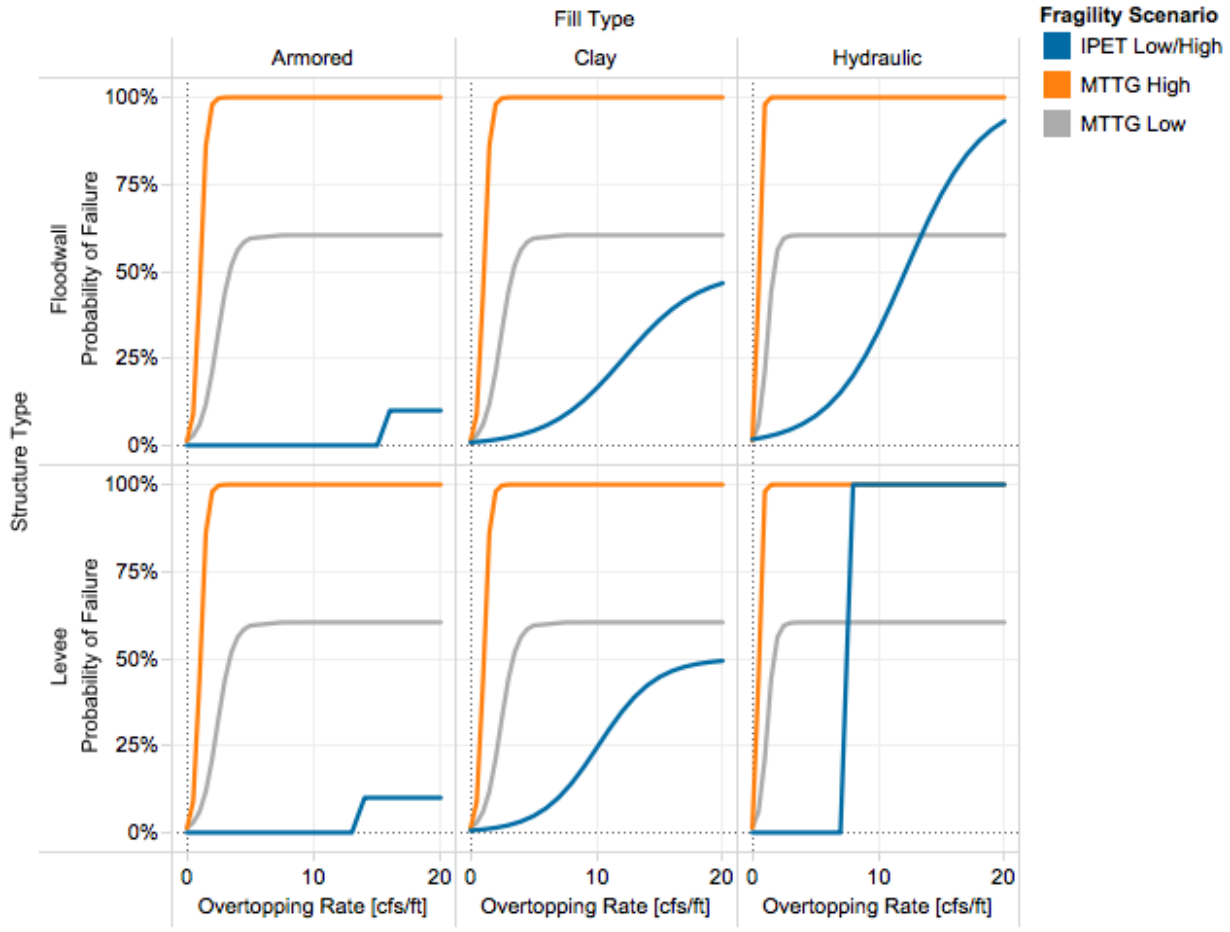

Note: the MTTG scenario uses the same fragility curves for both levees and floodwalls, while the IPET approach uses differing assumptions by structure type. MTTG also assumes that armored and clay fill levees have the same performance characteristics.

Figure 4-2: CLARA v2.0 2-D Erosion and Scour Fragility Curves by Fragility Scenario.

5.0 Parametric Uncertainty Assessment in CLARA

5.1 Overview and Motivation

CLARA v1.0 was originally designed to address uncertainty from key external factors such as sea level rise, land subsidence, and economic growth to assess plausible flood risk 50 years into the future. To estimate the performance of risk reduction projects with uncertainty, the model used a series of scenarios designed to span the range of plausible future conditions across drivers that could not be assigned believable likelihoods. Other than simulating system fragility, results calculated by the model were deterministic and resulted in point estimates for all output metrics.

The Science and Engineering Board (SEB) responsible for providing technical oversight to the 2012 Coastal Master Plan recommended that the systems models developed for coastal Louisiana provide for the estimation and propagation of parametric and model uncertainty. This was noted as particularly relevant for the integrated models used in the master plan analysis, in which outputs from one model are used as inputs to another. The SEB sought to better understand how well the "signal" of project effects could be detected through the "noise" of propagating uncertainty, an especially relevant concern for CLARA because the flood depth and damage calculations are among the final steps in the process.

With CLARA v1.0 as a foundation, the 2017 Coastal Master Plan model improvement process provided an opportunity to incorporate a variety of additional parametric and model uncertainties not previously addressed. This new framework provides multiple benefits. First, estimating uncertainty in model outputs, reported using statistical confidence intervals, brings the 2017 risk assessment more in line with standard methods for scientific investigation. Second, decomposing uncertainty into various component factors—such as DEM noise, statistical estimation of joint probability functions, and variability in overtopping rates—provides insight into the key drivers of uncertainty and may enable policy decisions to focus on targeting variables that matter the most. Finally, the new uncertainty approach allows CLARA to explicitly incorporate parametric uncertainty emerging from other systems models in the master plan analysis.

For example, the coastal landscape could vary greatly with different future conditions, and the landscape morphology estimates are subject to their own sets of uncertain parameters. This can be expressed as uncertainty in the land elevations that might be estimated in a given scenario. The propagation of land elevation uncertainty can be a major contributor to overall flood risk uncertainty (Tate, Muñoz, & Suchan, 2014). The physical systems models that feed into CLARA, including morphology, vegetation, and storm surge and waves, are used to estimate coastal flood depths. As a result, capturing uncertainty in the flood depth hazard experienced in a given location was given the highest priority when developing the parametric uncertainty framework for CLARA v2.0.

On the other hand, economic uncertainties, such as those related to the quantity and value of current structure inventories, are largely independent of the other systems models' outputs. Tate et al. (2014) conclude that these factors play a lesser role in total damage uncertainty than uncertainty propagated from estimates of flood hazard and landscape conditions. It is also likely that parametric uncertainty related to present-day structure inventories and valuation is much smaller in scale than the "deep" uncertainty related to future population and assets at risk 50 years from now currently addressed with scenario analysis. Further, adequately representing economic uncertainties requires higher-resolution data than was available when scoping model

improvements. In some cases, data was simply unavailable. For other uncertainties like depth-damage relationships, multiple estimates exist, but cannot be credibly combined within a parametric framework. As a result, assessing parametric and model uncertainty related to the flood hazard was deemed most critical for meeting the goals of the master plan process, and CLARA v2.0 does not specifically estimate parametric uncertainty related to assets at risk or depth-damage curves. The limitations related to economic uncertainties are discussed in more detail in Section 5.3.

This chapter divides potential sources of parametric uncertainty into flood depth and flood damage factors. The various sources of uncertainty are identified, along with a rationale for why each source was included or excluded from CLARA v2.0. For those sources addressed, implementation details are provided. Finally, each subsection concludes with a discussion of testing results or analysis of the source's importance in contributing to uncertainty in the model's flood risk estimates.

5.2 Flood Depth Uncertainty

CLARA's estimates of flood depths incorporate both aleatory and epistemic uncertainties (see the glossary included in this report for definitions of statistical terms). Uncertainty in CLARA is addressed through the use of three key approaches: 1) Monte Carlo simulation that impacts flooding on an individual-storm level, 2) resampling to generate confidence bounds around the exceedance curves summarizing the distribution of possible flood responses, and 3) scenarios designed to capture the variation due to deep uncertainty that impacts the flood response from all storms. Monte Carlo simulation is applied to estimate both aleatory and epistemic uncertainties at different points in the model. Resampling techniques and scenarios are used to characterize epistemic uncertainty.

Table 5-1 lists sources of uncertainty in estimates of coastal flood depths that are addressed by CLARA. Some of these sources have been addressed in prior publications; some will be described in detail in this document. Many of these sources of uncertainty are impossible to eliminate, but careful accounting can make model results more representative of the real world or inform future discussion.

Table 5-1: Sources of Flood Depth Uncertainty Addressed by CLARA.

Source of Uncertainty	Type of Uncertainty	CLARA Uncertainty Approach
Future state of the coastal landscape: sea level rise, subsidence, etc.	Deep	Scenario analysis
Future storm characteristics: changes to storm frequency, distribution of intensity, etc.	Deep	Scenario analysis
Variability in storm event characteristics	Aleatory	JPM-OS, parametric
Limited historical record of storms	Epistemic	Parametric, bootstrap sampling
Variability in surge and wave responses, given storm characteristics	Aleatory and Epistemic	JPM-OS, parametric

Source of Uncertainty	Type of Uncertainty	CLARA Uncertainty Approach
Limited observations of past surge and wave responses, given storm characteristics	Epistemic	Parametric
Impact of the chosen synthetic storm sample on exceedance estimates	Epistemic	*A posteriori* analysis
Impact of the chosen Monte Carlo and bootstrapping sample sizes on exceedance estimates	Epistemic	*A posteriori* analysis
Unknown geospatial correlations in surge and wave responses	Epistemic	Parametric, Monte Carlo simulation
Noise in ground elevation measurements	Epistemic	Parametric
Noise in input model (ADCIRC, UnSWAN) results	Aleatory	Parametric
Stochastic nature of levee and floodwall failure	Aleatory	Monte Carlo simulation
Incomplete understanding of levee and floodwall fragility	Epistemic	Scenario analysis
Variability in breach characteristics and failure consequences	Epistemic	Scenario analysis
Performance of pumping systems	Deep	Scenario analysis

In this chapter, how the uncertainties above are incorporated into CLARA are described, with a focus on those uncertainties not previously considered in CLARA v1.0 that are now addressed through parametric uncertainty analysis. Below, additional background about the methods used for incorporating these uncertainties into the model are provided below.

The CLARA model estimates flood depth exceedances: the probabilities of observing, in a given year, flood depths equal to or greater than estimated values (Fischbach et al., 2012a; Johnson et al., 2013). The exceedance values depend upon the relative likelihood of occurrence of different types of storms, which are estimated from the limited historical record of observed storm events. Because they are rare events, observed historical storms may not be representative of the true probability distribution of storm characteristics. To address this uncertainty, the bootstrap method is here applied to generate numerous samples containing different sets of storms, each of which is then used to separately estimate one or more exceedance probabilities. Specifically, bootstrap samples of observed historic storm events are used to analyze the uncertainty in estimates of storm probabilities associated with having a limited sample of observed storms in the historical record.

This section describes CLARA v2.0's approach for the implementation of parametric uncertainty analysis into flood depth estimates. As the methods and uncertainties differ by location type, separate descriptions are provided for flood depth estimates in unenclosed or enclosed areas, respectively.

5.2.1 Joint Probability Assessment and Flood Recurrence Statistics

5.2.1.1 Coastal Storm Characteristics

CLARA generates synthetic storms, simulates the flooding caused by these storms, and uses the resulting flood depths to estimate exceedance probabilities and other statistical measures of risk. Synthetic storms are defined by combinations of parameters, including: c_p, the minimum central pressure of the storm; R_{max}, the radius of maximum wind speeds; and the track angle θ_l, forward velocity, v_f, and location x (in degrees longitude) of the storm at the point of landfall. Landfall is defined by the point at which a storm's eye crosses 29.5 degrees North latitude (Resio, 2007). A summary of these parameters is provided in Table 5-2. The historical record of storms found in the National Oceanic and Atmospheric Administration's (NOAA) HURDAT database is used to obtain a historical record of the characteristics of observed storms making landfall near the study region (Hurricane Research Division, 2014).

Table 5-2: Summary of Modeled Storm Parameters.

c_p	*Central pressure*
R_{max}	*Radius of maximum wind speeds*
v_f	*Forward velocity*
θ_l	*Track angle at landfall (29.5° N)*
x	*Longitude at landfall (29.5° N)*

Flood depth exceedances are a measure of how likely it is that a location will experience a given level of flooding in any year. To estimate these values, three elements are needed: a way to predict the flood response associated with any given storm that may occur, a way to estimate the relative likelihood of a storm occurring with any given set of parameters, and an estimate of how frequently, on average, a storm might make landfall in the Louisiana coastal region.

The latter quantity is estimated by the frequency of observed storm events in the HURDAT data. The flood levels resulting from a storm are estimated using a response surface model, and the relative likelihoods of different storms are fit using historical data as described below.

5.2.1.2 Estimating Uncertainty in the Joint Probability Model

The Joint Probability Method with Optimal Sampling (JPM-OS) assumes that the marginal probability distribution of each storm parameter, Λ, conforms to a particular functional form (Resio, 2007). For example (see Equation 5-1), c_p is assumed to follow a Gumbel distribution with parameters a_0 and a_1 that depend on the landfall location x. The parameters of each distribution are estimated to maximize the likelihood of observing the historical record of storms identified from HURDAT. The fitted distributions are then used to assign probability masses to each synthetic storm run through CLARA. These probabilities indicate the relative likelihood of each synthetic storm's occurrence, and are used to calculate annual exceedance probabilities for quantities such as flood depths and damage.

$$\Lambda_1 = P(c_p|x) = \frac{\partial}{\partial x}\left\{\exp\left\{-\exp-\left[\frac{c_p - a_0(x)}{a_1(x)}\right]\right\}\right\} \quad (5\text{-}1)$$

Previous JPM-OS studies of Louisiana flood risk have fit the distributional parameters using a small, 22-storm "training set" of historical data. Statistical testing indicates that the fits are sensitive to additions or deletions to this sample. The training set did not, for example, include recent storms such as Hurricanes Gustav, Ike, or Isaac. As such, the flood depth AEP values calculated by CLARA are subject to uncertainty in the historical record.

To address this, bootstrapping is applied on the HURDAT data set. For each bootstrap sample, storms are sampled with replacement from the entire HURDAT database. These data contain many storms that did not make landfall in the Gulf of Mexico or were not sufficiently intense to be classified as hurricanes, so the resulting sample is then filtered to include only those storms which made landfall within 3 longitudinal degrees of the study region and had a central pressure less than or equal to 985 millibars (mb). As a result, each bootstrap sample may contain a different number of storms of interest.

It is assumed that the joint probability distribution of a storm's landfall point, landfall angle, maximum central pressure deficit, radius of maximum winds, and forward velocity are structurally of the same form used in the JPM-OS methodology. All storms of interest in a single bootstrap sample are used to fit the parameters of each marginal distribution. Probability masses are then assigned to each synthetic storm by partitioning the joint probability space of storm parameters in the same manner as previous CLARA versions (Johnson et al., 2013).

This procedure results in distinct sets of probabilities being assigned to every synthetic storm for each bootstrap sample. Annual exceedance probabilities are then calculated using the probability masses associated with each bootstrap sample. The resulting variation in AEP values over the bootstrap samples is used to produce median estimates and confidence bounds for each return period.

In some bootstrap samples, the number of storms of interest may be so small as to render the joint probability distribution impossible to fit. To avoid this problem, CLARA oversamples: instead of each bootstrap sample containing the same number of storms as the original HURDAT data set, nine times as many storms are sampled with replacement[22]. As in many statistical applications, a larger sample generally produces less uncertainty. Because the larger sample is artificial—it does not correspond to the actual sample size of the historical record—applying a statistically consistent adjustment to the confidence bounds estimated around each exceedance is used to compensate, as described by Chung and Lee (2001). More details on the estimation procedure and this adjustment are provided in later sections, since the confidence bounds incorporate Monte Carlo sampling in addition to the bootstrapping of the historical record.

5.2.1.3 Training Storm Selection

Alongside the joint probability model, a response surface model is needed to predict the surge and wave response of each synthetic storm. The model specification of the response surface itself is described in Section 5.2.2.1, but the corpus of storms used to fit the model is also an

[22] Experimentation showed that a factor of nine was sufficient to render it extremely unlikely that a bootstrap sample would produce an unidentifiable or pathological model fit.

important modeling choice. The training storms run through the ADCIRC and UnSWAN models can have a significant impact on the estimated response uncertainty. If storms with sufficient variation in the model fit parameters are not provided, or if too few storms wet a point, the model may be unidentifiable. The estimated coefficients will be more sensitive to outliers in the ADCIRC and UnSWAN model surge and wave values. Also, the estimated standard error associated with the predicted responses scales approximately as $1/\sqrt{n}$, where n is the number of storms used in the model fit.

Ideally, the flood model would be run with as large a storm set as possible. Resource constraints on computer memory and computation time, however, dictate that a set smaller than the total number of 446 available storms will be used for the production phase of the 2017 Coastal Master Plan study. The challenge, then, is to identify subsets of the full storm suite that, for a given subset size, produce unbiased estimates of flood risk and minimize the uncertainty associated with those estimates. Bias would result, for example, from adopting a training set consisting only of very slow-moving storms. Likewise, training sets with a limited range of values for central pressure and radius would produce a larger degree of uncertainty because the response surface would consist of more extrapolated estimates of surge elevations.

The choice of training set used to produce the synthetic storm suite represents a potentially significant uncertainty. Section 6.5 outlines the series of tests that were performed to evaluate the importance of storm selection, and the results of the analysis are provided in Section 6.5.

5.2.2 Flood Depths in Unenclosed Areas

In unenclosed locations, CLARA calculates the flood depths resulting from each individual synthetic storm as the sum of surge elevations and free wave crest heights, minus the ground elevation (relative to the NAVD88 datum). CLARA v2.0 accounts for uncertainty in estimated flood depths for each synthetic storm from three primary factors: 1) noise in the ADCIRC and UnSWAN models, 2) uncertainty in the response surface fits used to create synthetic storms from the training storms, and 3) noise in the DEM used to identify ground elevations. For testing purposes, the first and third factors were assumed to take constant values for all points and storms; later sections describe how they are integrated with uncertainty in the response surface model. The flood depth calculation steps for unenclosed areas are summarized in Table 5-3.

Table 5-3: Summary of Calculation Steps and Uncertainties in Unenclosed Areas.

Model Step	Individual Storms or Aggregate	Uncertainty Addressed	Method
Fit response surface	Aggregate		Regression model(s)
Predict surge elevations and wave heights	Individual	Storm behavior	Monte Carlo sampling
Calculate additional uncertainty	Individual	ADCIRC, UnSWAN noise	Propagation of uncertainty
Convert predicted flood elevations to flood depths	Individual	DEM noise	Monte Carlo sampling
Calculate synthetic storm probabilities	Aggregate		JPM-OS
Calculate flood depth exceedances	Aggregate	Small historic record	Bootstrap sampling

5.2.2.1 Response Surface Model for Surge Elevations and Wave Heights

CLARA v2.0's response surface model improves upon the previous, JPM-OS-based procedure in two ways: 1) by incorporating surge response from nearby points to increase the effective sample size used when fitting a point, and 2) by adding other geospatial covariates that relate the position of a point to the storm track.

In the 2012 Coastal Master Plan analysis, the predicted surge response at each point for a given synthetic storm was fit—using a training set of 40 storms run through ADCIRC and UnSWAN—as a function of central pressure, radius of maximum winds, and landfall track. The new response surface also incorporates landfall angle and forward velocity, the other two primary storm parameters in the JPM-OS joint probability function.

Geospatial covariates include the distance between a point and the point where a storm makes landfall (i.e., where it crosses 29.5 degrees North latitude). Linear, quadratic, and cubic powers of the distance from landfall are used. The model also controls for the azimuthal angle between the storm track and the point; see Figure 5-1 for an illustration of the azimuthal angle formed between a hypothetical storm track and the city of Thibodaux. Because the counter-clockwise rotation of tropical storms impacts the storm surge in different quadrants relative to the track, the model controls for $\sin(\theta_{az})$, where $\theta_{az} = 0$ for points 180 degrees clockwise from the storm track, and θ_{az} increases counter-clockwise. For example, if a storm is moving due north, then a point due east from the landfall point would have $\theta_{az} = \pi/2$ and $\sin(\theta_{az}) = 1$. A point due north from the landfall point would have $\theta_{az} = \pi$ and $\sin(\theta_{az}) = 0$.

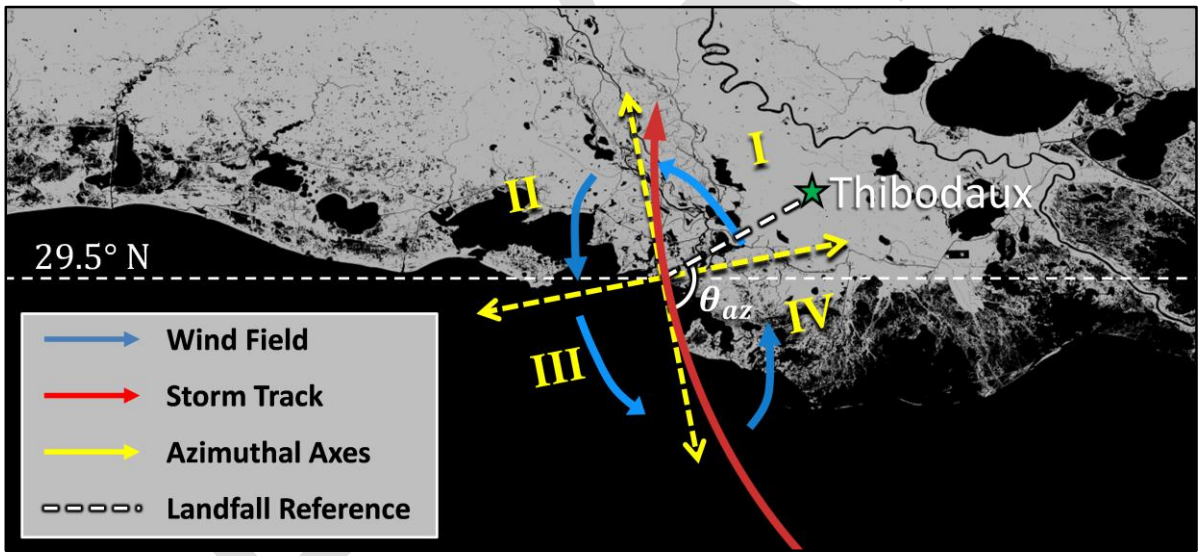

Figure 5-1: Illustration of Storm Wind Fields by Quadrant and Azimuthal Landfall Angle.

In CLARA v1.1, response surfaces were fit separately for each storm track. By contrast, the use of geospatial covariates in CLARA v2.0 allows us to fit a surface using data from all training storms simultaneously.

Model fitting is performed using conditional parametric locally-weighted regression (CPARLWR)(Cleveland & Devlin, 1988). This estimates a model of the form:

$$y = X\beta(z) + u \tag{5-2}$$

where y is the dependent variable of interest (here, surge elevations or wave heights), X is a vector of explanatory variables, z is a vector of spatial coordinates (latitude and longitude), β is a vector of coefficients, and u is a normally distributed residual term. As shown, the impact of the explanatory variables, β, is a function of a point's geographic location.

Further, the model is fit at each geographic point only using local points in the neighborhood of the fit point. Acknowledging that nearby points may display very different hydrodynamic behavior—because of the presence of floodwalls, elevated roads, or other weir features—points are only fit using neighboring points within a hydrodynamically similar region referred to as a watershed. CLARA's watershed boundaries were established using a shape file of the weir lines used by ARCADIS in their ADCIRC mesh (see Appendix 1). For sample size considerations, some small ADCIRC regions with low-lying weirs were joined together; in other cases, alternately, large ADCIRC regions were split apart into multiple watersheds. Figure 5-2 shows the CLARA v2.0 watersheds superimposed on the study region.

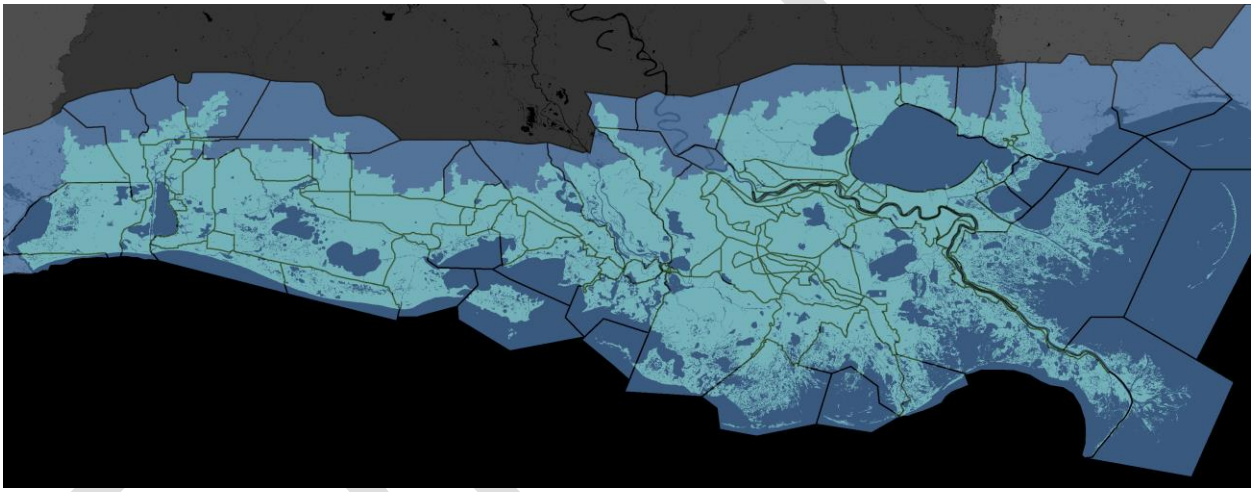

Note: Lines indicate watershed boundaries. Blue underlay shows model domain extent (Louisiana only).

Figure 5-2: CLARA v2.0 Watershed Boundaries.

A weight is applied to each point in the neighborhood according to a kernel weighting function $K(d/h)$, where d is the distance from the fit point to the neighboring point (calculated using a great circle formula) and h is a bandwidth parameter that determines how quickly the weights fall off with distance. The neighborhood of points available for fitting is restricted to all points within the same watershed. Depending on the number of points in a watershed, the model tries different values of h and attempts to identify an approximately optimal bandwidth by minimizing a cross-validation measure.

The model only fits using storms that produce wetting, meaning that the ADCIRC model produces some flood estimate (versus a null value). In some cases, very few storms wet a point, in which case the model fit cannot be identified due to the small sample size compared with the number of covariates to estimate. When this happens, CLARA then attempts to fit the response surface using a reduced-form model that does not include the geospatial covariates. Failing

that, a reduced-form model is attempted only with data at the specified point, and finally, only with data from storms on the same track.

If all of these models are not identifiable, then a stepwise procedure is used to predict the surge or wave response. This algorithm searches each combination of track and angle, looking for storms that wet a point. For any storm that does, the model assigns the same response value to any synthetic storm which is more extreme than the storm that wets. "More extreme" is defined by having a greater central pressure deficit, a larger radius, or a slower forward velocity. In practice, this backup procedure rarely produces new wetting storms, as there are very few cases in which a more extreme storm, using this definition, does not wet when a less severe storm does. It is primarily used for assigning response values to synthetic storms which are not a part of the training storm set. Table 5-4 provides a summary of the procedures attempted by the response surface model to fit surge elevations, s, and wave heights, w. The term s_i, w_i indicates that both surge elevations and wave heights are fit as a function of the same variables.

Table 5-4: CLARA v2.0 Response Surface Model Fit Priorities.

1. CPARLWR with full model specification:
$$s_i, w_i = \beta_0 + \beta_1 c_p + \beta_2 r_{max} + \beta_3 v_f + \beta_4 d_{il}^3 + \beta_5 d_{il}^2 + \beta_6 d_{il} + \beta_7 \theta_{il} + \beta_8 \sin \varphi_{il} + \beta_9 x + \varepsilon_i$$
a. Search for h minimizing a cross-validation measure

2. Point-by-point ordinary least squares regression with full model specification

3. Point-by-point ordinary least squares regression with reduced-form model:
$$s_i, w_i = \beta_0 + \beta_1 c_p + \beta_2 r_{max} + \beta_3 v_f + \beta_4 d_{il} + \beta_5 \sin \varphi_{il} + \varepsilon_i$$

4. Point- and track-level ordinary least squares regression with reduced-form model:
$$s_{i,x,\theta}, w_{i,x,\theta} = \beta_0 + \beta_1 c_p + \beta_2 r_{max} + \beta_3 v_f + \varepsilon_i$$

5. Step function assigning equal surge elevation and wave heights to any synthetic storms more extreme than wetting storms from training set

The predicted response values used for any given synthetic storm are the predicted values generated by the model fitting procedure. Even in cases where a synthetic storm's characteristics are identical to a storm in the training set, the predicted response is used rather than the training response to ensure consistency and avoid introducing bias. When one of the regression model fits is successful, standard error is estimated as the square root of the residual sum of squares. For lack of a basis on which to estimate it, no standard error is assigned under the stepwise procedure. Uncertainty does exist in this case, but the stepwise procedure is typically only applied at inland points which do not flood except under very extreme circumstances. As such, any uncertainty in the surge and wave response associated with storms modeled using the stepwise method likely makes only a small contribution to the overall uncertainty in the exceedances estimated at these points.

5.2.2.2 Converting Elevations to Depths

Surge elevations and wave heights are both fit under the assumption that errors are normally distributed. It is assumed that noise in the DEM is normally distributed; the standard error associated with a DEM measurement is also assumed to be 0.185 m (0.61 ft) (USACE, 2009b), but this can be changed to reflect more precise, updated LIDAR data, geospatial variation

according to land use type, or greater variance emerging from the Integrated Compartment Model (ICM) estimates of future landscape elevation as deemed appropriate for the 2017 Coastal Master Plan analysis.

For the preliminary testing analysis described in this document, a standard error of 0.15m (0.5 ft) was assumed for the combined effect of ADCIRC and UnSWAN noise based on initial guidance from ARCADIS (Cobell, 2013). Based on the most recent ADCIRC-UnSWAN model validation results, however, this error will be increased to 0.36m (1.2 ft) for the 2017 analysis (see Appendix 1). A separate analysis was also performed to better inform this parameter, and determine whether other uncertain factors not necessarily represented in the validation results suggest further increasing the assumed error for the 2017 Coastal Master Plan study (see Section 6.2).

The variance of the sum of normally-distributed random variables is the sum of their variances. This rule is directly applied to calculate the variance in the sum of surge elevations and wave heights (Equation 5-3). It is applied again to calculate the variance in the estimated flood depth, which includes contributions from the noise associated with the ADCIRC simulations and measurement error in the DEM values. The mean flood depth is calculated by subtracting the ground elevation from the sum of surge elevation and wave height (Equation 5-4). Although depths are non-negative by definition, this value is allowed to be negative when calculating the distribution of flood depths around the mean value (and associated quantities like confidence bounds).

$$s_{total}^2 = s_{surge\ response}^2 + s_{wave\ response}^2 + s_{ADCIRC}^2 + s_{DEM}^2 \quad (5\text{-}3)$$

$$d_f = \max\{surge + wave - elevation_{DEM}, 0\} \quad (5\text{-}4)$$

5.2.2.3 Resampling Schemes

Once flood depths have been estimated for each synthetic storm, they must be aggregated statistically in order to estimate flood depth exceedances at any return period of interest. An exceedance curve with many different AEP estimates, tracing out the "tail" of the flood risk distribution by estimating multiple points on the flood depth cumulative distribution function, is constructed at each geographic point using a single flood depth value and a single probability weight for each synthetic storm. However, the response surface model generates a probability distribution for flood depths, rather than a single value. The probability weights associated with each storm are determined by the joint probability distribution function of storm parameters (as developed in the JPM-OS methodology), and these, too, are uncertain.

These uncertainties are exploited to generate confidence bounds around any given return period value by resampling from its estimated distribution. Flood depths are sampled directly using the unconstrained (i.e., possibly negative) mean flood depth and standard error estimated by the response surface model. Once flood depths are sampled for calculating exceedances, negative values are replaced by zeroes. Thus, flood depths are treated as truncated normal random variables with some probability mass at zero.

Synthetic storm probability weights are sampled indirectly by bootstrapping from the observed historical record of storms, as described in Section 5.2.1. A single bootstrap sample is generated by sampling storms from the HURDAT data set with replacement. Probability masses are then assigned to each synthetic storm by partitioning the joint probability space of storm parameters in the same manner done by CLARA v1.0 (Fischbach et al., 2012a). CLARA v2.0 accounts for uncertainty associated with individual storm flood responses by generating Monte Carlo samples

from the estimated flood depth distributions associated with each synthetic storm. Uncertainty in the relative likelihood of each synthetic storm is addressed by fitting a joint probability function to each bootstrap sample. An exceedance curve is calculated for each combination of Monte Carlo and bootstrap sample, and confidence bounds around specified flood depth exceedances are produced by extracting the 10th and 90th percentile values of the empirical distribution of exceedances over the full sample. The point estimates reported in the Results chapter are the median values generated over the sampling scheme. Full details of this procedure are described in Section 5.2.4.

5.2.3 Flooding in Enclosed Areas

Due to the additional complexity introduced when flooding is simulated in enclosed areas, estimates of flood depth exceedances are subject to additional uncertainties. In addition to uncertainty in the response surface estimates of surge and wave heights, DEM noise, and uncertain probability weights assigned to each synthetic storm, CLARA v2.0 also addresses two other key sources of uncertainty: 1) uncertainty in the overtopping rates resulting from given surge and wave levels, and 2) uncertainty due to limited observed data and scientific knowledge regarding the likelihood of protection system failures. Table 5-5 summarizes the steps taken to estimate flood depth exceedances in enclosed areas, along with the uncertainties incorporated into each step.

As noted previously, the actual probabilities of system breaches—as a function of water levels and protection system characteristics—are deeply uncertain. Accordingly, five scenarios were developed for use in the 2017 Coastal Master Plan analysis: one in which systems do not fail, and four which utilize different forms for the fragility curves that govern breaching probabilities (see Section 4.3). What follows describes how the remaining parametric uncertainty is addressed within a given fragility scenario.

The previous version of CLARA uses a Monte Carlo simulation of system breaches to develop an empirical frequency distribution of flood elevations that account for the possibility of multiple points of failure. CLARA v2.0 further improves on this approach by incorporating uncertainty in overtopping rates into this simulation. Additionally, the model estimates the degree of uncertainty in the surge and wave levels that impact protection systems.

Table 5-5: Summary of Calculation Steps and Flood Depth Uncertainties in Enclosed Areas.

Calculation Step	Individual Storms or Aggregate	Uncertainty Addressed	Method
Fit response surface at surge and wave points (SWPs)	Aggregate		Regression model(s)
Predict surge and wave behavior	Individual	Storm behavior	Markov chain analysis, Monte Carlo sampling
Calculate additional uncertainty	Individual	ADCIRC, UnSWAN noise	Propagation of uncertainty
Estimate overtopping volumes	Individual	Overtopping water	Monte Carlo sampling
Simulate system breaches	Individual	System fragility	Monte Carlo sampling
Calculate breach volumes	Individual	Weir flows, characteristic length	Monte Carlo sampling
Distribute flood waters between Base Hydrologic Units (BHUs)[23]	Individual		Interior drainage module
Convert flood elevations to flood depths	Individual	DEM noise	Monte Carlo sampling
Calculate synthetic storm probabilities	Aggregate		JPM-OS
Calculate flood elevation exceedances	Aggregate	Small historic record	Bootstrap sampling

5.2.3.1 Exterior Surge and Wave Conditions

As described previously, surge elevations and peak wave heights at each point along the system boundary are modeled using a normal distribution, truncated below zero depth, with a standard deviation determined by 1) assumed noise in the ADCIRC and UnSWAN models, 2) measurement error in the DEM, and 3) uncertainty in the fit of the response surface model.

One way to address this variation in surge and wave levels would be to incorporate it into the Monte Carlo analysis. This poses several problems:

1. Breaching behavior, which represents aleatory uncertainty through a stochastic sampling process, can be radically different as surge and wave levels vary, and this might substantially increase the number of replications required for convergence (i.e., the number required to produce stable results if the simulation were repeated multiple times). The computational demands of the flood depth module make this infeasible without substantially greater computing resources.

[23] A base hydrologic unit (BHU) is the basic spatial unit of analysis in CLARA to determine final peak flood elevations in enclosed areas.

2. In unenclosed areas, surge and wave uncertainty manifests in the confidence bounds around flood depth exceedances. It is desirable for these factors to be included in the same manner in enclosed areas.

To address the effect of exterior surge and wave uncertainty on enclosed areas, CLARA v2.0 instead uses a similar approach to that used in unenclosed areas. For each synthetic storm, surge and wave levels on the boundaries of ring levee systems are resampled as part of the process of generating confidence bounds around exceedances. However, applying this process to interior flood depths introduces two complexities:

1. Flood waters on the system interior can originate from many places on the system boundary, because of the complexities of interior drainage between polders. There is not a one-to-one relationship between interior flooding and surge levels at all points on the system boundary. When sampling boundary conditions, then, CLARA should account for geospatial correlations between the surge and wave levels.

2. Every new sample of distinct boundary surge and wave levels must be run through the flood depth module (including the Monte Carlo simulation of overtopping and breaching). Computing resources thus demand that the number of samples be minimized.

5.2.3.2 Identifying Representative Variations

For each synthetic storm, CLARA v2.0 limits computational demands by developing a small set of "representative variations" that vary in their boundary surge and wave levels rather than directly sampling via Monte Carlo. The flood depth module is run for each variation, and the resampling procedure later draws the results from a lookup table.

Choosing the appropriate variations and their sampling weights is challenging. The spatial variation in surge and wave noise is not likely to be perfectly correlated, such that the 10th percentile of interior flooding could be found by running through the flood depth module a "surface" consisting of the 10th percentile of surge and waves everywhere along the system boundary. Instead, the model might underestimate water elevations outside the levees in some areas and overestimate it in others.

It is assumed that the boundary noise will typically be locally correlated, however. The probability distribution of surge and wave levels on the boundary was estimated in a previous step. Using this information, the distribution at each reach point is partitioned into a small number of bins. The surge values associated with each bin are defined as the value in the surge cumulative distribution function at the point midway between the bin's endpoints. For example, if five equally-sized bins are used, then the surge values for each bin would come from the 10th, 30th, 50th, 70th, and 90th percentile values of the estimated distribution. Values for wave heights are calculated and used in a similar manner.

Reach points are grouped into segments along the system boundary for this portion of the uncertainty analysis. The segments are generally defined as contiguous lengths of the protection system that are oriented in the same compass direction against oncoming surge. The segments defined for the Greater New Orleans Hurricane and Storm Damage Risk Reduction System (HSDRRS), for example, are shown in Figure 5-3.

For each segment, it is assumed that the surge at all reach points in the segment come from the same bin of their respective surge distributions—that is, all points within a segment are assumed

to be correlated and draw the same surge percentile. The bin assigned to each segment is determined by reconceiving the segments around each subsystem as links as a Markov chain[24]. The quantile bins form the state space. Transitions from one bin to another are only permitted between neighboring bins, and transition probabilities are chosen to produce a stationary distribution equal to the bin probabilities.

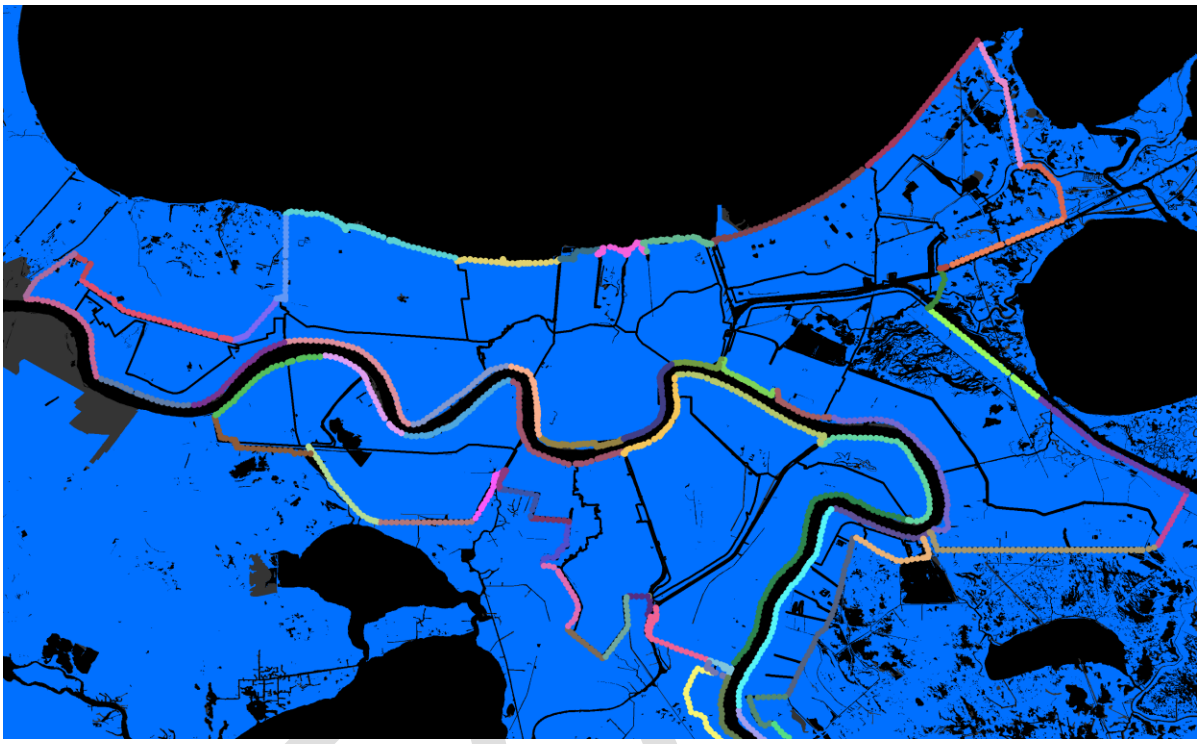

Figure 5-3: Greater New Orleans HSDRRS, as Divided into Segments.

For example, suppose the boundary surge distributions were divided into 3 bins, with the central bin representing 60 percent of the distribution, and the outer bins each having weights of 20 percent. If reach point A is assigned the surge value from its first bin, then adjacent reach point B can be assigned the value from its first or second bin, but not the third. The probability of being assigned the first bin is $20/(20+60) = 0.25$, and the probability of being assigned the second bin is $60/(20+60) = 0.75$.

Once the surge and wave values are determined for each reach point on the system boundary, the total volume of water entering the system via overtopping is calculated, but the fragility and interior drainage routines are not run. This process is repeated, generating thousands of Markov chains and producing a frequency distribution of total overtopping volumes. Chains that produce specified fractiles of total overtopping volume within each subsystem are chosen as the representative variations. This procedure is designed as a first-order way of approximating

[24] A Markov chain is a sequence of random variables in which the probability distribution and value of the next item in the sequence depends only on the current value of the system and not on the sequence of past values. A Markov chain system is defined by the set of valid states of the system, a transition matrix defining the probabilities of transitioning from one state to another, and an initial state of the system.

the uncertainty associated with surge and wave levels without dramatically increasing model runtimes by re-running fragility and interior drainage each time.

CLARA v2.0 generates surge Markov chains using five equally-weighted bins. The representative variations used are Markov chains which produce the 10th, 25th, 50th, 75th, and 90th percentile of overtopping volumes over a sample of 10,000 Markov chains. Each representative variation is run through the CLARA flood depth module; the resulting flood depths are resampled (as detailed in Section 5.2.3.5) as one of the uncertainties used to generate confidence bounds around exceedance estimates.

The net effect of this procedure is to produce a small number of variations of each storm that have locally correlated surge elevations. Further research is necessary to use empirical data to study the actual correlation structure. This research would allow us to adjust the transition matrices of the Markov chains to result in a stationary distribution consistent with the estimated geospatial correlations.

5.2.3.3 Overtopping Rates

USACE's LACPR analysis used the van der Meer overtopping equations to determine overtopping rates. Variability in overtopping rates was modeled by assuming that specific coefficients in the equations are uncertain and normally distributed (USACE, 2009c, p.46; van der Meer, 2002).

CLARA v2.0 adopts the same approach. The three coefficients varied by LACPR are treated as random variables with the same means and standard deviations used by LACPR (see Figure 5-4) and this variation is incorporated into the Monte Carlo simulation of each synthetic storm. In each replication, these parameters are assigned values by random draws from their assumed distributions, and the ensuing overtopping rate is then calculated. Parameter values are generated at every reach point along the exterior of ring levee systems, assuming spatial independence. Some spatial correlation likely exists, but addressing it would impose additional computational complexity; the total volume of water overtopping at each reach point will exhibit some correlation naturally because of the Markov chain methods used to address correlation in surge and wave levels. Future empirical studies could be used to calibrate the transition matrix used in the Markov chain procedure to emulate correlation in both the surge levels and the resulting overtopping volumes.

For the purpose of LACPR, the Van der Meer equations have been adopted to compute overtopping rates for levee sections. The overtopping formulations from Van der Meer are (see TAW document):

$$\frac{q}{\sqrt{gH_{m0}^3}} = \frac{0.067}{\sqrt{\tan\alpha}}\gamma_b\xi_0 \exp\left(-4.75\frac{R_c}{H_{m0}}\frac{1}{\xi_0\gamma_b\gamma_f\gamma_\beta\gamma_v}\right)$$

$$with \quad \max imum: \quad \frac{q}{\sqrt{gH_{m0}^3}} = 0.2\exp\left(-2.6\frac{R_c}{H_{m0}}\frac{1}{\gamma_f\gamma_\beta}\right) \qquad (1)$$

With:
q : overtopping rate [cfs/ft]
g : gravitational acceleration [ft/s^2]
H_{m0} : wave height at toe of the structure [ft]
ξ_0: surf similarity parameter [-]
α : slope [-]
R_c : freeboard [ft]
γ : coefficient for presence of berm (b), friction (f), wave incidence (β), vertical wall (v)

The coefficients -4.75 and -2.6 in Eq. 1 are the mean values. The standard deviations of these coefficients are equal to 0.5 and 0.35, respectively and these errors are normally distributed (see TAW document).

Eq. 1 is valid for $\xi_0 < 5$ and slopes steeper than 1:8. For values of $\xi_0 > 7$ the following equation is proposed for the overtopping rate:

$$\frac{q}{\sqrt{gH_{m0}^3}} = 10^{-0.92}\exp\left(-\frac{R_c}{\gamma_f\gamma_\beta H_{m0}(0.33+0.022\xi_0)}\right) \qquad (2)$$

The overtopping rates for the range $5 < \xi_0 < 7$ are obtained by linear interpolation of eq. 1 and 2 using the logarithmic value of the overtopping rates. For slopes between 1:8 and 1:15, the solution should be found by iteration. If the slope is less than 1:15, it should be considered as a berm or a foreshore depending on the length of the section compared to the deep water wave length. The coefficients -0.92 is the mean value. The standard deviation of this coefficient is equal to 0.24 and the error is normally distributed (see TAW document).

Source: (USACE, 2009c, p.46)

Figure 5-4: Van der Meer Overtopping Equations and Random Coefficients Used by LACPR.

5.2.3.4 System Failure and Breaches

The probabilities of failure at each reach point, and the consequences of breaching, are determined by the fragility scenarios described in Section 4.0. Breaches are simulated using random draws for each replication of the Monte Carlo simulation, and the consequent flood depths are calculated using the same approach as in CLARA v1.1. Breaches and overtopping rates are simulated simultaneously in a single-stage Monte Carlo design. This is intentional, as the two processes are intimately related. Because CLARA v2.0 calculates the probability of a breach as a function of overtopping rates, it makes sense to calculate peak overtopping rates and estimate the resulting probabilities of failure for each replicate, and then take random draws from those distributions to simulate breaches. However, including both uncertainties in the same Monte Carlo simulation procedure implies that a larger number of replicates may be

necessary for convergence of the calculated frequency distribution of flood elevations. This is explored as part of the specification testing described in Section 6.0.

5.2.3.5 Resampling Schemes

Exceedance curves define the probability of observing flood depths that meet or exceed specific values in any given year. CLARA constructs these curves empirically by combining the flood depths caused by each synthetic storm with a probability mass associated with each synthetic storm. Flood levels are calculated using CLARA's response surface in unenclosed areas, and the flood depth module in enclosed areas. Probability masses are determined by fitting the characteristics of storms from the observed historical record to a joint probability distribution (in accordance with JPM-OS). Scenario assumptions regarding potential changes to future storm frequency or intensity are compared with the historical record and also modify these probability weights when projecting future conditions.

When modeling system fragility, CLARA v1.1 complicates this procedure by producing a probability distribution of flood depths rather than a single value for each synthetic storm. In CLARA v2.0, this probability distribution is still generated, but now incorporates variability in overtopping rates in addition to the uncertainty associated with breaching consequences.

As in unenclosed areas, CLARA v2.0 incorporates both Monte Carlo simulation and bootstrap sampling to generate confidence bounds around the exceedance values at each return period. The historical record of observed storms is boostrapped to generate the probability weights associated with each synthetic storm. The flood elevations produced by each synthetic storm's representative variations are sampled according to the sampling weights assigned to each variation. To complete the process, exceedance curves are generated for each combination of bootstrap sample and Monte Carlo replicate.

5.2.4 Integrated Flood Depth Uncertainty Calculations

In both unenclosed and enclosed areas, CLARA v2.0 produces a set of exceedance curves from a full factorial combination of Monte Carlo replicates, elevation or depth values, and bootstrap samples of the relative likelihoods of each synthetic storm. To avoid samples in which the joint probability function cannot be fit, the number of storms from the historical record is oversampled by a factor of nine. This requires a post-hoc adjustment to the resulting confidence bounds to account for this oversampling. The method described by Chung and Lee (2001) is applied, but in a modified form because of the additional complexity of integrating bootstrap sampling with the Monte Carlo sampling.

Denote the y-year exceedance calculated for Monte Carlo replicate i and bootstrap sample j as $\hat{\theta}_{ij}^{y}$. Assume that the historical record contains n storms and that each bootstrap sample contains m storms. (In CLARA v2.0, $m = 9n$.) Denote the exceedance associated with Monte Carlo replicate i and the historical record of storms as $\theta_{h,i}^{y}$. Let the β-quantile value of $\hat{\theta}_{ij}^{y}$ over all bootstrap samples be $\hat{\mu}_{\beta,i}$.

Then a standard α-level confidence interval for θ^{y} in the case where $m = n$ is

$$\left[\hat{\mu}_{\frac{1-\alpha}{2},i}, \hat{\mu}_{\frac{1+\alpha}{2},i}\right] = \left[\hat{\theta}_{h,i}^{y} + \left(\hat{\mu}_{\frac{1-\alpha}{2},i} - \hat{\theta}_{h,i}^{y}\right), \hat{\theta}_{h,i}^{y} + \left(\hat{\mu}_{\frac{1-\alpha}{2},i} - \hat{\theta}_{h,i}^{y}\right)\right] \quad (5\text{-}5)$$

By Chung and Lee(2001), a α confidence interval adjusted for oversampling is

$$\left[\hat{\theta}_{h,i}^{y} + \sqrt{\frac{m}{n}}\left(\hat{\mu}_{\frac{1-\alpha}{2},i} - \hat{\theta}_{h,i}^{y}\right), \hat{\theta}_{h,i}^{y} + \sqrt{\frac{m}{n}}\left(\hat{\mu}_{\frac{1-\alpha}{2},i} - \hat{\theta}_{h,i}^{y}\right)\right] \quad (5\text{-}6)$$

Therefore, an order-preserving transformation of $\hat{\theta}_{ij}^{y}$ is made for every Monte Carlo replicate and bootstrap sample:

$$\gamma_{ij}^{y} = \hat{\theta}_{h,i}^{y} + \sqrt{m/n}\left(\hat{\theta}_{ij}^{y} - \hat{\theta}_{h,i}^{y}\right) \quad (5\text{-}7)$$

With this adjusted test statistic, the empirical $(1-\alpha)/2$ and $(1+\alpha)/2$ quantile values of γ_{ij}^{y} can now be used to form confidence bounds for θ^{y}.

Additionally, the decomposed variance of θ^{y} can be estimated by calculating the sample means of $\hat{V}\left(\gamma_{ij}^{y}\right)$ separately over the Monte Carlo replicates or over the bootstrap samples.

The above procedure is applied to flood depth exceedances in unenclosed areas and BHU flood elevation exceedances in enclosed areas, respectively. To convert the latter to flood depth exceedances by grid point, the flood elevation confidence bounds are used to estimate an implied variance around each exceedance, under an assumption of normality (testing has indicated that this is a reasonable assumption). That variance is summed with the assumed variance of DEM noise to estimate the total variance associated with interior flood depth estimates.

5.2.5 Sources of Flood Depth Uncertainty Not Considered

The development of CLARA v2.0 represents a significant step forward in the use of uncertainty analysis in flood risk modeling. It incorporates a variety of statistical methods to produce confidence bounds around flood depth exceedances that account for a wider range of environmental, physical, technological, and statistical uncertainties than any prior study known to us.

Despite this, many important uncertainties remain outside of CLARA's scope. Some of these are structural (model) uncertainties that run counter to the model's design philosophy, or cannot be addressed given current computational limits. One example of this is the impact of CLARA's simplified interior drainage model that ignores the time dynamics of routing water between polders. In order to quickly run many scenarios and hundreds or thousands of synthetic storms, CLARA was purposefully not designed as a hydrodynamic model. Related uncertainties, like the time in the surge hydrograph at which breaches occur, are also not explicitly analyzed.

CLARA also focuses primarily on flood depths from storm surge and waves, and the new version of the model does not capture uncertainty in the coupling between tropical storms and rainfall. Rainfall is modeled in the same manner as in CLARA v1.0, which produces point estimates for rainfall volumes by polder in enclosed systems.

The joint probability model has uncertainty beyond that which is captured by the bootstrapping procedure, which is designed to address uncertainty in the joint distribution of hurricane parameters. Further study is necessary to adequately understand the potential bias associated with estimates, even bootstrapped estimates, based on a small set of observed historical events.

Each bootstrap sample results in a different fit of the joint distribution, producing different estimates of the probability weights assigned to each synthetic storm. However, the short historical record provides a small number of storms from which to sample. If, by coincidence, the historical record is not representative of the underlying distribution of storm characteristics, then bootstrapping from this skewed sample may still produce skewed results.

This poses less of a problem in theory than it does in practice, because CLARA is currently restricted to running a limited set of 446 available JPM-OS storm simulations. Recent storms, such as Hurricane Isaac, reinforce the possibility of storms with parameters and behavior outside of the range of characteristics embedded in the JPM-OS storm model. This suggests that not only is there additional uncertainty in the joint probability fits, but also that the limited set of available may not be representative of the range of possible storm events. If so, the existing set of idealized synthetic storms may not produce statistically unbiased exceedance estimates.

Testing during the 2012 Coastal Master Plan process indicated that the probability of levee failures due to seepage or slope instabilities is generally much smaller than the probability of failure through overtopping and scour. As such, uncertainty in the estimated factors of safety and critical exit gradient values affecting these failure modes was ignored.

In other cases, CLARA simplifies certain aspects of flood behavior to a degree which may result in bias. For example, the model does account for uncertainty in ground elevations (DEM), but in reality, errors in ground elevations also imply errors in the interior stage-storage curves and interflow elevations. These factors are not modified in the flood model to assess their impact because of the computational complexity required to do so.

5.3 Damage Estimation Uncertainty

In CLARA v2.0, probabilistic uncertainty from the flood depth estimates, including uncertainty associated with the ground elevation at each grid point, is carried forward into the damage calculations. In addition, scenario analysis is used to estimate the effect on damage of deep uncertainties such as future economic development patterns, which alter the quantity and value of assets at risk in the coastal region. However, other sources of damage estimation uncertainty are not included in the new version of the model. Table 5-6 summarizes various sources of uncertainty in flood damage estimates, including several that are not considered in CLARA v2.0.

This section describes the current state of knowledge about each of the excluded uncertainties and discusses the reasons why they were not implemented in the latest model version.

Table 5-6: Sources of Damage Estimation Uncertainty.

Source of Uncertainty	Type of Uncertainty	CLARA Uncertainty Approach
Future population and asset growth	Deep	Scenario analysis
Future distribution of assets by location	Deep	Scenario analysis
Distribution of flood elevations in areas with assets	Deep and epistemic	Scenario, parametric analysis
Noise in ground elevation measurements	Epistemic	Parametric

Source of Uncertainty	Type of Uncertainty	CLARA Uncertainty Approach
Present-day structure inventory	Epistemic	Not included
Asset valuation	Epistemic	Not included
Depth-damage relationships	Epistemic	Not included

5.3.1 Present-Day Structure Inventory

The count of current economic assets in the coastal region is derived from multiple data sets that originate from different points in time and include different spatial resolutions. This introduces uncertainty that CLARA's economic database may not accurately tally the existing number, location, and characteristics of structures at risk. Older data, such as the original LACPR database dating to the second quarter of 2005, are projected forward using a combination of estimates of past growth (from the 2010 US Census and other sources) and an assumption that growth since 2010 has proceeded on the same trajectory as the scenario-dependent future growth assumptions. Recent reconstruction efforts may vary significantly from future long-term trends, so the performance of these projection methods to arrive at a baseline inventory is uncertain.

As in the 2012 Coastal Master Plan analysis, CLARA v2.0 does not analyze this uncertainty in the current inventory of economic assets or the location of structures; no methods have been proposed to date that incorporate such an approach into the Hazus-derived damage assessment methodology. The procedures described in Section 3.1 are limited to producing a single point estimate of these quantities. The economic inventory is thus constrained by the quality and resolution of available data; this also affects estimates of asset characteristics such as foundation elevations. This uncertainty is compounded in future damage estimates because it is the basis for future growth projections.

Future research and addition data collection could improve accuracy and resolution of the current inventory of assets. In addition, where multiple data sources have measured the same inventories, exploitation of different data set characteristics might yield estimates of the accuracy of the data. For example, data from the West Shore Lake Pontchartrain Feasibility Study (USACE, 2013e) is estimated at the tax parcel level and is considerably more recent than the LACPR study. Assuming negligible uncertainty in the parcel data—itself a potentially poor assumption—one could hindcast estimates from the time of the LACPR study, or calibrate the growth rates implied between the two data sets. These findings could then be applied to other areas to estimate uncertainty in places where parcel data are not available.

This type of study could help bound current damage estimates, but could provide a false level of precision and would likely not improve future flood risk estimates for the 2017 Coastal Master Plan. This is because economic growth uncertainty over the 50-year period of analysis is likely to be much greater than current inventory uncertainty. As a result, estimating current inventory uncertainty was not included in the scope of the current round of model development.

5.3.2 Asset Valuation

Valuation of economic assets is performed following the procedures and data used by the Hazus model, which produces only point estimates of value. CLARA expands upon this approach by implementing three approaches to estimating depreciation, either by disregarding it altogether (replacement value) or by calculating actual cash value (ACV) or an NFIP-compliant depreciation scheme.

However, these are more analogous to deep uncertainties, in that the different methods may each be most appropriate in different accounting scenarios. Hazus does not provide any insight into the level of uncertainty associated with different elements of its valuation method, such as uncertainty in structure square footage or replacement costs per square foot.

CLARA thus lacks a solid basis for developing estimates of this uncertainty. Use of point estimates for structure valuation was instead deemed suitable for comparing the risk reduction impacts of different proposed structural and nonstructural projects, provided that the same method is applied consistently coast wide when assessing each type of project and scenario.

5.3.3 Depth-Damage Functions

In the economic module, uncertainty in the depth-damage relationships was considered but not implemented. Naturally, there is stochastic variability in the amount of damage an asset would experience under a given level of flooding. The depth-damage relationship also varies systematically between certain circumstances, such as fresh versus salt water inundation, or flooding in A-zones versus V-zones (FEMA, 2011).

Different curves are thus more appropriate under different circumstances. Previous studies have found that flood damage estimates are sensitive to the choice of depth-damage curve, but the CLARA development team is aware of no studies that suggest credible weightings between curves that could be used to produce parametric estimates of damage uncertainty related to this factor. (Tate et al., 2014), for one, concluded that variation in different depth-damage relationships from Hazus is responsible for less total uncertainty in damage estimates than factors such as the choice of DEM, uncertainty in the flood hazard, or uncertainty in structure inventories.

CLARA's depth-damage curves are taken from the Hazus model, which in some cases does provide multiple candidate curves. When multiple curves are available for the same set of conditions, the RAND team has selected the curve deemed most appropriate for use in modeling local conditions. Specifically, CLARA adopts depth-damage curves associated with salt water, long-duration flooding developed by the USACE New Orleans District based on historical observed flood damage data in coastal Louisiana. This is consistent with the methods used by LACPR (USACE, 2009b) and in other recent USACE Feasibility Studies. Curves produced by the USACE New Orleans District, or those published most recently, were assumed to be more relevant than older functions or curves based on data from other regions. Louisiana-specific curves were also favored over composite "universal" curves, like those developed by the Federal Insurance and Mitigation Administration (FIMA). The adoption of curves based on local data specifically for Louisiana helps to ameliorate some of the uncertainty associated with the choice of depth-damage relationship.

Even if depth-damage curves from multiple data sources were applicable to a particular asset category, the fundamental problem with incorporating multiple curves is that no basis exists for

weighting different functions to construct a single curve or distribution. Further, the amount of variation around any point in the curve, across assets of the same type, is also unknown. For a given curve, FEMA or USACE only report point estimates at each flood depth interval.

The depth-damage relationship is more accurately considered as a scenario uncertainty at present. Any consideration of its uncertainty would best be implemented using scenario analysis, similar to how system fragility is handled. However, the variation in damage that could result from different depth-damage scenarios is likely outweighed by the additional complexity and communication issues associated with adding a new dimension of scenario uncertainty to CLARA's flood risk analysis.

Figure 5-5 shows one example of these curves: the variation in depth-damage relationships associated with short-duration and freshwater flooding for a one-story, single-family residence on a pier foundation. The first four curves are drawn from the same source, the USACE New Orleans District, as provided in the Hazus model. The other curves are consensus curves developed by USACE Institute for Water Resources (IWR) and FIMA, respectively. This illustrates that alternative curves, even for circumstances (such as freshwater flooding) that do not correspond to storm surge events, are often quite similar. This is especially true given CLARA's assumption that a structure receiving damage equal to 50 percent of its value or greater would be demolished and reconstructed.

The set of salt water, long-duration curves appropriate for each structure and foundation type, as shown in Figure 5-5 are the functions adopted for use in CLARA. These curves are most specific to the circumstances of storm surge-based flooding in Louisiana, and are also the most conservative (i.e., most rapidly increasing damage with flood depth) of the functions shown. Consistent with Hazus methodology, it is assumed that any structure which receives damage greater than 50% of replacement cost is demolished and rebuilt.

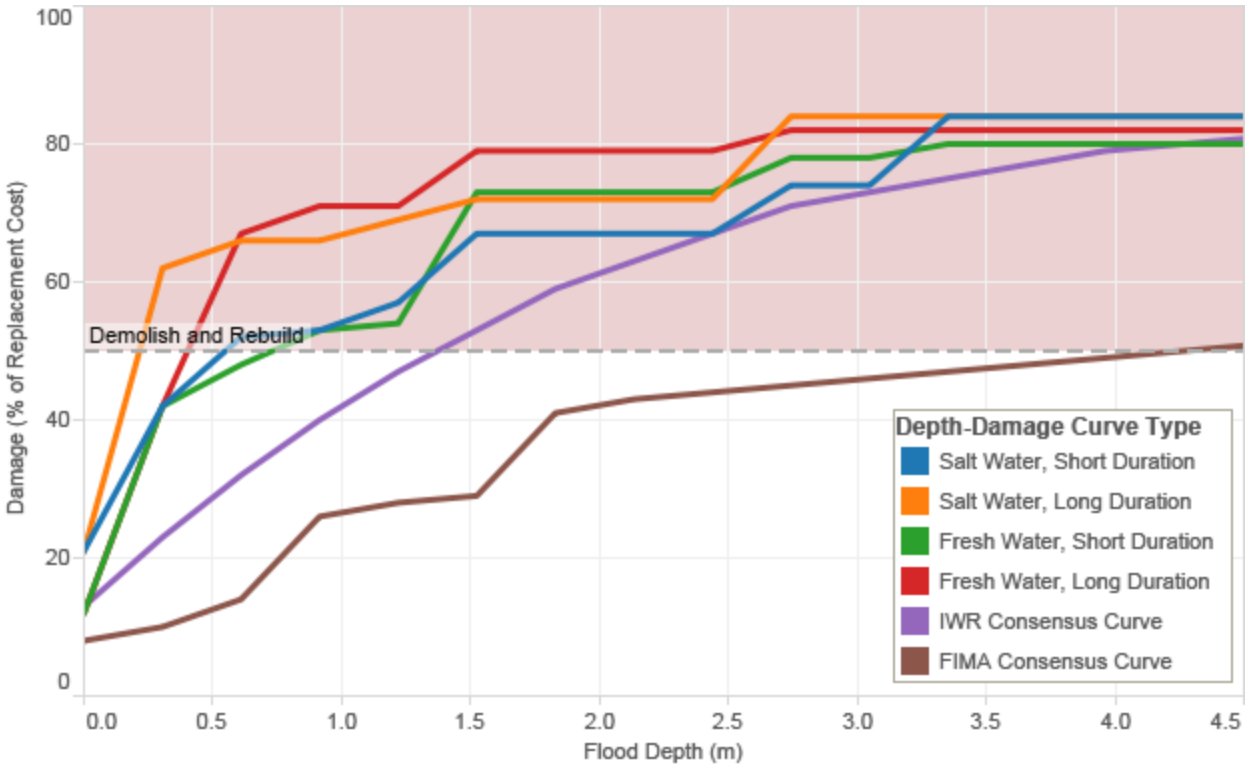

Source: Hazus.

Figure 5-5. Structural Damage as a Function of Flood Depth for Single-Family Residences (One Story, Pier Foundation).

For the reasons outlined above, the Risk Assessment team has not incorporated multiple depth-damage relationships into the CLARA v2.0 economic module. However, if deemed necessary it is feasible to treat the depth-damage relationship as an additional scenario uncertainty, though this could limit the number of other scenario uncertainties considered. CPRA will need to weigh the information presented here with runtime considerations from the other flood depth and damage modeling steps in order to select the set of scenario variables to be used in the 2017 Coastal Master Plan analysis.

5.4 Storm Frequency Modifications

Estimating statistical metrics such as flood depth exceedances or EAD requires assumptions about the overall frequency of hurricanes impacting the coastal area, expressed as the average number of storms per year. For CLARA, the relevant frequency value to be used in model calculations depends on the types of storms represented in the modified JPM-OS procedure. Johnson et al. (2013) outlines the method used by previous versions of CLARA; risk analysis supporting the 2012 Coastal Master Plan directly applied frequency values reported by Resio (2007), which were expressed as the expected number of storms with a minimum central pressure of 965 mb of lower per year per degree of longitude in the study region.

In 2012, the surge and wave analysis was restricted to examining risk associated with Atlantic cyclones with a minimum central pressure of 965 mb, corresponding approximately to Category 3 or greater storms on the Saffir-Simpson scale. The appropriate frequency depends on the

range of AEP values to be estimated,[25] the intensity of storms being modeled, and the range storm tracks included in an analysis. For example, an ongoing assessment of proposed Lake Pontchartrain Barrier alignments only considers storms from the eastern five primary tracks in the original JPM-OS storm suite (labeled tracks E1 through E5). Naturally, fewer storms per year have occurred in the historic record for this area alone than have occurred within the range of both the eastern and western tracks.

In preparation for the 2017 Coastal Master Plan analysis, the CLARA v2.0 scope has been expanded to model risk associated with any Atlantic cyclone attaining a minimum central pressure deficit of 985 mb or lower, corresponding to storms of Category 1 intensity and higher. Including less intense storms allows for the estimation of a wider range of depth and damage AEPs and improves EAD estimates, because a wider range of the damage probability distribution is directly modeled. By including less intense storms, however, the overall frequency of storms represented by CLARA's storm suite has increased.

CLARA v2.0 makes several changes to accommodate flexibility in the types of storms included in a given risk assessment. Previously, CLARA v1.0 calculated flood depth exceedances using a storm frequency formulated as an expected number of storms impacting the coast, per year and per degree of longitude in the study region. The average frequency per year per degree of longitude (0.052 under current conditions, approximately 1 storm every 19 years) was small enough that the probability of "clustering"—that is, experiencing more than one storm in the same degree of longitude—was ignored.

However, by formulating exceedance calculations in terms of the frequency of storms per year throughout the entire study region expanding the universe of relevant storms to include all hurricanes (985 mb central pressure or lower), the probability of experiencing more than one relevant storm in a given year is non-trivial. To address this, CLARA v2.0 now models the number of hurricanes experienced in a year as a Poisson process, in which flood events are independent and the time between them follows an exponential distribution. The mean inter-arrival rate of storms during a hurricane season, α, is estimated using HURDAT data by counting the number of storms making landfall (at 29.5 degrees North latitude) since 1950, within the region defined by the JPM-OS storm tracks and with a minimum central pressure of 985 mb or less.

Previous studies using JPM-OS have constructed flood depth CDFs by estimating either 1) the probability of each synthetic storm occurring in a given year; or 2) the relative likelihood of each synthetic storm, conditional upon a storm occurring. These approaches then exponentiate the CDF by the assumed average frequency to account for the fact that no storms may occur in some years. Using the Poisson process instead explicitly incorporates the possibility of seeing multiple storms in a single year, such that the maximum flooding observed on an annual basis is the maximum over all the storms occurring in a given year. This more accurately represents how storms recur year-by-year, as evidenced by Hurricane Katrina and Hurricane Rita both striking Louisiana in 2005.

When modeled as a Poisson process, the probability of observing i storms of interest in a given year is

$$P(i) = \frac{e^{-\alpha}\alpha^{i}}{i!} \quad (5\text{-}8)$$

[25] Resio (2007), for instance, focused on storm surge AEP estimates in approximately the 100- to 1000-year range to support structure design for the New Orleans HSDRRS improvements.

The n-year flood depth exceedance, d_n, is the depth for which the maximum flood depth occurring in a given year has probability $1 - 1/n$ of being less than or equal to d_n. The law of total probability then dictates that the probability of the maximum flood depth in a given year being less than or equal to d_n is

$$F_{annual}(d_n) = \sum_{i=0}^{\infty} F_{storm}(d_n)^i \cdot P(i) = e^{-\alpha} \sum_{i=0}^{\infty} \frac{F(d_n)^i \cdot \alpha^i}{i!} \quad (5\text{-}9)$$

where F_{annual} represents the cumulative distribution function of maximum annual flood depths and F_{storm} represents the cumulative distribution function of flood depths from a single storm event.

CLARA v2.0 implements this new method for calculating annual flood depth exceedances, accounting for the possibility of observing multiple storms in a given year. Under this framework, exceedance estimates should only increase with any expansion of the universe of relevant storms. More specifically, expanding the number of storm tracks considered in the JPM-OS analysis, or including less intense storm such as the set of JPM-OS storms with a central pressure of 975 mb[26], only increases the objective probability of observing a given level of flooding at a particular point. Expanding the universe of relevant storms can alter the conditional probability distribution of experiencing a given flood depth, conditional on a storm occurring, but the overall frequency of storms increases in a manner such that the annual exceedance must be the same or greater than the value estimated using a more restricted storm suite.

Expected annual damage calculations are also a function of the overall frequency of storms, but damages from multiple storms in a single hurricane season are not likely to be independent (because areas affected by the first storm would not be constructed by the next). CLARA v2.0 makes a simplifying assumption that if multiple storms were to impact the same geographic point within the same hurricane season, the total damage received to assets is equal to the maximum damage that would occur from any of the storms in isolation. In other words, it is assumed that damage is not additive over multiple storms in a single year; this is a reasonable approximation of reality, given the length of time required for reconstruction after a damaging event.

In this case, CLARA answers a slightly different question: if n storms impact the study region in a year, what is the probability that the most severe event is a storm of return period x? Equivalently, given n storms, what is the probability that flooding from every storm is less than or equal to the x-year flood depth exceedance?

Suppose that the model estimates flood depth exceedances for a set of return periods, X, where x_i is ordered from high frequency to low (for example, if $x_1 = 5, x_2 = 10$, etc.). Then for x_1, the desired probability is just

$$P_{n,1} = F(x_1)^{n/\alpha} \quad (5\text{-}10)$$

[26] As noted earlier in this section, the JPM-OS storm suite of 446 storms is intended to accurately produce statistics representing flood risk from Atlantic cyclones with central pressures of 985 mb or lower (approximately Category 1 or greater hurricanes on the Saffir-Simpson scale). Storms in the JPM-OS suite have minimum central pressures of 900, 930, 960, or 975 mb. As such, the 142 storms with 975 mb central pressure are intended to represent all storms with central pressures ranging from 985 mb to 967.5 mb.

where $F(x_1) = 1 - 1/x_1$ is the CDF corresponding to the x_1-year return period. Inductively, for x_{i+1},

$$P_{n,i+1} = F(x_{i+1})^{n/\alpha} - \sum_{j=0}^{i} P_j \tag{5-11}$$

This provides the probability weight that should be applied to the damage exceedance associated with each return period in order to calculate EAD. Thus, if D_x represents the damage resulting from the x-year flood depth exceedance, then

$$EAD = \sum_{n=0}^{\infty} \sum_{i} P_{n,i} \cdot D_{x_i}. \tag{5-12}$$

Except where noted, this new frequency approach is applied for depth and damage estimates provided in the subsequent sections of this report.

6.0 Preliminary Analysis to Support Model Improvement

The many methodological advances in CLARA v2.0 require extensive testing to verify that results do not violate informed intuitions about system performance and risk, and that results are similar—to the degree expected—to those produced by CLARA v1.1 under similar initial conditions. This chapter describes how each new component of CLARA v2.0 was tested. It also provides illustrative results from the model tests and preliminary risk estimates for current conditions and in the Less Optimistic future scenario.

The tests performed fall into four primary categories: 1) sensitivity tests to better understand how different sampling steps or sources of uncertainty contribute to the overall parametric uncertainty ranges; 2) model specification tests, used to determine recommended simulation sample sizes and other model settings; 3) storm selection tests, in which model runs based on different training sets are compared to examine the tradeoffs between training set size, the characteristics of selected training storms, expected bias, and residual uncertainty; and 4) scenario comparisons, where the model is run across multiple scenarios, using default model settings, to compare the estimated flood depth and damage between different scenarios (including comparisons to 2012 Coastal Master Plan results). Sensitivity testing was also performed on the ADCIRC and UnSWAN models. The experimental setup and design used to conduct these initial tests is described below.

Results in this section are estimated for AEPs ranging from the 10-year (10 percent AEP) to the 2,000-year (0.05 percent AEP) flood or damage event, as well as in terms of expected annual damage. In addition, parametric uncertainty ranges around each of these estimates are shown, using the 10th, 50th (median), and 90th percentiles to summarize this variation. These intervals were chosen to align with values typically applied by USACE to set margins of error for design purposes--for example, the maximum overtopping rate threshold for which federal levee design heights are set (Department of the Army, 2010).[27]

6.1 Data Sources

The Storm Surge and Wave team provided storm outputs from ADCIRC and UnSWAN for current conditions and the Less Optimistic landscape scenario from the 2012 Coastal Master Plan. Each test set consisted of the full 446 storms available from prior studies. No changes were made to ground elevations or protection feature crest heights from those used in 2012. Although the 2017 production runs will utilize an updated landscape mesh for the 2065 time horizon, the 2061 landscape used in 2012 provided a suitable approximation for testing that allowed more direct comparison to previous results.

Storm probabilities were fit using the HURDAT set of historical storm data described in Section 5.2.1.

[27] The current USACE criteria for federal certified levees is that the overtopping rate with a 1 percent AEP does not exceed 0.009 m^3s^{-1}/m (0.1 cfs/ft) with a "90 percent non-exceedance probability" or "90 percent assurance," meaning that 90th percentile estimate of the 1 percent AEP overtopping rate is used to set the minimum design height (Department of the Army, 2010, Appendix D, p. D-7).

Economic damage projections were based on the updated geospatial units detailed in Section 2.2 and the updated asset inventories described in Section 3.0, but were otherwise calculated in the same way as in the 2012 Coastal Master Plan analysis to facilitate comparisons with CLARA v1.0. Growth was modeled with an annual coastal growth rate of 0.67 percent to project asset inventories forward to 2065; this is the same rate as the default value used in the 2012 Coastal Master Plan. . The default value used in 2012 for the dispersion parameter—the proportion of assets located in urban areas—was the value present in the baseline economic inventory, representing no projected change in urbanization. The dispersion parameter used in these analyses differs slightly from the 2012 value but was also set equal to the value determined by the baseline inventory of assets. Thus, while the economic assets and flood depths analyzed have been updated, the analysis presented here makes similar assumptions about future growth as applied in 2012.

6.2 ADCIRC Raised-Feature Interpolation Methods

One question addressed by this sensitivity analysis was whether there are additional sources of epistemic uncertainty that emerge from the ADCIRC model that are not necessarily captured in the assumed standard error (0.15m for the test analysis or 0.36m for model production, respectively). Specifically, ARCADIS noted that different methods for incorporating raised features (weirs) into the ADCIRC mesh could yield different estimates of the final water elevations behind or nearby those features, potentially introducing bias or additional variance into the results.

6.2.1 ARCADIS Bias Investigation

To investigate this question further, ARCADIS conducted an experiment with ADCIRC, using three different proposed methods for incorporating raised features into the ADCIRC mesh: maximum value, averaging, or 2σ averaging. ARCADIS applied each method to the Louisiana coastal domain and ran the 40-storm 2012 Coastal Master Plan sample to test each approach. These results were then compared to consider the possible bias introduced by selecting one method versus another. The detailed setup and results of this investigation are described separately in Appendix 3 of this document.

ARCADIS ultimately determined that the averaging method is likely to bias surge elevations behind these raised features, understating the value of protection features. The 2σ averaging method, in contrast, produces results more consistent with the maximum value approach previously applied while helping to avoid overestimation of the height of protection features in close proximity to other raised features. They recommend using either the 2σ averaging or maximum value method in the 2017 Coastal Master Plan analysis, noting that the maximum value is likely to provide a more optimistic assessment of the protection value of these features.

6.2.2 Surge and Wave Uncertainty

The results from the raised-feature experiment were also provided to the RAND Team to support this investigation of parametric uncertainty. Rather than evaluate the bias introduced by one method relative to another, these results were used to identify the maximum variation that occurs between the different methods on a coast wide basis for storm surge elevations and wave heights. In turn, this might suggest changing the assumed standard error associated with the storm surge and wave inputs in CLARA v2.0.

To evaluate the variation, statistical analysis was performed directly on the individual 40 storms inputs instead of running each of the separate methods through the CLARA model.[28] This approach was based on the results described in Appendix 3 and an assessment of the potential variation after summarizing the raw data inputs.

The maximum deviation (spread) across all three methods for each CLARA grid point and each storm was first calculated, and then the maximum deviations were summarized from the 40-storm sample by grid point or by watershed. Figure 6-1 shows a map of the maximum storm surge deviation for each point, filtered to focus only on points where the maximum deviation is greater than 0.36m (1.2 feet)—that is, greater than the level of noise that will be assumed in the ADCIRC and unSWAN simulation outputs for the production runs.

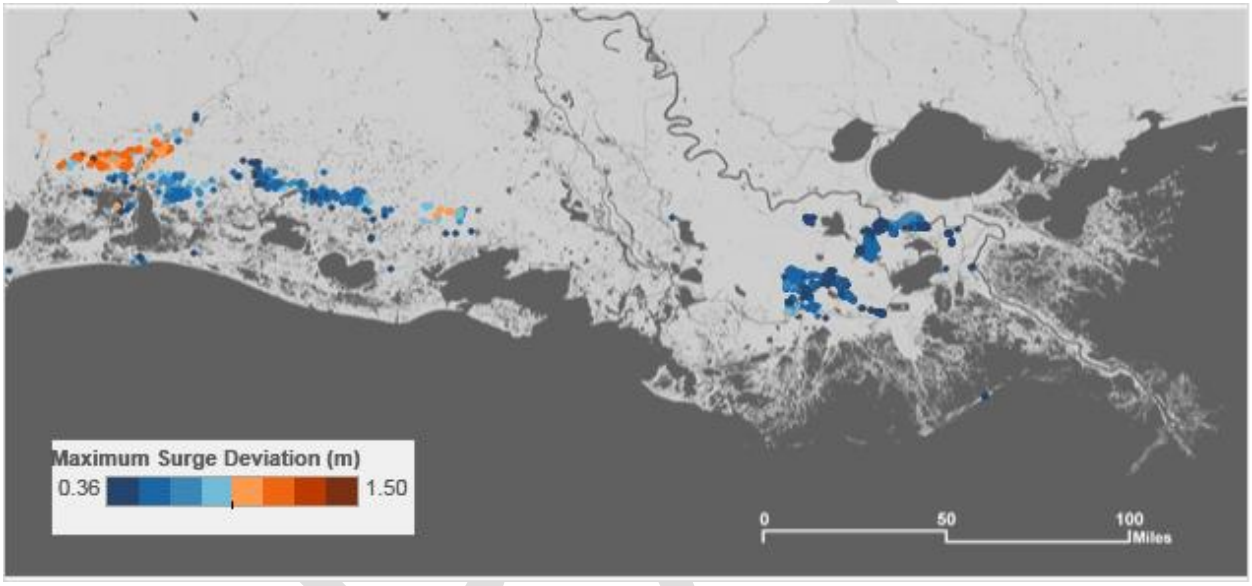

Note: Map shows only points with a maximum deviation of at least 0.36 m (1.2 feet).

Figure 6-1: Maximum Surge Deviation by Grid Point Across Three Interpolation Methods.

In general, non-zero surge variation is observed across the methods at about one-quarter of the CLARA grid points. Approximately 4 percent of points varied more than 0.36m across the methods in at least one storm simulation. The areas where variation most commonly occurs is in the vicinity of Lafourche Parish, Lake Charles, and along the northern boundary of the modeling domain in the western half of the state. In many cases, the maximum variation is driven by only 1 or 2 storms, though in the west this is likely due to the very limited sample of storms that produce flooding there in the 40-storm set.

Because the surge variation only occurs in certain weir-influenced areas and under selected storm conditions, the RAND Team recommends not changing the average standard error associated with all surge input values based on this analysis. In general, this variation appears to be a relatively minor factor compared with other sources of uncertainty discussed in this report.

[28] A follow-on evaluation using the CLARA model can be performed if CPRA deems it necessary based on the initial investigation described here.

Wave deviation results show a similar spatial pattern (not shown), but the maximum deviation at any point and storm combination is 0.44m, and only 1 point yields a deviation greater than 0.32m. No changes to the wave analysis or assumed noise are indicated by these results.

6.3 Contributions to Parametric Uncertainty in Unenclosed Areas

In this investigation, a better understanding of the relative contribution to parametric uncertainty from each step of the sampling process was sought for unenclosed areas. Recall that the bootstrapping sampling is designed to capture the uncertainty when an estimation of the likelihood of storms with different characteristics from a limited set of observed historical storm events is sought, while the Monte Carlo sampling in unenclosed areas incorporates uncertainty from the surge response surface predictions, ADCIRC/UnSWAN variance, and noise in the DEM.

Due to computational limits, this investigation did not include a decomposition of the uncertainty by each input. Instead, the analysis focused on the relative contributions of the bootstrap uncertainty (historical storms) and Monte Carlo uncertainty (all other parametric uncertainties) using the methods described below.[29]

6.3.1 Approach and Experimental Design

In unenclosed areas, the Monte Carlo sampling is designed to analyze the combined uncertainty associated with the response surface predictions, ADCIRC and UnSWAN model noise, and measurement error in the elevations contained in the DEM. By retaining the flood depth exceedances associated with each combination of Monte Carlo and bootstrap sample, the relative contributions of each can be examined. To do this, one sample was held fixed and calculated the variance in test statistics over the other type of samples. Taking the 100-year exceedances as an example, the procedure takes every bootstrap sample, holds it as fixed, and then calculates the standard deviation of the exceedance value over all Monte Carlo replicates. If this procedure is repeated for each bootstrap sample and the mean of the resulting standard deviations is taken, this quantity represents an estimate of the average variation in 100-year exceedances associated with the Monte Carlo sampling.

Stated another way, there are many possible values for the standard deviation of estimates of the exceedance value with respect to the Monte Carlo sampling, depending on which bootstrap sample they are interacting with. That all bootstrap samples are equally likely has been asserted, so this represents a sample mean of the standard deviation with respect to the Monte Carlo over all of its realizations determined by the set of bootstrap samples.

Likewise, if the Monte Carlo replicates are held fixed and the standard deviation of the exceedance values is calculated over the set of bootstrap samples, an estimate of the average standard deviation with respect to the bootstrap samples can be calculated. Comparing the quantities produced by these two procedures, an estimate of the relative contribution of each sampling scheme to the overall uncertainty can be obtained.

[29] Note that the sensitivity testing results presented in this section use a lower overall storm frequency assumption than what is presented through the remainder of Section 6, and reflects the initial frequency approach used in CLARA v1.0 rather than the updated methods described in Sec. 5.2.1.1 above. This difference in approach is not expected to meaningfully affect the results or conclusions drawn in this portion of the testing.

6.3.2 Sensitivity Testing Results

Coast wide summary results, representing the average contribution to standard deviation from each sampling step, are shown in Figure 6-2. The relative contribution from the Monte Carlo sampling (orange line) and bootstrap resampling of the historical record (blue line) is shown at AEPs ranging from the 10-year to 2,000-year exceedance. The ratio between them at each AEP is shown with the thick red line (right-axis).

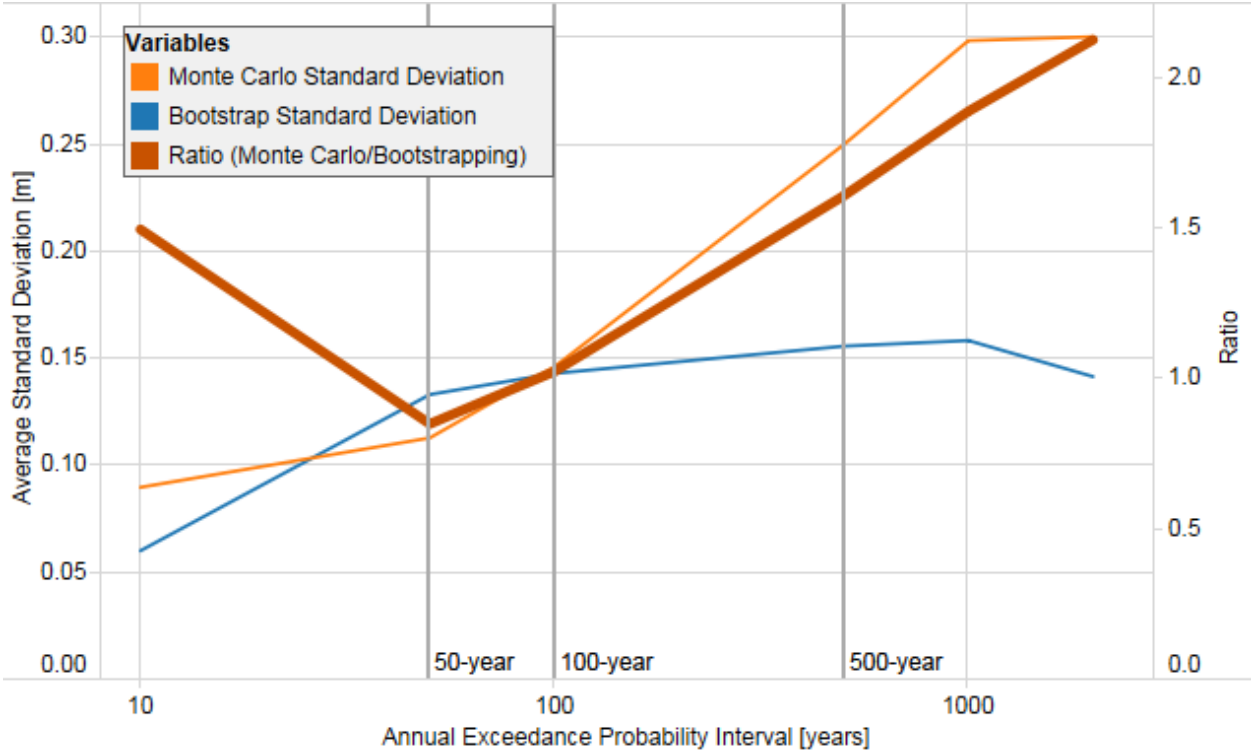

Figure 6-2: Relative Contribution to Standard Deviation by Sampling Step in Unenclosed Areas.

These average coast wide results suggest an intuitive pattern: at more frequent intervals (50-year, for instance) the relative contributions from both sources are relatively equal, ranging from 0.05-0.15m from each, and the ratio is close to 1. From that point, however, the Monte Carlo contribution continues to increase at more extreme intervals, increasing to 0.3m by the 1,000-year interval, while the bootstrapping contribution stays relatively constant (approximately 0.15 m). As a result, the ratio between both increases with exceedance interval, ranging from 2:1 (500-year interval) to nearly 3:1 (2,000-year interval).

This pattern can be explained by the nature of the calculations that use the different samples. A bootstrap sample of the historic storm record is used to fit the probabilities assigned to each synthetic storm. A simplified explanation of CLARA's statistical model is that the synthetic storms are ordered by their associated flood depth response, and then exceedances are determined by the cumulative sum of the probabilities. For extreme return periods, in the range of the 1,000-year event and beyond, there is little probability mass left in the tail of the distribution, and correspondingly few synthetic storms that can produce the 1,000-year levels of flooding. Those storms are also likely to produce very similar flood depths as they asymptotically approach a maximum surge response. Therefore, the contribution of the bootstrapping procedure to total uncertainty is constrained at the high end of the flood distribution.

In contrast, the uncertainty associated with Monte Carlo sampling is expected to increase for storms further in the tail of the distribution. Although the uncertainty associated with model and DEM noise is considered to be fixed, the prediction intervals produced by the response surface model grow wider when making extrapolated predictions for storms outside of the parameter range spanned by the training storm set.

This shows that the uncertainty captured in the Monte Carlo sampling is a more significant driver for larger storm surge and wave events in unenclosed areas. A similar pattern emerges in enclosed areas, as described in the next subsection.

The pattern described above can be shown at each grid point as well, though some clear spatial variation emerges. Figure 6-3, for example, shows the same Monte Carlo to bootstrap standard deviation ratio by grid point for the 50-year (top pane), 100-year (middle panel), and 500-year (lower pane) AEP intervals. Blue colors indicate where the ratio is less than 1, and orange colors greater than 1. The mapped results clearly show that bootstrap uncertainty is more dominant in the western half of the state at the 50-year and 100-year intervals. Alternately, the ratio is more balanced in the east at the 50-year and begins to tilt towards the Monte Carlo uncertainties by the 100-year interval. By the 500-year interval, however, the Monte Carlo contribution is dominant at nearly every grid point coast wide, except along the northern edge of the study boundary at points that rarely flood. Figure 6-4 reinforces this pattern, showing the separate contributions of Monte Carlo and bootstrap uncertainty at the 500-year interval.

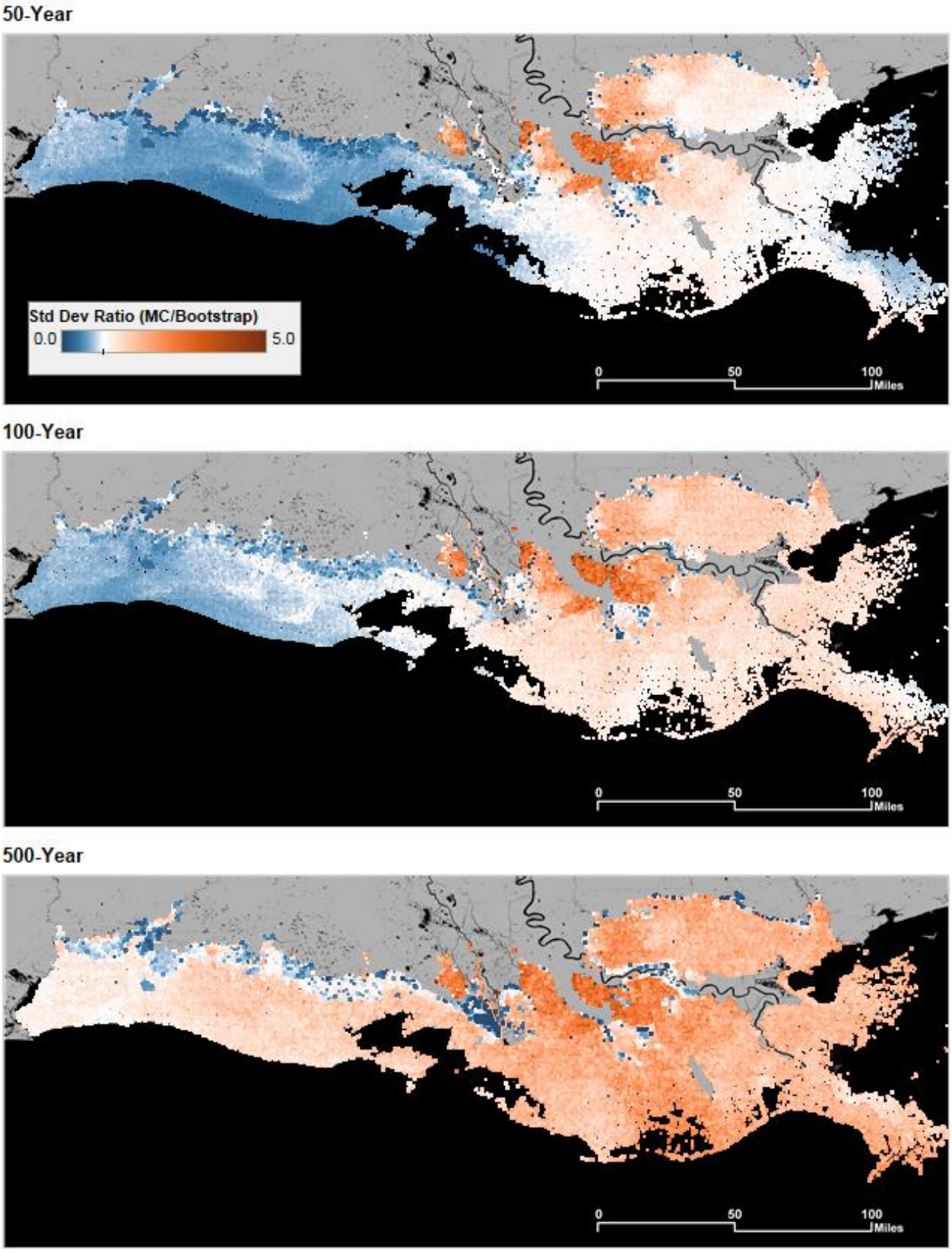

Figure 6-3: Relative Contribution to Standard Deviation by Grid Point at three AEP Intervals.

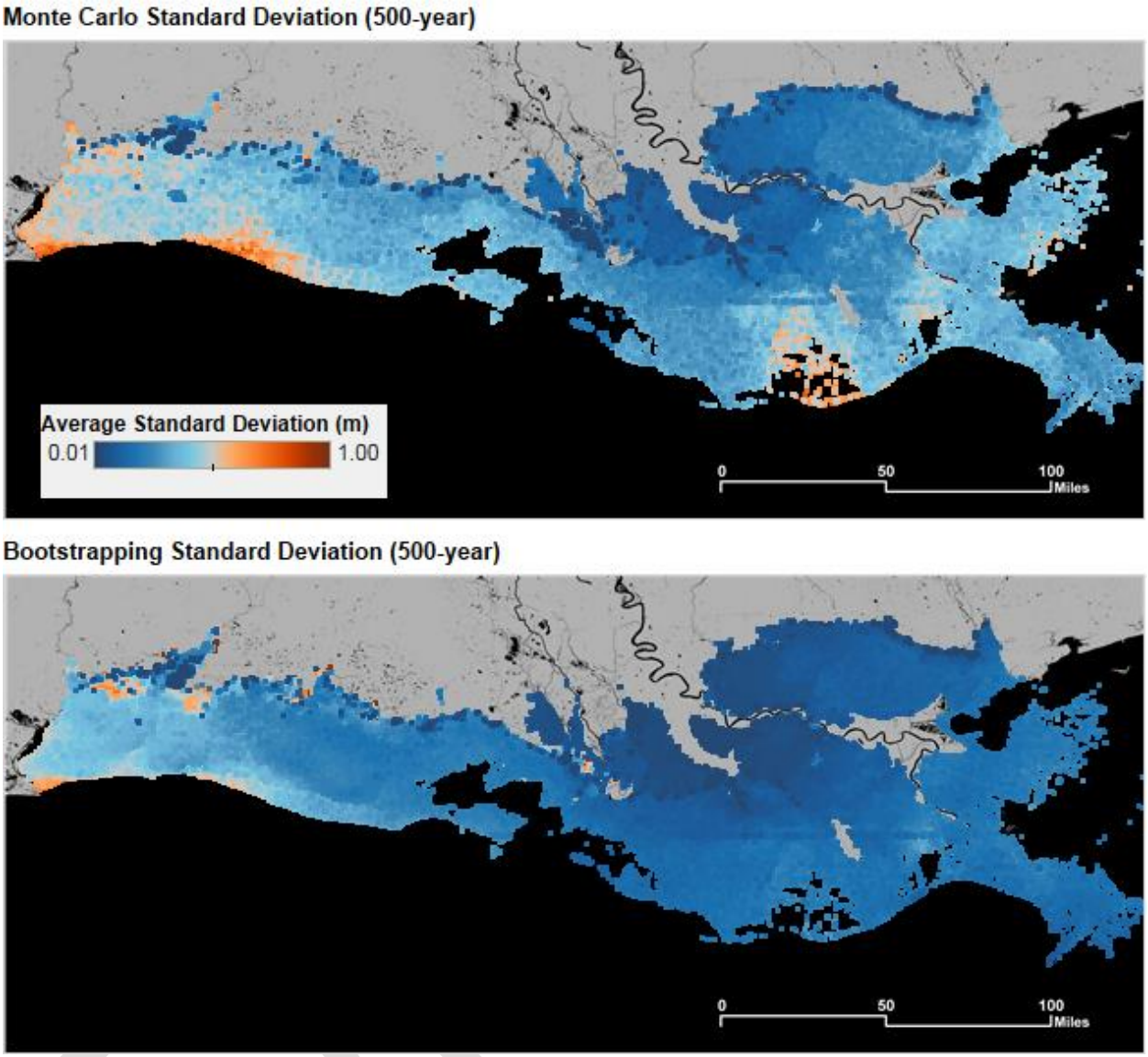

Figure 6-4: Monte Carlo and Bootstrap Standard Deviation by Grid Point, 500-year AEP Interval.

6.4 Testing Sample Sizes in Enclosed Areas

CLARA v2.0's implementation of parametric uncertainty analysis requires a multi-stage sampling design that uses random samples of various model elements at both the individual storm level and the aggregate statistical level. In unenclosed areas, Monte Carlo sampling is used to generate synthetic storm flood depths by drawing from a distribution determined by the response surface fitted at each point, noise in the surge and wave models, and measurement error in ground elevations. Bootstrap samples of historic storms are used to estimate the relative likelihood of different synthetic storms. In enclosed areas, Monte Carlo simulation contributes to the flood distribution associated with synthetic storms by sampling overtopping rates and breaches. The model also samples Markov chains to simulate geospatial correlations in surge variation. Bootstrap samples are used in the same way as in unenclosed areas, and measurement error in ground elevations are also treated identically.

The flood depth exceedances estimated by CLARA are affected by the sample sizes of each of these simulations. The results of a particular model run based on any combination of sample sizes are unbiased with respect to the outputs that would be generated by a run with infinite samples. However, larger sample sizes could reduce the variance associated with the model. This portion of the sensitivity analysis was conducted to test the uncertainty associated with different sample sizes on CLARA v2.0's flood depth estimates in enclosed areas. The goal was to assess whether the sample sizes for the bootstrapping, Monte Carlo, and Markov chain Monte Carlo steps in enclosed areas were sufficient to achieve convergence, as well as to better understand how interior flooding varies across CLARA v2.0's new estimates of parametric uncertainty. Because of the additional complexity modeled in enclosed areas, a set of sample sizes convergent on the interior was judged to be sufficient in exterior regions.[30]

6.4.1 Screening Analysis Experimental Design and Results

The relationship between sample size and variance cannot be determined *a priori* given the model's complexity. Further, re-running an entire model case—which includes all synthetic storms and all sampling steps described above—hundreds to thousands of times, as might be called for in a formal analysis of convergence, is computationally infeasible. Instead, the analysis described here uses a two-stage process to provide insight on suitable sample sizes for enclosed areas.

Certain scenario parameters were fixed to conduct these experiments for the interior flood model. Specifically, the Less Optimistic FWOA landscape scenario was run through the model, assuming 50 percent pumping capacity and using the "MTTG Low" fragility assumptions. Various combinations of sample sizes for the Monte Carlo, representative Markov chain variation, and historical bootstrap simulations were run, with some combinations omitted due to processing time constraints.

In the first "screening" stage, the model was run once for each of several combinations of sample size parameters for the three sampling steps. In this stage, outputs from these single model runs were compared to the largest sample sizes run to note any difference in results. The goal was simply to determine whether there is, in fact, variation occurring between different sample sizes for each sampling step.

[30] Note that the sensitivity testing results presented in this section use a lower overall storm frequency assumption than what is presented through the remainder of the sensitivity testing results, and reflects the initial frequency approach used in CLARA v1.0 rather than the updated methods described in Sec. 5.2.1.1. This difference in approach is not expected to meaningfully affect the results or conclusions drawn in this portion of the testing.

Table 6-1: Simulation Cases Run for Specification Testing (Screening Analysis).

All cases merged with 50 exterior flood depth Monte Carlo replicates		Monte Carlo replicates of overtopping rate/fragility uncertainty		
Markov chain replicates of surge level uncertainty	**Bootstrap samples of historical record**	**50**	**100**	**200**
50	50	x (*run twice*)	x	x
50	100	x	x	x
50	200	x	x	x
100	50	x	x	x
100	100	x	x	x
100	200	x	x	x
200	50	x		
200	100	x		

Each sample size combination was then compared to the largest sample size considered overall, which included 200 Monte Carlo replicates, 100 Markov chain replicates, and 100 bootstrap samples (Table 6-1, yellow highlight). The average difference in flood elevation was then calculated, as shown in Figure 6-5. This comparison uses the flood elevation across the entire AEP curve, provided as an average for the East and West Bank HSDRRS areas, respectively, as well for all enclosed areas outside of HSDRRS collectively. Results from all experiments across all AEP intervals are shown at their 50th percentile values, with one pane for each sample size combination.

This figure shows that the Monte Carlo sample, rather than the Markov chain replicates or bootstrap sample size, shows the most variation when examining different samples and sample sizes . Looking across the columns, for instance, it can be seen that variation nearly disappears as the Monte Carlo sample gets closer to the largest sample size. By contrast, looking down the first column, for a fixed Monte Carlo sample size, using the smallest sample sizes for the Markov chain and bootstrapping procedures has very little effect on the results. In addition, Figure 6-5 shows that the large majority of variation across sample sizes occurs in the HSDRRS, with little-to-no variation noted on average in non-HSDRRS enclosed areas.

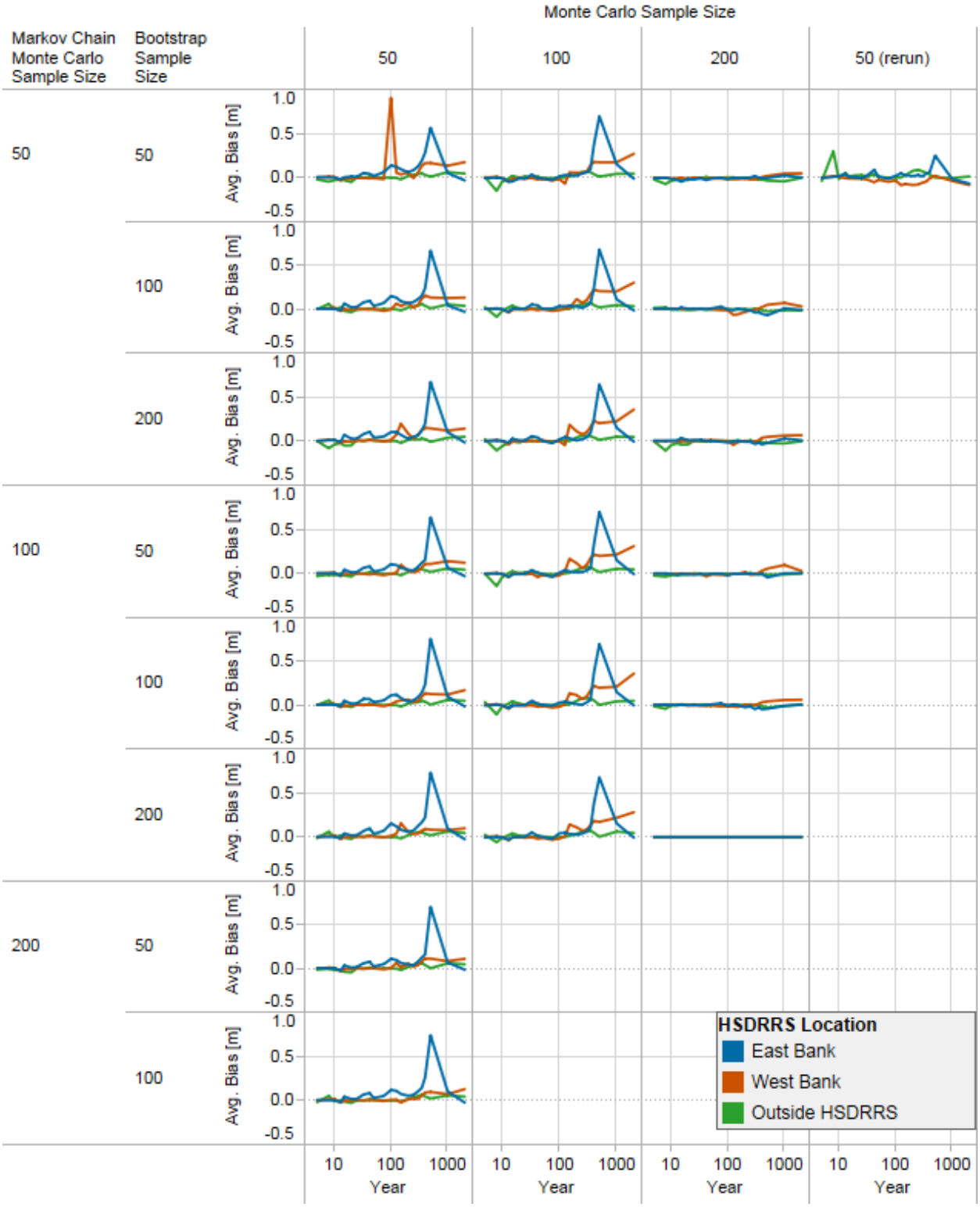

Figure 6-5: Average Flood Elevation Variation from All Sample Sizes Versus Largest Sample Size Tested, by Enclosed Area Location.

The results of this initial screening are suggestive only, because they rely on comparisons of single model runs. A more complete comparison of variation would instead utilize resampling to better isolate the contribution to variance from sample sizes, and to determine whether a larger sample size would reduce the final standard deviations.

6.4.2 Detailed Analysis in the New Orleans HSDRRS

In the second stage, a more detailed resampling analysis was conducted, focused on the Monte Carlo sampling step only. This sampling step was identified as yielding the greatest variation due to sample size (Figure 6-5). In this re-analysis, the Markov chain and bootstrap sample sizes were held fixed at 50 replicates, and a Monte Carlo sample of 1,000 replicates was run through the model. Next, a separate bootstrap resampling analysis was conducted by repeatedly drawing different Monte Carlo sets (with replacement) from the 1,000-replicate sample, with sizes ranging from 50 to 400 replicates. This resampling was used to construct empirical standard deviations for flood elevations and flood depths. The goal was to compare standard deviations constructed from different sample sizes, and determine whether variance is reduced, on average, with increased sample size. Only the New Orleans HSDRRS was considered in this step, both to improve runtime and in light of the variation in these areas noted in the initial screen.

Ten sets of results were generated for each number of replicates considered. For a given number of Monte Carlo replicates, looking across all of the HSDRRS BHUs yields a distribution of flood elevation standard deviations. Comparing the different distributions obtained when different numbers of replicates are used helps to indicate if the variation in standard deviation decreases across the BHUs as sample size increases. Figure 6-6 shows a boxplot comparing the distributions of the standard deviations of flood elevation results as a function of the number of Monte Carlo replicates (N Mc) at the 500-year AEP. No clear trend is discernable, and no evidence has been found that increasing the number of Monte Carlo replicates reduces the variance of model results. This suggests that 50 replicates is adequate for production runs, because model variance between runs is not appreciably lessened by increasing the sample size beyond 50.

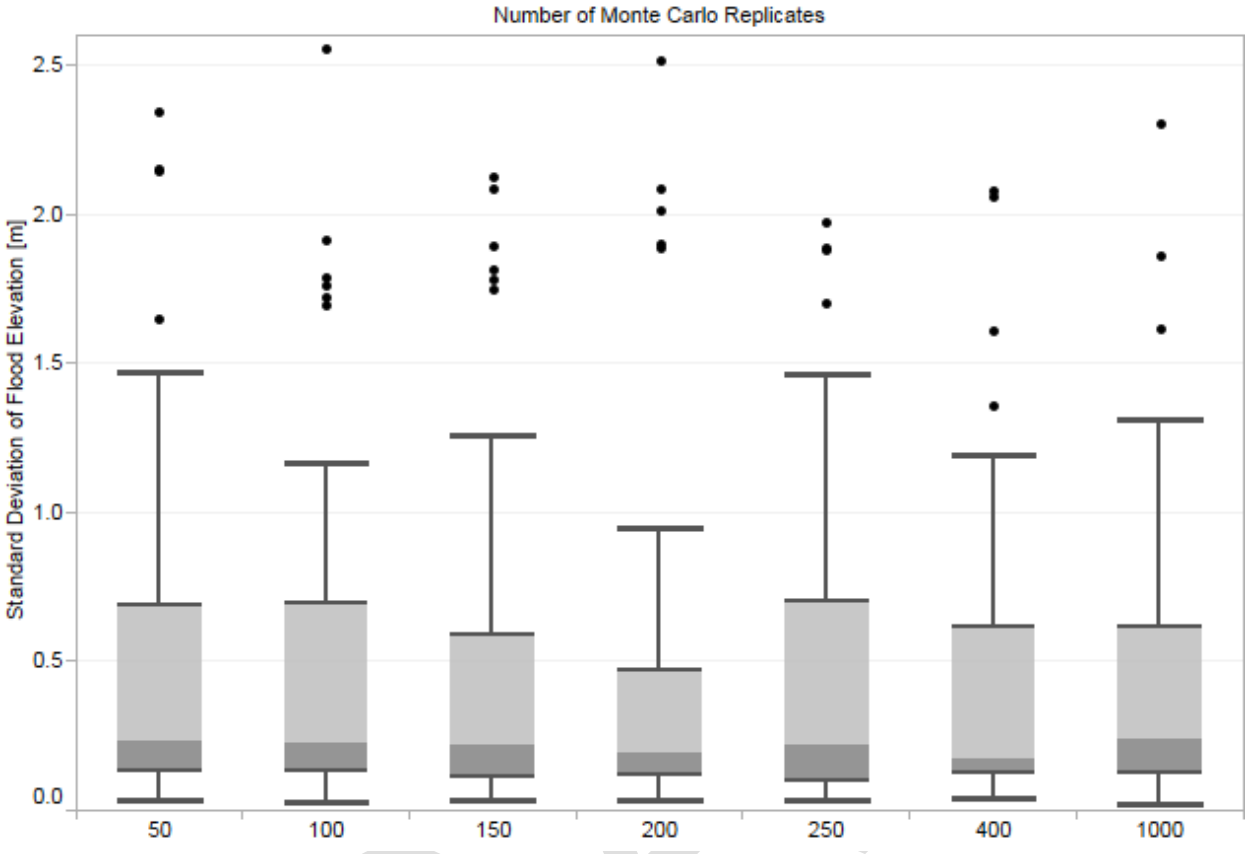

Figure 6-6: Distributions of Standard Deviations of Adjusted Flood Elevation Observations Obtained when Varying the Number of Monte Carlo Replicates, New Orleans HSDRRS (500-year AEP).

The discussions above focused on flood elevations for each BHU, but CLARA produces results at the level of individual grid points. Figure 6-7 is similar to Figure 6-6, showing results for the 500-year return period in the New Orleans HSDRRS, but compares the distributions of standard deviations of flood depth results at different grid points as a function of the number of Monte Carlo replicates. In this case, grid points which experienced no flooding in any sample have been excluded from the graph to avoid skewing the results; the testing was intended to examine variability in flood depths, so points that never flood are not informative. The implied median standard deviation of flood depths by point over each run, for all sample sizes tested, is less than 0.4m (slightly greater than 1 foot). Again, there exists no clear evidence that increasing sample size decreases the variance associated with model outputs.

The existence of grid points with high standard deviations greater than 1 meter was expected. These correspond to some of the lowest-elevation points within BHUs. As their ground elevation is near the minimum elevation in a BHU's stage-storage curve, great differences in flood depth can be produced by relatively small volumes of flood water.

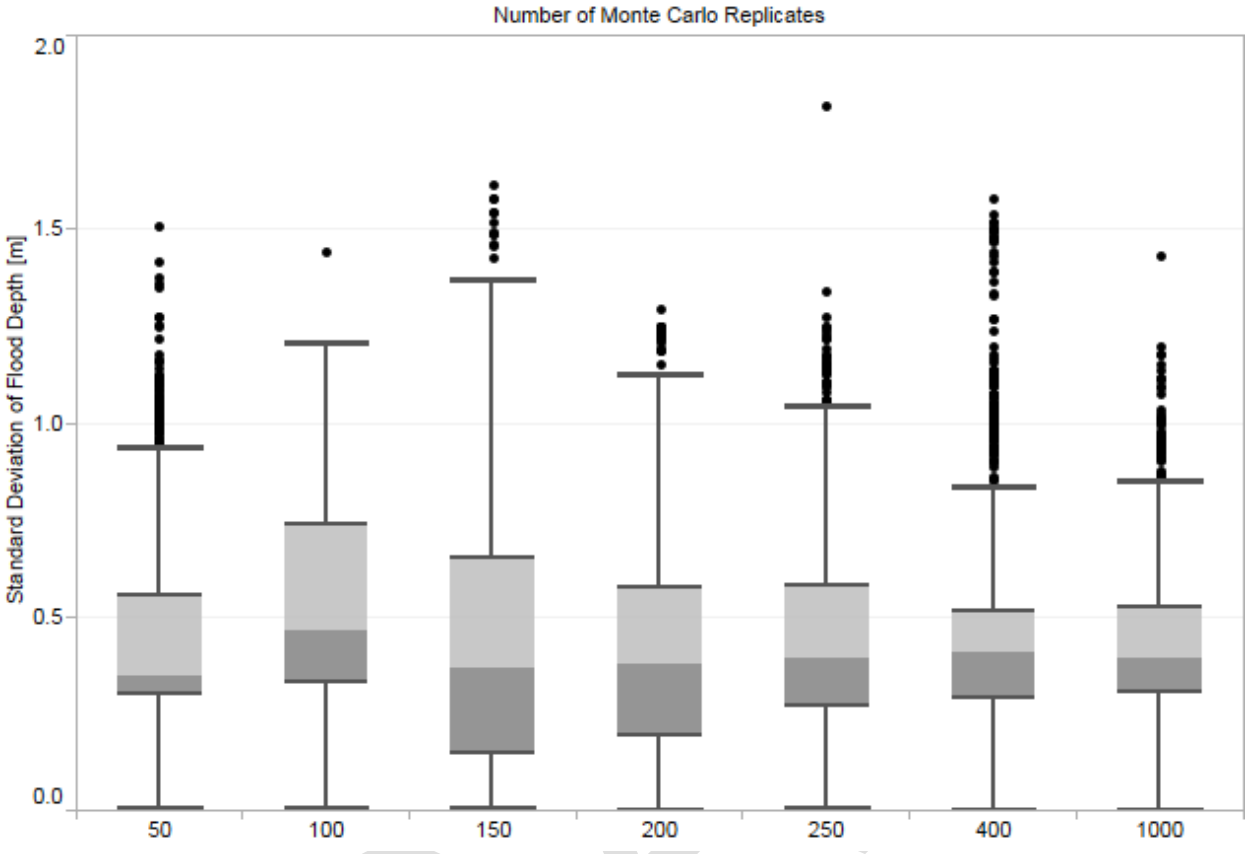

Figure 6-7: Distributions of the Standard Deviations of Flood Depths Obtained by Different Numbers of Monte Carlo Replicates, 500-year AEP.

The specification testing conducted did not reveal any clear benefit, in terms of reduced variance associated with model outputs, from using larger sample sizes for the Monte Carlo and bootstrapping simulations. A sample size of 50 for each appears to be sufficient for production runs.

6.5 Storm Selection Analysis

A key goal to address using the revised CLARA v2.0 model and new parametric uncertainty approach was to better understand the potential tradeoffs CPRA should consider when using a smaller subset of storms as a training sample for its statistical analysis of flood depths and damage. Fischbach et al. (2012a) describe an initial evaluation of potential bias—comparing the subset of 40 storms chosen for the 2012 Coastal Master Plan analysis to a larger set of storms—but this evaluation still relied on a relatively small set to compare against (154 storms), and could not account for the additional parametric uncertainty introduced when reducing the training sample size.

To support the 2017 Coastal Master Plan analysis, a more thorough investigation was conducted to investigate the use of smaller subsets of training storms. The first step in the investigation was to conduct an initial screening by comparing a relatively large number of plausible subsets (sixteen in total, inclusive of the original 40-storm Master Plan Storm Set and the complete 446-storm set) comparing flood depth results in a limited number of non-enclosed watersheds (Figure 5-2). Subsets were formed by eliminating storms from the full 446-storm in ways that, it was hoped,

would introduce minimal bias. For example, some subsets consist only of storms with a forward velocity of 11 knots, discarding storms from the 446-storm set with faster or slower progression. Other sets eliminate storms that follow "off-angle" tracks, or they may only include storms with minimum central pressures of 960 mb or lower.

The performance of each storm subset was evaluated by examining bias in predicted flood depths at various return periods, relative to the results from the full 446-storm set. The estimated standard errors associated with exceedance estimates was also analyzed. Promising subsets were identified from this initial screening, as well as further storm sets added after discussion with CPRA and The Water Institute. These proposed sets were then evaluated using the complete CLARA v2.0 depth and damage models for all areas of the coast.

Results from the detailed coast wide depth and damage comparisons are presented in this section, including experimental design, setup, and results. Bias was calculated by comparing results from each subset against the outcomes from the full 446-storm reference set (Set 1 in Table 6-2), by grid point, at each annual exceedance probability. Summary maps and coast wide statistics were then developed, and the results were encoded into a Tableau-based interactive storm selection workbook (Appendix 5). This subsection then includes preliminary recommendations and a discussion of tradeoffs for CPRA to consider.

6.5.1 Experimental Design

For model development and testing, ARCADIS provided full 446-storm data sets representing current conditions and the 2012 Coastal Master Plan Less Optimistic, Future Without Action landscape scenario, respectively. To produce the flood depth and damage results for storm selection, all 446 storms from the Less Optimistic scenario were run through the flood model, and the statistical outputs generated by using all storms (Set 1 in Table 6-2) were used as a benchmark for comparison. Analysis focused on the Less Optimistic scenario rather than current conditions because the higher baseline level of risk allows more information about bias to be drawn from a wider range of return periods.

The ten tracks used in the 2012 Coastal Master Plan analysis are sometimes referred to as primary tracks, and were labeled E1 through E5 and W1 through W5 for tracks in the eastern and western halves of the coast, respectively. Secondary storm tracks correspond to paths in between the primary tracks and were denoted by a B at the end of the track name (e.g., track E1B). Tracks also vary by their angle of incidence made with the coastline upon landfall. Tracks with a mean landfall angle, as estimated using historic data, are referred to as central-angle tracks; those making landfall at angles 45 degrees less or greater than the mean angle are referred to as off-angle tracks. Similarly, a majority of storms in the 446-storm set have a forward velocity of 11 knots, referred to as the central value for v_f; faster- or slower-moving storms are sometimes called off-velocity storms.

The listed subsets were chosen to be collections of storms with easily interpretable and describable characteristics, to have variation in the total number of storms, and to have variation in the types of storms represented over the subsets. They were also chosen to avoid groups of storms that could cause identifiability or other performance issues in the response surface model. CPRA also identified a need for storm sets with fewer than 154 storms—and preferably fewer than 100 storms—that could be used to evaluate a range of individual structural protection projects during 2017 Coastal Master Plan model production using available computing resources.

Initial screening results (not shown) suggested that including higher-frequency storms with 975 mb central pressure improved statistical performance. By contrast, secondary storm tracks and storms with non-central values for forward velocity did not yield similar improvement and were generally not included in the final testing and results. The final sets tested in this analysis, including number of storms and a description of key characteristics, are shown in Table 6-2 below.

Table 6-2: Characteristics of Storm Sets Selected for Detailed Investigation.

Set	Storms	Description
1	446	Reference storm set
2	40	2012 MP storm set: 10 storm tracks, 4 storms per track that vary c_p and r_{max}
3	60	2012 MP storm set expanded to 5 storms per track that vary c_p and r_{max}, plus storms with 975 mb c_p and central values for r_{max}
4	90	2012 MP storm set expanded to 9 storms per track that vary c_p and r_{max}
5	90	7 storms per track (excludes 1 930 mb and 1 900 mb storm) with 975mb storms using extremal (rather than central) r_{max} values
6	92	Set 3, with 960 mb and 975 mb storms on off-angle tracks only in E1-E4
7	92	Set 3, with 960 mb and 975 mb storms on off-angle tracks only in W3-W4, E1-E2
8	100	All central-angle, primary-track storms with 11-knot v_f, plus 975 mb storms with central r_{max}
9	110	All central-angle, primary-track storms with 11-knot v_f, plus 975 mb storms with extremal r_{max}
10	120	All central-angle, primary track storms with 11-knot v_f, including 975 mb storms
11	154	Set 4, plus all 960 mb and 975 mb storms on primary, off-angle storm tracks

Results from the detailed screening are summarized below, with full analysis results across all grid points, annual exceedance probabilities, and storm sets considered made available separately through an interactive Tableau workbook.

6.5.2 Results

6.5.2.1 Flood Depth Bias and Variance Comparisons

Figure 6-8 summarizes the average coast wide 100-year flood depth bias (root mean squared error, y-axis) and coefficient of variation (point size) for each set, plotted against number of storms (x-axis). Colors indicate whether the set includes 975 mb storms, and shape indicates whether off-angle tracks are included. Bias is estimated relative to the flood depth results from Set 1, the reference set.

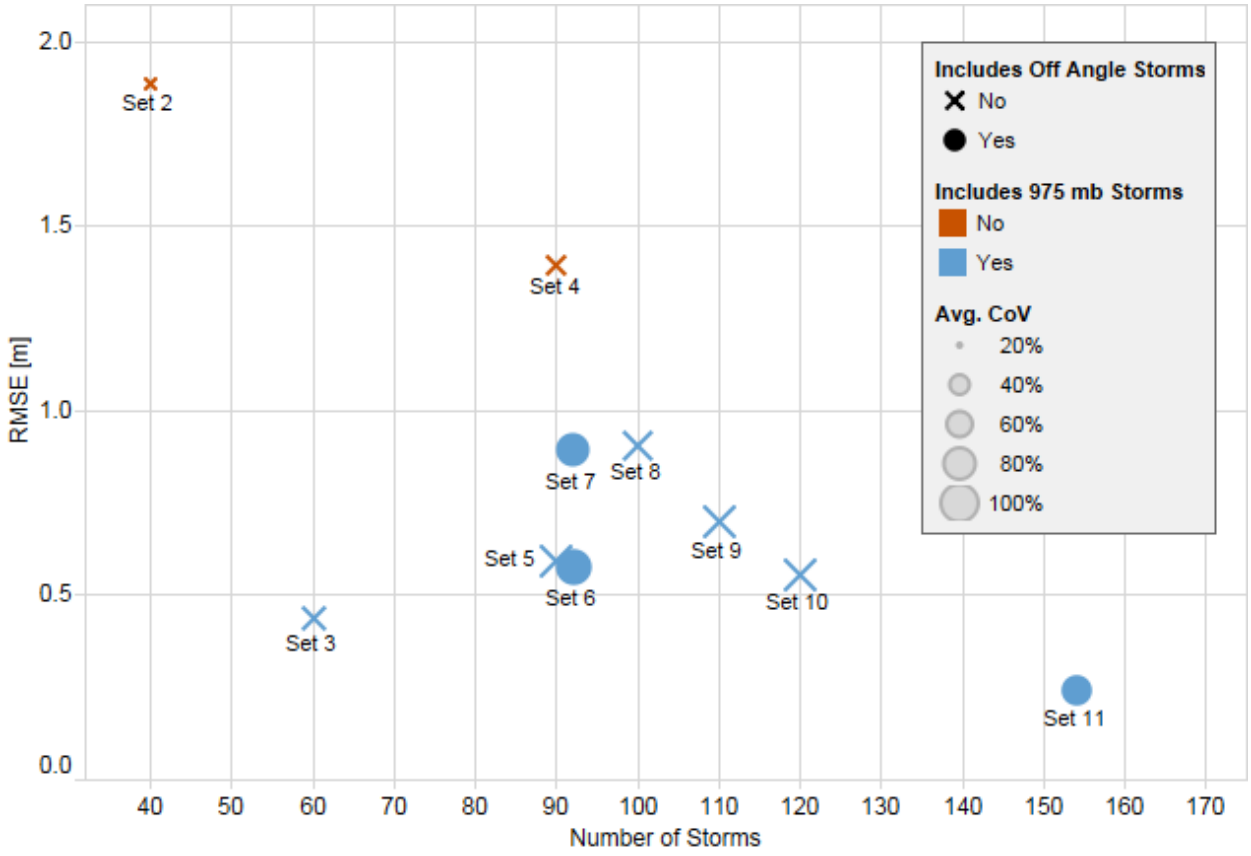

Note: Bias is calculated relative to Set 1, the reference set.

Figure 6-8: Average Coast Wide Bias and Variation by Number of Storms, 100-Year Flood Depths.

Summary results show that average flood depth bias by point at the 100-year interval varies from less than 0.25m to nearly 2.0m, depending on the storm sample. Substantial bias is observed for Set 2—the 2012 Coastal Master Plan set—compared with the other candidate sets tested. All additional sets with more than 40 storms improve upon the 40-storm results. In fact, increasing the number of storms to 60 (Set 3) leads to substantial improvement in itself, reducing average bias by more than a meter. Similar results are observed at other AEP levels.

Note: Bias is calculated relative to Set 1, the reference set.

Figure 6-8 suggests that in general, sets that include 975 mb storms generally outperform sets that exclude storms with these characteristics, even with similar numbers of storms included. The pattern is less evident when off-angle tracks are included, however, especially for sets in which only certain off-angle tracks were included (e.g., Sets 6 and 7).

Figure 6-9 below illustrates how the average bias, again measured by RMSE, changes for each storm subset at different return periods of the flood depth distribution. The x-axis shows the return period on a logarithmic scale, and the line thickness denotes the coefficient of variation as a measure of estimated uncertainty around the point estimates.

With few exceptions, such as Set 5, the relative order of performance across storm subsets is consistent over a wide range of return periods. Sets 2 and 4 are conspicuous in their poor average performance; neither set contains any storms with central pressures of 975 mb, illustrating the importance of including higher-frequency events in the training set. Interestingly,

this effect is still particularly apparent in the tail of the distribution beyond the 100-year AEP interval, indicating that exclusion of higher-frequency events from the response surface model also skews the model's predictive accuracy for more extreme synthetic storms.

In general, average bias is smaller at 50-year and more frequent return periods. This is due to the large number of points in which no flooding occurs for these exceedances. The absolute error is more likely to be small when the depth estimates themselves are small. Set 11, with 154 storms, outperforms the other sets across most of the distribution. Of the sets with fewer than 100 storms, Set 3 clearly shows the best performance in terms of average bias across the exceedance distribution.

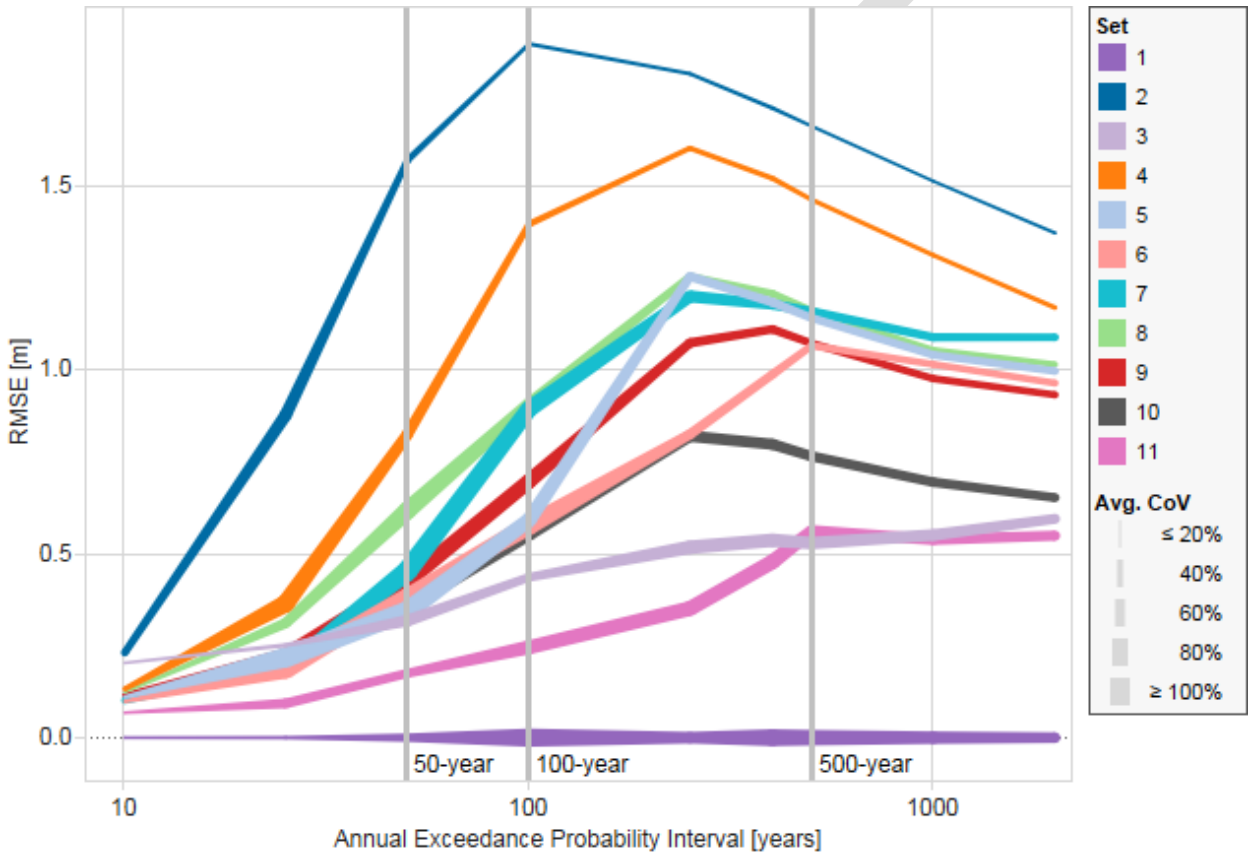

Figure 6-9: Average Bias and Variation by Exceedance.

The decline in bias at low-frequency (more extreme) AEP intervals observed in some sets is driven by points in enclosed areas, which comprise approximately 42 percent of the points with assets included in Figure 6-9 and approximately one-third of the total grid points. The hypothesis is that this relates to the level of protection levees are designed to provide; the peak bias will tend to occur at the point in the depth probability distribution where system fragility starts to play a large part in the flood dynamics, causing an upturn in the risk distribution at this point. Well beyond the designed level of protection, at 500-year and more extreme return periods, flood levels approach the crest heights of protection features on the system boundaries irrespective of the storm subset, which results in a lower average bias.

Figure 6-10 shows a sequence of maps to display the spatial patterns of bias for all storm sets tested, relative to Set 1, in the selected watersheds used for the initial storm selection screening. When examining the spatial distribution of bias, some interesting patterns emerge. The Set 2

results in Figure 6-10, showing the 2012 Coastal Master Plan 40-storm sample, shows a substantial overestimate of flood depths across nearly the entire study region. This effect occurs because of the types of storms excluded from Set 2. It only contains central-angle storms on primary tracks, and thus leaves out both 975mb and off-angle storms. For instance, Set 2 excludes off-angle storms that pass well to the east of New Orleans. These storms would tend to lower the estimated flood depth exceedances in St. Bernard Parish, so as a result Set 2 has positive bias in that region.

Set 3, which includes 60 storms, improves dramatically on the Set 2 results. Some positive bias is still noted in the western portion of the coast and many areas east of the Mississippi River, but the magnitude is notably lower than Set 2. In addition, Set 3 actually shows an underestimate of 100-year flood depths compared with Set 1 in some enclosed areas, including the East Bank of the New Orleans HSDRRS and Plaquemines Parish.

Set 11 yields the lowest overall bias, and similarly shows balanced results coast wide when looking at mapped outcomes. Positive bias is still observed in the western parishes, but again with a lower magnitude than Sets 2 or 3. There are some instances where the 100-year flood depth estimates are both positively and negatively biased within the same watershed. When these differences in flood depths are translated into damage, the coastal and parish-level results are more similar to Set 1, with the values averaging out as grid points are aggregated to larger spatial units.

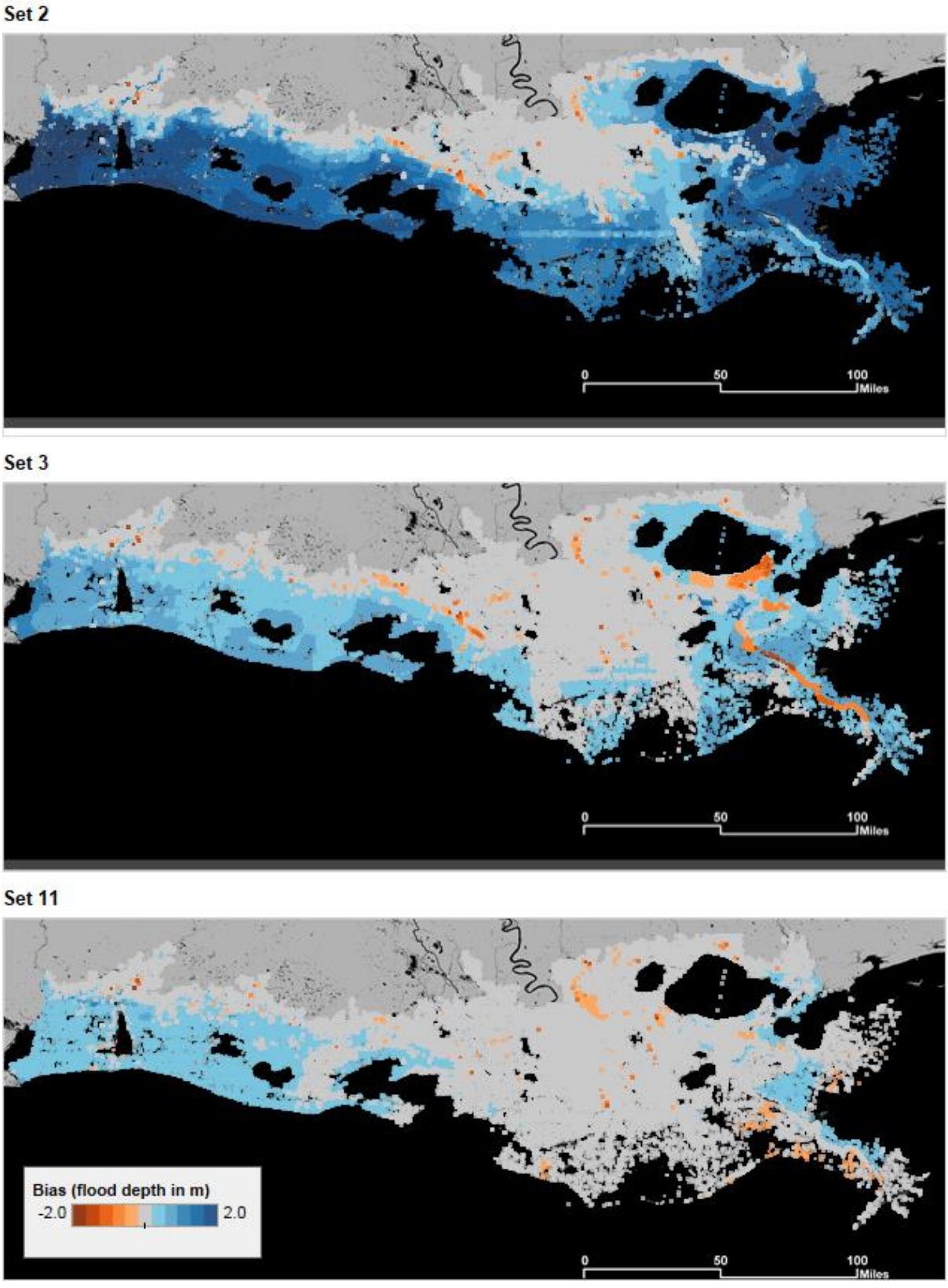

Figure 6-10: Map of Bias by Grid Point for Sets 2, 3, and 11, 100-Year Flood Depths.

Figure 6-11 focuses in on differences in storm set performance for enclosed and unenclosed areas. Specifically, results are split out for enclosed points into the East and West Bank areas of the Greater New Orleans HSDRRS, respectively, as well as other non-HSDRRS enclosed areas and unenclosed points.

At the 500-year AEP interval shown here, results are most uncertain and show the greatest variance in the East and West Bank areas. Except for Set 2, all sets considered yield an average bias of approximately 0.3m (1 foot) or less in unenclosed locations; similarly, Sets 3 through 11 also result in less than 1m of bias in non-HSDRRS enclosed areas (e.g., Larose to Golden Meadow, Slidell), with many sets also yielding less than 0.3m in these areas.

Figure 6-11: Average Bias and Variation, 500-Year Flood Depths (All Points, Split by Location).

The figure confirms that Set 11 is the best or near-best performer in terms of bias across all enclosed areas. For sets with fewer than 100 storms, performance depends on HSDRRS location. For instance, similar to what was observed in Figure 6-10, Set 3 yields a downwards average bias in the East Bank HSDRRS system, but the magnitude is smaller at the 500-year level than from other sets. Set 3 performs substantially worse, however, on the West Bank, as do most other sets considered.

By contrast, Set 7 was specifically selected to improve performance in the West Bank of HSDRRS. This set adds additional storms to Set 3, including off-angle tracks for the middle of the coast with landfall locations observed to have the greatest effect on this portion of HSDRRS. The results bear this out: Set 7 is the best overall set in terms of bias in the West Bank, slightly better than the larger Set 11. However, Set 7 produces much greater bias in the East Bank HSDRRS, and is among the worst performers when looking at enclosed areas other than the West Bank.

6.5.2.2 Damage Bias Comparisons

An understanding of how the potential bias from different promising storm subsets in terms of flood depth translates to damage bias was next sought. Figure 6-12 below shows the same spatial breakdown as Figure 6-11, for instance, but instead showing bias in terms of damage (EAD, median results) estimated by the CLARA v2.0 damage model. Set 2, which yields very high EAD bias overall and will not be recommended for the 2017 Coastal Master Plan analysis, is omitted from the figures below for clarity.

Figure 6-12 confirms the performance noted above, with roughly the same overall ranking of sets by EAD bias as with flood depths. Set 11 is the best overall performer using the median EAD results, but Set 3 shows good performance as well while using many fewer storms (60 versus 154). Set 3 is also the only set with fewer than 100 storms that does not produce a substantial overestimate of damage in the East Bank HSDRRS area; instead, as expected this set shows a slight downwards bias at the 500-year interval.

Increasing the number of storms from 60 up to 90-110 does not substantially improve EAD performance for enclosed areas, except in the West Bank HSDRRS. In this area, Set 7 produces nearly zero EAD bias compared to the 446-storm set, whereas all other sets except for Set 11 overestimate EAD by at least $1 billion.

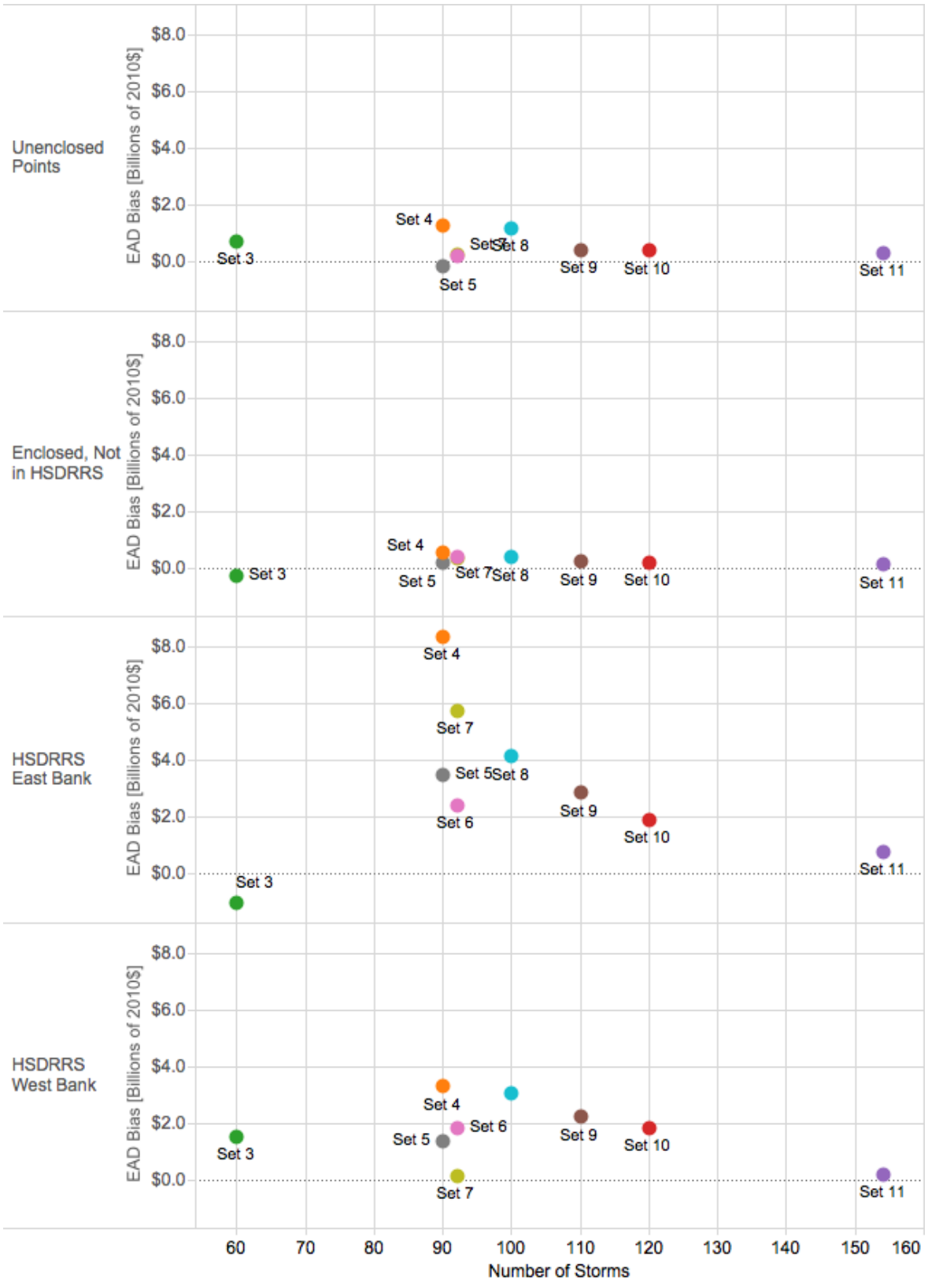

Figure 6-12: EAD Bias (50th Percentile, All Points, Split by Location).

Similarly, Figure 6-13 shows a summary by parish of bias in EAD. Some storm sets produce large bias in selected parishes. For example, Set 4 produces nearly three times as much damage in Jefferson Parish as the 446-storm comparison set. In turn, this leads to a substantial upwards bias in coast wide EAD because Jefferson Parish contains such a large concentration of assets (Figure 6-14).

Once again, Set 11 is the best performing subset using this measure. The maximum bias for any parish from Set 11 is just over 100 percent in St. Bernard Parish, which includes relatively few assets. Each of the other subsets have several parishes with biases as large or larger. Sets 3 and 11 are the only subsets tested in the detailed analysis that perform well in Orleans and Jefferson parishes. Of the sets with fewer than 100 storms, Set 3 yields the lowest percentage of EAD bias by parish at the 50th percentile, though still somewhat greater than that noted in Set 11. EAD performance across non-HSDRRS parishes, by contrast, is similar across nearly all sets tested in this round of analysis. Note that Set 7 shows EAD bias in Jefferson Parish because the parish straddles both banks of the HSDRRS system.

	Set								
Parish Name	3	4	5	6	7	8	9	10	11
Acadia	7%	9%	3%	5%	14%	9%	1%	3%	14%
Ascension	25%	35%	10%	18%	7%	33%	18%	18%	10%
Assumption	2%	5%	-4%	-5%	-4%	3%	-1%	-2%	-4%
Calcasieu	26%	28%	11%	26%	44%	30%	19%	20%	25%
Cameron	-1%	0%	-4%	-1%	4%	0%	-2%	-2%	2%
Iberia	2%	5%	-3%	3%	7%	5%	0%	1%	8%
Jefferson	37%	314%	134%	119%	151%	225%	167%	121%	32%
Jefferson Davis	10%	15%	0%	10%	20%	15%	9%	9%	16%
Lafourche	-5%	6%	-3%	3%	0%	4%	-1%	1%	0%
Livingston	13%	18%	7%	7%	3%	17%	10%	10%	5%
Orleans	-41%	450%	172%	144%	249%	214%	133%	97%	29%
Plaquemines	-7%	48%	28%	25%	-6%	45%	30%	33%	3%
St. Bernard	115%	444%	241%	313%	284%	325%	234%	192%	106%
St. Charles	7%	33%	12%	7%	15%	15%	10%	7%	4%
St. James	-9%	7%	-21%	-10%	-19%	6%	-18%	-19%	-24%
St. John the Baptist	21%	29%	9%	11%	5%	28%	18%	18%	12%
St. Martin	0%	3%	-5%	-2%	-3%	2%	-1%	-2%	-2%
St. Mary	-9%	9%	-5%	10%	4%	7%	2%	1%	1%
St. Tammany	12%	18%	10%	9%	9%	17%	12%	12%	10%
Tangipahoa	12%	16%	6%	6%	2%	15%	9%	9%	5%
Terrebonne	6%	12%	-3%	3%	0%	11%	3%	3%	2%
Vermilion	7%	9%	1%	7%	8%	9%	4%	4%	8%

EAD Bias (percent)

-100% 400%

Figure 6-13: Bias in Expected Annual Damage by Parish (percent), 50th percentile.

The results discussed so far have portrayed the median (50th percentile) outputs over the sampling design, with the coefficients of variation in some plots giving some information about the parametric variation across different sets. Figure 6-14 illustrates the distribution of EAD in another way. The y-axis indicates the bias in coast wide EAD relative to the full 446-storm Set 1;

the three points for each subset, from bottom to top, represent the bias associated with the 10th, 50th, and 90th percentile values, respectively, of EAD.

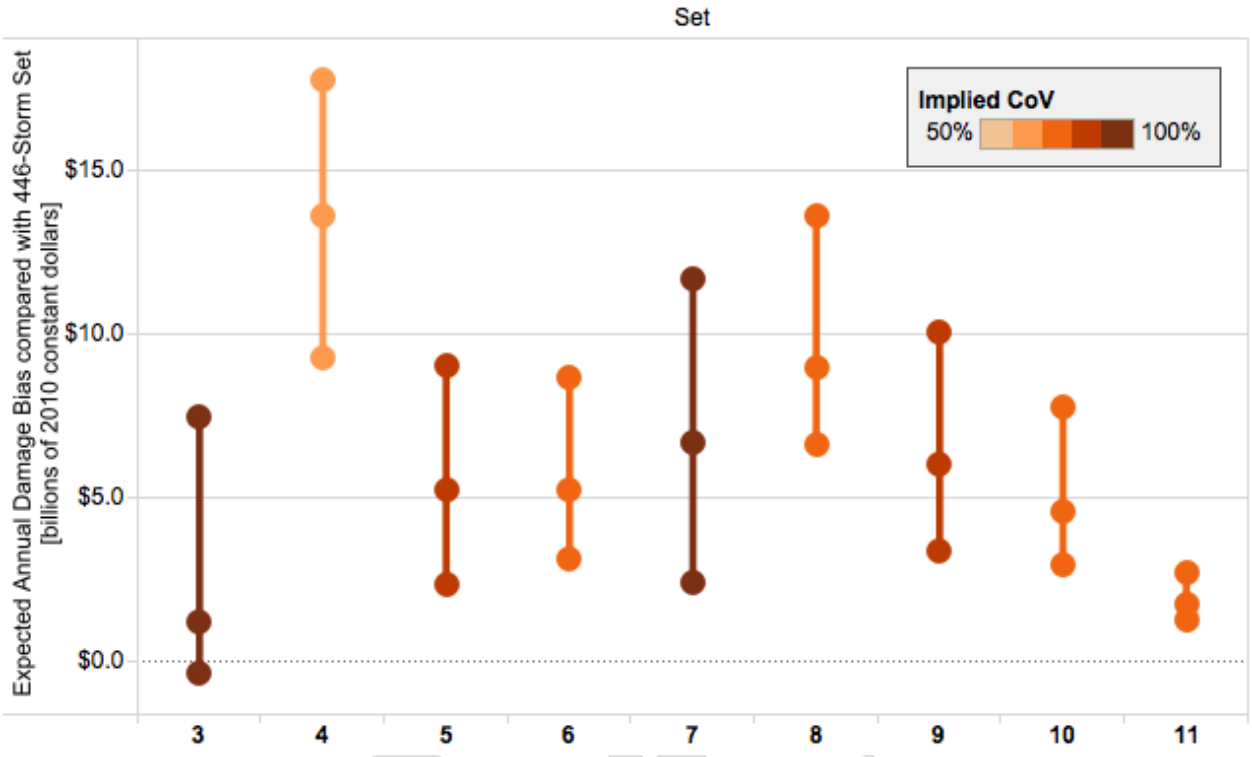

Figure 6-14: Coast Wide Bias in Terms of Expected Annual Damage (billions of 2010 dollars).

Again, the primary takeaway is that Set 11 yields a much smaller variation in bias over the experimental design tested, compared to the other subsets. Considering only sets with fewer than 100 storms, Set 3 is the best performer at the median, but includes a wider range of results across the parametric distribution, and it has performance comparable to Sets 5-11 when comparing the 90th percentile results. However, Set 3 is the only subset that actually crosses zero bias coast wide in its results, largely due to the underestimate of East Bank HSDRRS damage, with all other subsets consistently overestimating EAD relative to the 446-storm set.

6.5.3 Discussion

The storm selection analysis shows a tradeoff between the number of storms and the resulting bias when compared with the reference set of 446 storms. Results show that nearly all storm sets tested produce lower bias when compared with the 2012 Coastal Master Plan 40-storm set (Set 2). Substantial improvement is noted when storms with 975-mb central pressure were included, as well as with the addition of off-angle storms in some cases.

Of the subsets tested, Set 11 (154 storms) appears to yield the best balance of results. This set shows relatively low bias compared with the reference set in terms of both flood depth and damage, no concerning spatial patterns of bias, and reasonable performance in enclosed areas (particularly Greater New Orleans).

However, Set 3 produces the best results among the smaller sets, and, given the much smaller number of storms required and notable overall performance, is also a potential candidate for

the comparison of individual structural risk reduction projects during model production. If CPRA is concerned about performance on the West Bank HSDRRS system from Set 3, another option would be to use Set 7, which includes 92 storms, when considering projects that affect the West Bank HSDRRS. Set 3 is a proper subset of Set 7, and the Set 3 subset of storms could be extracted from Set 7 for use in non-West Bank areas to improve the overall results.

CPRA will need to take into account the results of this analysis, together with cost and runtime considerations for the surge and wave hydrodynamic models, in order to select a suitable storm set for the 2017 Coastal Master Plan analysis.

6.6 CLARA v2.0 Test Results with Uncertainty

The final discussion in this section provides summary flood depth and damage results from the analysis conducted with the testing version of CLARA v2.0. These results were created from the 446-storm set for current conditions and the Year 50 Less Optimistic future scenario, and reflect the default CLARA v2.0 sample sizes discussed in Section 6.4. Selected flood depth results are shown separately for unenclosed areas and enclosed areas, respectively, ranging from the 10-year to the 2,000-year AEP interval. Parametric uncertainty is represented with 10th, 50th, and 90th percentile results by interval. Damage results are shown coast wide at the same AEP intervals and percentile values, and also include coast wide summaries of EAD with uncertainty.

The figures shown below are intended to be a snapshot of the testing results, and to provide the reader with a sense of the variation in results across the new parametric uncertainty calculations and CLARA v2.0's revised fragility scenarios. Results remain preliminary, however, as part of the model improvement and testing process. As a result, brief explanations for the setup of each figure are provided, but policy implications are not discussed.

6.6.1 Flood Depth in Unenclosed Areas with Parametric Uncertainty

The first set of results displays flood depths in unenclosed areas of the coast. With the broader training sample of storms used, a 10-year AEP interval with CLARA could be estimated for the first time. This new 10-year result across the 10th, 50th, and 90th percentile estimates in the Less Optimistic future scenario is shown in Figure 6-15, with each pane showing one percentile outcome.

Next, the primary AEP intervals used in the 2012 Coastal Master Plan analysis—50-, 100-, and 500-year flood depth estimates—at the 90th percentile estimate are shown, showing a more extreme value from the estimated range. Specifically, Figure 6-16 shows these results under current conditions, Figure 6-17 has the same display for the Year 50 Less Optimistic future without action scenario (FWOA), and Figure 6-18 shows the change in flood depths between current and future conditions at these intervals, also at the 90th percentile.

Figure 6-19 compares the results from this analysis to the original results produced with CLARA v1.0 during the 2012 Coastal Master Plan analysis. To perform this comparison, each grid point was assigned the value from the nearest 2000 census block centroid from the 2012 analysis. The median results from the CLARA v2.0 test analysis are shown to represent central tendency and to facilitate this comparison, as the 2012 analysis results can be thought of as average values. In this figure, blue shading indicates where the 2012 results showed larger flood depths than the CLARA v2.0 results, while red shading shows where depth values show an increase with the new model version.

Finally, Figure 6-20 provides a detailed snapshot of one grid point in CLARA v2.0. A sample point was selected in the town of Houma and shows the entire AEP curve for this point, ranging from the 10- to 2,000-year intervals, under both current and FWOA conditions. Median results are shown with the blue line, and uncertainty around this estimate—the 10th and 90th percentile estimates—is shown with the light orange bounds. The 2012 Coastal Master Plan results are also included (green points) at the 50, 100, and 500-year intervals for this location to provide a better understanding of how the previous results related to the new estimates with parametric uncertainty bounds.

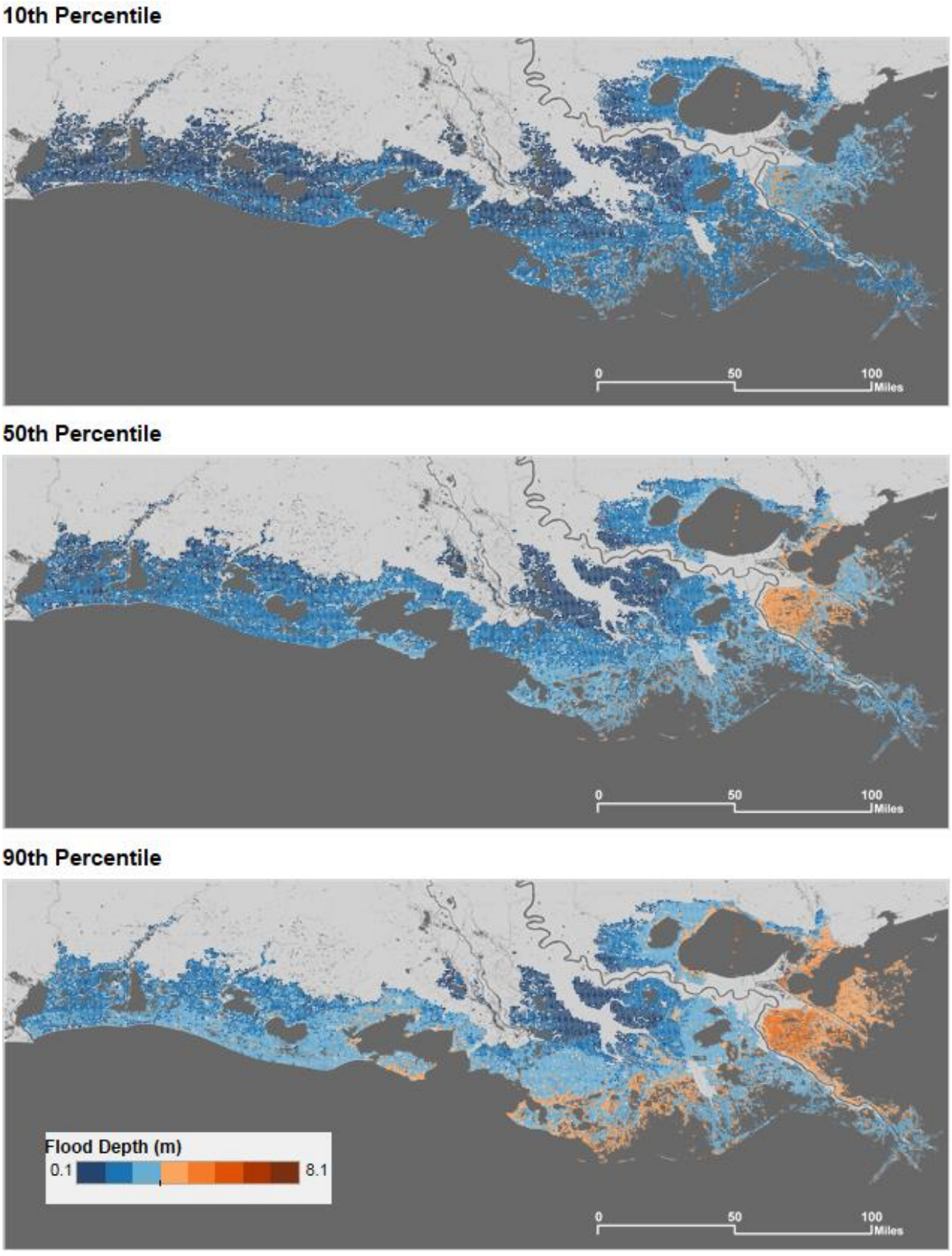

Note: Only grid points with positive flood depths shown.

Figure 6-15: 10-Year Flood Depths by Grid Point, Year 50 FWOA Less Optimistic Scenario.

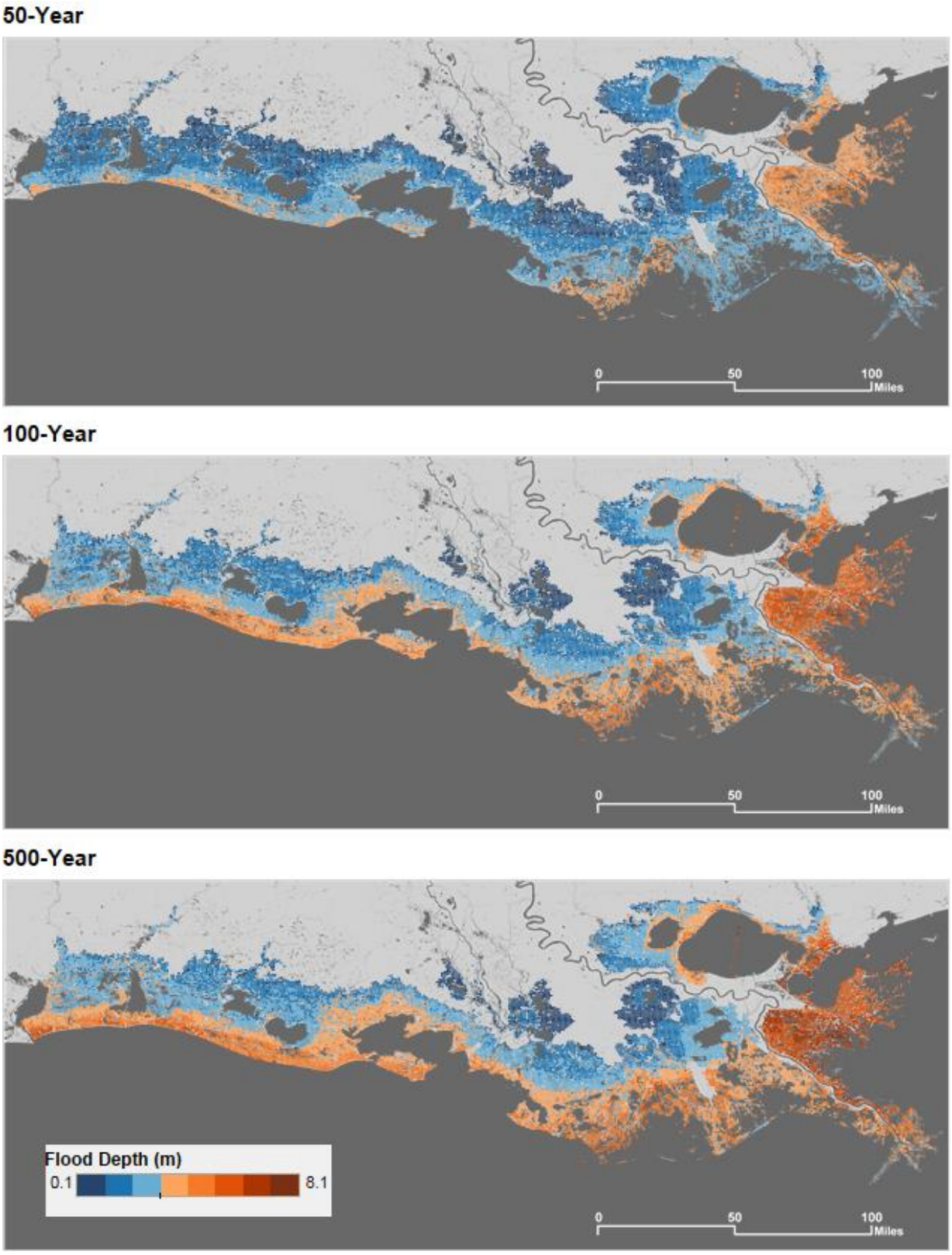

Note: Only grid points with positive flood depths shown.

Figure 6-16: 90th Percentile Flood Depths by Exceedance, Current Conditions.

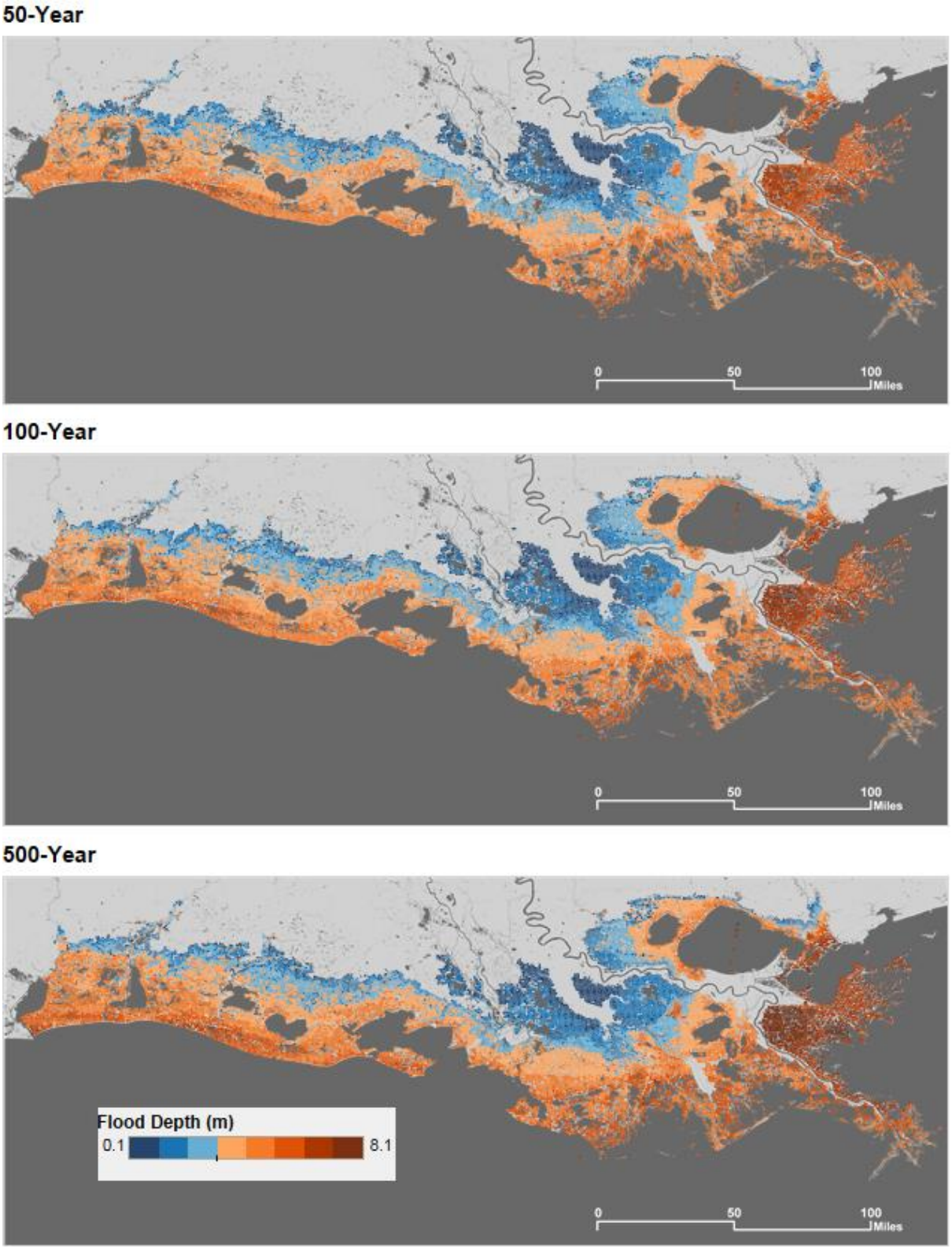

Note: Only grid points with positive flood depths shown.

Figure 6-17: 90th Percentile Flood Depths by Exceedance, Year 50 FWOA Less Optimistic Scenario.

50-Year

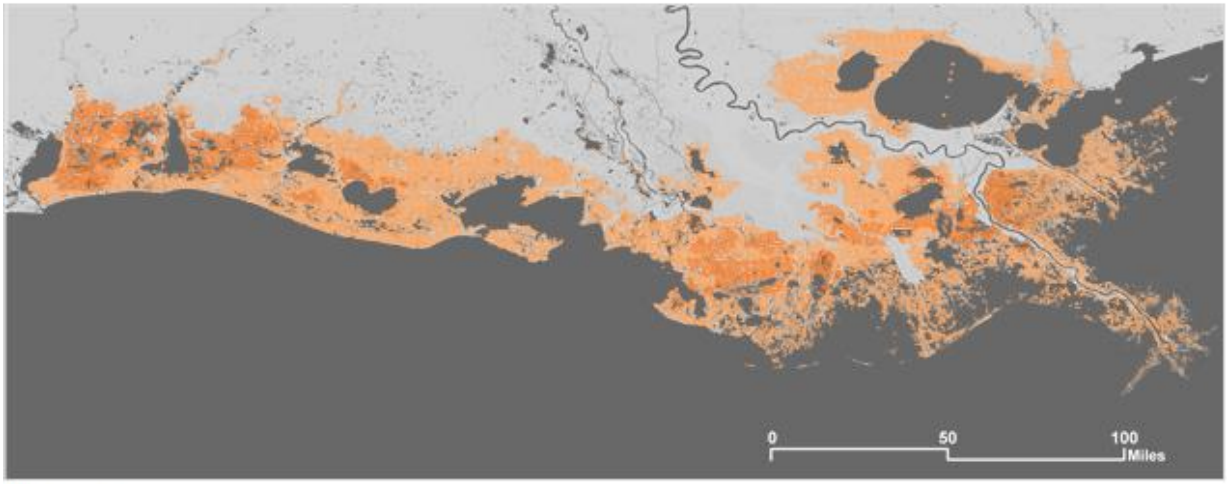

100-Year

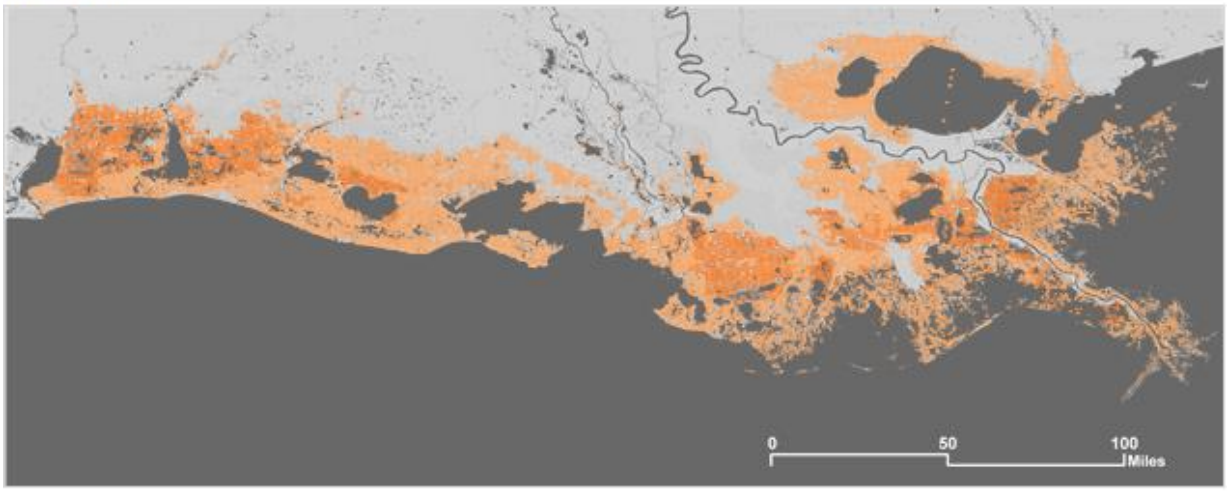

500-Year

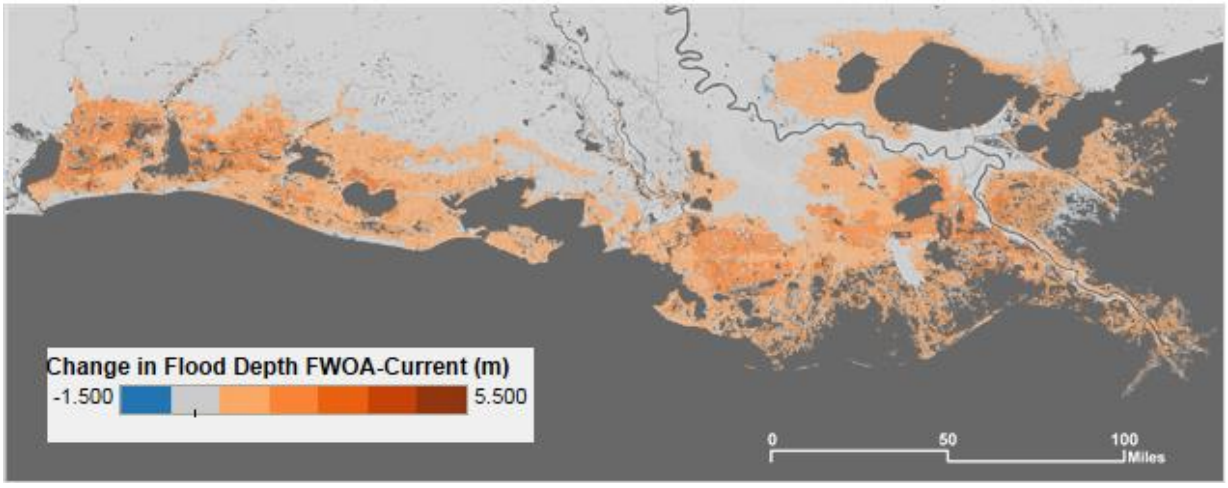

Note: Only grid points with positive flood depths shown.

Figure 6-18: Change in 90th Percentile Flood Depths by Exceedance (FWOA-Current Conditions).

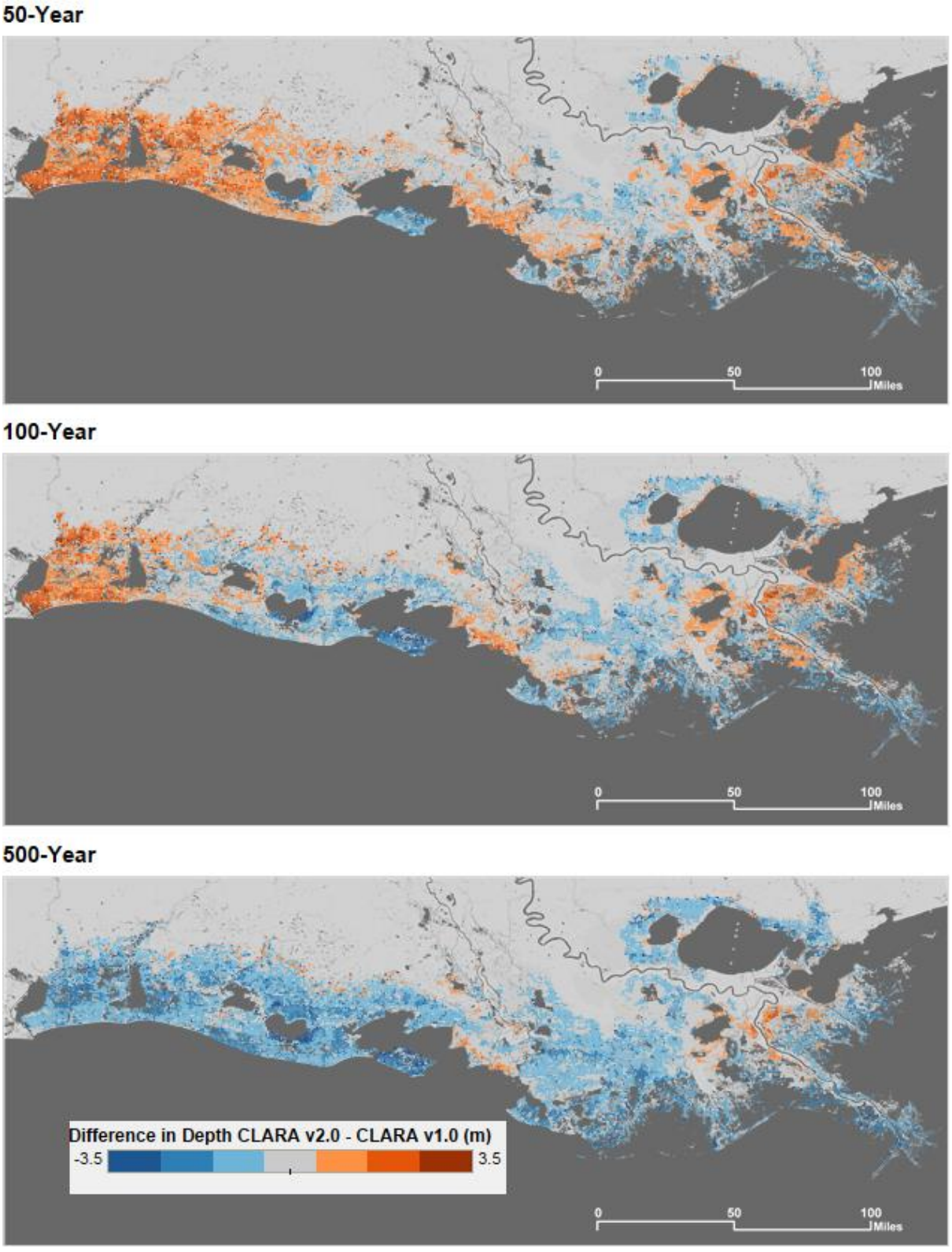

Note: Only grid points with positive flood depths shown.

Figure 6-19: Difference in Flood Depth between CLARA v2.0 (50th Percentile) and CLARA v1.0, Year 50 FWOA Less Optimistic Scenario.

Note: Orange lines show the 10th and 90th percentiles surrounding the median (blue line). Green dots show point value estimates for this location calculated with CLARA v1.0 in the 2012 Coastal Master Plan analysis.

Figure 6-20: Flood Depth Annual Exceedance Probability Curve at a Sample Point Near Houma.

6.6.2 Flood Depths in Enclosed Areas with Parametric Uncertainty

Finally, this subsection provides a similar snapshot of flood depth results for enclosed areas. The tests described in previous sections examined settings and inputs that govern how the model operates. In both cases, results were compared to some reference case used as a benchmark. The analysis centered around the performance of a particular model setup relative to the more complex benchmark run. By contrast, these scenario comparisons are focused on the actual risk estimates produced by different model scenarios. The primary differentiator between runs is the fragility scenario used. The full 446-storm set was run, under both current conditions and in the Less Optimistic future scenario, using five different fragility curve assumptions. Each of the four fragility curves described in Section 4 was run, along with a case in which no breaches were allowed to occur.

This resulted in a set of 10 model runs. For computational tractability during the testing phase, each run used a sample size of 50 for the exterior Monte Carlo, interior overtopping and fragility Monte Carlo, Markov chain Monte Carlo, and bootstrapping simulations. The results of these initial runs represent draft estimates of current and future risk. The goal is to display variation due to both parametric uncertainty and across the range of fragility scenarios described in Chapter 4. Both figures provided below show the 500-year AEP interval in the Less Optimistic FWOA scenario. In addition, for this analysis interior pumping was set at 50 percent of rated capacity, the current default setting in the model.

The first plot (Figure 6-21) shows results from the MTTG-Low fragility scenario for all enclosed areas, divided by pane into the 10th, 50th, and 90th percentiles. This breakdown makes clear that

variation in flood depth can occur across the parametric uncertainty range when holding other factors constant, depending on the exceedance probability and scenario considered.

Next, a more detailed snapshot of Greater New Orleans in the Less Optimistic future scenario is provided. Figure 6-22 shows 90th percentile results from each of the four new fragility scenarios. As expected, substantial variation between scenarios is evident here, confirming the need for a range of fragility scenarios when assessing risk reduction project performance and benefits for the New Orleans HSDRRS.

10th Percentile

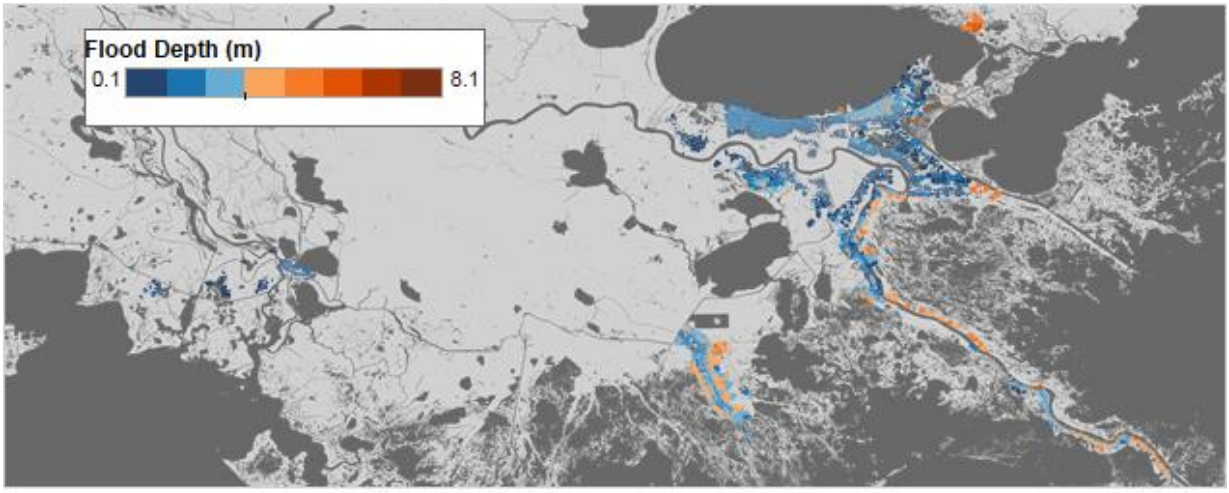

50th Percentile

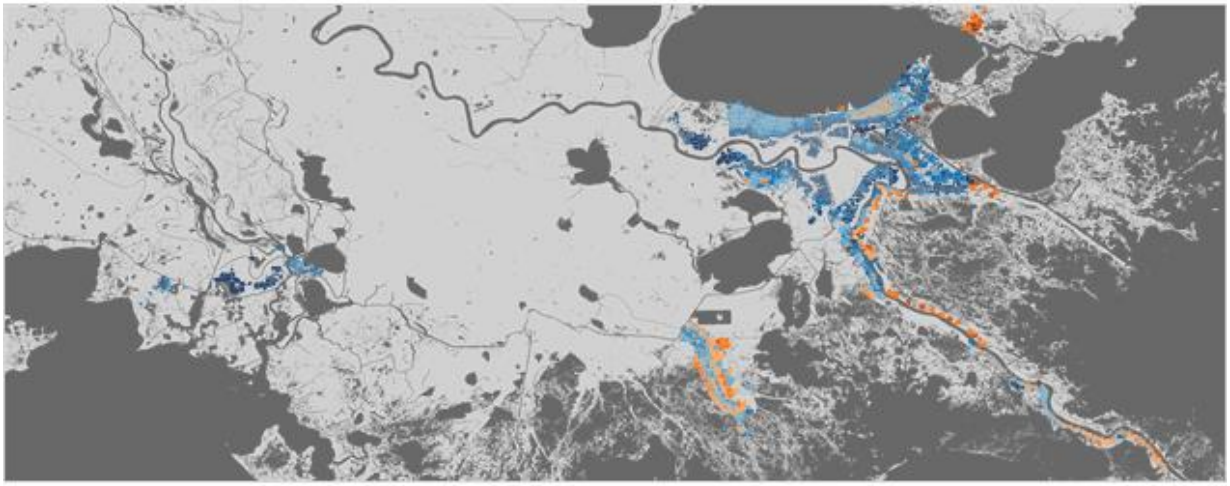

90th Percentile

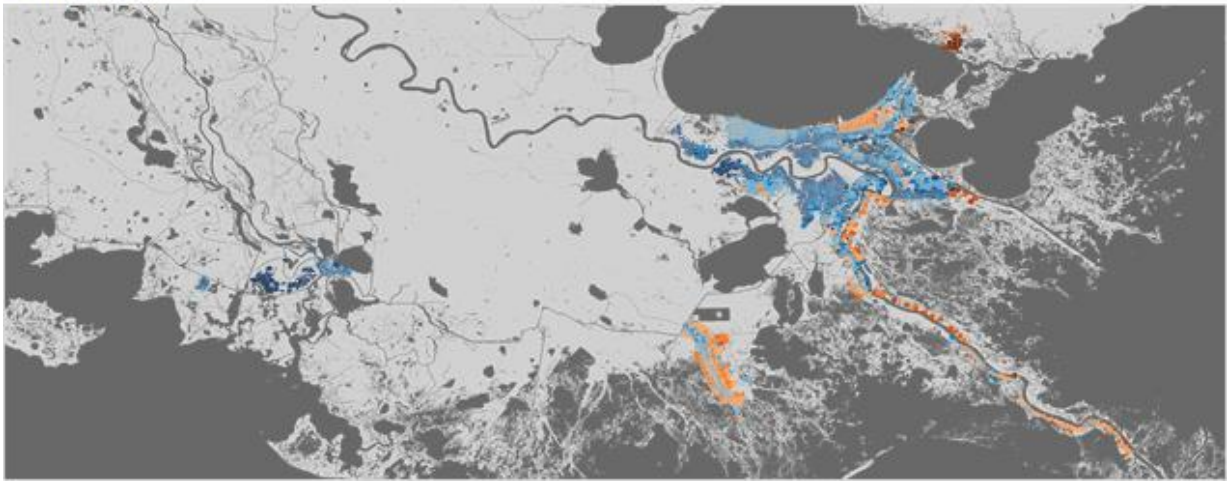

Note: Only grid points with positive flood depths at the 90th percentile shown.

Figure 6-21: 500-Year Flood Depths, MTTG Low Fragility, Year 50 FWOA Less Optimistic Scenario.

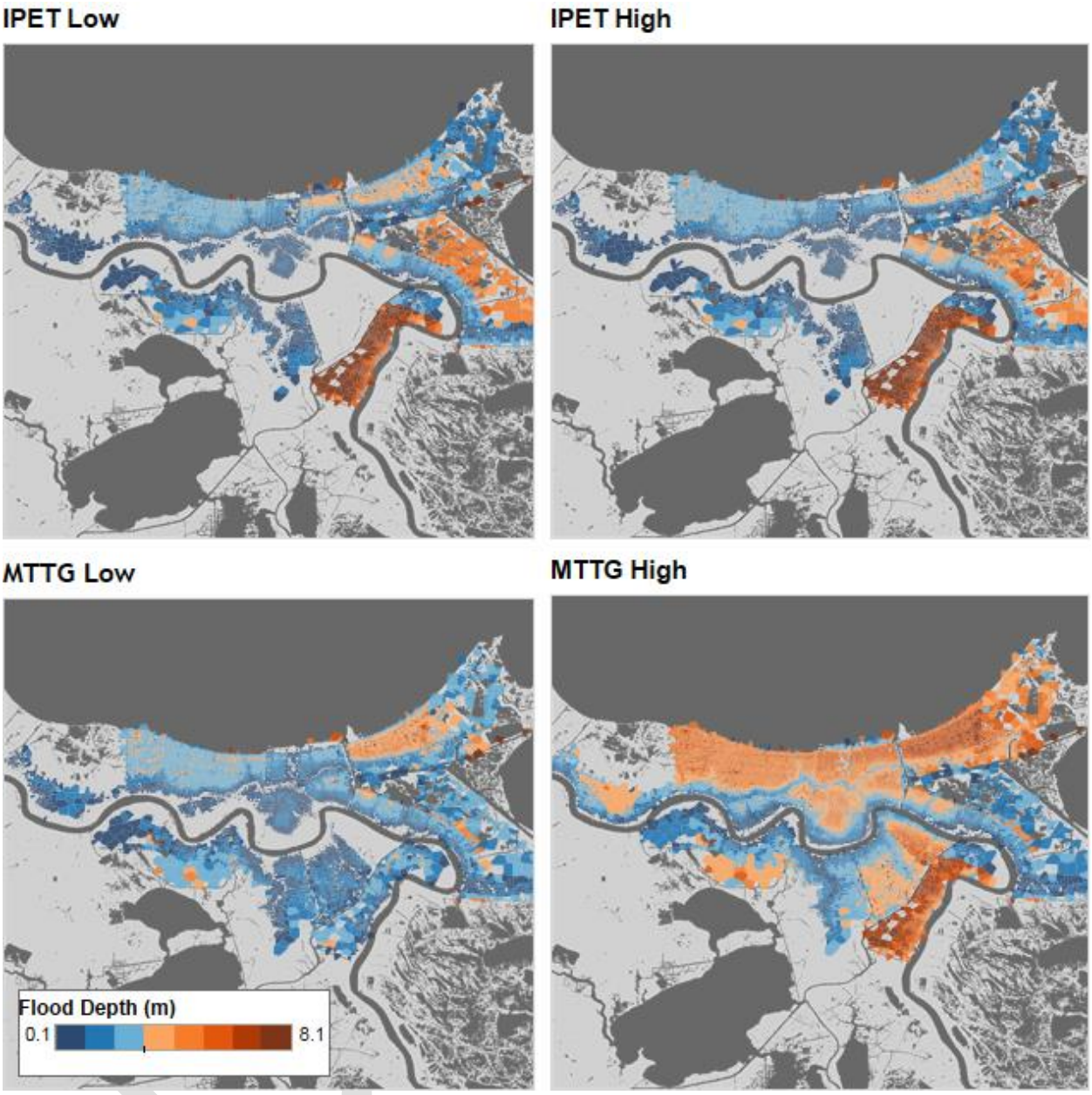

Note: 90th percentile values shown at grid points with positive flood depth.

Figure 6-22: 500-Year Flood Depths by Fragility Scenario in Greater New Orleans, Year 50 FWOA Less Optimistic Scenario.

6.6.3 Flood Damage with Parametric Uncertainty

Lastly, this subsection shows summary results with uncertainty produced with the CLARA damage model. The same caveats noted above apply in this section. Figure 6-23 shows an estimate of the damage AEP curve summed across the entire coast under current (left pane) and future (right pane) conditions, under the MTTG Low fragility scenario. The median is shown with the blue line, while the percentile bounds are again indicated in light orange. This plot shows the dramatic increase in damage from current conditions to the Less Optimistic future scenario. It

also reveals the wide range of possible outcomes at more extreme intervals emerging from the parametric uncertainty analysis. For instance, the 1,000-year coast wide damage AEP estimate ranges from $475 billion (10th percentile) to $875 billion (90th percentile) in the Year 50 Less Optimistic FWOA scenario.

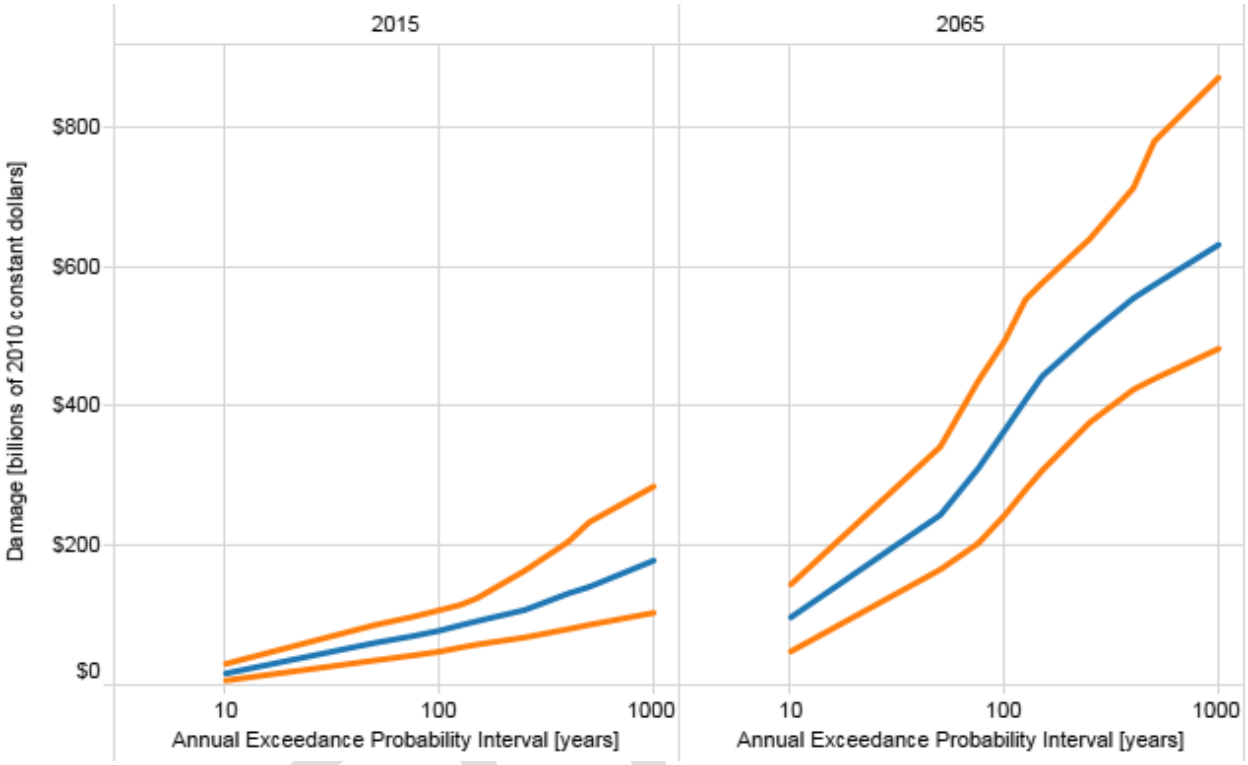

Note: MTTG Low fragility scenario shown.

Figure 6-23: Sum of Coast Wide Damage by AEP Interval, Current and Future Conditions.

Figure 6-24 instead shows damage results in terms of EAD. This figure shows three maps of EAD by grid point, under current conditions (top pane), the Less Optimistic FWOA scenario (middle pane), and the change from current to future conditions in this scenario (bottom pane). 90th percentile results are shown, again assuming the MTTG Low fragility scenario. This map mirrors the results shown previously in Section 3.4 (see Figure 3-1, for example)—only grid points with substantial assets in place show substantial average annual damage using this metric.

Finally, several barplot summaries of coast wide EAD (Figure 6-25) in current and FWOA conditions in two different fragility scenarios, bracketing the most optimistic (IPET Low) and most pessimistic (MTTG High) approaches are shown. The barplots are also stacked to show the relative contribution from each asset class included, with commercial, industrial, and single family residential assets contributing the majority of damage across cases. This plot again shows the dramatic increase in EAD that could occur over the next 50 years, as well as the range of outcomes produced by the divergent fragility approaches.

Current Conditions

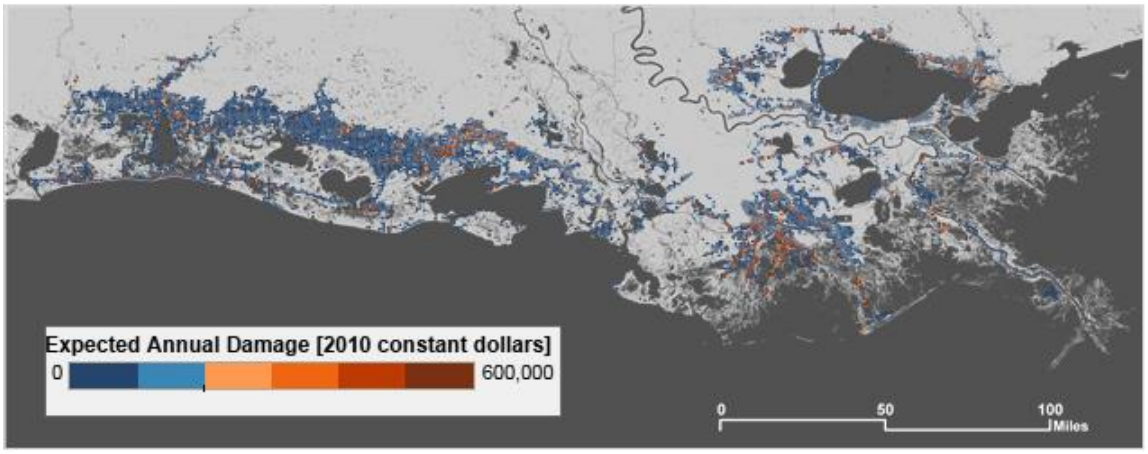

Year 50 FWOA Less Optimistic Scenario

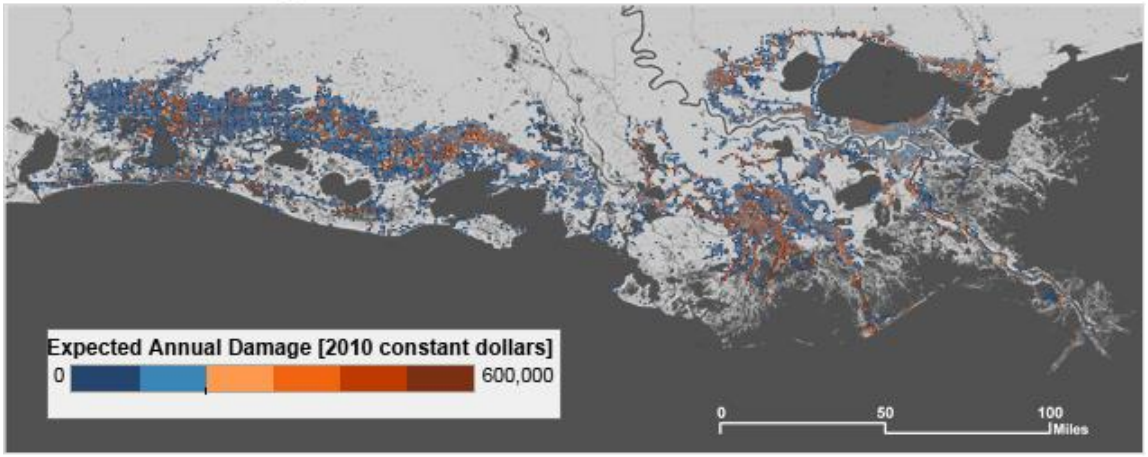

Change in EAD (FWOA - Current Conditions)

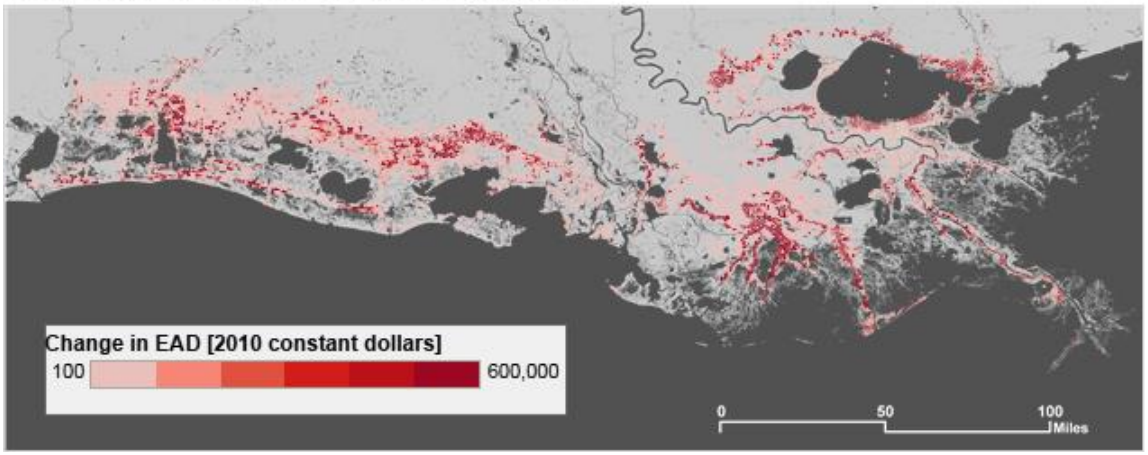

Note: MTTG Low fragility scenario shown at the 90th percentile.

Figure 6-24: Current, Future, and Change in EAD over Time.

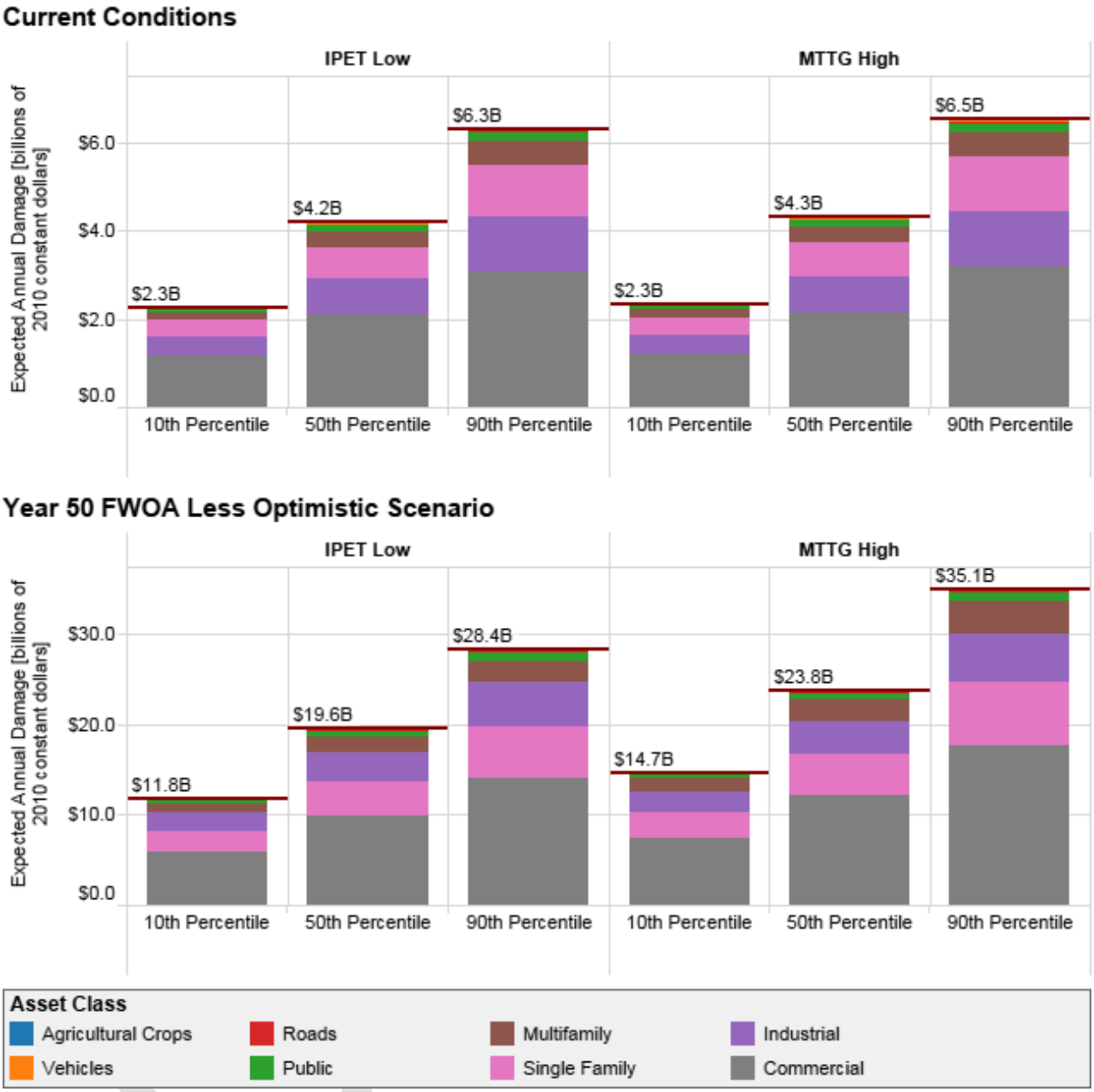

Figure 6-25: Coast Wide EAD in Two Fragility Scenarios, All Percentiles, Current and Future Conditions (billions of 2010 constant dollars).

As discussed in Section 3.1.4, some types of critical infrastructure are not included in damage calculations. Table 6-3 is an example of the model outputs for critical infrastructure, showing the number of assets inundated to 1 ft (0.3m) or more at the 100-year return period. Results can be generated by parish, as shown in Table 6-3; alternatively, Table 6-4 aggregates the asset counts over the entire Louisiana study region but compares results over multiple return periods. Both tables represent inundation in the Year 50 FWOA, Less Optimistic scenario, using the MTTG Low fragility assumption for enclosed areas. The color of text in Table 6-4 denotes the proportion of the total number of assets of each type that are inundated.

Table 6-3: Number of Critical Infrastructure Assets Inundated by Type and Parish (1% AEP; Year 50 FWOA, Less Optimistic Scenario, MTTG Low Fragility Assumption).

Parish	Airport	Electric Power Plant	Electric Substation	Gas Proc.	Gov't/ Military	LOOP	LNG	Manuf./ Chem.	Nuclear Power	Port	Petrol. Pump Station	Refinery	Sewerage	Strat. Petrol. Reserve	Water Supply
Acadia			0								1				
Ascension	1		1								1		0		0
Assumption	0		1	1				2							
Calcasieu	6	4	12	3		1		5			3	3	2		
Cameron	17	2	7	11		1		1		1	2		1	1	
Iberia	3	2	5	2				1		2	0		0		
Jefferson	6	1	7	1				1			3	0	0		
Jeff. Davis	2		0									1			
Lafayette	0														
Lafourche	8	0	7	3			2	3		1	9		2		
Livingston			1												
Orleans	2	2	4		0			1		0			1		1
Plaquemines	16	4	4	3	0			0		1	3	2			
St. Bernard	0	0	2	2						0		0	0		
St. Charles	0	0	2	1				0	0		1	0	0		
St. James	0	1	2								0	0			
St. John the Baptist	1	0	2	0				1				0			
St. Martin		1	1								1		1		
St. Mary	13	6	4	5				4		1	0		0		
St. Tammany	2	1	5										1		0
Tangipahoa	1		0												
Terrebonne	8	2	7	6							1				
Vermilion	14	1	6	15						1	3				
Grand Total	**100**	**27**	**80**	**53**	**0**	**2**	**2**	**19**	**0**	**7**	**28**	**6**	**8**	**1**	**1**

Table 6-4: Number of Critical Infrastructure Assets Inundated by Type and Return Period

Critical Infrastructure Type	50-year	100-year	500-year
Airport	95	100	116
Electric Power	20	27	36
Electric Substation	60	80	112
Gas Processing	51	53	55
Government/Military	0	0	2
LNG	2	2	2
LOOP	2	2	2
Manufacturing/Chemical	16	19	22
Nuclear	0	0	0
Port	7	7	7
Pump Station	27	28	29
Refinery	5	6	7
Sewerage	7	8	14
Strategic Petroleum Reserve	1	1	1
Water Supply	0	1	1

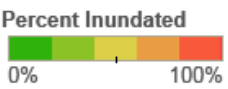

Note: Year 50 FWOA, Less Optimistic Scenario, MTTG Low Fragility Assumption shown.

6.7 Summary

This section described the results from a series of testing and sensitivity experiments conducted by the RAND Team designed to gain insight into the performance of the new CLARA v2.0 model. These experiments were also designed to inform modeling decisions to be made by CPRA, the MDT, and the CLARA development team leading into the production phase of the 2017 Coastal Master Plan analysis. Additional steps based on these results, however, will emerge from subsequent CPRA and MDT discussion and deliberations.

7.0 Model Comparisons: Hurricane Isaac

The original development of the CLARA model did not include a validation of the model using a historically observed storm. The lack of relevant, available data and the development timeline for the 2012 Coastal Master Plan precluded such an analysis. To effectively compare depth and damage results from CLARA to an observed event, a validation approach would require as model inputs accurate representations of a past storm event's surge and wave characteristics, past landscape and levee configurations, and past inventories of economic assets. Representing all of these elements in CLARA would have entailed a significant effort to reconstruct historical conditions. For example, the levee configurations and crest height data available for use by the 2012 Coastal Master Plan represented an upgraded New Orleans HSDRRS that included reconstruction projects that were either under way or funded by 2012. The 2012 system is very different from the system impacted by recent storms like Hurricane Katrina in 2005.

Instead, during CLARA 1.0 development individual components of the model were evaluated independently where possible, with extensive comparisons made to other published studies to ensure that any differences in outcomes were expected given different parameter inputs or methods. For example, flood depths and overtopping rates were compared to quantities from the IPET investigation (IPET Vol. VIII, 2009), accounting for the differences in levee heights between the systems modeled by each study. In other cases, however, portions of the CLARA framework—such as statistical projections of future flood depth and damage exceedances—cannot be validated using individual events.

Hurricane Isaac presents a unique opportunity for comparing elements of the CLARA model to the behavior and consequences from an observed event, as it impacted protection systems in New Orleans and Plaquemines Parish that were nearly identical to how they are represented in CLARA's Current Conditions scenario. This section describes how data elements from Isaac were used to assess CLARA's economic asset database, response surface model, interior flood model, and damage calculations.

7.1 Overview

Hurricane Isaac made two separate landfalls on the Louisiana coast in late August 2012. Isaac was a storm with unique characteristics that present challenges for fitting it into CLARA's JPM-OS framework. On crossing 29.5 degrees north latitude, Isaac had an r_{max} value of 30 nautical miles, a forward velocity of 4 knots, a central pressure of 973 mb, and a landfall angle of 41 degrees west of north. These values are on the extreme end or outside the range of parameters captured by synthetic storms in the current JPM-OS 446-storm suite. For instance, the majority of storms in the JPM-OS suite have a forward velocity of 11 knots, and even the slowest storms move at 6 knots.

In this respect, the comparison exercise should not be viewed solely as an evaluation of the CLARA model. It is also an exploration of the extent to which the JPM-OS synthetic storm and response surface approaches, designed to produce statistical measures of flood risk, can be used to simulate individual events. Hurricane Isaac's previously unobserved characteristics also suggest the possibility that the JPM-OS storm suite does not adequately span the range of possible storm parameters that could reasonably occur. This is noted as a current limitation, but updates to the storm suite itself are beyond the scope of this investigation.

Four main analyses were performed for this comparative exercise, with some building upon the results of others. Specifically, this section includes comparisons of:

- the number of residential structures in Plaquemines Parish, by municipality, to the corresponding assets in the CLARA economic database;
- peak flood depths, surge elevations, and high-water marks experienced during Isaac in unenclosed areas to the flood depths predicted by CLARA's response surface model for a synthetic storm with "Isaac-like" storm parameters (a synthetic storm with JPM-OS parameters set to those listed above, as described in more detail in Section 7.3.2.1);
- flood depths in enclosed areas from the "Isaac-like" synthetic storm to the flood depths experienced behind the Plaquemines and HSDRRS protection systems; and
- damage to residential assets from Hurricane Isaac to the damage produced by running the Isaac-like synthetic storm through CLARA.

Together, these four comparisons are helpful for evaluating CLARA's baseline inventory estimates and assessing the extent to which the JPM-OS framework and CLARA's overtopping, fragility, and interior drainage routines can be combined to represent flood depths and damage from real storm events. While no levee breaches were observed during Hurricane Isaac, other than an intentional back levee breach in Braithwaite, a fragility analysis was also conducted and included in the flood depth analysis described in the third bullet above.

7.2 Hurricane Isaac Storm Data

Observed storm surge levels, wave heights, and flood depths have been reported based on temporary and permanent U.S. Geological Survey (USGS) monitoring stations, National Oceanic and Atmospheric Administration (NOAA) monitoring sites, and high-water marks (HWM) surveyed post-event by USGS (McCallum et al., 2012). This produced a total of 378 points throughout Louisiana, Mississippi and Alabama. Figure 7-1 shows the estimated peak flood depths from Hurricane Isaac at a selection of these points in the areas most affected.[31].HWMs and storm tide measurements are expressed in terms of height above the NAVD88 datum, so depths are calculated by subtracting local ground elevations obtained from the current conditions DEM used in the 2012 Coastal Master Plan analysis. Storm surge from the above sources is expressed in terms of height above normal tide levels, so these are converted to flood depths by first converting to a storm tide value. For selected parishes, inundation levels are summarized in Table 7-1.

In Louisiana, the sample points provide the best coverage of unenclosed areas near populated Northshore Lake Pontchartrain communities, like Mandeville and Slidell, and West Shore Lake Pontchartrain communities like Laplace. Coverage is considerably more sparse along the HSDRRS and Plaquemines levee exteriors.

Many of the locations where flood depths were measured are adjacent to a levee, floodwall, or drainage canal. Some points referenced in the National Hurricane Center report (Berg, 2013) denote whether the monitoring station was interior or exterior to the elevated feature, but this is not the case for the large majority of points. The reported latitude and longitude of the sample

[31] Some points further inland in Louisiana, in Alabama, or in areas of western and central Louisiana have been omitted for clarity.

points are also not precise enough to determine the exact distance of the stations from the floodwall or levee centerlines.

This presents a challenge for data comparisons, then, because it cannot always be determined whether a measurement represents inundation on the protected or unprotected side of a levee. This could lead to inappropriate comparisons between, for example, an exterior observed measurement and an enclosed CLARA grid point which is run through the interior flood model. Further, estimates of inundation from sensor measurements are subject to errors due to the precision of the digital elevation model (DEM) used to identify the prevailing ground elevation. CLARA (and the ADCIRC model used by the Storm Surge and Wave Team) uses a DEM with a 30-meter resolution, insufficient for capturing deviations in ground elevation from levees and other raised weir features. Where monitoring stations are situated on levee exteriors, measurements also reflect surge pile-up against the protection features, meaning that the measured values are likely higher than the surge elevations at nearby unenclosed points.

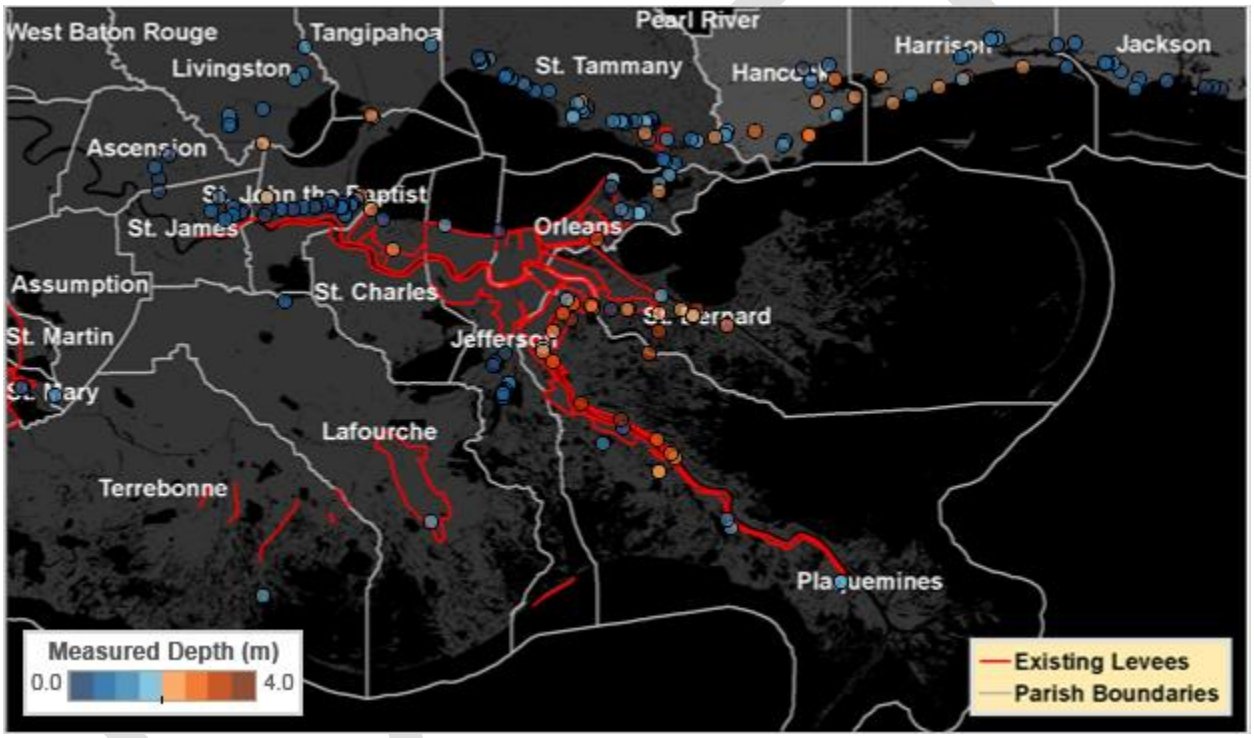

Figure 7-1: Hurricane Isaac Maximum Flood Depths (m), Compiled from Various Data Sources.

Table 7-1: Measured Peak Inundation Levels from Hurricane Isaac, by Selected Parish.

Parish	Depth (m)
Plaquemines	3.0 - 5.2
St. Bernard	2.4 - 3.7
Orleans	1.2 - 2.4

St. Tammany	1.2 - 2.4
Jefferson	0.9 - 1.8
Tangipahoa	0.9 - 1.8
St. John the Baptist	0.2 - 0.9
St. Charles	0.2 - 0.9

Source: Berg (2013)

Still-water elevations (equivalent to peak surge values) from a simulated reconstruction of Hurricane Isaac were also provided by ARCADIS. These values, converted to flood depths, are shown in Figure 7-2, and a comparison of the ADCIRC simulation to the observed flood depths is provided in Figure 7-3. Figure 7-2 only shows points where flooding occurred; by contrast, Figure 7-3 includes all observations, including points where no flooding was either observed or predicted.

The simulation was created by running reconstructed estimates of the Isaac wind fields through the ADCIRC model. Multiple versions of the simulated storm were produced using different multipliers on the wind fields, but the expert judgment of the Storm Surge and Wave team is that the reconstructions are of poor quality (Cobell, 2013). For this reason, and because of the issues described above related to extrapolating values sampled near protection features to other areas, the ADCIRC simulations were ultimately not used to create a synthetic version of Isaac for use in CLARA. (The ADCIRC model was also coupled with UnSWAN to produce wave data, but the decision not to use the hydrodynamic simulations was based on an evaluation of the surge predictions.) Instead, a synthetic storm was created by fitting the JPM-OS response surface to the entire 446-storm current conditions test dataset and then using it to predict the surge and wave behavior of a synthetic storm with parameters set equal to Hurricane Isaac.

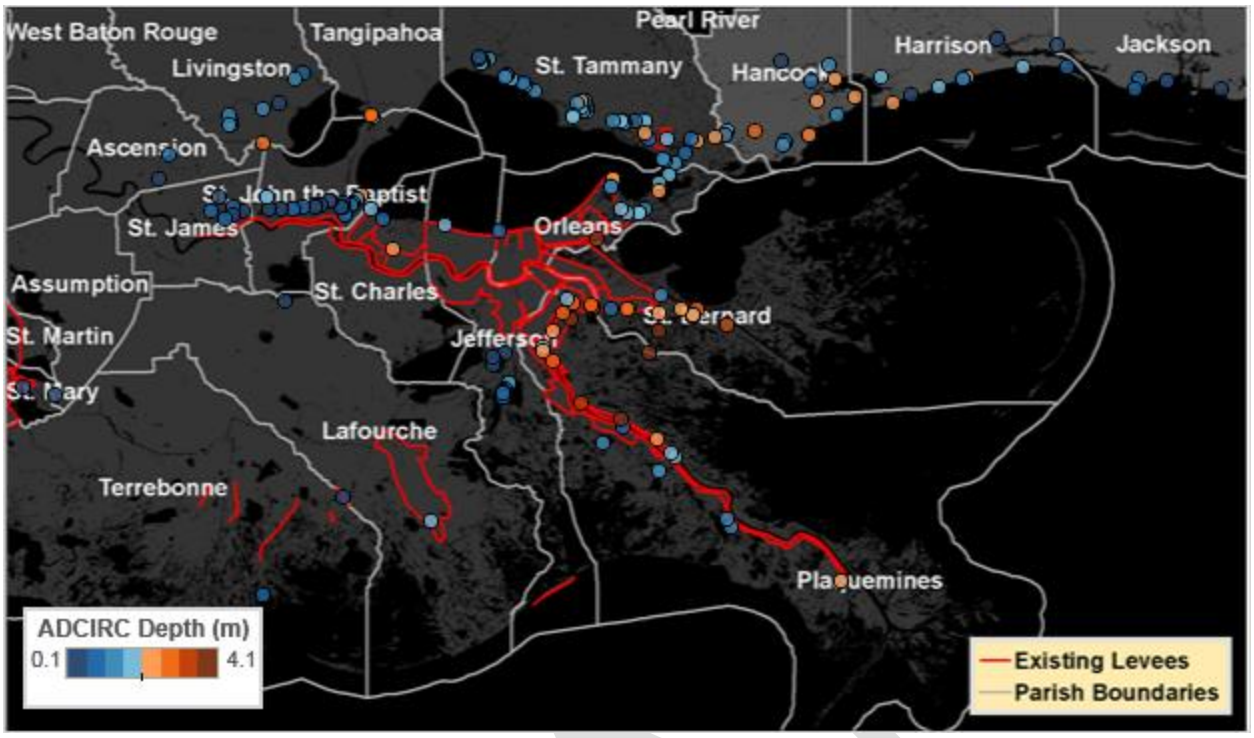

Figure 7-2: Flood Depths Produced by ADCIRC Simulation of Hurricane Isaac (0.9 Wind Multiplier).

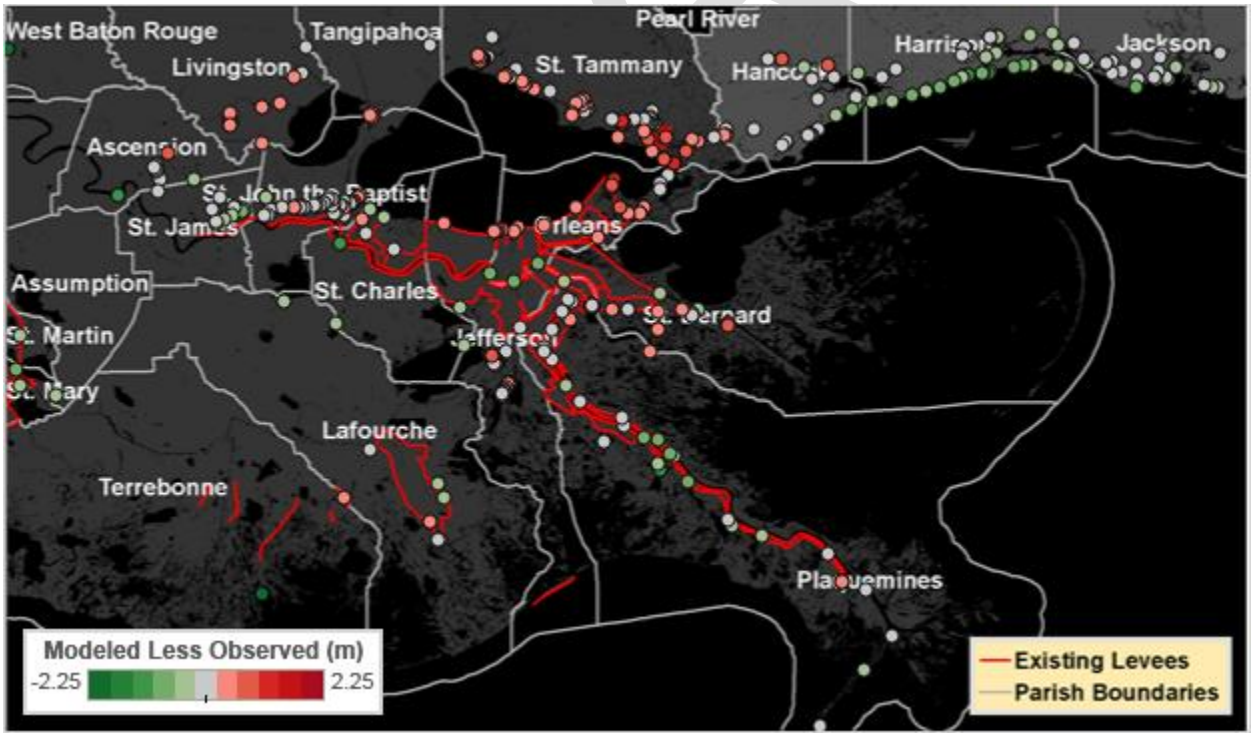

Figure 7-3: Difference between ADCIRC Simulation of Isaac and Observed HWMs (0.9 Wind Multiplier).

Economic damage data is primarily derived from two sources: a Community Development Block Grant (CDBG) proposal submitted by Plaquemines Parish after the storm (Plaquemines Parish, 2013), and a summary of damage produced by the Governor's Office of Homeland Security and Emergency Preparedness (GOHSEP, 2012). Both sources focus on residential housing stocks and are further described in Section 7.3.1.

7.3 Comparison Results

7.3.1 Comparison of Residential Structure Inventories

The economic inventory used in CLARA v2.0 (see Section 3.1) was evaluated in this analysis by comparing the estimated number of structures in CLARA's economic database against totals available from other data sources. As a result, the exercise focused on Plaquemines Parish, which reported housing units by municipality in its recent CDBG application (Plaquemines Parish, 2013).

For this comparison, the economic inventory in CLARA v2.0 was divided into a subset to include only those grid points that fall within Plaquemines Parish. This subset was merged with the US Census Populated Places Areas GIS layer (2010), such that each grid point was linked to its corresponding community. The boundaries mapping each point to a named location within Plaquemines Parish are shown in Figure 7-4.

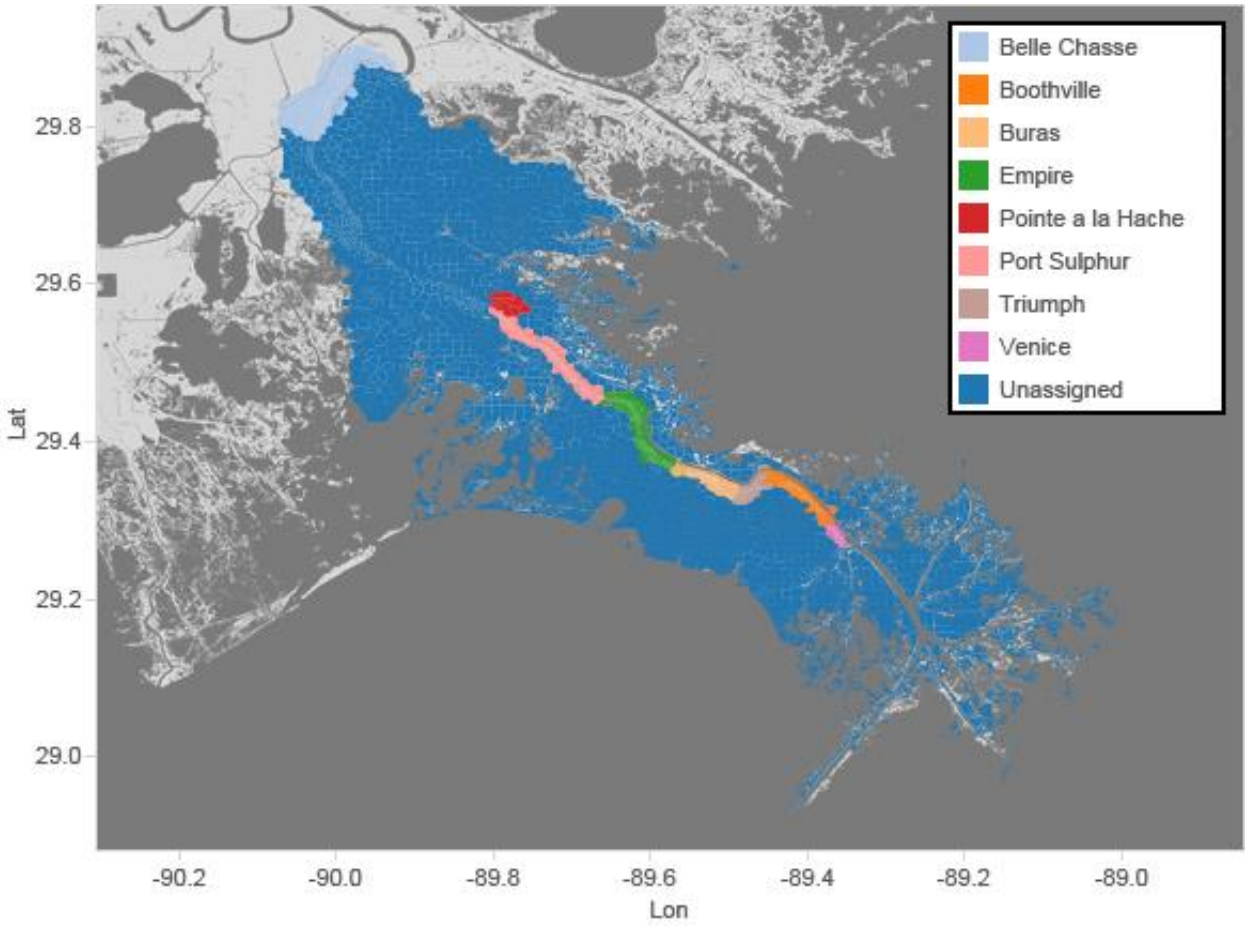

Figure 7-4: Boundaries of Named Locations in Plaquemines Parish.

The inventory of residential structures in CLARA v2.0 was aggregated to the municipality level, allowing for a direct comparison between the CLARA and CDBG estimates. Table 7-2 shows the results of the comparison between these datasets for each community in the Plaquemines Parish.

Table 7-2: Comparison of Plaquemines Housing Units to CLARA Residential Inventory.

Location	Single Family (CLARA)	Multi-Family (CLARA)	Housing Units (CLARA)	Housing Units (CDBG)
Belle Chasse	4,712	722	5,433	4,828
Boothville	385	22	406	443
Buras	572	29	600	427
Empire	416	36	452	501
Pointe a la Hache	75	0	75	96
Port Sulphur	713	26	739	659
Triumph	221	2	224	118
Venice	106	6	112	119
Unassigned	1,736	33	1,769	2,405
Grand Total	8,936	875	9,811	9,596

Note: Single family structures also includes CLARA's Manufactured Homes asset class, and Multi-Family includes both the Small Multi-Family and Large Multi-Family asset classes.

Taken as a whole, the CLARA inventory matches up well with the CDBG data, containing 2% more housing units than the figures reported by Plaquemines Parish, with a greater concentration of homes in Belle Chasse. Census data shows that the parish population declined by 14% between 2000 and 2010, but Belle Chasse's population increased by 22% over the same period. CLARA's inventory reflects a baseline year of 2015, compared to the CDBG application's use of 2010 US Census data. Thus, if trends have continued over the past five years, then a further concentration of assets in Belle Chasse is consistent with the model's projections of housing stock, but the total number of structures would be less than what is estimated by CLARA. As discussed in Section 3, CLARA's inventory has been updated using parcel-level data sets in some regions of the model study area. This has not been done for Plaquemines Parish due to lack of available data, but this comparison nevertheless suggests that the model's existing asset inventory is of good quality.

7.3.2 Comparison of Flood Depths in Unenclosed Areas

As noted in Section 7.2, a relatively small number of observations of actual Isaac flood depths were available for comparison, relative to the size of the affected area. Monitoring data and HWMs measured post-storm are primarily located near protection features and do not cover the affected area of the coast adequately to reconstruct estimates of flood depths throughout the affected area. Points on opposite sides of the HSDRRS or Plaquemines protection systems will clearly experience very different storm surge behavior during an extreme event, as will points on opposite shores of Lake Pontchartrain or at different points along the Mississippi River levee system. This further reduces the sample size of points that could be used to estimate surge elevations and wave heights at other coastal points.

Multiple methods of reconstructing the storm through simulation were considered. The ADCIRC simulations of Hurricane Isaac were not considered to be of sufficient quality for use in this exercise, as previously discussed. Alternative approaches included making adjustments to the ADCIRC outputs to improve quality, or using a synthetic storm with Isaac's storm characteristics.

For the former alternative, a bias-corrected version of the Hurricane Isaac simulation from ADCIRC was considered, with correction factors applied as a multiplier at observed sample

points to bring simulated values in line with the observed storm data. Bias correction factors were interpolated spatially at other points; interpolations at points in any given watershed did not utilize observed points from other watersheds. In cases where an interpolated value could not be identified because of the small sample size, watersheds were successively joined until values could be identified; joining watersheds on opposite sides of the Mississippi River or on opposite sides of a federal levee system was still avoided. However, the interpolated correction factors suffered from the same issues as interpolations of the surge values themselves. Some of CLARA's watersheds (see Section 5.2) do not contain any sample points, so interpolations using the sparse observed data set would likely be inaccurate.

Consequently, instead of using the bias-corrected ADCIRC results, a synthetic "Isaac-like" storm was constructed to perform flood depth comparisons. Storm parameters derived from HURDAT data on Hurricane Isaac were used to predict surge and wave behavior using the response surface fit from the full set of 446 JPM-OS storms under the current conditions landscape.

7.3.2.1 Joint Probability Parameters Derived from Hurricane Isaac

The storm parameters used in the JPM-OS analysis were extracted from HURDAT information to obtain the parameter values that would be used if Hurricane Isaac were added to the set of historical events used to fit the joint probability function. Specifically, parameter values were taken from the characteristics of Hurricane Isaac as it crossed the JPM-OS definition of landfall: crossing $29.5° N$ latitude (see Figure 7-5).

At this point, the storm center was at $90.6° W$ longitude, with a bearing of 40.9 degrees west of North. This placed it most closely on the "E2, -45 degrees" off-angle track. Other parameters were $c_p = 973$ mb, $v_f = 4$ knots, and $r_{max} = 30$ nm. The value for r_{max} was estimated using available windspeed data at the time of landfall and comparing similar windspeed estimates from other historic storms to the r_{max} values assigned to those storms.

Source: New York Times

Figure 7-5: Map of Hurricane Isaac's Track.

7.3.2.2 Predicted Surge Elevations and Wave Heights

The "Isaac-like" synthetic storm was formed by predicting surge and wave behavior using CLARA v2.0's response surface algorithm. The surface was fit using the 446 storms in the JPM-OS storm suite for the Current Conditions scenario, and surge elevation and wave height values were predicted for a synthetic storm with the above parameter values.

In unenclosed areas, CLARA v2.0 estimates the uncertainty associated with DEM measurement and the response surface goodness of fit. This uncertainty is modeled for each synthetic storm, including the Isaac-like storm, resulting in estimates of the 10th, 50th (median), and 90th percentile values. Figure 7-6 through Figure 7-8 show the predicted flood depths at each percentile. The spatial patterns of flooding from the Isaac-like storm are consistent with the actual Isaac event at all quantiles, with the greatest inundation occurring in Plaquemines and St. Bernard parishes. The observed flood depths are within one foot of the median predicted value at 74% of the points.

CLARA-estimated depths were next compared to the observed sample points by taking the values from the CLARA grid point closest to each observed point. The results of this comparison for each percentile are shown in Figure 7-9 through Figure 7-11. The figures show points where flooding was predicted to occur (differences in the extent of flooding are discussed later in the section). Generally, the flood depths derived from HWMs lie between CLARA's 10th- and 90th-percentile estimates. Some observed depths, however, are significantly higher or lower than all of the CLARA predictions. Points where this occurs were inspected in greater detail. Some observation points adjacent to elevated protection features were matched to CLARA grid points on the opposite side of the weir; in other cases, as previously mentioned, it was impossible

to determine where the observation point lies relative to the weir. This is a possible explanation for the discrepancies at such points; errors in the provisional high water mark data are another possibility.

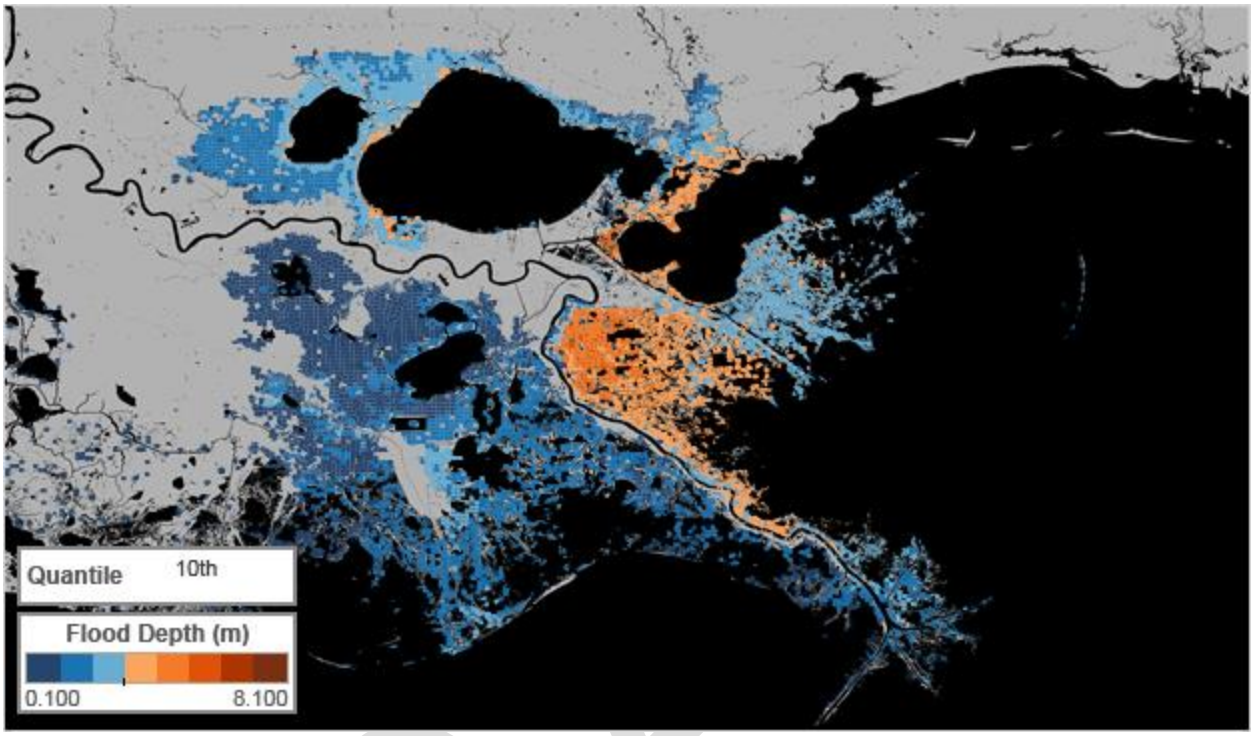

Figure 7-6: Flood Depths from an "Isaac-Like" Synthetic Storm (CLARA v2.0, 10th Percentile).

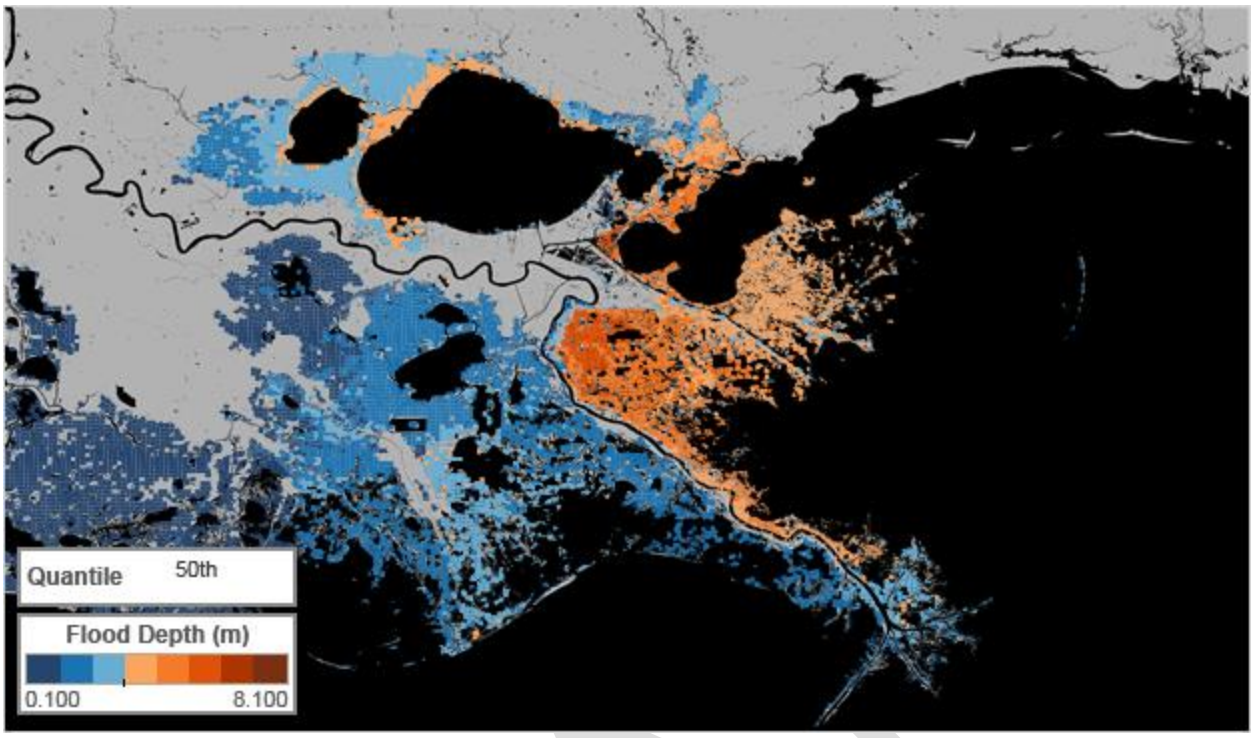

Figure 7-7: Flood Depths from an "Isaac-Like" Synthetic Storm (CLARA v2.0, 50th Percentile).

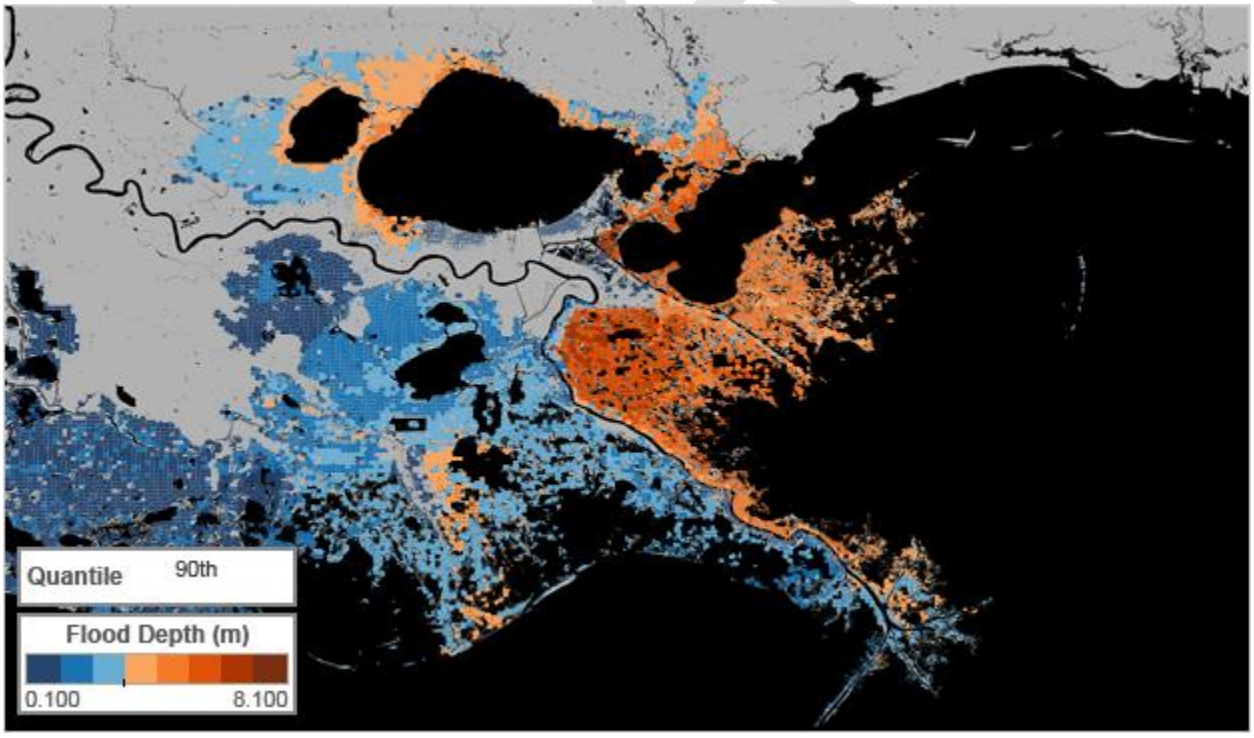

Figure 7-8: Flood Depths from an "Isaac-Like" Synthetic Storm (CLARA v2.0, 90th Percentile).

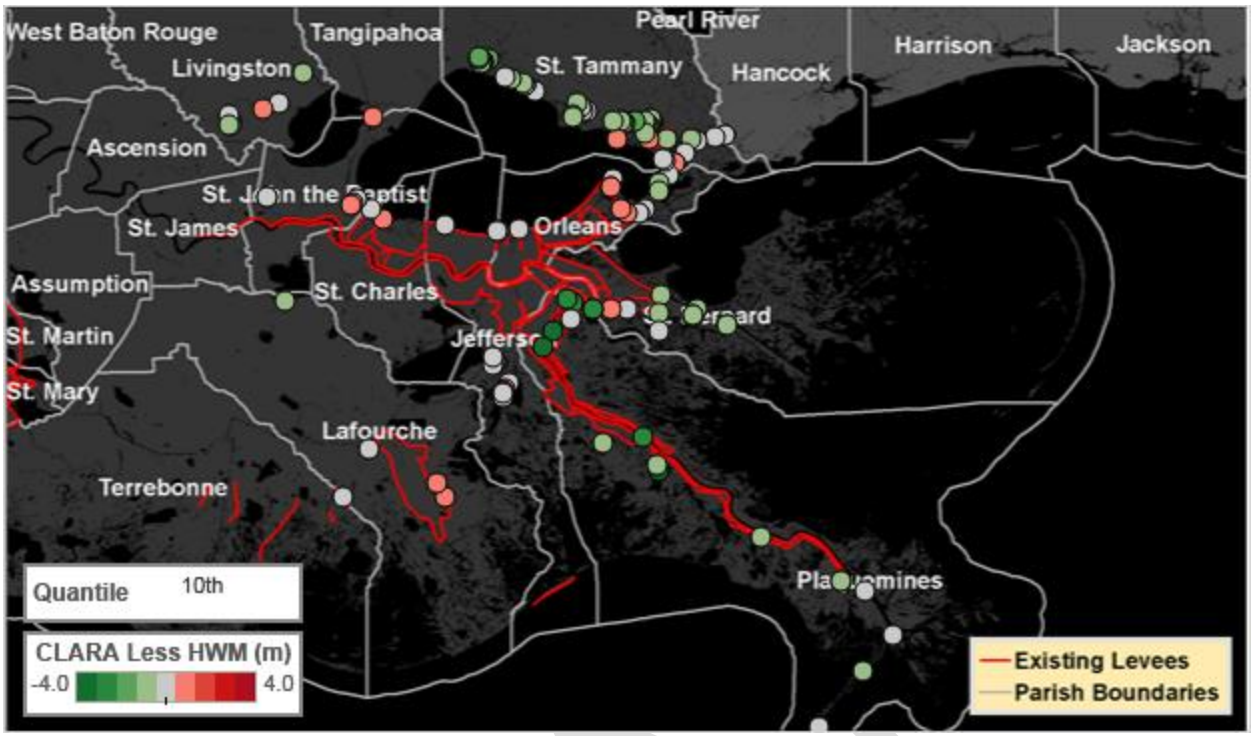

Figure 7-9: Flood Depths from the CLARA "Isaac-Like" Synthetic Storm, Less Flood Depths from Observed High-Water Marks (10th Percentile).

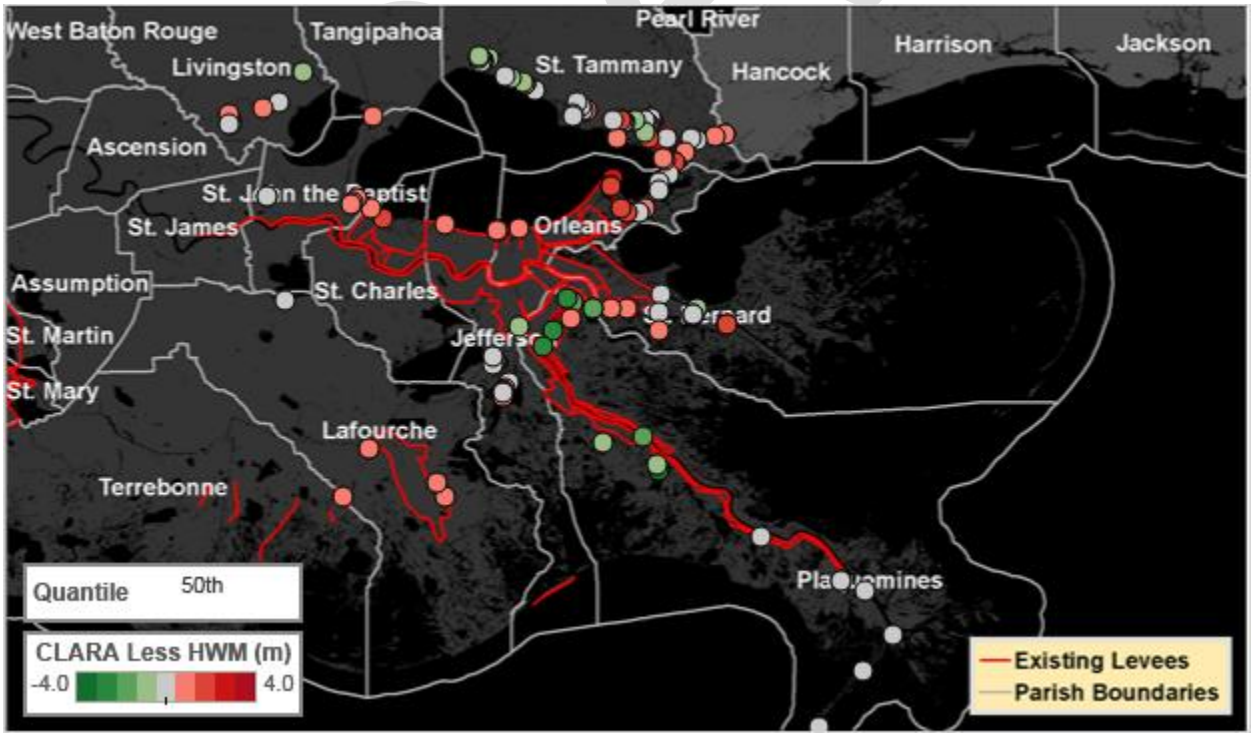

Figure 7-10: Flood Depths from the CLARA "Isaac-Like" Synthetic Storm, Less Flood Depths from Observed High-Water Marks (50th Percentile).

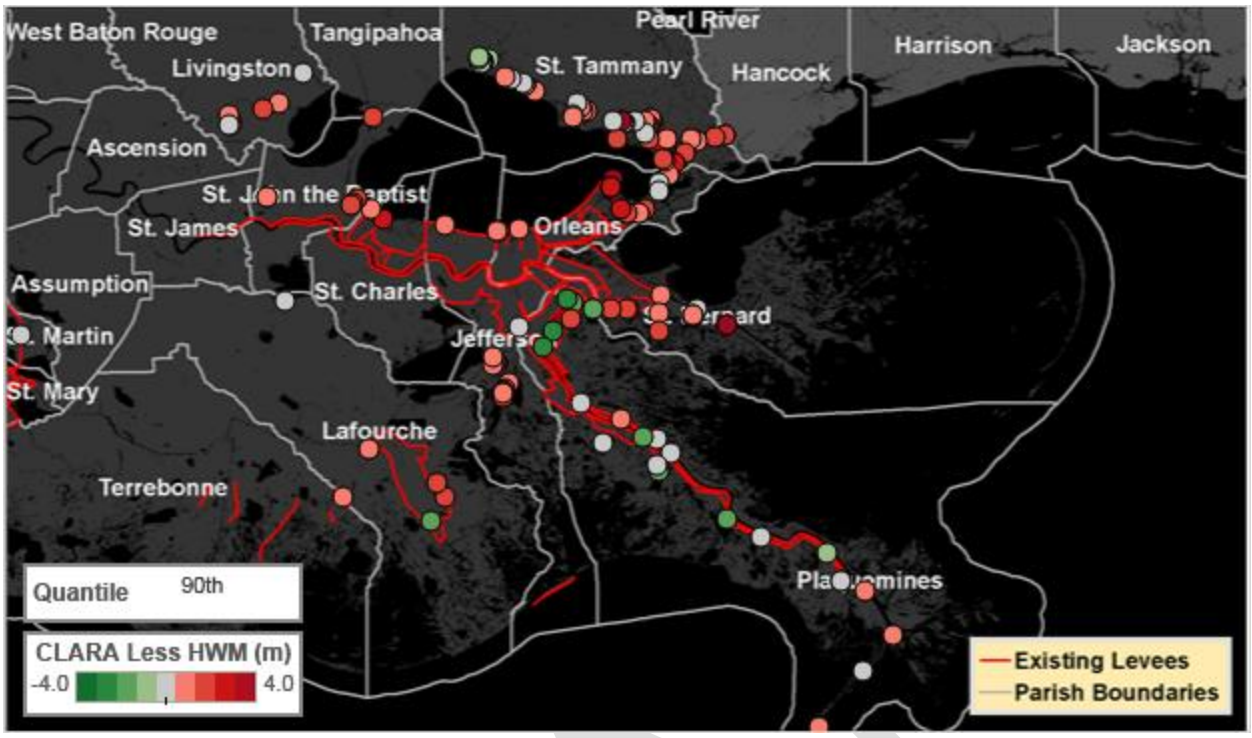

Figure 7-11: Flood Depths from the CLARA "Isaac-Like" Synthetic Storm, Less Flood Depths from Observed High-Water Marks (90th Percentile).

The above comparisons were only made at points in Louisiana where CLARA predicted flooding to occur. Notably, the predicted extent of flooding did not cover most of the populated areas of Laplace between Highway 10 and US-61. This had a major impact on the damage estimated in St. John the Baptist Parish, as noted in Section 7.3.4. Despite experiencing much lower flood depths than some other communities, the high concentration of assets in this area resulted in St. John the Baptist Parish receiving more severe damage than any other parish.

Flooding in Laplace and other parts of St. John the Baptist Parish came largely from storm surge building from Lake Pontchartrain. Isaac's large size and slow progression inland resulted in sustained winds blowing counter-clockwise from the lake into populated areas. This lake-borne flooding was not predicted by the CLARA response surface. Median estimates of flood depths over the predicted CLARA uncertainty range are shown in Figure 7-12; in each of the following figures in this section, US Census-defined urban areas are displayed in yellow and indicate the most highly-developed areas with concentrated assets. The discrepancy in the predicted extent of flooding is likely a consequence of the JPM-OS storm suite not containing any storms as large or slow-moving as Isaac; it is possible that no storms in the JPM-OS suite produce such extensive flooding by the same mechanism.

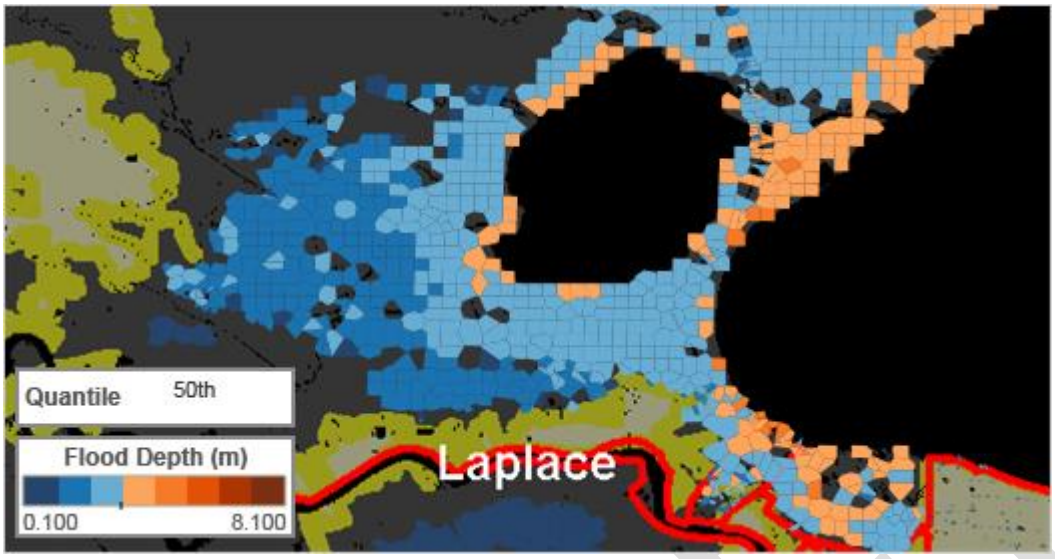

Figure 7-12: Flood Depths in St. John the Baptist Parish (CLARA, 50th Percentile).

On the Northshore, CLARA's Isaac-like storm more accurately reproduces observed flood depths in the Mandeville area. Median estimates of flood depths are shown in Figure 7-13, with comparisons to observed HWMs in Figure 7-14.

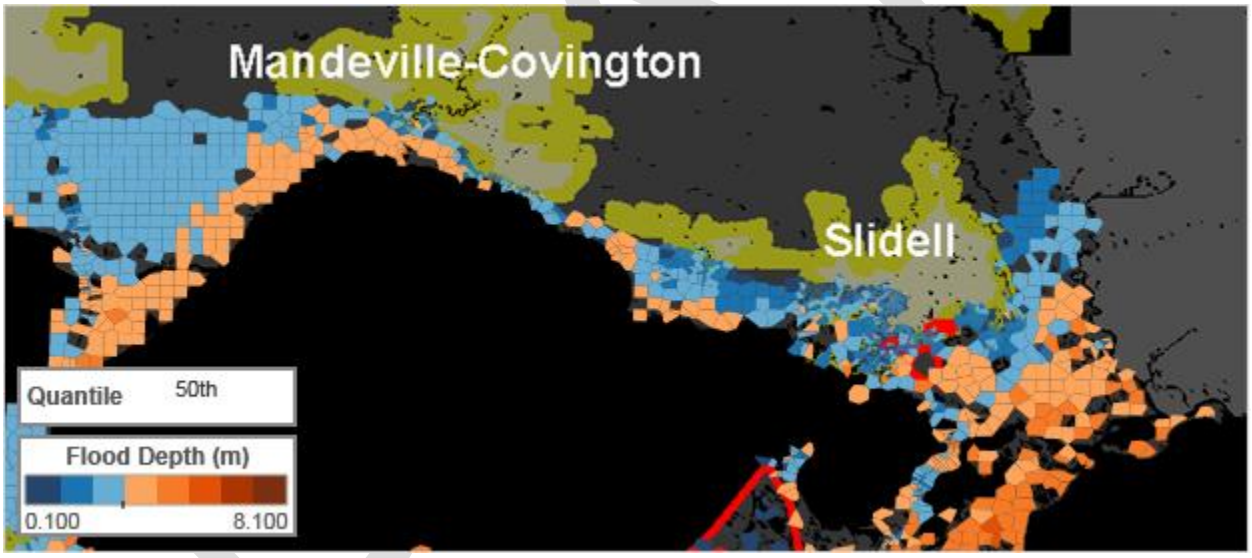

Figure 7-13: Flood Depths in St. Tammany Parish (CLARA, 50th Percentile).

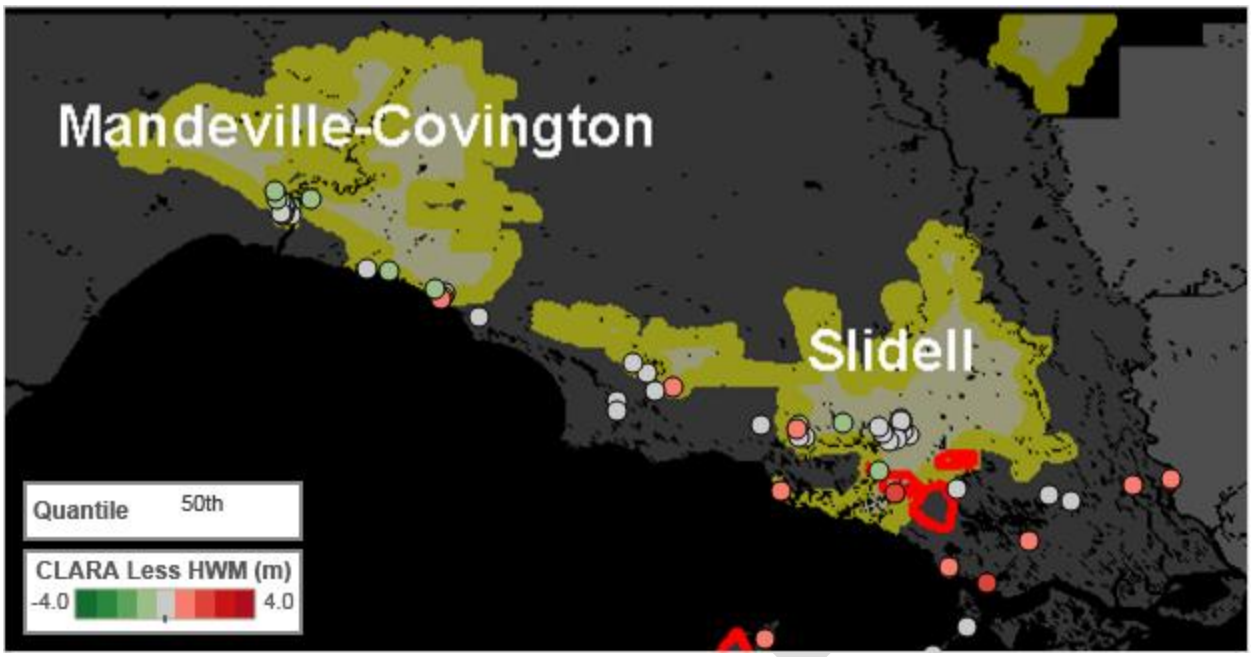

Figure 7-14: CLARA Flood Depths (50th Percentile) in St. Tammany Parish, Less Flood Depths from Observed High-Water Marks.

While observed HWMs are within a meter of CLARA's median projections, the model predicted flooding to extend further into Slidell (Figure 7-13) than actually occurred. This may be attributable to local levees or weir features not adequately represented in the DEM used by the ADCIRC model, or it may be related to the general difficulty, previously noted in Section 5.2.2.1, of accurately predicting wetting from individual storm events. This had a major impact on CLARA's damage estimates in St. Tammany Parish, as discussed in Section 7.3.4.

7.3.3 Comparison of Flood Depths in Enclosed Areas

The same Isaac-like synthetic storm approach was used to produce flooding estimates in enclosed areas. The CLARA response surface was fit using the 446 JPM-OS storms to predict storm behavior at the CLARA Surge and Wave Points (SWPs), including surge hydrographs. The Isaac-like storm was run through the model's overtopping, fragility, and interior drainage routines, using the "MTTG Low" fragility curve assumption previously described. This generated a probability distribution of flood depths that accounts for uncertainty in surge and wave levels, the resulting overtopping volumes, the possibility of system failures, and noise in the DEM measurements.

Figure 7-6 through Figure 7-8 illustrate the flood depths estimated by CLARA in enclosed areas such as New Orleans, Belle Chasse, and Larose. During Hurricane Isaac, New Orleans saw little-to-no flooding within HSDRRS that originated from storm surge. CLARA results are consistent with the observed outcomes—the model predicts negligible flooding in populated areas within HSDRRS except at the 90th percentile, at which point flooding occurs in portions of Metairie, Kenner, and West Lake Forest.

Figure 7-15 shows an inset of predicted flooding in Plaquemines Parish (90th percentile). While the greatest flooding occurs in unenclosed areas of Breton Sound, significant flooding (1 to 4 m) is predicted in all areas enclosed by the federal levees from Pointe a La Hache on the East Bank,

through Port Sulphur down to Venice on the West Bank. Flooding also occurs behind non-federal back levees in Braithwaite (East Bank) and Alliance (West Bank). (Figure 7-16 shows the location of each named place in this section.)

During the actual Hurricane Isaac, flood waters overtopped the 8-foot (2.4 m) non-federal back levee in Braithwaite, and backed up against the federal Mississippi River levee, eventually peaking at about 14 feet (4.3 m). The substantial overtopping did not, however, cause this levee to erode or breach. Instead, water levels were not relieved until the back levee was intentionally breached near Caernarvon, at the north end of Braithwaite, creating an escape valve for flood waters to flow back out of the polder (Adelson, 2012). A map illustrating where back levees were overtopped is shown in Figure 7-16.

Flood depths near Caernarvon were predicted by CLARA to peak at about 3.5 m at the 90th percentile. This resulted from surge elevations greater than the levee heights in that area filling the polder. However, the predicted depths were still less than those observed during the actual storm. This is likely because of the proximity of the federal levee on the Mississippi River. CLARA's interior drainage model assumes that interior flood depths cannot exceed either the levee heights surrounding a polder or the lowest peak surge occurring along the levee boundary, whichever is greatest. The model assumes that if flood levels were to rise beyond that level within a polder, water would begin flowing back out to the unenclosed area. In the case of Hurricane Isaac, surge waters overtopping the back levee at Braithwaite continued to flow into the polder until reaching the Mississippi River levee. Surge then piled up against the back of the river levee. CLARA does not model this type of time-dependent hydrodynamic effect in enclosed areas and was not able to capture this effect.

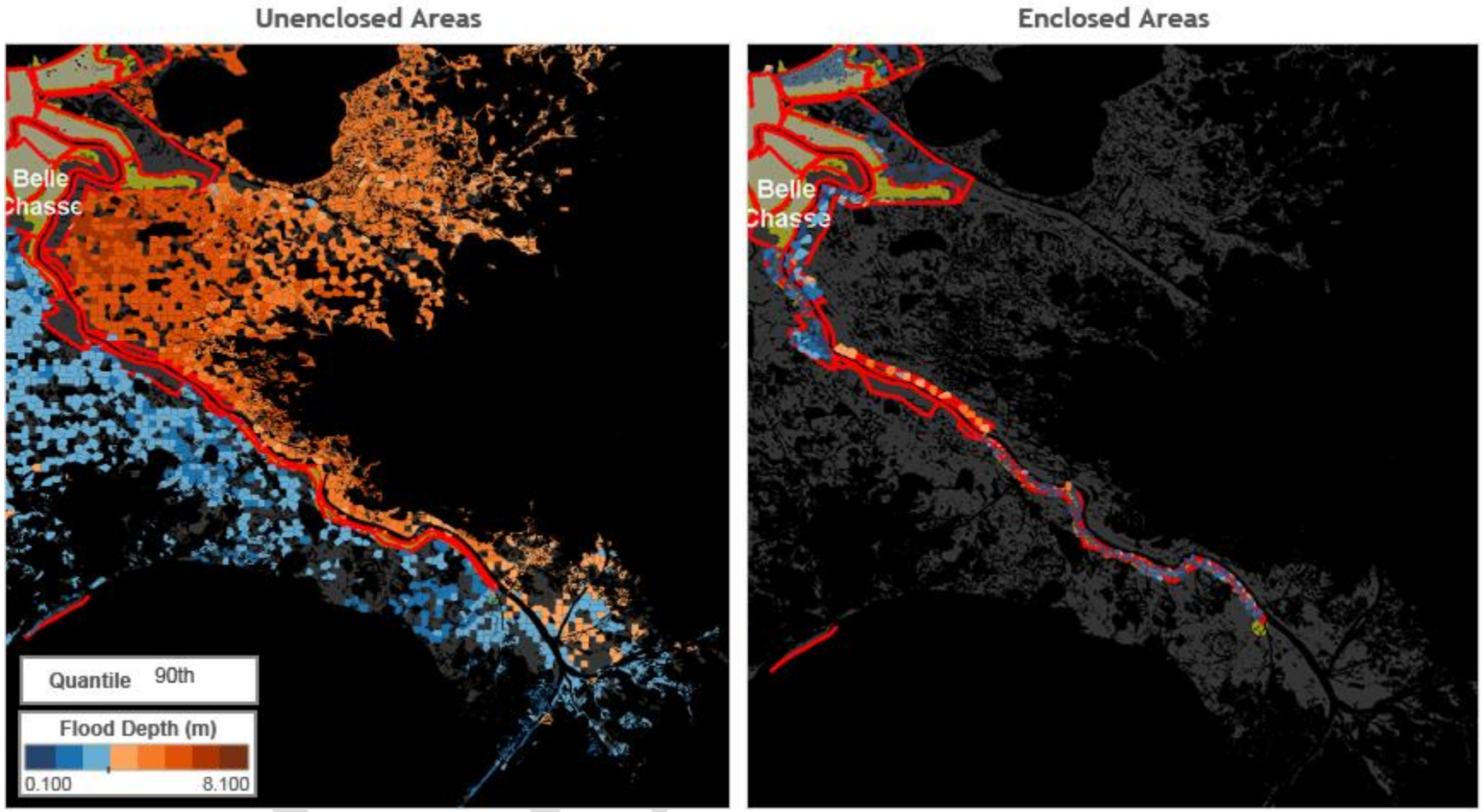

Figure 7-15: Flood Depths in Plaquemines Parish, Unenclosed and Enclosed Areas (CLARA, 90th Percentile).

Figure 7-16: Detail of Plaquemines Federal and Non-Federal Levee System.

7.3.3.1 Determinants of Predicted Flooding in Enclosed Areas

Flooding in enclosed areas can develop through several mechanisms. Water can enter a polder by surge or waves overtopping protection features. If system failures occur, additional water flows in through the breaches. Finally, rainfall can produce flooding if pumping rates are exceeded.

USACE inspection found little to no evidence of overtopping into New Orleans over HSDRRS levees, floodwalls, and gates or other transition features (USACE, 2013c). Nearly 10,000 homes saw damage in Orleans Parish during Hurricane Isaac, but this was primarily caused by flash flooding from rainfall (Mitigation Assessment Team, 2013). In Plaquemines Parish, however, flooding resulted from extensive overtopping.

Both of these results are consistent with CLARA's predictions for an Isaac-like synthetic storm. Levee heights, shown in Figure 7-17, reach up to 32 feet (9.8 m) along the Mississippi River and in St. Bernard Parish, but are considerably lower in Plaquemines Parish. As a result, HSDRRS encountered no overtopping from the peak surge levels of up to 14 feet (4.3 m). Overtopping was most severe in Plaquemines Parish along an 18-mile stretch of back levee from Braithwaite south to White Ditch, but other communities downriver also saw overtopping.

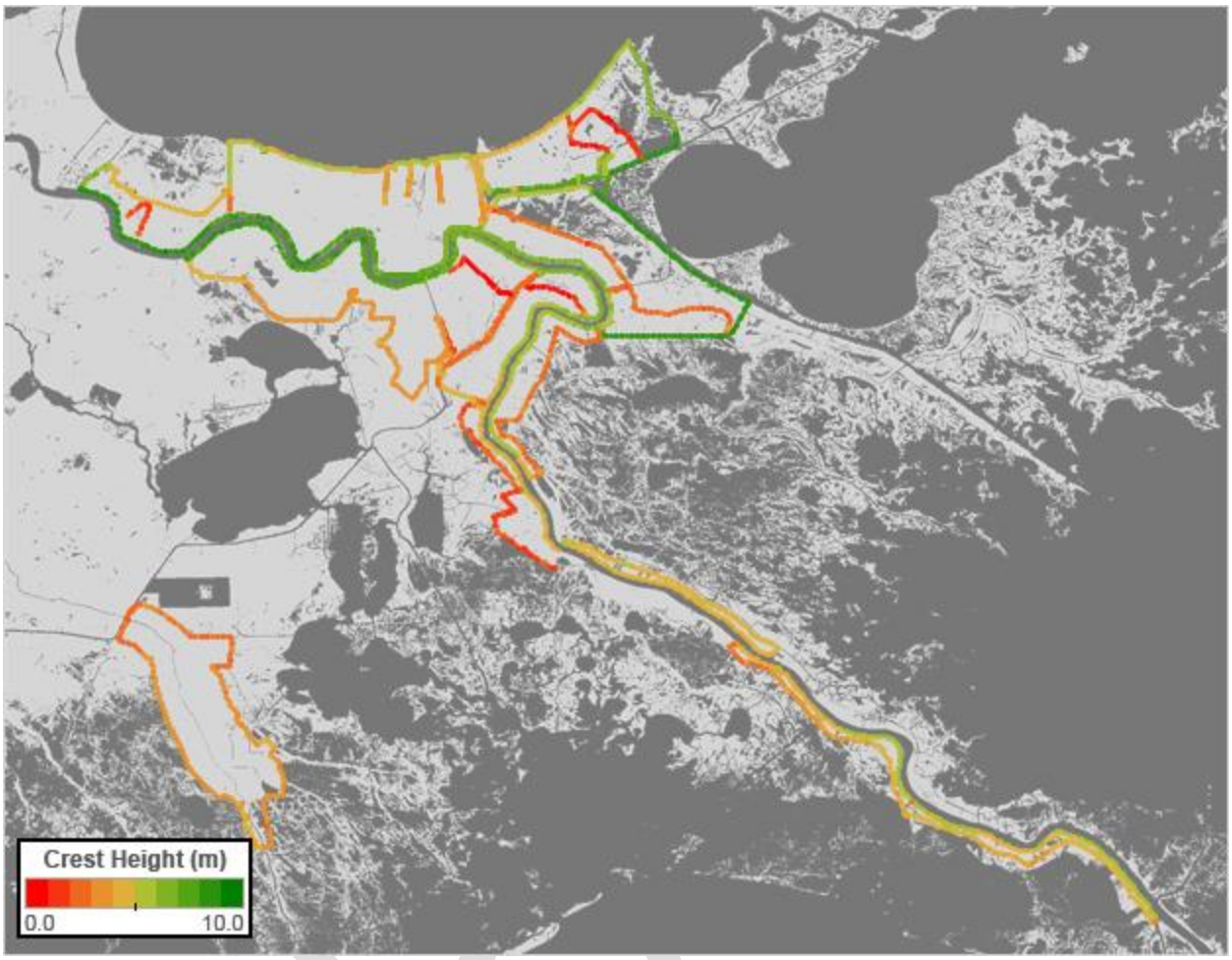

Figure 7-17: HSDRRS, Plaquemines, and Larose to Golden Meadow Protection System Reach Heights.

The modeled CLARA overtopping volumes are depicted in Figure 7-18, expressed as cubic meters of water overtopped per linear meter of levee or floodwall over the entire duration of the storm. Only characteristic reaches with overtopping volumes of at least $1\ m^3$ are shown. In agreement with the actual Isaac experience, overtopping into HSDRRS is negligible, and the most severe overtopping occurs along the Braithwaite back levee. The only other area where significant overtopping is predicted is on the west bank in Myrtle Grove, just south of Braithwaite; as predicted, a seven-mile stretch of Highway 23 in Myrtle Grove experienced 1 m (3 ft) of flooding during Isaac due to overtopping of the non-federal levee there (Alexander-Bloch, 2013).

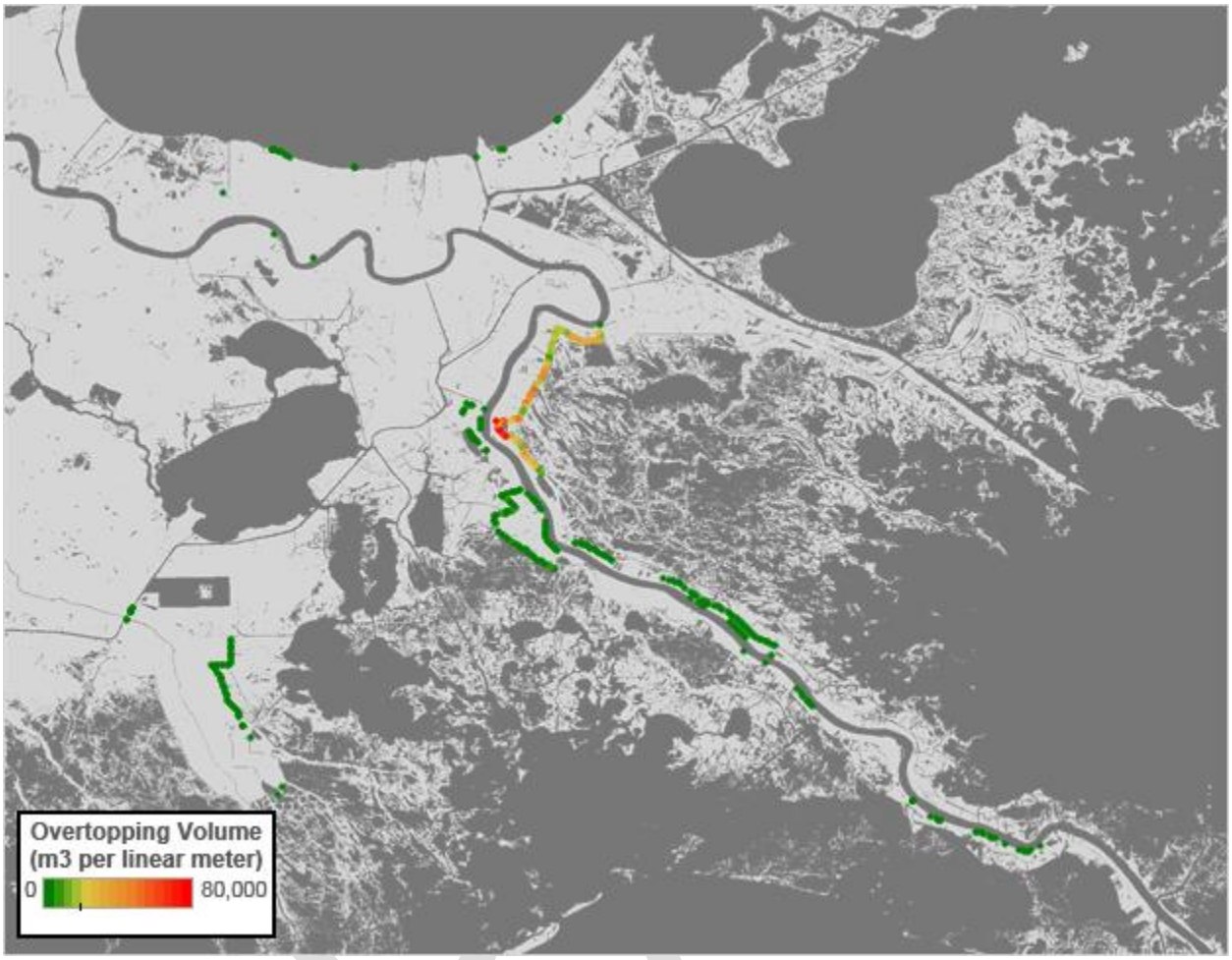

Figure 7-18: Calculated Overtopping Volumes from an Isaac-Like Synthetic Storm (CLARA, Median Values).

The probability of levee failure in CLARA v2.0 is a function of overtopping rates. To consider failure probabilities in this investigation, the Isaac-like synthetic storm was run using the model's MTTG Low fragility curve assumption, as described in Section 4.3. The peak overtopping rate experienced during a storm—whether observed or simulated—is a function of surge elevations, wave heights, wave periods, and protection feature characteristics. For a given reach, the peak overtopping rate generally occurs when surge levels are at their peak (assuming wave characteristics do not change). Thus, it is correlated with the total overtopping volume passing over a reach, but not perfectly so; a wider hydrograph with a lower peak surge elevation could produce overtopping for a longer duration of time, but at a lower rate than a hydrograph that sharply rises to and recedes from a higher peak surge level.

In this case, however, the probabilities of failure predicted by CLARA in Plaquemines Parish, shown in Figure 7-19, are very strongly correlated to the total volume of overtopping water from Figure 7-18 ($r^2 = 0.82$). Failure probabilities have been normalized on the figure to represent the probability of failure per characteristic reach length, to account for differences in the lengths represented by each CLARA reach point. CLARA v2.0 addresses uncertainty in the surge levels produced by a given storm, as well as uncertainty in the overtopping rates that are produced by a given level of surge. Figure 7-19 depicts the median probabilities calculated at each point over every replicate of the simulation.

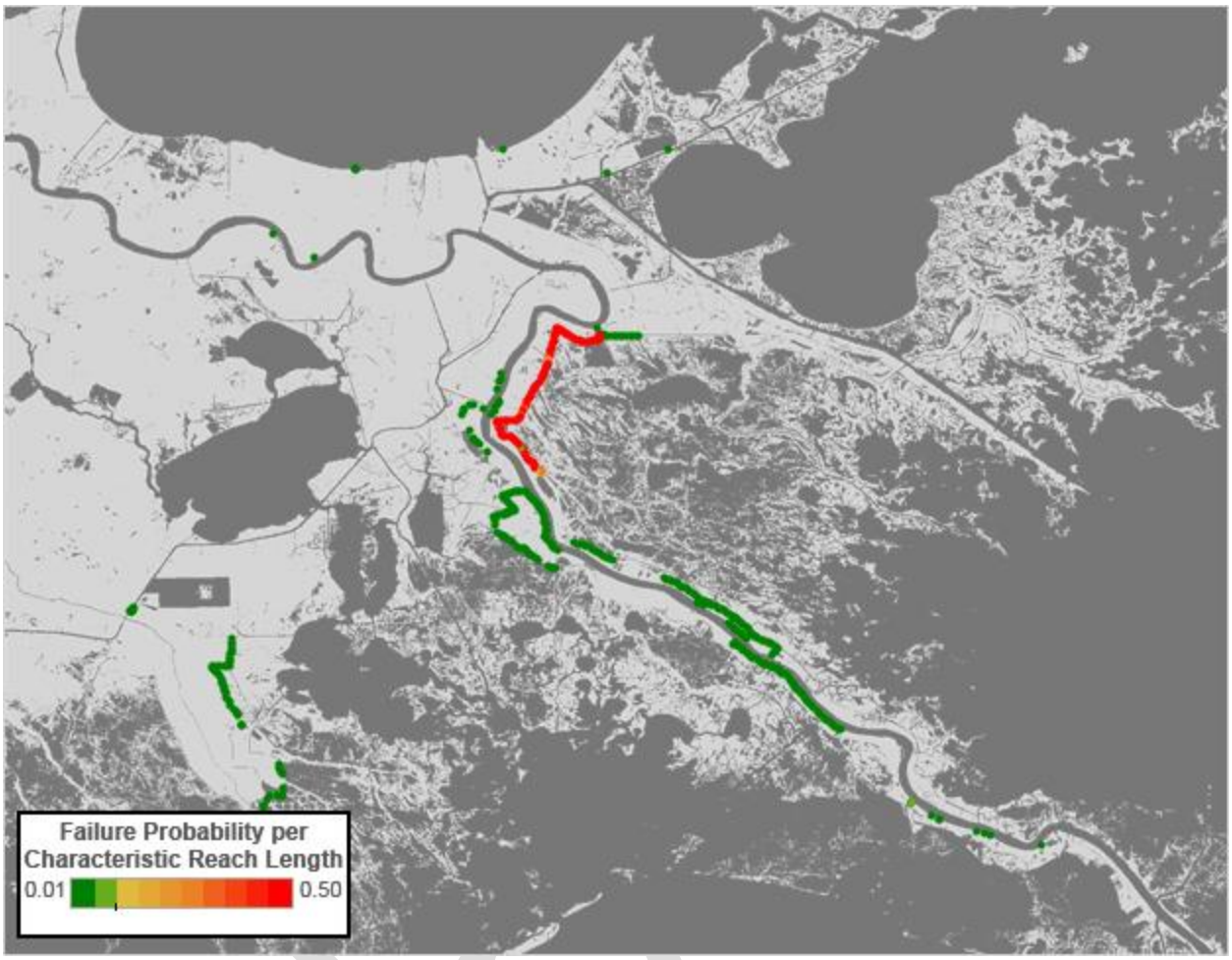

Figure 7-19: Probability of System Failure from an Isaac-Like Synthetic Storm, Normalized as the Probability per Characteristic Reach Length (Median Values).

Failure probabilities are consistently between 0.3 and 0.5 along the entire length of the Braithwaite back levee, and less than 0.02 everywhere else but a handful of points on the back levee protecting Myrtle Grove. Failures occurred in the simulation at an average of 40 reach points, representing approximately 12 km (7.4 miles) of levee subject to failures from backside scour. Given that the Braithwaite back levee is a non-federal levee, additional study would be required to determine why breaches from backside erosion did not occur at this location during Hurricane Isaac.

The controlled breach of the Braithwaite back levee at Caernarvon allowed flood waters to escape the Braithwaite polder after peak surge had already occurred. CLARA v2.0, by contrast, assumes that breaches occur at the point of peak surge. Introducing a forced failure in CLARA at the point of the controlled breach does not significantly change modeled flood depths in the area. Surge levels in the region were sufficiently above the levee heights that, because of the small size of the polder, overtopping still fills the polder to the same depth even when the levees do not fail (aside from the intentional breach).

7.3.4 Comparison of Damage to Residential Assets

Nearly 59,000 homes in Louisiana were damaged by Hurricane Isaac, with the most severe losses occurring in St. John the Baptist and Plaquemines Parishes (GOHSEP, 2012; Mitigation Assessment Team, 2013). As sustained winds and gusts from Isaac were below design level wind speeds, wind damage was minor; for the purpose of this exercise, it is assumed that the number of homes receiving wind damage without flood damage was negligible. Of these, 47,200 homes were in parishes where all major population centers are in the CLARA study region. Over half of the homes damaged were located in Jefferson, Orleans and St. John the Baptist Parishes. Table 7-3 compares the counts of damaged residences by parish to the numbers estimated by CLARA at the 10th, 50th, and 90th percentiles of flooding.

Table 7-3: Homes Damaged by Hurricane Isaac, Observed (Left Column) Versus Modeled.

		CLARA Percentile		
Parish		10th	50th	90th
Assumption	562	299	452	513
Jefferson	12,912	2,496	3,092	11,910
Lafourche	2,103	1,390	1,943	2,614
Orleans	9,777	623	648	10,778
Plaquemines	2,983	573	1,125	3,291
St. Bernard	2,257	343	343	343
St. Charles	1,368	2,296	3,535	3,833
St. James	953	7	10	25
St. John The Baptist	6,871	146	156	156
St. Mary	1,127	29	257	388
St. Tammany	4,572	8,557	11,836	13,499
Terrebonne	1,695	1,369	3,044	5,132
Grand Total	47,180	18,128	26,439	52,483

Relative Difference

-100% 200%

The number of homes damaged during Isaac falls within CLARA's uncertainty bounds for four of the parishes, with two others being less than 10 percent from the actual numbers at the 90th percentile. CLARA-estimated counts are consistently greater than the actual values in St. Charles and St. Tammany Parishes. Conversely, projections in St. Bernard, St. James, St. John the Baptist, and St. Mary are all significantly less than the actual damaged structure totals.

There are many possible explanations for why CLARA might under- or over-estimate actual damage counts. The most obvious is related to uncertainties in the extent of flooding. Large differences could occur if CLARA fails to predict flooding in an urban area with concentrated assets; likewise, if CLARA projects that a particular city would experience flooding, damage counts may overshoot the actuals.

Careful examination of the damage outcomes from the synthetic Isaac-like storm suggests that the simulation overestimated the number of damaged structures in at least two major urban areas, the most prominent of which is St. Tammany Parish. Figure 7-20 shows the geographic distribution of damage on the Northshore of Lake Pontchartrain by depicting the number of

homes damaged by the Isaac-like synthetic storm in each grid point under the 90th percentile of flood depths (census-defined urban areas are underlaid in yellow below the grid points). Much of the projected damage is concentrated in Slidell, with about 9,000 homes projected to receive some amount of damage at the 50th percentile (about 10,400 at the 90th percentile). In reality, only 500-600 homes were damaged in Slidell. This difference explains nearly the entire difference in the parishwide total for St. Tammany. The extent of flooding in Slidell is difficult to ascertain with certainty from the small number of observed HWMs and pressure sensor readings, but a difference in estimated damage this large is likely due to a discrepancy in the projected extent of flooding; see the next section for more discussion of this effect.

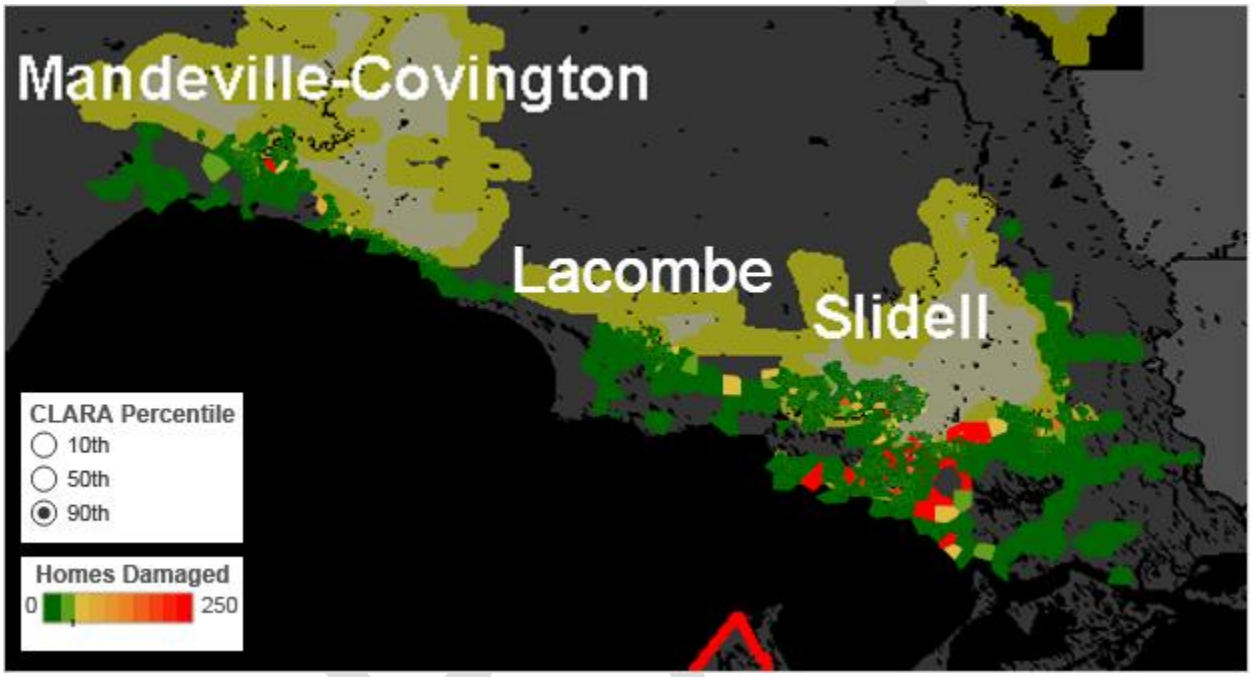

Figure 7-20: Homes Damaged by Grid Point (CLARA, 90th Percentile).

By contrast, the Isaac-like synthetic storm underestimated the extent of flooding in St. John the Baptist Parish, as discussed in Section 7.3.2. Figure 7-12 showed that flooding there was not projected to cross Highway 10 south into Laplace or other communities on the Mississippi River. Consequently, very few homes were projected to see damage in CLARA, compared with the nearly 7,000 that actually did. As previously discussed, the flood discrepancy in St. John the Baptist is very likely due to limitations in the current suite of JPM-OS storms, which is missing a storm as large and slow-moving as Hurricane Isaac that could reproduce the observed surge dynamics in Lake Pontchartrain.

Plaquemines Parish's CDBG application contains more detailed data about the number and type of residences damaged. These are reproduced in Table 7-4; note that the Mobile Home and Travel Trailer categories are both counted as Mobile Homes in this table, and the Houses category also includes Condos and Townhouses. The Mobile Home and House totals provided in the CDBG application consist only of owner-occupied housing; a separate column in Table 7-4 provides the total across both categories for renter-occupied housing.

Table 7-4: Observed and Simulated Count of Damaged Residences by Area and Housing Type, Plaquemines Parish (CLARA, 90th Percentile).

Location	Mobile Homes (CDBG)	Mobile Homes (CLARA)	Houses (CDBG)	Single Family (CLARA)	Small Multi-Family (CLARA)	Large Multi-Family (CLARA)	Rentals (CDBG)	Total (CDBG)	Total (CLARA)
Belle Chasse	163	11	161	21	0	0	54	324	31
Boothville	147	221	25	99	1	18	31	172	339
Buras	138	277	24	179	5	13	9	162	475
Empire	190	150	21	74	2	23	32	211	248
Pointe a la Hache	90	32	12	43	0	0	24	102	75
Port Sulphur	349	169	43	100	0	14	51	392	284
Triumph	19	106	1	61	0	1	4	20	168
Venice	17	51	2	36	0	3	1	19	91
Unassigned	793	502	567	1,046	22	8	292	1,356	1,579
Grand Total	1,906	1,519	852	1,660	31	81	498	3,256	3,290

Overall, CLARA estimates damage to almost exactly the same number of homes reported in the CDBG application. However, the distributions of damaged assets by location and type do not match up as closely. Some areas overestimate the number of homes, while others underestimate. Differences in the inventory of exposed assets, as discussed previously, would certainly contribute to differences in the number of damaged assets.

In Belle Chasse, fewer homes were projected to receive damage, and inspection of Figure 7-15 reveals that this is likely because the Isaac-like synthetic storm's flooding envelope hardly extends into the community.

Other possible explanations exist. Aside from the number of homes in each area, limitations or errors in the data about the characteristics of these homes—in particular, information about the foundation height of residences—could also contribute to errors in the modeled results. As reconstruction occurs after extreme events, the average foundation height of homes is likely to rise. Because CLARA relies on an older 2008 estimate of structure characteristics for Plaquemines Parish, this would tend to cause CLARA to overestimate the number of homes that would receive damage from a given storm.

Naturally, any differences between the actual and simulated extent of flooding will also result in differences in estimated damage. Analysis of monetary damage estimates was restricted to Plaquemines Parish, because the counts of damaged homes are in close agreement. Damage estimates are also available separately for houses and mobile homes in the Plaquemines Parish CDBG application.

The CDBG application lists the total FEMA Verified Loss (FVL) values in each Plaquemines location and for each type of home. FVL is based on a cursory inspection of a home and represents FEMA's estimated cost to make critical repairs to the structure. It does not estimate the cost of fully restoring the home to its pre-storm condition, so it does not represent full replacement cost (Illinois Department of Commerce and Economic Opportunity, 2013). It generally underestimates the actual damage incurred by homeowners, in that it also does not include damage to home contents or other items which may be insurable.

As such, it is inappropriate to compare FVL to the entire damage estimate modeled by CLARA. Instead, results have been compared to CLARA's estimates of Structure Damage only. Comparisons are shown for both CLARA's Actual Cash Value (ACV) estimate, which incorporates depreciation based on an effective age calculated for each structure, and also CLARA's estimate of full replacement costs (RC; the model's default option).

Another estimate of actual repair costs can be made using Small Business Administration (SBA) disaster loans. By May 1, 2013, SBA had approved 347 home loans in Plaquemines Parish worth about $24.4 million. Assuming that the proportion of loans given for mobile homes is the same as the proportion of mobile homes damaged compared to houses, this represents an average loan of about $113,200 per house and $23,400 per mobile home, respectively. These averages may be biased by a selection effect if homes able to secure loans by May 2013 received systematically greater damage than those not issued loans at that point.

SBA disaster loans can include up to $40,000 to repair or to replace home contents and vehicles. The loans can also be increased by up to 20 percent above the real estate damage if improvements are made to reduce the risk of future property damage (SBA, 2015). It is not likely that all loans included these additional funds (loans are also reduced if they would duplicate insurance benefits), but assuming their presence can provide a lower bound for estimating structure damage using SBA loan values.

The estimates of average structure damage by various methods are summarized in Table 7-5. CLARA values correspond to damage resulting from the median and 90th percentile estimate of flooding. Using either valuation method, the average damage from the median flood depths is less than the corresponding estimate resulting from the 90th percentile flood depths.

Table 7-5: Estimated Average Structural Damage Per Home in Plaquemines Parish, by Estimation Method.

Method	Single-Family	Mobile Homes
CDBG (FVL)	$ 24,235	$ 5,016
SBA (Lower Bound)	$ 40,675	$ 8,419
SBA (Upper Bound)	$ 113,211	$ 23,434
CLARA (90th, RC)	$ 111,027	$ 43,154
CLARA (90th, ACV)	$ 77,737	$ 30,225
CLARA (50th, RC)	$ 96,354	$ 29,268
CLARA (50th, ACV)	$ 67,470	$ 20,555

All of the CLARA estimates for single-family residences fall between the upper and lower bounds of the estimates produced using SBA loan data. For mobile homes, the average damage estimated using three of the four CLARA methods is greater than the SBA upper bound.

Given the same flood depth, damage estimates from CLARA could deviate from official estimates due to three primary factors. The first is the calculated value of a home, which follows Hazus methods and depends on the type of home, square footage, and replacement cost per

square foot. When modeling ACV, this also relies on accurate assessment of a home's effective age and an appropriate depreciation schedule. The second is the depth-damage relationship used to determine the proportion of a structure's full replacement cost damaged by a given level of flooding. The third is the foundation height, which alters the effective flood depth experienced by a particular residence. Without more detailed data, the relative importance of these factors in producing bias here is difficult to determine. The error contributed by each likely varies geographically, but it can be reduced by obtaining better quality data; for example, bias from these factors is likely smaller in the communities where parcel-level data has been obtained.

7.4 Discussion

As shown in Section 7.3.4, damage projections in CLARA are sensitive to differences in the projected extent of flooding from individual events like Hurricane Isaac. Previous model documentation has discussed the difficulty of modeling the threshold where storms start to wet a given point using the JPM-OS response surface approach (Fischbach et al., 2012b). Statistical metrics such as 100-year flood depths are less sensitive to errors in identifying the storm parameters where this threshold occurs, however, because storms with parameters near the boundary only represent a small fraction of the entire space of possible synthetic storms.

A summary of the key findings and conclusions from the Isaac comparison exercises is given below, with more detailed discussion to follow:

- Data quality in CLARA's economic inventory was good: housing units in Plaquemines Parish, for example, were within 2 percent of reported values, and discrepancies between named communities in the parish are consistent with continuation of settlement trends observed in the last decade.

- Simulated surge elevations from synthetic storms based on the parameters of real, observed storms like Hurricane Isaac are of mixed quality. Further, evaluation of synthetic storm performance in this regard is made difficult by the small number of monitoring sensors and their typical proximity to levee systems.

- Predicted overtopping and flooding in enclosed areas coincided with observed locations during Hurricane Isaac. CLARA calculated that levee failures were likely where none actually occurred, though due to the polder configurations in Plaquemines Parish, this had little impact on modeled flood depths within the polders.

- Differences in economic damage assessments were primarily due to differences in the predicted extent of flooding, as opposed to differences in flood depths where flooding did occur in both reality and the modeled synthetic storm.

Errors and uncertainty in the quantity and characteristics of economic assets at risk could be reduced by additional data collection. These are data elements with verifiable values. Several tax parcel-level datasets developed by USACE for other recent studies have been integrated into CLARA's economic database, including some areas that received heavy damage from Hurricane Isaac such as St. John the Baptist Parish. However, these detailed surveys do not yet cover the entire coast (see Section 3.1).

CLARA's damage estimates—both the number of properties and direct economic losses—are a function of many different storm and economic characteristics. Because of this, it can be very difficult in some cases to determine the precise reason(s) why modeled results deviate from real

losses. Uncertainty propagates through each step of the model calculations, so final results are generally more sensitive to differences in earlier steps. As illustrated by the Isaac-like synthetic storm, the accuracy of modeled foundation heights in a particular community does not matter if the model does not project flooding to extend into that area.

The quality of damage projections from individual storm events is highly sensitive to the predicted extent of flooding from the event; statistical results like damage exceedances are much less sensitive to accurate identification of flood extents. This illustrates the importance of having a greater number of monitoring stations and pressure sensors deployed in locations not adjacent to protection features that alter ground elevations or surge patterns. The extent to which CLARA and the JPM-OS framework can be used to simulate real storm events depends greatly on having a larger number of observed data points in order to better evaluate the fit of the modeled surge elevations, wave heights, and flood depths. The quality of a simulated historic storm within CLARA also relies on having an appropriate set of similar synthetic storms in the JPM-OS corpus to produce a good response surface fit.

Validating CLARA's economic module would be aided by having access to a database of FEMA inspection results for the over 120,000 home inspections performed in the months after Hurricane Isaac. This would have provided a much better understanding of flooding extent and depths than the approximately 350 HWMs, tide gages and pressure sensor locations. Without this information, it is difficult to ascertain whether differences in economic outputs stem from differences in economic characteristics or errors propagated from the flood module.

Even several years after the event, reconstructions of Hurricane Isaac's wind fields are of poor quality. If synthetic storms based on observed storm parameters can produce a reasonable approximation of observed flood depths, models like CLARA could be used to quickly estimate economic impacts in the period immediately after a storm. However, the model's sensitivity to the extent of flooding implies that results are much more reliable areas such as Plaquemines Parish, where flooding is substantial and widespread. Results from the Isaac-like synthetic storm were significantly less accurate in areas like Laplace and Slidell that, despite suffering heavy monetary losses, experienced maximum water depths of 1 meter or less.

Hurricane Isaac was an anomalous storm, larger than previous storms of record and slow-moving enough to stall out and make landfall twice on the Louisiana coast. This presented a challenge to the JPM-OS framework that was known from the outset of this exercise. Specifically, extrapolating from a storm suite that does not contain any storms with parameters like Isaac's introduces significant uncertainty to response surface-based predictions of flooding. Some major biases in model outputs have been traced to the response surface's difficulty in identifying the envelope of flooding produced by Hurricane Isaac. Particularly when considering the possibility of more intense storms in the future, adding storms with more extreme parameter values to the JPM-OS storm suite could help to mitigate this issue and yield more accurate projections of plausible flooding.

Additional study is needed before concluding whether results are generalizable to storms with features more similar to those already in the JPM-OS suite. The current analysis suggests that the idealized Isaac-like synthetic storm drawn from the current storm suite replicates some impacts of the actual hurricane. It does not, however, reproduce flood depths across the entire coast accurately enough to conclusively validate the depth and damage estimates from CLARA, or to serve as a means of estimating flood impacts rapidly after a storm event.

8.0 Nonstructural Vulnerability Analysis

The 2012 Coastal Master Plan analysis, and subsequent analysis such as Johnson et al. (2013), suggests that applying nonstructural mitigation to all structures vulnerable to storm surge flood damage would be prohibitively expensive. In addition, the cost-effectiveness of nonstructural measures varies widely across different coastal communities. To address this challenge and support future resilience planning in coastal Louisiana, this section describes a detailed analysis to identify areas of the coast that are most vulnerable to flood damage—with and without the structural measures included in the 2012 Coastal Master Plan—and where nonstructural measures could be applied to cost-effectively reduce current and projected future flood damage.

The analysis described below serves a dual purpose. Baseline estimates of flood risk, spatial vulnerability, and the effectiveness of nonstructural measures can support project planning and investment decisions made by Louisiana's Flood Risk and Resilience Program. The 2017 Coastal Master Plan can also utilize this work to define nonstructural projects—application of mitigation measures using particular decision rules over a particular spatial domain—for evaluation alongside proposed structural risk reduction projects.

This section first summarizes the 2012 Coastal Master Plan's nonstructural analysis and describes the basic mechanisms by which the modeled nonstructural measures reduce flood damage. Several improvements to CLARA's nonstructural modeling capabilities are then described. This includes an outline of the mathematical basis used to identify the most cost-effective mitigation heights for a given set of scenario assumptions. The results of the cost-effectiveness analysis are presented next. Illustrative results are shown for a set of projects with a total cost of $10.2 billion to facilitate comparisons to 2012, but results can be generated using any budget constraint. Finally, the chapter concludes with a discussion of spatial clustering of vulnerable areas and areas where nonstructural measures are most effective. This spatial clustering was done to inform the definition of nonstructural project areas for the 2017 Master Plan process, which will replace the "target communities" used in 2012.

8.1 Overview and Background

CLARA's economic damage module has the capability of estimating the risk reduction effects of various nonstructural mitigation measures. This was originally done to support the inclusion of nonstructural projects for consideration in the 2012 Coastal Master Plan. Four policy options were modeled in support of the 2012 Coastal Master Plan: residential structure elevation, residential floodproofing, non-residential floodproofing (of commercial and industrial assets), and residential property acquisitions. Elevation was modeled by raising first floor heights above local Base Flood Elevations (BFEs), plus either one or four feet (0.3 or 1.2 m) of additional freeboard (referred to as BFE+1 and BFE+4, respectively).

If attaining that level, referred to as the mitigation standard, would require elevating a residence beyond 18 feet (5.5 m) above the ground elevation (the highest elevation of adjacent grade, or HEAG), assets were modeled as being acquired by a voluntary buyout. An easement was then placed against future development. Alternately, if the mitigation standard was three feet or less above existing structure elevations, floodproofing was applied rather than elevation.

These measures were applied to each census block, according to the difference in mean block elevation and the local BFE. Nonstructural projects were defined by the collective nonstructural

mitigation efforts applied over all blocks within each target community from the 2012 Coastal Master Plan, along with the mitigation standard used (BFE+1 or BFE+4). The number of structures mitigated varied by a scenario parameter, the participation rate assumed for each nonstructural measure. The 2012 Coastal Master Plan results primarily reflected the Medium-High participation rate: 80% participation in residential floodproofing, and 70% participation for the other measures.

Elevation and floodproofing costs were modeled as a function of the elevation height and a structure's square footage. Buyout costs were proportional to the assessed value of the property, plus a fixed cost for both the structure acquisition and the easement. For all results presented here, costs for the acquisitions measure also include the cost of easements.

Residential elevation mitigates risk by reducing the effective depth of flooding experienced by a structure. Floodproofing acts to eliminate damage up to the level where floodproofing stops (i.e., up to three feet [0.9 m] above the building foundation). Acquisitions reduce risk by removing an asset from the floodplain entirely.

8.2 Cost-Effectiveness Analysis

Elevating all coastal residences and floodproofing commercial and industrial properties to a BFE+1 or BFE+4 level would cost much more than the initial allocation of funding to nonstructural risk reduction in the 2012 Coastal Master Plan, and could cost more than the master plan's entire $50 billion budget (Johnson et al., 2013). As a result, decision criteria are needed to prioritize where scarce nonstructural funds should be allocated. In 2012, the reduction in EAD with a project in place was used as a measure of cost-effectiveness; this metric was applied to both nonstructural and structural projects. The updated analysis presented here adopts the same metric. CLARA also calculates the residual damage by return period; selected exceedances are also shown in the results.

Nonstructural projects considered in 2012 were defined geographically using a set of 56 target communities spanning the Louisiana coast. Cost-effectiveness was assessed for entire target communities, despite the possibility that a community may encompass some regions with high potential for nonstructural mitigation and other regions where mitigation would be less cost-effective. This was indeed the case: for example, some of the initial target communities, such as Jefferson Parish, contain population centers both interior and exterior to the New Orleans HSDRRS.

The 2012 Coastal Master Plan designated $10.2 billion for nonstructural mitigation. The funding level was selected using the Planning Tool, which is a tool developed to help prioritize projects based on multiple decision metrics and to visualize tradeoffs between criteria and differences between modeled scenarios (Groves et al., 2012). The funding level was based upon the cost of implementing a BFE+1 strategy in 42 of the 56 target communities. However, the plan specified that funding be made available to all communities coast wide. The new analysis provided here instead examines cost-effectiveness at the grid point level to enable the construction of more homogeneous geographic project definitions (see Section 8.3).

Subsections 8.2.1 and 8.2.2 describe updates to the CLARA model that specifically address recognized limitations of the 2012 Coastal Master Plan analysis or add new functionality related to nonstructural modeling. Subsection 8.2.3 presents the results of a cost-effectiveness analysis based on the preliminary flood risk data available during the 2017 Model Improvement phase.

8.2.1 Changes and Additions in CLARA v2.0

The nonstructural strategies considered for the 2012 Coastal Master Plan were based on existing BFEs provided by FEMA at the time of plan development. However, using these BFEs as the reference standard for future mitigation is challenged by several shortcomings. First, the effective BFEs in some NFIP jurisdictions and municipalities are outdated, with some dating back to the 1970s. Many of the effective Flood Insurance Rate Maps (FIRMs) do not yet incorporate recent improvement to flood risk estimation methods, changes in risk associated with upgrades to structural protection systems, or the change in risk in recent decades due to sea level rise and land subsidence. In addition, FEMA BFEs are static, and do not yet take into account potential future changes to flood depths. Finally, FEMA BFEs are typically provided as 100-year (1 percent annual exceedance probability (AEP)) flood elevations only in support of the federal flood insurance program, with 500-year estimates (0.2 percent AEP) also provided only in select cases. The 1 percent AEP flood elevation is intended to support the implementation of the federal flood insurance program first and foremost, and may or may not provide cost-effective damage reduction when considering the full range of plausible storm surge events.

As a result, mitigation standards measured relative to the BFEs may not be the most cost-effective mitigation heights in all areas. Depth-damage curves and the costs of mitigation are each non-linear—elevating a structure becomes more expensive, per foot of elevation, as the desired elevation increases. As such, the cost-effectiveness of a nonstructural mitigation strategy can vary substantially as a function of the mitigation standard used.

To improve the ability to select cost-effective nonstructural projects, two major changes were made to how they are modeled in CLARA v2.0. Firstly, the definition of a mitigation standard is more flexible. They no longer must be tied directly to FEMA BFEs; instead, standards are based on estimates of flood depths produced by CLARA.

Secondly, standards are no longer tied to a particular flood depth exceedance (as BFEs are ostensibly based on 100-year flood depths), and they do not have to be defined *a priori*, independent of cost-effectiveness. Instead, CLARA v2.0 calculates the most cost-effective elevation for mitigation; details for how this is accomplished are in the next subsection. Strategies are defined by elevating residential structures up to this level (as noted earlier, elevation is generally not possible for non-residential structures). Freeboard is not added beyond the most cost-effective elevation height in this initial analysis.

However, because cost-effectiveness depends in part on risk reduction, the most cost-effective elevation can vary depending on the assumed probability distribution of flood depths. This is scenario-dependent, so a nonstructural strategy is now defined by the scenario used as the basis of the flood depth calculations.

This analysis presents risk reduction results from the 2012 Coastal Master Plan's Less Optimistic FWOA scenario in 2065. The analysis considers nonstructural strategies with elevation reference standards no longer tied to the FEMA BFEs, but based instead on either the 2012 Coastal Master Plan current conditions scenario ("2015 Basis Year") or the 2065 Less Optimistic scenario ("2065 Basis Year"). Both of the reference standards also assume that none of the structural projects recommended in the 2012 Coastal Master Plan are in place.

To support the goals of the Flood Risk and Resilience program, CLARA v2.0 also allows for the possibility of removing residential floodproofing from the mix of nonstructural policy options. Project results with and without this option are presented, allowing analysis of how cost effective nonstructural mitigation strategies might be without elevation. The elevation threshold beyond

which properties are acquired has been lowered to 14 feet (4.3 m) based on additional guidance from CPRA. In addition, this analysis restricts non-residential floodproofing to commercial properties, excluding industrial and public assets that were included in 2012.

New cost curves for each measure were recently developed to support 2017 Coastal Master Plan analysis. Updated values were not available at the time of this analysis, so the results presented here are based on the same cost estimates used in the 2012 Coastal Master Plan analysis.

8.2.2 Derivation of Maximally Cost-Effective Mitigation Standards

The cost-effectiveness of nonstructural mitigation is a function of three factors: the cost of mitigating an asset; the probability distribution of flood depths at the asset's location; and the depth-damage relationship between flood depths and the extent of damage the asset experiences, expressed as a proportion of its actual cash value or total replacement cost.

Assume a home with square footage s is to be mitigated. Elevating the building to a height of h above the current foundation would incur some cost $C(h,s)$.

Denote the depth-damage function as $D(e)$, a monotonically increasing function of e, the elevation of flooding relative to a building's ground floor or the top of its foundation. Define $f(e)$ to be the probability distribution function (PDF) of flood elevations the home might encounter, conditional on some storm event occurring.

Elevating a home directly reduces the effective flood depth it experiences relative to its foundation. The expected loss from a flood, L, expressed as a proportion of its value, can therefore be defined as

$$L(h) = \int_{-\infty}^{\infty} D(e)f(e+h)de = \int_{-\infty}^{\infty} D(e-h)f(e)de \quad (8\text{-}1)$$

These two definitions are equivalent; the variable substitution will be used later.

Define the cost-effectiveness ratio, $R(h)$, to be the change in expected damage per dollar spent on mitigation. The objective is to maximize

$$R(h) = \frac{L(0) - L(h)}{C(h,s)} \quad (8\text{-}2)$$

Denoting the change in expected loss as $\Delta(h) = L(0) - L(h)$, then the goal is to identify h^* such that

$$h^* = \underset{h}{\operatorname{argmax}} \frac{\Delta(h)}{C(h,s)} \quad (8\text{-}3)$$

The optimal mitigation height h^* is thus the height for which the derivative of Equation 8-2 is equal to zero. This then implies that

$$\Delta'(h^*)C(h^*,s) = \Delta(h^*)C_h(h^*,s) \quad (8\text{-}4)$$

where C_h denotes the partial derivative of $C(h^*,s)$ with respect to h. Using the variable substitution in Equation 1 on the left-hand side,

$$C(h^*,s)\int_{-\infty}^{\infty} D'(e)f(e+h^*)de = C_h(h^*,s)\int_{-\infty}^{\infty} D(e)[f(e)-f(e+h^*)]de \quad (8$$

Rearranging terms yields

$$\int_{-\infty}^{\infty}\left[\frac{C(h^*,s)}{C_h(h^*,s)}D'(e)+D(e)\right]f(e+h^*)de = \int_{-\infty}^{\infty} D(e)f(e)de \quad (8\text{-}6)$$

The right-hand term is just the expected damage in the unmitigated case. Using variable substitution again on the left-hand side yields

$$\mathbb{E}\left[\frac{C(h^*,s)}{C_h(h^*,s)}D'(e-h^*)+D(e-h^*)\right] = \mathbb{E}[D(e)] \quad (8\text{-}7)$$

$$\Longrightarrow \mathbb{E}[D'(e-h^*)] = \frac{C_h(h^*,s)}{C(h^*,s)}\mathbb{E}[D(e)-D(e-h^*)] \quad (8\text{-}8)$$

$$\Longrightarrow \mathbb{E}[D'(e-h^*)] = \mathbf{E}C(h^*)\frac{\mathbb{E}[D(e)-D(e-h^*)]}{h^*} \quad (8\text{-}9)$$

where $\mathbf{E}C(h^*)$ is the elasticity of the cost function with respect to mitigation height, the ratio of the percentage change in cost with respect to a percentage change in height.

The most cost-effective mitigation height h^* must satisfy Equation 8-9, a more straightforward relationship between the expected risk reduction produced by additional mitigation and the additional costs incurred. Put more plainly, the optimal mitigation height is the height at which the cost elasticity is equal to the elasticity of the expected damage, accounting for the fact that the damage is uncertain and depends on the probability distribution of flooding.

CLARA v2.0 identifies the scenario-specific h^* for each grid point as a function of the probability distribution of flood depths and the characteristics of assets located at that point (for example, the model accounts for the current foundation heights of existing homes). The mitigation cost function and depth-damage curves are the same coast wide.

8.2.3 Results

8.2.3.1 Cost-effectiveness of Nonstructural Mitigation Measures

Following the Planning Tool's use of cost-effectiveness as a decision criterion, grid points have been ranked by the cost-effectiveness of nonstructural mitigation, expressed as the reduction in EAD per dollar spent on mitigation. The most cost-effective mitigation measure varies across the coast, depending on the probability distribution of flooding at each point and the height of existing structure foundations. The most cost-effective measure—elevation, floodproofing, or

acquisition—for each point where nonstructural mitigation does reduce some flood damage is shown in Figure 8-1. Floodproofing is generally the most cost-effective option in New Orleans, where the baseline expected damage is relatively low due to HSDRRS. Buyouts are the most cost-effective measure in a few selected regions of the coast, particularly around Lake Charles, Braithwaite, and portions of Slidell without structural protection.

Figure 8-2 shows the actual cost-effectiveness of nonstructural mitigation when the most cost-effective mitigation measure is applied to each asset class; grid points with no residential or commercial assets that can be mitigated are excluded, as are points where mitigation does not reduce risk (i.e., where assets are projected to have zero expected annual damage). Residential floodproofing is included in the mapped results, and the mitigation standard is based on flood depths in the 2065 FWOA Less Optimistic scenario (2065 Basis Year). Some risk reduction is achieved in 49,542 grid points. Of these, floodproofing is the most cost effective measure in 33,789 points.[32] Elevation is the most cost-effective option in 13,316 points, and acquisitions are the most cost effective in 2,437 points.

If residential floodproofing is not considered as an option, elevation is always the next-best measure. In Figure 8-2, excluding residential floodproofing would only remove the small number of points where homes could be floodproofed, but where no commercial structures otherwise exist. A summary of the number of points where a given option is selected, and the total cost of implementing the measure at those points under High participation, is found in Table 8-1. Throughout this section, Medium-High participation denotes 80% participation in residential floodproofing (when offered) and 70% participation in other measures; High participation denotes 90% participation in all measures.

The degree of homogeneity and clustering apparent in Figure 8-1 indicates that the most cost-effective measure in a given census block tends to align well with the risk in surrounding areas. Points where acquisitions are the most cost-effective option are points with high risk, and they generally form easily-recognizable clusters. Few of these points are isolated or surrounded by points for which another option is more cost-effective. In New Orleans, floodproofing is overwhelmingly the most cost-effective option. Elsewhere, floodproofing and elevation are somewhat mixed, due to local differences in flood risk, ground elevation, or average foundation heights of existing assets.

[32] This pattern is not readily apparent on the map because of the high density of grid points in New Orleans.

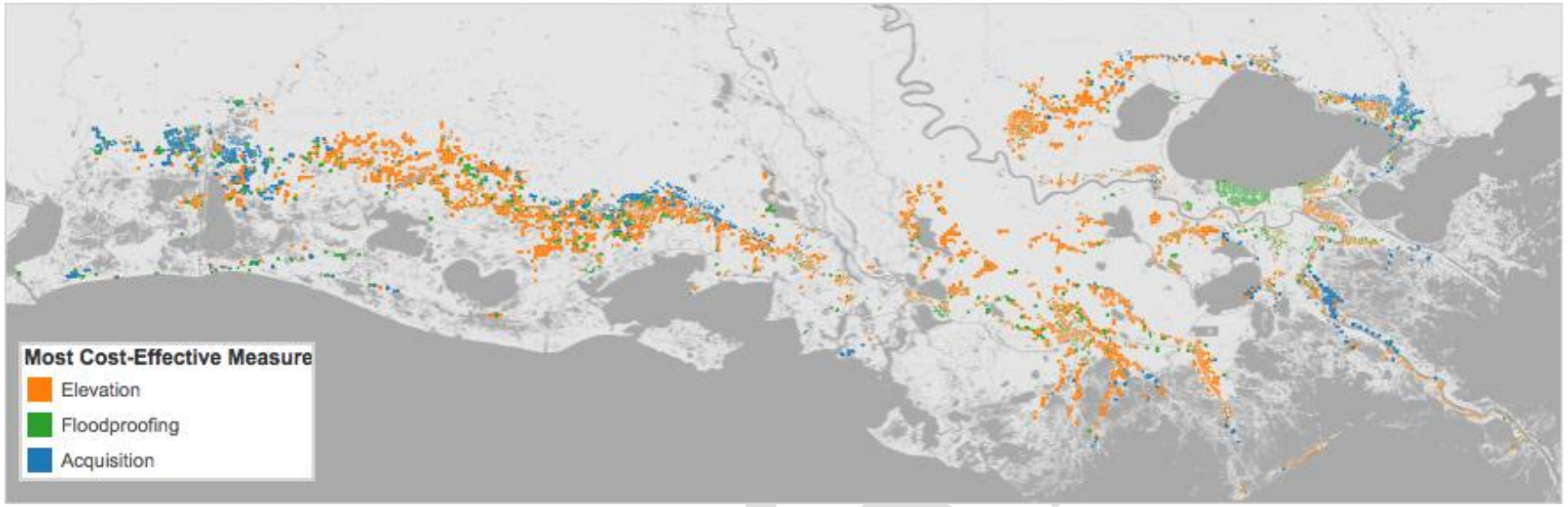

Figure 8-1: Most Cost-Effective Mitigation Measure by Grid Point (Single-Family Residences, 2065 Basis Year; FWOA).

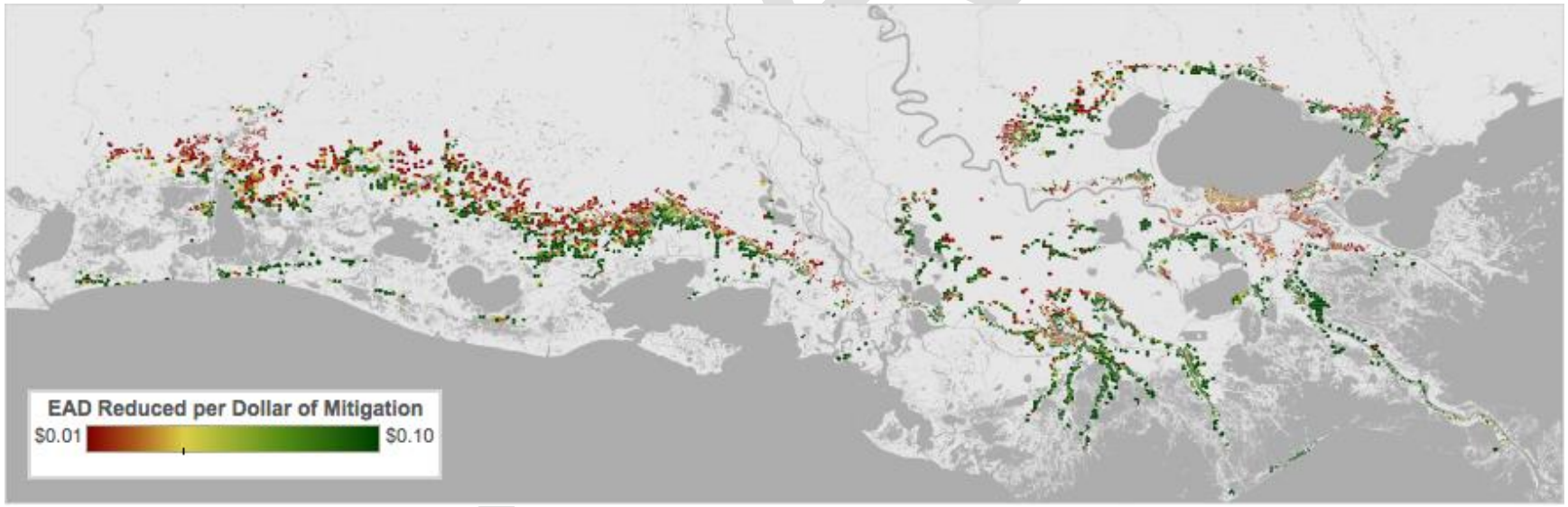

Figure 8-2: Cost-effectiveness of Nonstructural Mitigation, by Grid Point (Residential Floodproofing Allowed; 2065 Basis Year; FWOA).

Table 8-1: Number of CLARA Grid Points by Most Cost-Effective Nonstructural Measure, Including Total Cost Under High Participation (2065 Basis Year, Residential Floodproofing Offered).

Measure	Points	Cost
Floodproofing	31,519 (73%)	$14.1B
Elevation	8,834 (21%)	$26.3B
Acquisition	2,548 (6%)	$40.5B
Total	42,901	$80.9B

One simple way to allocate nonstructural funds would be to distribute funding to the most cost-effective areas. Successively less cost-effective points would be funded until the program's budget runs out. Figure 8-3 shows the reduction in EAD achieved by nonstructural programs, as a function of cost, using this method of allocation. The $10.2 billion nonstructural budget from the 2012 Coastal Master Plan is provided as a reference line, illustrating that the marginal benefit from spending more than this constraint tails off quickly in all scenarios modeled. In general, excluding residential floodproofing from the program (the lighter lines of each color) has less of an impact on overall cost-effectiveness than does having a lower participation rate or adopting the mitigation standard based on current conditions.

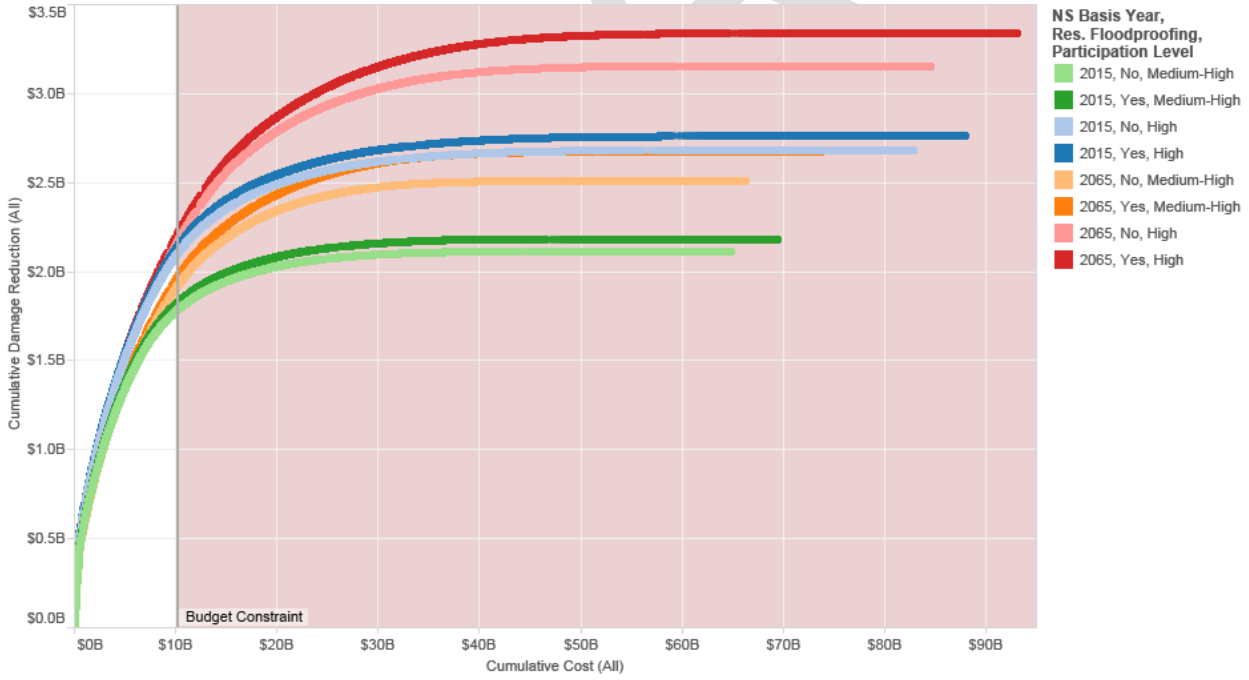

Figure 8-3: Cumulative Damage Reduction as a Function of Program Cost.

The end of each line in Figure 8-3 represents the total risk reduction that could be achieved with unlimited funding in each scenario. Under the allocation method based on cost-effectiveness, residential floodproofing is only selected for the program when it is more cost-effective than other options, so it always reduces greater risk for the same cost than the same strategy with the

measure excluded. Allowing, but not requiring, residential floodproofing results in greater efficiency.

Figure 8-4 shows the portion of the marginal damage reduction curve from Figure 8-3 below a $10.2 billion program cost. Additional points show the cost and EAD reduction estimated for selected structural protection projects recommended in the 2012 Coastal Master Plan. These are shown as a reference and to illustrate that the 2012 plan included structural projects with both higher and lower cost-effectiveness than the nonstructural measures analyzed here.

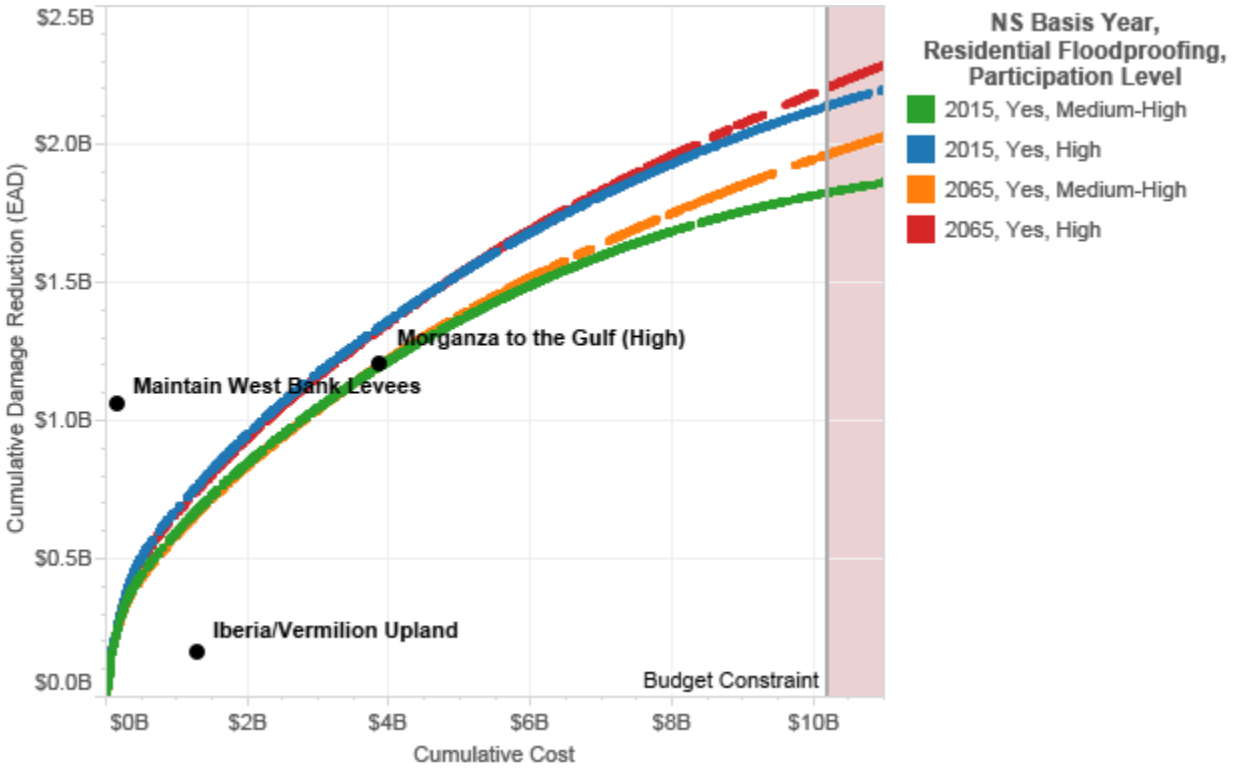

Figure 8-4: Cumulative Damage Reduction as a Function of Program Cost (Comparison to 2012 Coastal Master Plan Structural Projects).

Under a $10.2 billion budget constraint, damage reduction primarily hinges on participation rates. This is an intuitive result; if property owners in the most cost-effective areas do not participate, allocations shift down to less cost-effective areas, producing less benefit for the same cost. With high participation, expected annual damage reduction in 2065 under the Less Optimistic FWOA scenario is approximately $3.1 billion, versus only about $2.2 billion in the Medium-High participation scenario.

8.2.3.2 Geographic Allocation of Nonstructural Funding

Figure 8-5 shows which grid points would be included in a nonstructural mitigation program under a $10.2 billion budget constraint in a future without action in which no additional structural protection is assumed. The program shown does not include residential floodproofing, and a Medium-High participation rate is assumed. The excluded points (orange), with lower cost-effectiveness, are generally either further inland, or are within the New Orleans HSDRRS and have a lower baseline level of expected damage. Exceptions include some points in Cameron Parish and lower Plaquemines Parish.

For grid points included in this strategy under a $10.2 billion budget constraint, Figure 8-6 shows the proportional damage reduction achieved by the strategy, illustrating where it provides substantial risk reduction, as well as where relatively high levels of risk would remain even with the strategy in place. Figure 8-7 details how funds are distributed among parishes, alongside the reduction in expected annual damage produced by the program. In all of the modeled scenarios, St. Tammany and Terrebonne Parish see the greatest funding levels and benefits.

The color of each bar in Figure 8-7 indicates the proportion of EAD from the Future Without Action case that is reduced using the nonstructural mitigation strategy. Note that unlike the cost-effectiveness measure, proportional risk reduction depends partly on the number and type of assets at risk in a given area. Low proportional risk reduction does not necessarily indicate that nonstructural measures are ineffective. Instead, it may indicate that the area has a large number of assets that cannot be mitigated, such as roads or agriculture. In terms of absolute risk reduction, elevation is more effective than floodproofing, because it can be used to protect a structure up to a higher level. Therefore, a low proportional risk reduction may also indicate a larger number of assets, such as commercial and industrial properties, that cannot be mitigated using elevation.

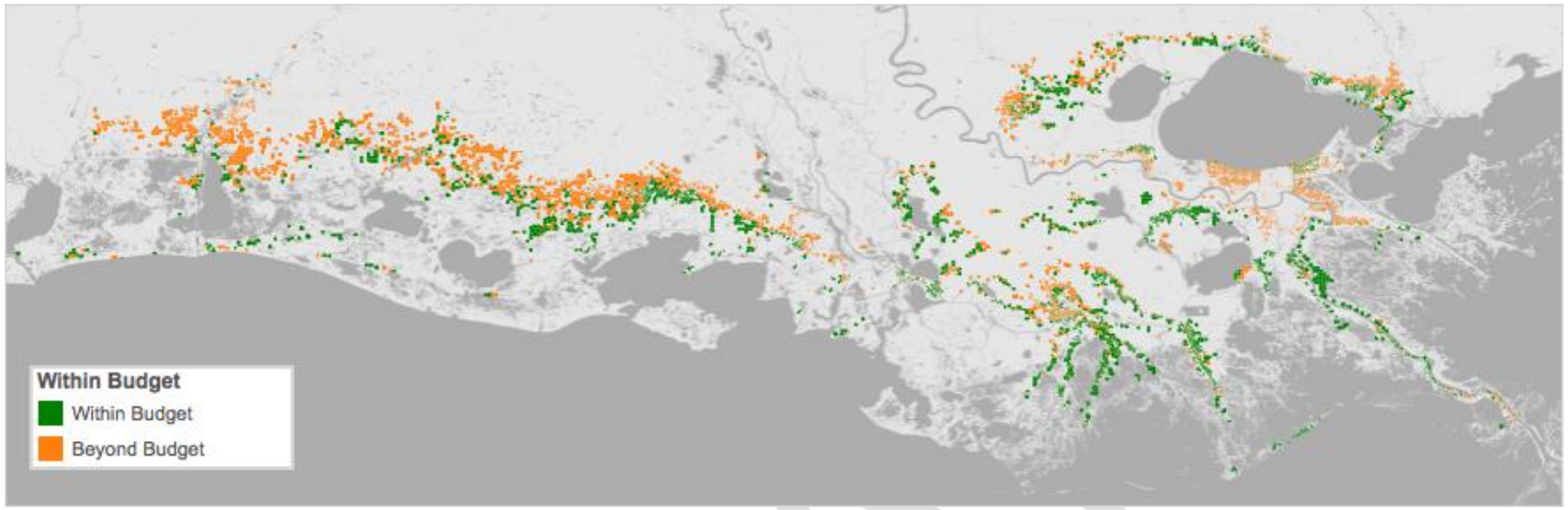

Note: Residential Floodproofing Excluded; 2065 Basis Year; Medium-High Participation; FWOA.

Figure 8-5: Points Included in a $10.2B Nonstructural Mitigation Program Based on Cost-Effectiveness.

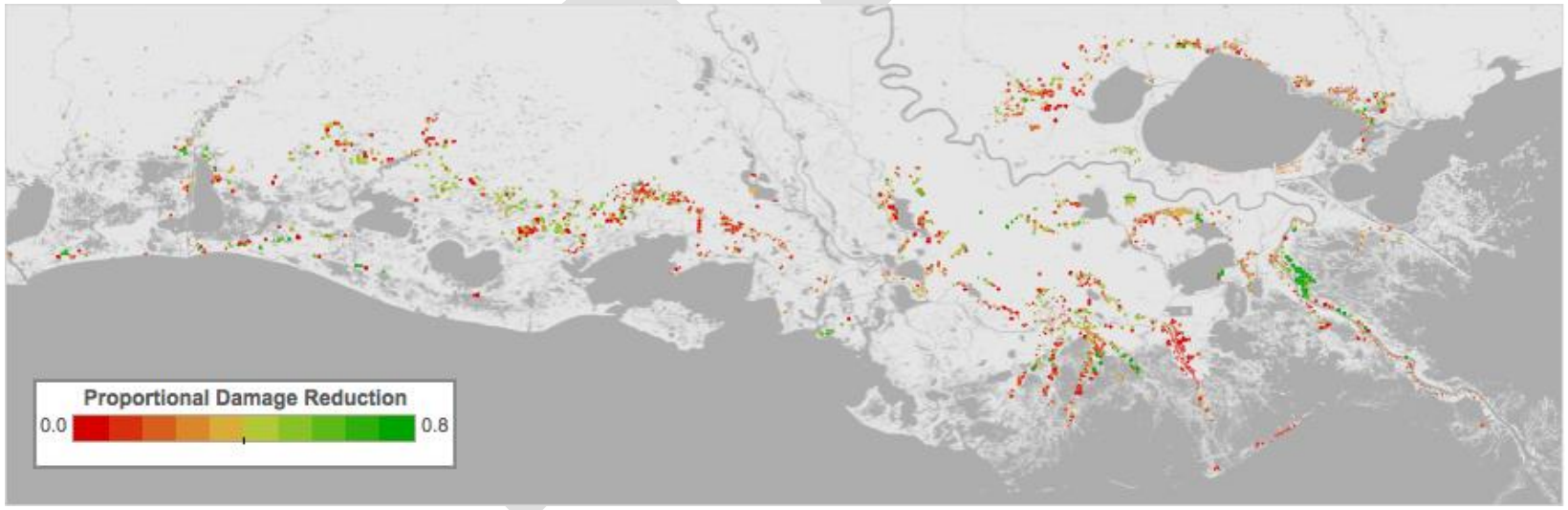

Note: Residential Floodproofing Excluded; 2065 Basis Year; Medium-High Participation; FWOA.

Figure 8-6: Proportional Damage Reduction from a $10.2B Nonstructural Mitigation Program.

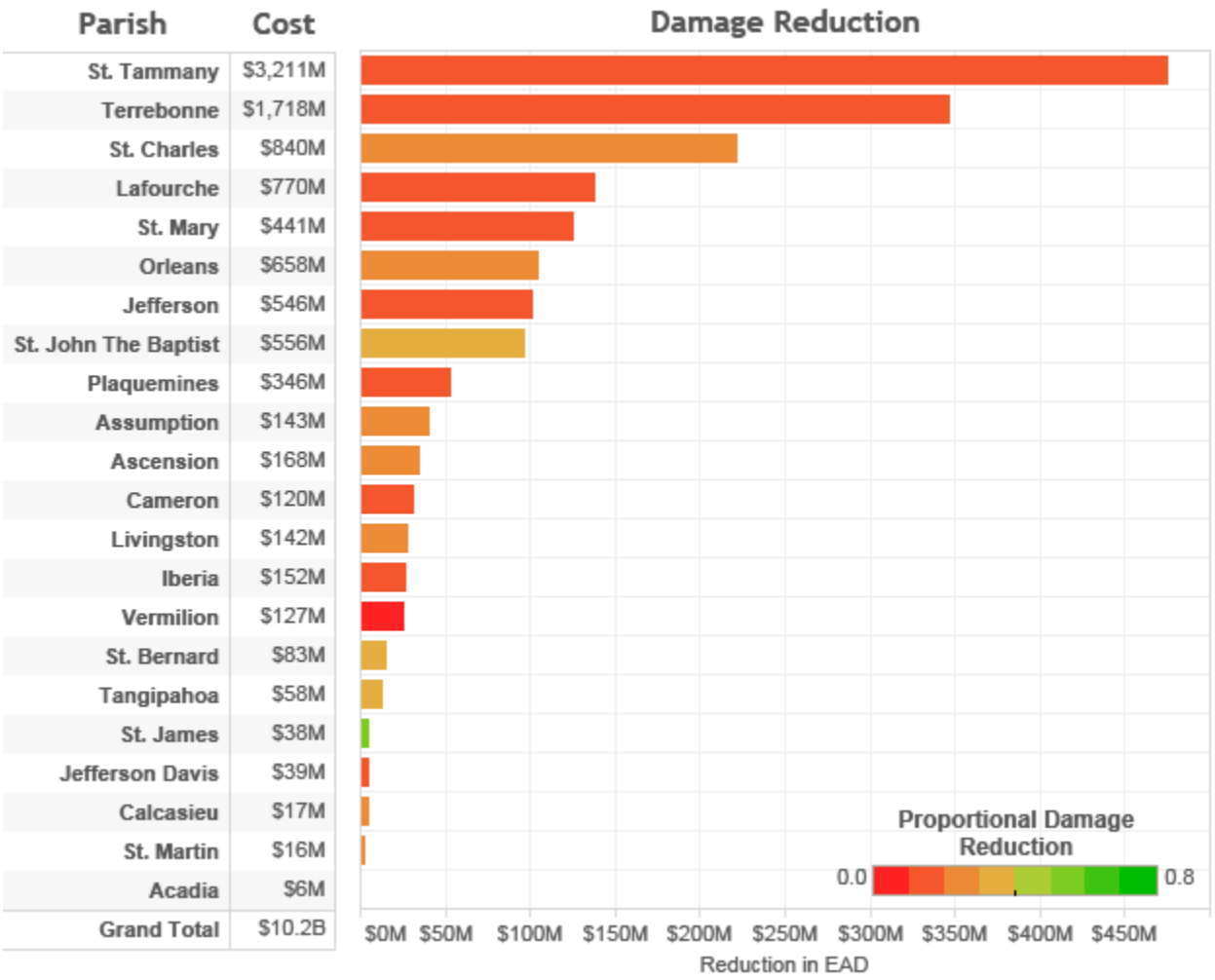

Figure 8-7: Distribution of Funds and EAD Reduction by Parish Based on Cost-Effectiveness (Residential Floodproofing Excluded; 2065 Basis Year; Medium-High Participation; FWOA).

Programs could also incorporate other decision rules. For example, Figure 8-8 shows the points that would be funded by a $10.2 billion program, depending on whether or not funding is only provided to areas which do not have structural protection (both currently and with the 2012 Coastal Master Plan's structural projects in place). For ease of comparison, only areas that remain unprotected with implementation of the 2012 plan are shown. The top pane of Figure 8-8 is therefore identical to Figure 8-5 except that it does not show points that have structural protection.

Some funding could still be allocated to areas with structural protection, provided that it is still relatively cost-effective to use nonstructural measures to mitigate the residual risk. Excluding areas with structural protection from the nonstructural program allows a greater number of assets in unprotected areas to be mitigated.

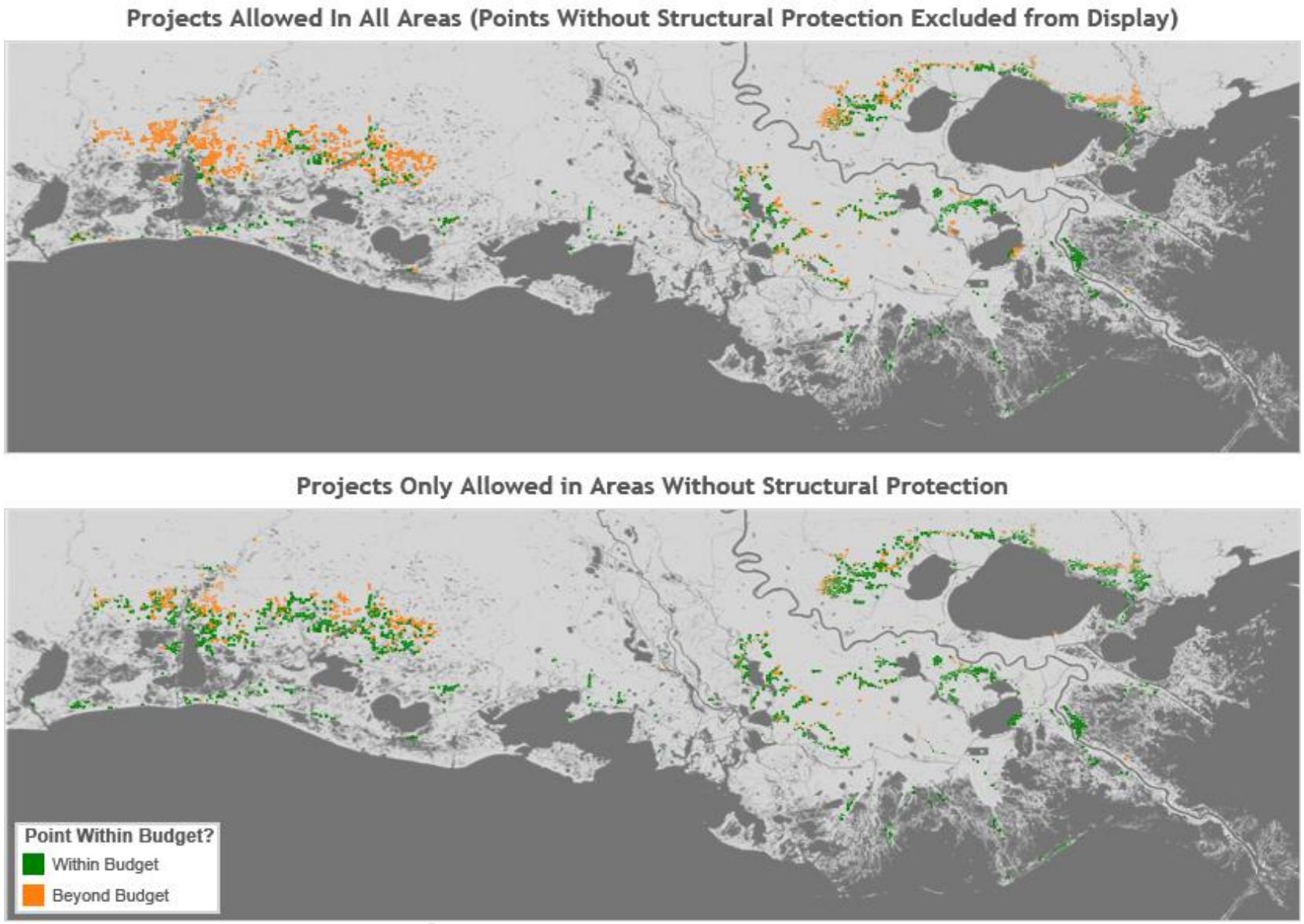

Figure 8-8:. Unprotected Areas Included in a $10.2 Billion Program (Areas with Structural Protection under the 2012 Master Plan Included in (Top) or Excluded from (Bottom) the Program.

The more inclusive program described above decides if areas should receive funding on the basis of cost-effectiveness in the FWOA scenario, in which no new structural projects are built. However, the investment performance of nonstructural risk reduction might differ greatly if and when protection alignments identified in the 2012 Coastal Master Plan are constructed. In Terrebonne Parish, for example, damage reduction from nonstructural might be dramatically different with the Morganza to the Gulf project (USACE, 2013b) in place. Development of an effective nonstructural mitigation program thus depends on assumptions made about what, and when, structural projects will be constructed.

This can dramatically shift the distribution of costs and benefits of the program. Figure 8-9 shows the distribution of costs and benefits by parish under the exclusionary strategy. In this case, the benefit to Terrebonne Parish is reduced due to exclusion of points which would receive structural benefits from the Morganza to the Gulf levee project.

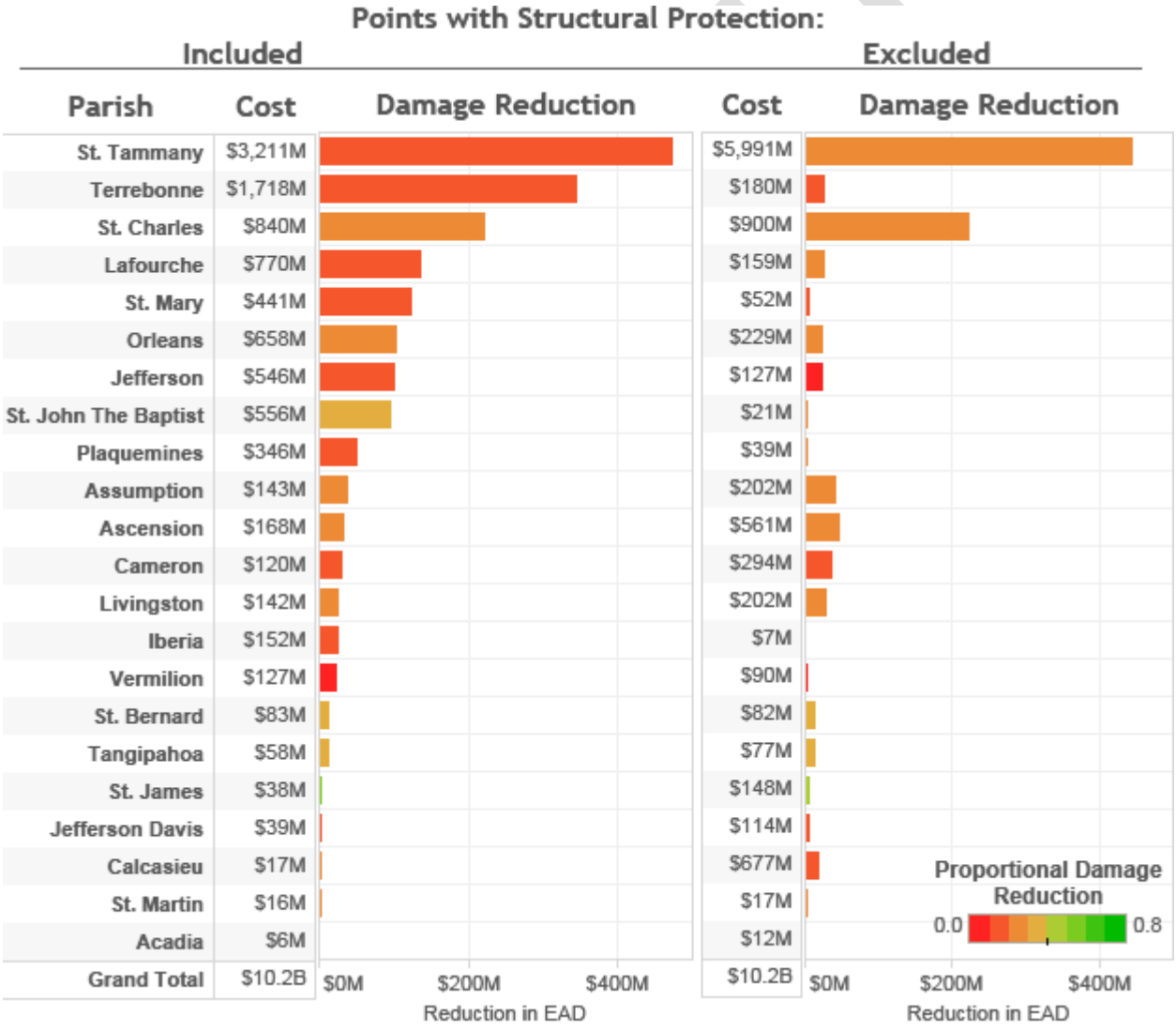

Figure 8-9: Distribution of Funds and EAD Reduction by Parish, Points with Structural Protection Included or Excluded from Nonstructural Program(No Residential Floodproofing; 2065 Basis Year; Medium-High Participation).

Figure 8-9 also shows several other notable results. First, the amount of damage reduction in some areas (e.g., St. Tammany Parish) remains nearly constant despite a much larger investment cost. This is because some points receiving structural protection from the 2012 Coastal Master Plan would be cost-effective for nonstructural mitigation in the scenario being modeled (FWOA, where said projects are not built). As a result, the overall cost-effectiveness goes down; the figure clearly shows that total damage reduction coast wide is greatly decreased, though the $10.2 billion budget is constant. When points receiving structural protection are excluded, unprotected points in St. Tammany are still cost-effective enough, relative to other parishes, that St. Tammany receives the majority of funding. However, the damage reduction achieved by those funds is slightly decreased compared to the less restrictive strategy.

In addition, the proportional damage reduction (color scale) for each parish changes depending on whether areas behind structural protection are included or excluded, also because the baseline damage is different in each case.

8.2.3.3 Distribution of Nonstructural Mitigation Costs and Benefits by Asset Class

Given that elevation has greater potential for effectiveness than floodproofing, it is not surprising that the majority of the benefit from a $10.2 billion program would accrue to residential properties. Figure 8-10 shows this breakdown by asset class. The far left column represents EAD in the Future Without Action case, while other columns show the reduction in EAD achieved by different strategies. The values are colored by the proportional risk reduction achieved by the strategies for each asset class. Breaking out the results by asset class clearly shows that residential assets, where elevation is a possibility, achieve a much greater level of risk reduction than property types that can only be floodproofed or acquired.

Expected Annual Damage (Future without Action)		Reduction in EAD by Asset Class NS Basis Year / Participation Level / Residential Floodproofing							
		2015				2065			
		Medium-High		High		Medium-High		High	
		Excluded	Included	Excluded	Included	Excluded	Included	Excluded	Included
Single Family	$3,684M	$1,172M	$1,210M	$1,366M	$1,401M	$1,186M	$1,238M	$1,342M	$1,376M
Manufactured Homes	$407M	$137M	$138M	$149M	$154M	$121M	$121M	$127M	$127M
Small Multi-Family	$72M	$19M	$19M	$22M	$23M	$19M	$21M	$22M	$23M
Large Multi-Family	$1,824M	$49M	$49M	$44M	$43M	$151M	$149M	$121M	$115M
Commercial	$10,302M	$404M	$403M	$513M	$513M	$435M	$428M	$546M	$540M
Grand Total	$20,313M	$1,780M	$1,820M	$2,094M	$2,133M	$1,912M	$1,957M	$2,157M	$2,181M

Proportional Damage Reduction
0.0 0.8

Figure 8-10: EAD in Future Without Action, and Reduction in EAD by Asset Class and Scenario.

Figure 8-11 breaks out the EAD reduction by parish for the case of a $10.2 billion program using the 2065 basis year with residential floodproofing excluded and high participation. The proportional damage reduction is similar by parish for the other scenarios run.

Parish	Single Family	Mobile Homes	Small Multi-Family	Large Multi-Family	Commerce	Grand Total
Acadia	$1.2M	$0.1M	$0.0M	$0.0M	$0.1M	$1.5M
Ascension	$20.6M	$5.2M	$0.7M	$0.2M	$14.0M	$40.6M
Assumption	$36.9M	$6.0M	$0.4M	$1.1M	$7.8M	$52.2M
Calcasieu	$1.8M	$0.3M	$0.0M	$0.0M	$4.4M	$6.5M
Cameron	$3.1M	$1.4M	$0.0M	$0.6M	$28.4M	$33.5M
Iberia	$16.5M	$3.2M	$0.9M	$0.3M	$9.0M	$29.8M
Jefferson	$86.6M	$15.2M	$2.8M	$5.6M	$11.8M	$122.1M
Jefferson Davis	$5.3M	$0.4M	$0.2M	$0.0M	$0.8M	$6.7M
Lafayette	$0.0M	$0.0M	$0.0M	$0.0M	$0.1M	$0.1M
Lafourche	$99.9M	$18.5M	$0.8M	$1.0M	$37.9M	$158.1M
Livingston	$27.4M	$6.6M	$0.2M	$0.0M	$0.9M	$35.2M
Orleans	$13.1M	$0.1M	$0.9M	$45.5M	$57.2M	$116.8M
Plaquemines	$37.1M	$10.1M	$0.9M	$2.2M	$8.8M	$59.0M
St. Bernard	$10.2M	$1.6M	$0.1M	$6.7M	$0.2M	$18.8M
St. Charles	$227.3M	$5.1M	$3.7M	$0.1M	$49.2M	$285.4M
St. James	$7.2M	$0.2M	$0.1M	$0.0M	$0.1M	$7.5M
St. John The Baptist	$81.6M	$0.1M	$0.1M	$0.0M	$29.2M	$111.0M
St. Martin	$4.1M	$0.6M	$0.0M	$0.0M	$0.4M	$5.1M
St. Mary	$80.9M	$4.2M	$3.4M	$3.1M	$65.0M	$156.6M
St. Tammany	$342.6M	$9.3M	$6.6M	$52.4M	$48.0M	$458.9M
Tangipahoa	$13.8M	$2.2M	$0.0M	$0.0M	$0.2M	$16.2M
Terrebonne	$210.8M	$35.0M	$0.0M	$2.0M	$158.2M	$406.0M
Vermilion	$13.3M	$1.5M	$0.0M	$0.0M	$14.7M	$29.5M
Grand Total	$1,341.6M	$126.9M	$21.7M	$120.8M	$546.2M	$2,157.1M

Figure 8-11: Reduction in EAD by Asset Class and Parish (FWOA; 2065 Basis Year, High Participation, Residential Floodproofing Excluded; $10.2 Billion Budget).

Figure 8-10 demonstrates that a major driver of risk reduction is the participation rate associated with a program. Higher participation means that the most cost-effective areas can be more completely mitigated, achieving a greater amount of total risk reduction when summing over the entire coastal region. The tradeoff is that higher participation results in fewer grid points receiving funding, so benefits would accrue to a smaller number of communities. Another major factor influencing the remaining risk is the limitation that floodproofing can only extend protection up to three feet beyond foundation heights. Because most of the residual risk shown in Figure 8-10 is to commercial properties, this indicates that the traditional measures explored in this analysis do not adequately protect these types of assets. While elevation has the potential to mitigate a large proportion of expected damage to homes, businesses would not receive the same level of benefits. In the event of a major future flood, homeowners might be able to return

home soon after the storm passes, but damage to the local economy could still hamper a quick recovery.

The large benefit to residential assets comes at a price, however. Elevation is a more expensive policy option on a per-square-foot basis. For all strategies modeled with a $10.2 billion budget constraint, more than half of the program cost goes to home elevation, with the next-largest expenditures being residential buyouts and commercial floodproofing. This is summarized in Table 8-2. Note that large multi-family residences are treated separately from other residential assets. Their multi-unit structures are generally too large to elevate in place; as such, strategies that exclude residential floodproofing as an option still allow large, multi-unit residences to be floodproofed. In this sense, they can be viewed more like commercial properties.

Table 8-2: Distribution of Costs by Asset Type and Mitigation Measure, $10.2 Billion Program.

		NS Basis Year / Participation Level / Residential Floodproofing							
		2015				2065			
		Medium-High		High		Medium-High		High	
		Excluded	Included	Excluded	Included	Excluded	Included	Excluded	Included
Residential (Small)	Elevation	$7,703M	$7,523M	$8,199M	$8,092M	$5,801M	$5,478M	$6,289M	$6,087M
	Floodproofing	$0M	$232M	$0M	$133M	$0M	$451M	$0M	$393M
	Acquisition	$1,586M	$1,534M	$1,171M	$1,152M	$2,462M	$2,427M	$2,195M	$1,945M
Residential (Large)	Elevation	$0M	$0M	$0M	$0M	$0M	$0M	$0M	$0M
	Floodproofing	$30M	$33M	$30M	$30M	$314M	$301M	$326M	$288M
	Acquisition	$321M	$317M	$168M	$166M	$879M	$868M	$531M	$509M
Non-Residential	Elevation	$0M	$0M	$0M	$0M	$0M	$0M	$0M	$0M
	Floodproofing	$558M	$556M	$627M	$625M	$739M	$673M	$850M	$805M
	Acquisition	$0M	$0M	$0M	$0M	$0M	$0M	$0M	$0M

Table 8-3 shows the number of structures mitigated under each of the strategies whose costs are broken out in Table 8-2. The number of structures that would be mitigated by a smaller, $5 billion program is shown in Table 8-4. The most striking difference is between strategies, with the same basis year and participation rate, that include or exclude residential floodproofing. As expected, strategies that exclude this measure result in fewer structures being floodproofed (the remaining numbers represent commercial properties). Excluding residential floodproofing results in many fewer structures being mitigated, however. This illustrates that floodproofing is simply a less expensive option than the other measures considered.

Another useful result is that in all cases, the number of structures acquired increases as the participation rate decreases. This is a consequence of acquisitions typically being more expensive and less cost-effective than other measures. A larger number of buyouts are included in a cost-constrained program only when residents decline to participate in areas with more cost-effective options.

No similar rule applies to floodproofing or elevation; in some cases, the number of structures receiving each treatment increases with program participation, and in other cases each decreases. This relates to the findings shown in Figure 8-1, that floodproofing and elevation are of similar cost-effectiveness in several areas of the coast, with the more cost-effective measure varying frequently among neighboring grid points.

Table 8-3: Number of Assets Mitigated by Measure and Nonstructural Strategy, $10.2 Billion Program.

NS Basis Year / Participation Level / Residential Floodproofing	2015				2065			
	Medium-High		High		Medium-High		High	
	Excluded	Included	Excluded	Included	Excluded	Included	Excluded	Included
Elevation	44,934	43,888	53,090	52,222	34,535	32,857	41,643	39,779
Floodproofing	1,078	9,229	1,239	7,498	1,674	15,742	2,020	15,888
Acquisition	4,631	4,467	4,135	4,095	6,677	6,576	6,322	6,205
Grand Total	50,643	57,583	58,464	63,815	42,885	55,176	49,985	61,872

Table 8-4: Number of Assets Mitigated by Measure and Nonstructural Strategy, $5 Billion Program.

NS Basis Year / Participation Level / Residential Floodproofing	2015				2065			
	Medium-High		High		Medium-High		High	
	Excluded	Included	Excluded	Included	Excluded	Included	Excluded	Included
Elevation	22,915	22,596	26,300	25,781	19,013	18,760	22,302	21,828
Floodproofing	756	4,165	1,066	4,703	1,073	7,886	1,414	7,992
Acquisition	1,943	1,919	1,318	1,246	3,288	3,049	2,303	2,227
Grand Total	25,613	28,680	28,684	31,730	23,374	29,695	26,019	32,048

The results presented here focus on programs that are restricted to the budget constraint approved for nonstructural risk reduction in the 2012 Coastal Master Plan. However, CLARA estimates the cost and damage reduction from nonstructural mitigation at each grid point, independent of the decision criteria that decides which parts of the coast and which policy measures are included in a nonstructural project. One example of this flexibility is the exclusion of residential floodproofing from some of the results shown in this chapter, but results can also be produced using any specific budget constraint.

8.3 Defining Nonstructural Project Areas

CLARA divides coastal Louisiana into thousands of small areas represented as grid points. Points differ in terms of severity of flood risk as well as cost-effectiveness of mitigation options. Geography is relevant in both cases; grid points close to one another are likely to have similar levels of flood risk (except where protection structures are present) and mitigation cost-effectiveness results, relative to grid points farther away.

Nonstructural mitigation is often planned and conducted by local communities or local floodplain managers. These areas can be thought of as contiguous geographic regions that contain multiple grid points. The goal may be to focus on areas with a given level of risk or areas amenable to specific mitigation options. Here, finding regions with similar grid points would clearly be desirable. Alternatively, the goal may be to focus on covering a diverse group of grid points to ensure policies are put in place to mitigate flood risk across all types of areas. Here again, it would help to aggregate grid points into similar regions, and then to examine how policies fare across these regions.

This section describes an approach to define new nonstructural risk reduction project areas for the 2017 Coastal Master Plan analysis and results from the initial analysis. Damage reduction, cost-effectiveness, and other attributes will be evaluated separately for each of the project areas defined through this process. This process included several steps. First, the asset database was carefully reviewed to filter down and identify assets and locations likely to be eligible for nonstructural investment, according to the methods described in the subsection below. Next, methods for defining similarity between points and identifying similar contiguous regions were applied. The goal was to describe a set of clusters that, coupled with existing municipal boundaries, existing or proposed levee alignments, and other natural geographic boundaries, could be used to identify a new set of target communities for nonstructural risk reduction in the 2017 Master Plan. Finally, a common method was applied to the CLARA v2.0 coastal domain, using both geographic and non-geographic data, to produce draft nonstructural project areas. Methods and results for each step is detailed below.

8.3.1 Identifying Grid Points Eligible for Nonstructural Investment

To finalize the nonstructural project areas, the Thiessen polygons for grid cells were examined to determine whether they contained assets liekly to be eligible for nonstructural risk reduction, focusing on residential and commercial asset classes. In this careful review, grid points were excluded from nonstructural damage analysis if they met at least one of the following criteria:

- The grid point fell on public land (state wildlife management areas, state/national parks, other state-owned/-leased land) which did not contain residential or commercial structures.
- The grid point was located on barrier islands other than Grand Isle.
- The grid point was associated with a census block containing entirely vacant or secondary homes.
- Both of the following:
    - The Thiessen polygon contained less than 1 total computed residential/commercial structure.
    - The grid point was associated with a census block containing at least 80 percent vacant or secondary homes as identified in the 2010 US Census.

Grid points included after this review process were then used to define nonstructural project areas using the methods described below.

8.3.2 Spatial Clustering Analysis

8.3.2.1 Approaches to Clustering

Prior research efforts have identified methodologies for dividing a geographic area into regions that are similar in terms of one or more variables. The problem has been given various names, including regionalization (e.g., Assunção, Neves, Câmara, & da Costa Freitas, 2006), contiguity-constrained clustering (Murtagh, 1985), spatial clustering (Cao, Wang, Forestier, Puissant, & Eick, 2013), and region-based segmentation. Assunção et al. (2006) surveyed existing efforts and categorized these methodologies.

The underlying concept for any clustering analysis is to separate a set of items into subsets which are similar under some definition of similarity. The items considered here are geospatial points, but in the general case, items need not have locations. Further, even when clustering points, the similarity metric need not be a function of the points' geospatial characteristics; it could be a function of one or more other variables associated with each point.

There are several possibilities for incorporating geospatial information into a clustering algorithm. Conventional cluster analysis can be performed on non-geographic variables, ignoring spatial information; each individual cluster can then be separated into [one or more] contiguous regions. Other methods use conventional cluster analysis based on both geographic and non-geographic data. A third approach first determines which points or areas are adjacent to others. These adjacency relations are then used in customized clustering algorithms where clusters must contain linked points or areas.

Intuitively, the first of the three approaches mentioned above works best when points in close geographic proximity are likely to be similar in terms of the non-geographic variables of interest. Otherwise, each of the clusters constructed when clustering without consideration of geographic data will have to be split into a large number of small clusters. In addition, it is difficult to control how many regions will be created when applying this approach.

The second approach is arguably the easiest approach to implement; existing clustering algorithms can be directly applied. One complication is the need to select a framework or weights when combining geographic and non-geographic variables to determine the similarity or difference between distinct points. This is similar, however, to choices that must be made when clustering on any set of more than one variable. The approach also cannot guarantee that the resulting clusters will form contiguous geographic areas without overlap or exclaves. The developer has some control here, as increasing weights on geographic data results in more geographically coherent clusters.

The third approach, in contrast to the second, always produces clusters consisting of geographically connected areas. This approach is, generally speaking, the most difficult to implement as it requires one to define adjacency relations and then cluster based on these adjacency relations. The results are not necessarily more pleasing to the eye when plotted. For example, many algorithms generate a tree connecting adjacent points that are also similar in terms of non-geographic variables. Links of this tree are then removed to yield clusters of similar points. The resulting clusters can be long and narrow when plotted on a map, as links were chosen without consideration of spatial patterns other than that the final cluster be contiguous.

8.3.2.2 Clustering Analysis Results

The results presented here were produced using the second approach identified above. The latitude and longitude of each point were combined with statistics on flood risk and the cost-effectiveness of mitigation options by point. K-means clustering—in which the grid points are divided into k clusters, such that all points in a cluster have a functional value closer to the mean value of points in its own cluster than to the means of other clusters–was applied multiple times to the resulting data set. The relative importance of the different variables was altered until the k-means algorithm produced clusters that divided up the coast into regions that made intuitive sense, looked sensible when plotted on a map, and contained points that were relatively similar in terms of the non-geographic data.

The specific variables of interest, which were combined with geospatial location when clustering, included the proportional (Figure 8-12) and absolute (Figure 8-13) damage reduction

achievable via nonstructural mitigation measures, the cost-effectiveness of those measures (Figure 8-14), and the count of properties that have experienced severe repetitive losses (SRL) caused by flooding (Figure 8-15). For all but the SRL clusters, analysis is based on output metrics from the FWOA case, the 2065 Basis Year, and with residential floodproofing allowed and full participation. This set of parameters was used to evaluate clusters based on the full potential for nonstructural mitigation.

Clusters based on proportional and absolute damage reduction exhibit similarities in the total numbers of clusters (thirteen in each case), and overlap in many areas. Despite both being metrics related to damage reduction, this is not necessarily an obvious or expected result. Nearby points could have similar potential for damage reduction in absolute terms, but the proportional reduction could vary depending on different numbers, types, or values of assets. Finding such similarity is significant, then, and suggests that geospatial location is a reasonable proxy for other characteristics related to the asset inventory. This is more intuitive, given that populations naturally exhibit spatial clustering into towns and cities. In both cases, existing federal levee centerlines coincide closely with the resulting clusters, with distinct regions being identified within structurally protected areas like Berwick, Larose to Golden Meadow, lower Plaquemines, and the east and west banks of New Orleans. This suggests that a final set of clusters could be derived from these results by manually adjusting or separating cluster boundaries based on some combination of levee lines, municipal or parish boundaries, and natural features like the Mississippi River. This would produce a final set of nonstructural project areas similar in number to the structural projects being considered by the Master Plan process. Recommended project boundaries formed using these selection criteria are discussed in the next section.

The clusters produced by cost-effectiveness estimates and SRL properties are less instructive, largely because of a paucity of data. Cost-effectiveness can only be calculated at points with assets that can be cost-effectively mitigated, and the number of points experiencing repetitive losses is small relative to the entire set of grid points. Some of the same patterns emerge, however, if one were to imagine expanding the clusters to cover the entire coast. Large clusters tend to encompass the western half of the state, with a single cluster covering Cameron and Calcasieu through Vermilion parishes, and another roughly from Iberia to Terrebonne parishes. Clusters generally respect the Larose to Golden Meadow, HSDRRS, and Lower Plaquemines system boundaries.

The clustering method applied here favors circular or somewhat square-shaped clusters over regions shaped like thin strips or bands. Despite this, the clusters based on cost-effectiveness and on absolute damage reduction exhibit this banding effect to some extent. Particularly in the eastern third of the state, clusters are loosely separated by latitude into an extreme coastal wetlands zone, a near-coastal zone, communities on the west shore of Lake Pontchartrain between the Mississippi River and Lake Maurepas, and Northshore communities like Mandeville and Slidell. This indicates that nonstructural measures are generally less cost-effective in areas further inland with lower baseline risk, and also that extreme coastal areas are less developed, resulting in less potential for absolute damage reduction.

8.3.3 Defining Nonstructural Project Areas

The four sets of clusters share some common characteristics, as discussed in the previous section. However, Figure 8-12 through Figure 8-15 illustrate that clustering on different variables and performance metrics can produce different spatial clusters that cover the Louisiana coast in different ways and to varying degrees of completeness. In some cases, clusters cross parish or levee boundaries or have other characteristics that may be undesirable when designing project

definitions for consideration in the master planning process. Communication using complicated spatial regions would be difficult, and crossing parish or municipal boundaries might create needless complexities for future analysis or funding allocations.

For this reason, the spatial clusters serve only as a starting point and were not themselves be used to define project areas. Instead, the clustering maps, along with additional geospatial data describing existing or proposed levee systems and jurisdictional boundaries, were used to guide the process of developing and refining nonstructural project areas. Specifically, preliminary project area boundaries were identified by converting the spatial clusters into contiguous regions and overlaying parish and municipal boundaries with existing levee centerlines and structural projects under consideration for the 2017 Coastal Master Plan as of May 2015. Projects are never allowed to join across parish boundaries, which in some cases leads to very small project areas.

The preliminary nonstructural project areas were then refined. Small areas in southwestern Louisiana and areas without any nonstructural grid points were combined with their logical neighbor, based on adjacency and the number of grid points in the neighboring polygons, resulting in 48 distinct areas. The Thiessen polygons belonging to the remaining nonstructural analysis grid points were then combined based on which nonstructural area they fell inside, as shown in Figure 8-16. Finally, these rough nonstructural project areas were smoothed out, to produce the final nonstructural areas shown in Figure 8-17. Note that this also involved several rounds of review, refinement, and customization based on feedback from CPRA.

This process produced a proposed set of 48 nonstructural project area boundaries (Figure 8-17).

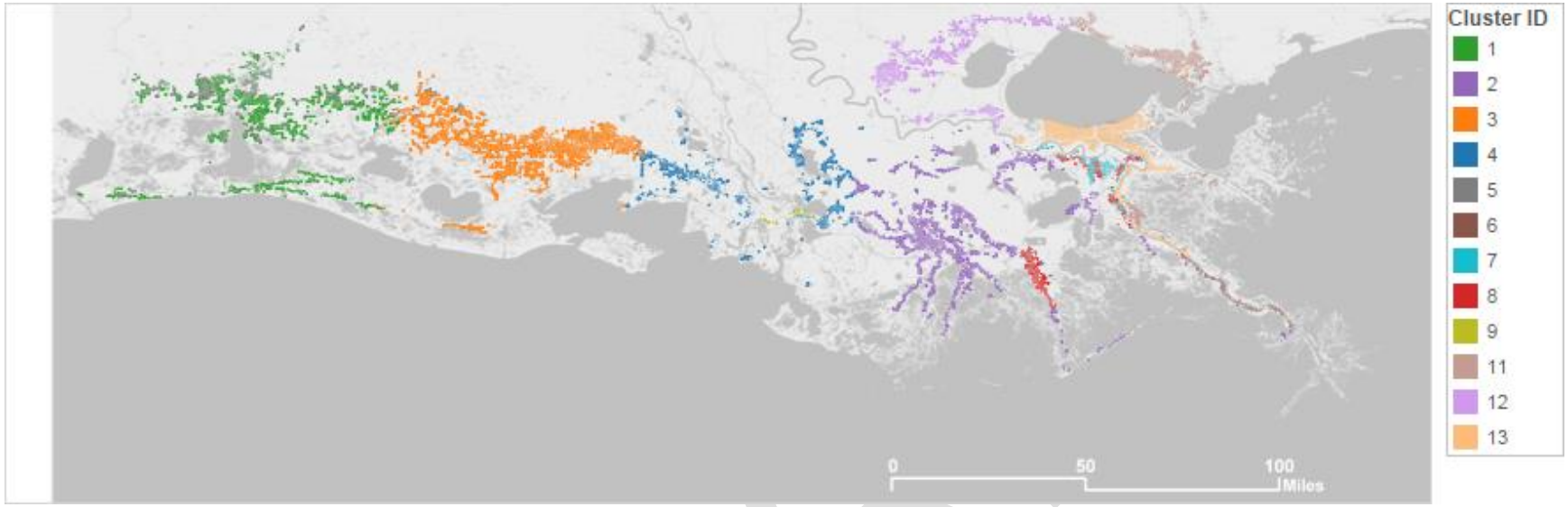

Figure 8-12: K-means Clusters Produced Using Geospatial Location and Proportional Damage Reduction.

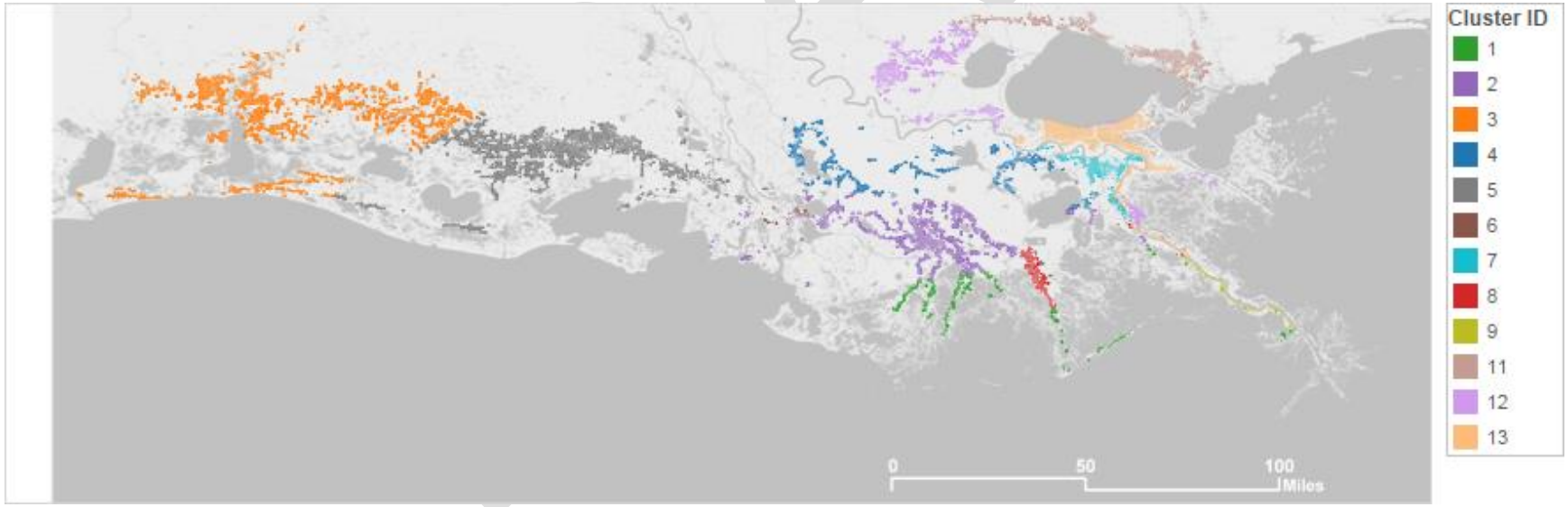

Figure 8-13: K-means Clusters Produced Using Geospatial Location and Absolute Damage Reduction.

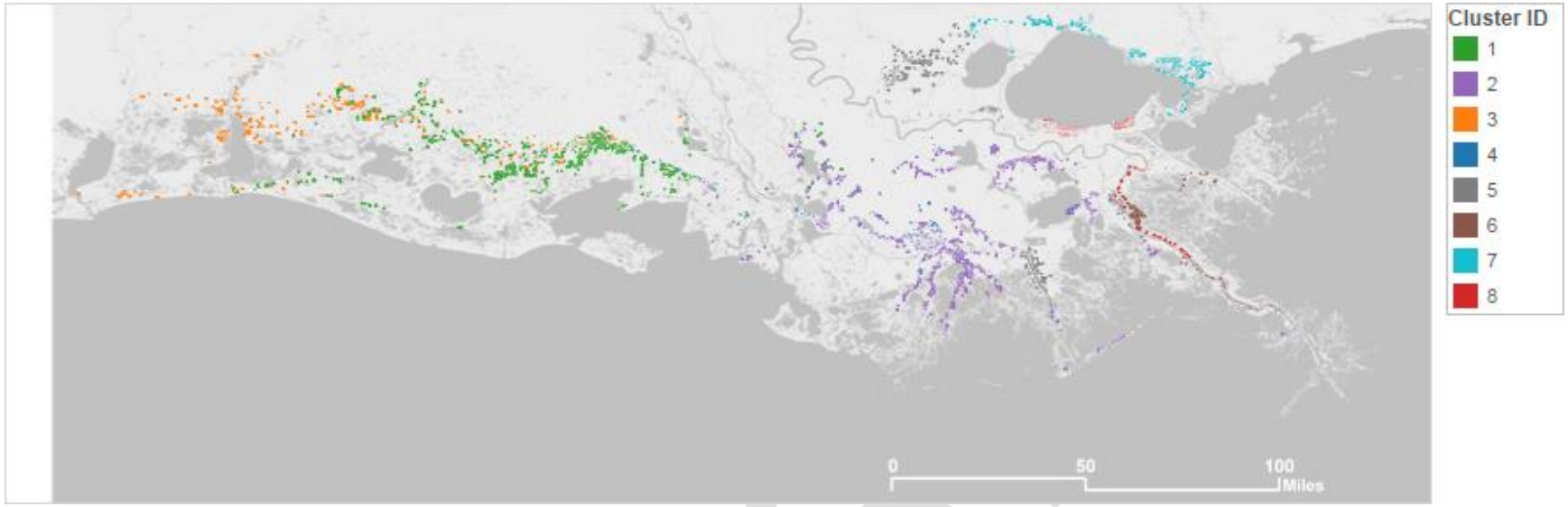

Figure 8-14: K-means Clusters Produced Using Geospatial Location and Nonstructural Cost-effectiveness.

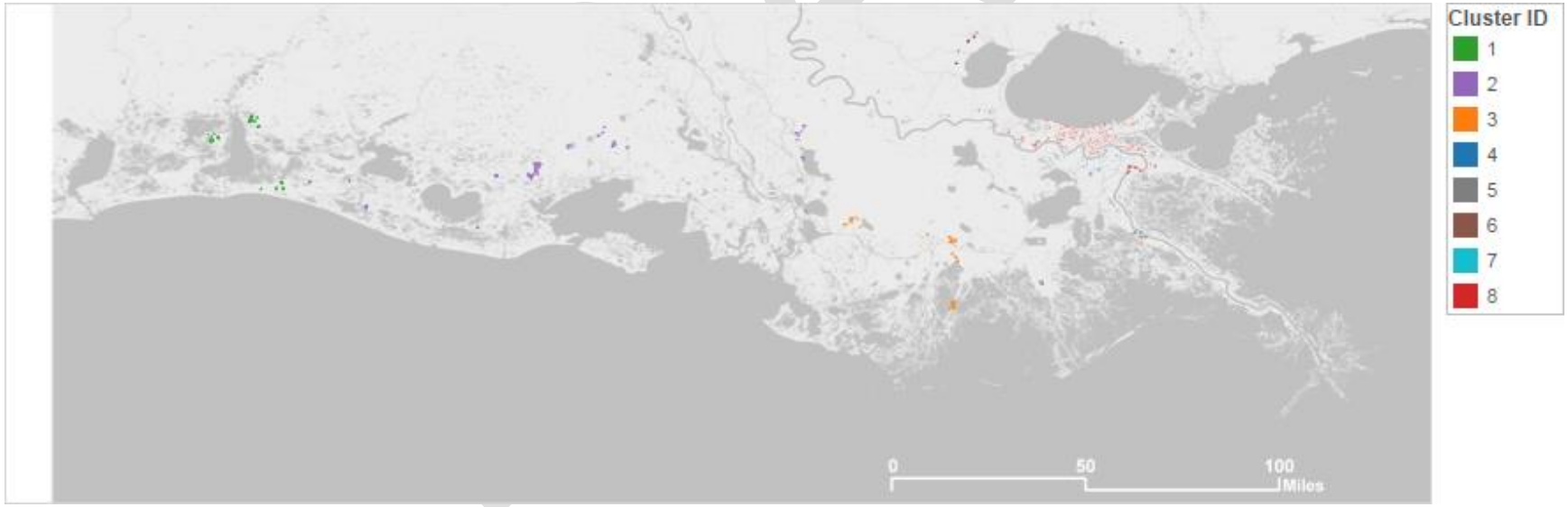

Figure 8-15: K-means Clusters Produced Using Geospatial Location and Repetitive Loss Events.

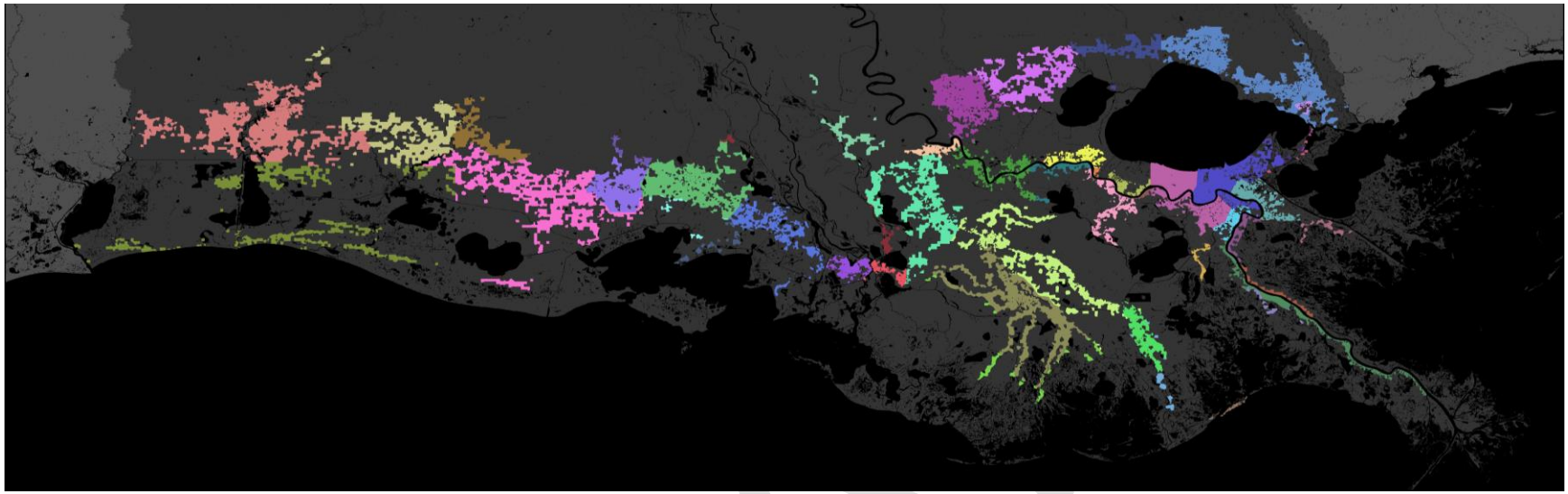

Figure 8-16: Proposed Rough Nonstructural Project Area Definitions.

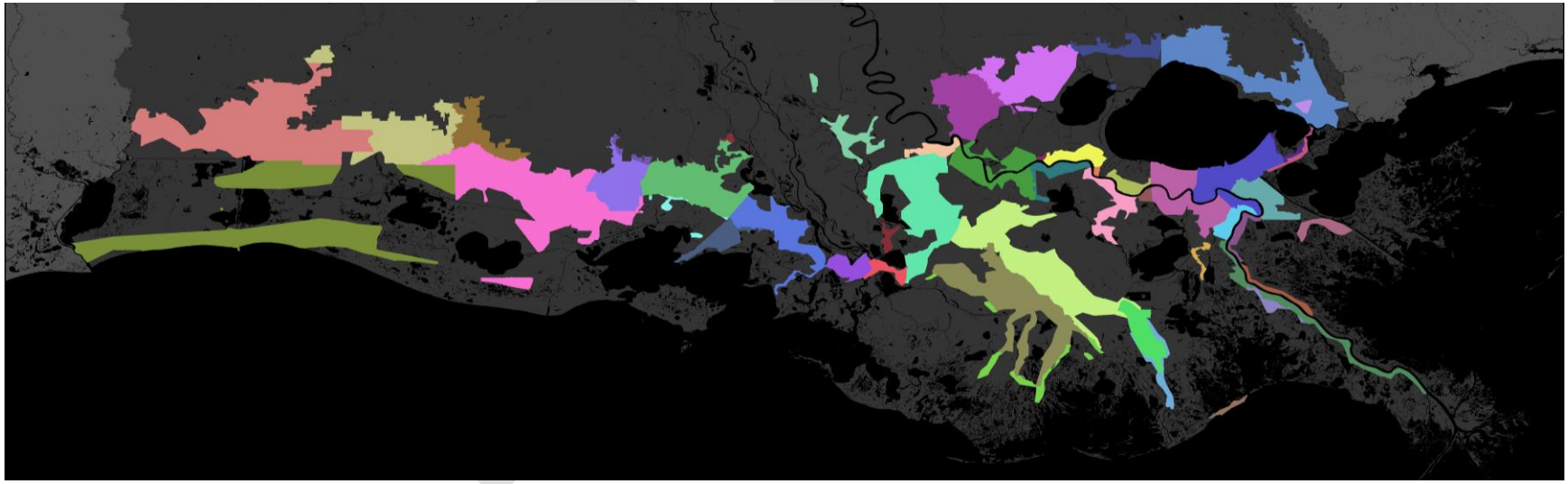

Figure 8-17: Proposed Smoothed Nonstructural Project Area Definitions.

9.0 Scenarios of Future Population and Asset Growth for the 2017 Coastal Master Plan

9.1 Introduction

In the 2012 Coastal Master Plan, the flood risk analysis considered uncertainty related to the future growth and distribution of assets at risk in the coastal floodplain using scenario analysis. CLARA v1.0 implemented a simplified scenario approach that projected plausible population growth and geographic distribution over the 50-year period of analysis. The scenario approach utilized two scenario parameters: a **coast wide growth rate** for the population of all parishes in the study area, and a **growth dispersion parameter** that represented the proportion of the population living in urban versus rural census blocks. This scenario approach assumed that asset growth and distribution would track population change.

Given the substantial population disruption caused by Hurricanes Katrina and Rita in 2005, this analysis used historical population data (including U.S. census data from 1950 to 2000) and assumed that long-term growth in population is more likely to follow pre-Katrina/Rita growth trends. Consequently, in the "nominal" or default growth scenario, the population growth rate for the entire study region was set at 0.67 percent year over year, approximately equal to the average annual rate of growth in population from 1990 to 2000. The nominal scenario favors simplicity and transparency, avoiding, for example, the development and parameterization of a statistical model to detail a gradual decline in population growth rates that some readers may anticipate.

Instead, we use scenario analysis to consider other plausible future outcomes. Alternative scenarios ranged from a "no-growth" scenario on the coast—one in which the population stagnates or growth in one region is balanced by declines in others—to a 1.5-percent annual growth rate, somewhat higher than the average annual growth rate for the coastal region from 1950 to 2000. The latter scenario resulted in a doubling of the coastal population over the 50-year time span. All asset types except for agricultural structures, agricultural crops, and roads were assumed to grow in direct proportion with changes in population (Fischbach et al., 2012a). Counts of the other asset types were also assumed to remain constant (Ibid.). Further discussion of the link between assets at risk and population growth is included in the next subsection of this document.

The dispersion parameter was designed to reflect changes in the distribution of population between concentrated (urban) and distributed (rural) asset areas. Urbanization was defined using the urban areas defined by the US Census. According to the 2000 Census, 81 percent of the study area population in south Louisiana lives in areas designated as urban. In 2012, CLARA v1.0 modeled a scenario in which urbanization remained constant, as well as scenarios with 5-percentage-point increases or decreases in coastal urbanization over 50 years, respectively.

For the 2017 Coastal Master Plan, CPRA asked RAND to revisit and update this scenario approach. The overall goal was the same: to create plausible scenarios for the growth and geographic distribution of assets at risk in the coastal region, spanning a wide range of possible outcomes, while applying a relatively simple approach. For this analysis, however, an added objective was to represent long-term drivers of risk from the physical environment—including land loss rates, anticipated flood recurrence, and changes to anticipated flood risk from new or upgraded structural protection alignments. These changes would allow CPRA to consider how

future patterns of asset growth in different parts of the coast might vary with changes to the physical landscape over a 50-year period.

Specifically, the distribution of population and assets 50 years into the future might change substantially in response to long-term drivers, and plausible changes should be represented in the scenario range developed here. In addition, a new approach should be dynamic, allowing for growth rates to vary over time in response to changing coastal conditions, including increasing land loss rates or the implementation of structural protection projects that might encourage additional development in the newly protected area ("induced development"). This improves on the 2012 approach, which assumed constant growth rates and urbanization as a simple linear function of time, and did not incorporate plausible migration patterns in response to long-term coastal process changes.

As part of this update, recent social science investigations of the link between social vulnerability, response to disasters, and near- or long-term effects on coastal population growth were also considered. It was determined that, while there are demographic data that can be used to quantify the social vulnerability of various populations and model disaster response, existing models have not yet matured sufficiently to incorporate into definitions of scenarios of future population and asset growth for the 2017 Coastal Master Plan.

The focus of this additional investigation is on defining plausible scenarios of population growth, rather than economic growth defined more broadly. Recall that CLARA estimates direct economic damage to physical assets along the coast, and does not consider effects on the local, regional, or national economy from coastal storms. Historical data suggests that asset growth in the Louisiana coastal area closely tracks population changes. For example, among the census tracts in the CLARA v2.0 study region and using the model's current conditions economic inventory data, there is a strong correlation between population and the number of single-family residences ($r = 0.78$). The correlation is weaker, but still strong, when measured at the census block level ($r = 0.63$). The model assumes that commercial and industrial assets grow in proportion with population growth at the census tract level, where the correlations are moderately strong ($r = 0.53$ for commercial properties, $r = 0.42$ for industrial structures). As a result, projecting plausible future population patterns provides a relatively simple, convenient, and understandable means to project scenarios of future asset distribution, and avoids the substantial complications and high level of effort involved in trying to develop 50-year economic projections with a general equilibrium model.

This section proposes new methods for developing growth scenarios for use in the 2017 Coastal Master Plan analysis. The section first provides a brief literature review of relevant social science investigations and the conclusion, mentioned above, that the literature does not yet point to a single, established method that supports defining vulnerability and using it to project population growth and distribution in coastal Louisiana looking out 50 years.

A new framework and methods for scenario development are described next, drawing in part on the literature review. The approach is based on applying general methodological principles derived from the literature review. In this new approach, an index is defined based on environmental factors, and this index is then used to define future population and asset growth rates.

The new method has two components: one that constructs an index value for each 2010 census block group in the study area, and another that assigns a differential growth rate to each block group based on its projected index value. New scenario parameters, with corresponding parameter ranges, are also proposed for incorporation into the 2017 analysis. The section

includes preliminary population growth and asset distribution results using the new framework, providing a range of results to support CPRA's subsequent selection of a small number of growth scenarios for economic assets in the 2017 Coastal Master Plan. However, the initial parameters and assumptions selected for this analysis are preliminary, and subject to change pending further discussion with CPRA and the Model Decision Team. The section concludes with a brief discussion and preliminary recommendations.

9.2 Literature Review

In this subsection, the literature on internal migration and environmental and social vulnerability impacts on migration is reviewed. This review had two primary goals:

1. Investigate existing methodologies linking vulnerability and migration patterns that could be adopted for the new scenario approach; and
2. Support the selection of input variables for the index that will be used to define population and asset distribution across the coast.

The review describes the role of environmental threats on migration, then summarizes related case studies based in coastal Louisiana. One of the key findings of the review is that prior studies are primarily based on environmental disasters (Hurricanes Rita and Katrina), rather than gradual environmental degradation. It also briefly describes the literature on "social vulnerability" and methods to construct a "Social Vulnerability Index" (SoVI), which help to inform the new population and asset scenario methodological approach.,

9.2.1 Environmental Impacts on Migration

The characteristics of internal migrants and the decades-long decline in internal migration have been well documented (see, e.g., Hunter, White, Little, & Sutton, 2003; Long, 1988; Molloy, Smith, & Wozniak, 2011; Wolpert, 1966). In general, economic prospects are among the most significant drivers of migration, especially at younger ages. Unemployed individuals, those under age 45, and renters (versus homeowners) are the most mobile, while nonwhite, foreign-born, and individuals with children in the home are the least ((Hunter et al., 2003; Long, 1988; Molloy et al., 2011; Wolpert, 1966).

Driven by environmental change, particularly climate change, interest in the environmental drivers of migration is growing, but empirical research is still limited. Research suggests that natural hazards will increase in both frequency and intensity due to climate change (Goldenberg, Landsea, Mestas-Nuñez, & Gray, 2001). Even minimal rises in sea levels would affect commercial piers, military bases, harbors, and residential areas along coastlines around the country (Constable et al., 1997; Curtis & Schneider, 2011).

However, most scholars reject the hypothesis that climate change and mass migration are currently directly linked. Instead, linkages between the environment and migration are complex and operate through social, political, economic, and demographic drivers, with migration being just one of many possible adaptations to environmental change (Black et al., 2011; Fussell, Hunter, & Gray, 2014; McLeman, 2013; McLeman & Smit, 2006; Piguet, Pécoud, & De Guchteneire, 2011). As of yet there are too few studies investigating these complex linkages to make conclusive generalizations about the extent to which environmental factors directly or indirectly shape human migration patterns (Jäger, Frühmann, Grünberger, & Vag, 2009; Kniveton, Schmidt-Verkerk, Smith, & Black, 2008; McLeman, 2013; Piguet, 2010; Warner, 2011).

The majority of environmental migration studies focus on developing countries and rural populations and on the immediate impacts of disasters (see for example the EACH-FOR series of studies, Warner, 2011). There has been relatively little research examining migration out of urban settings in response to gradual environmental change; the bulk of research in this context concerns population response to environmental disasters such as hurricanes and temporary flooding, rather than incremental environmental encroachment.

9.2.2 Environmental Impacts on Migration in Coastal Louisiana

Numerous studies of the population impact of Hurricanes Rita and Katrina on the coastal communities and especially New Orleans have been conducted (see, e.g.,Finch, Emrich, & Cutter, 2010; Frey & Singer, 2006; Fussell, Sastry, & VanLandingham, 2010; Plyer, Bonaguro, & Hodges, 2010; Stringfield, 2010; Zaninetti & Colten, 2012). These studies all generally identify whiter, wealthier residents return to affected areas. The research points to gradual recovery in New Orleans, but also to an exacerbated population decline throughout the area that was already occurring prior to the hurricanes (see, e.g., Finch et al., 2010; Frey & Singer, 2006; Fussell et al., 2010; Myers, Slack, & Singelmann, 2008; Plyer et al., 2010; Stringfield, 2010; Zaninetti & Colten, 2012).

Many coastal parishes are losing population, with some communities shifting inland or shrinking (Dalbom, Hemmerling, & Joshua A. Lewis, 2014). Population loss is most concentrated in neighborhoods that suffered inundation, primarily due to the higher costs of restoring damaged properties (Myers et al., 2008). Three years after Hurricane Katrina, neighborhoods in Orleans parish with no flooding had returned to 96% of the pre-Hurricane population, while medium flood depth (less than 2 feet) areas reported a 78% return, and areas with flooding greater than 4 feet had only a 52% return (Finch et al., 2010). Private mitigation efforts, such as raising houses on stilts, were not financially feasible for many residents. As a result, the African-American population decline in urban cores accelerated after the hurricanes; displaced populations largely relocated to the suburbs and eastern part of the West Bank of New Orleans (in continuation of previous trends) (Zaninetti & Colten, 2012). Prior to the Hurricane, African Americans comprised 68% of the New Orleans population and 20% of the suburban parishes, but currently comprise less than 60% of the central city population, and 23% of the suburban parishes (Zaninetti & Colten, 2012). Conversely, non-Hispanic whites increasingly moved to the city center and formed a larger part of the total metropolitan population – from 25% of the total city population prior to the storm to 30% (Zaninetti & Colten, 2012). A relatively small number of places absorbed a large share of the dislocated population. Importantly, the evacuated population was from largely economically and socially disadvantaged places (Myers et al., 2008). The overall resettlement pattern has tended to push population growth to higher ground, and less flood-prone development patterns have emerged.

Much of the population of southeast Louisiana is employed in various natural resource extractive industries, such as oil and gas, fishing, and agriculture (Finch et al., 2010); and are located in areas that FEMA has designated as Special Flood Hazard Areas in the 100-year floodplain – including more than half (55%) of the census blocks in Jefferson, Lafourche, Orleans, Plaquemines, St. Bernard, St. Charles, St. James, St. John the Baptist, and Terrebonne parishes (Dalbom et al., 2014). The rural communities located along coastal Louisiana are sparsely populated, and many are in areas where structural protection is not provided. These populations remain especially vulnerable to natural hazards and risks, and they primarily come from historically disadvantaged demographic groups.

9.2.3 Social Vulnerability

The concept of "social vulnerability" provides a link from the catastrophic environmental hazard literature to models of population change in response to gradual environmental change. In one of the few studies considering migration in response to non-catastrophic, incrementally changing environmental conditions, Dalbom et al. (2014) argue that migration and relocation will be highly influenced by the degree of social vulnerability of impacted communities. However, they also note that factors linked to vulnerability (such as the lack of income, lack of transportation, age, gender, and minority status) are all also linked to a community's ability to relocate in response to environmental change. Thus, while economic factors—particularly the loss of business and employment opportunities—will be key drivers of outmigration, it is possible that migration at the extremes of economic disadvantage will be curtailed.

Cutter and colleagues' (2003) Social Vulnerability Index is one commonly used vulnerability model that captures the majority of these dimensions (except the explicit inclusion of "resilience" and scalar ability), and is referred to as a "hazards of place" model. The SoVI was developed as a response to the lack of consensus about social vulnerability or its correlates and is intended to provide a multidimensional model of social vulnerability to environmental hazards through a combination of social inequality and geographic inequality (based on characteristics of communities and the built environment).

Cutter et al. (2003) reviewed a large number of studies that included social vulnerability concepts and their metrics – 17 broad concepts and dozens of individual metrics. Using these studies as a starting point, they examined 42 variables using national 1990 Census data at the county level. Using these 42 variables, factor analysis was used to identify 11 latent factors explaining 76.3% of the variance among all counties in the US. The factor scores were then summed in an **additive model**, producing a composite **SoVI score** for each county. The additive model was explicitly used so that no *a priori* assumptions about the particular importance of any factor to overall vulnerability were introduced. This approach – identifying key latent vulnerability factors and summing them into an index – is a defining characteristic of the SoVI approach, regardless of the context in which it is applied.

SoVI scores are rescaled in terms of standard deviations from the mean providing ordinal levels of vulnerability. For example, in an analysis similar to the Cutter et al. (2003) focused on the Gulf Coast, Finch et al. (2010) use of a cutoff of 0.5 standard deviations below the mean to reflect the least vulnerable areas, and 0.5 standard deviations above the mean to reflect the most vulnerable areas, respectively.

Although most SoVI literature focuses on post-disaster recovery, Myers et al. (2008) sough to take an additional step and link SoVI to migration (county level net migration for one year [July 1, 2005-July 1, 2006]) as a percent of population at the beginning of the period to estimate the impact of Hurricanes Rita and Katrina. Further, and most importantly, they also looked at each dimension of vulnerability and how it related to migration by regressing the percent net migration on each dimension of social vulnerability. They present unstandardized regression coefficients, so we are only able to assess valence and significance – but this is a unique attempt to investigate the salience of specific components of vulnerability on migration. More disadvantaged populations and more densely built environments both predicted greater outmigration, as did percent of housing units that were damaged.

At a high level, the SoVI literature identifies variables relevant to models of population growth and movement as well as methods for combining these variables based on summing scaled independent factor variables and then rescaling the result. However, the degree to which the

SoVI framework can support projections of long term future population growth and distribution as a function of gradual environmental degradation remains unclear. Therefore, although the methods described below use a similar methodological approach to define lower and higher growth areas, a direct application of a SoVI-type approach relying on demographic and socioeconomic data is not being pursued here.

9.3 Scenario Development Methods

9.3.1 Overview of Approach

This subsection describes an approach for developing plausible scenarios for population growth and alternate growth patterns across coastal Louisiana over the next 50 years. The approach involves the use of a **composite index** that takes on different values in distinct geographic areas and is subsequently used to define location-specific population growth rates. The index is based on population density (similar to the 2012 analysis), land loss or gain, and projected flood depths.

In the 2012 Coastal Master Plan, the study area was bifurcated into urban and rural areas, with distinct and fixed average growth rates applied in each of the two areas depending on the scenario assumptions (Fischbach et al., 2012a). In this proposed update, the study area is split into three areas based on binning a composite index that summarizes relevant variables. Because the new composite index is defined in part by drivers that will change over time in a future without action or with-project condition, the corresponding growth rates in these areas can also vary dynamically with these changes, as opposed to the fixed approach used in 2012. In addition, defining three different types of areas allows some areas to grow rapidly, others to grow more slowly or remain at constant levels, and others to contract over time, with the variation between these areas depending on the scenario assumptions defined below.

Note that the new approach can be viewed as a generalization of the 2012 approach that focused exclusively on population density. The use of three bins, in particular, allows the model to soften the binary nature of the previous approach, where an arbitrarily small change in population density could lead the growth rate assigned to an area to shift from the lowest to the highest growth rate considered.

This approach uses two scenario parameters to develop a separate growth rate for each bin. The first is an overall **coast wide growth rate**, mirroring the 2012 approach. The second is a **rate difference between bins**, which is a simple scaling that adds a fixed percentage of growth to each successive bin. The model translates these parameter values into population growth rates for each geographic area based on the areas' land loss rates, flood depth estimates, and population density.

For example, assume a coast wide annual growth rate of 0.55% and that growth in any given bin occurs at a rate 0.5 percentage points greater than that of the next bin. Let there be three regions, one representing each bin of the composite index. Suppose the total population is 10,000 people, consisting of 2,000 in the low growth area, 3,000 in the high growth area, and 5,000 in the remaining area. Under an annual growth rate of 0.55%, the total population will grow to 10,055 in one year. The model would solve for the final populations of each area: 2,000, 3,030, and 5,025, corresponding to growth rates of 0%, 1%, and 0.5%, respectively. This produces the required total of 10,055 people across the entire region and conforms to the initial assumption about differences in growth rates between bins.

Figure 9-1 shows a flowchart to summarize the overall scenario development approach. Current population, land change, and flood depth data are merged to yield initial composite index values assigned to each grid point. These values are then compared to set thresholds, and grid points are assigned to high, medium, or low growth bins, respectively. The growth rate of each bin is then determined using the equations defined later in this section to ensure that the coast wide growth rate and the separations in growth rates between bins match pre-specified input values. These growth rates are then used to define plausible annual population change at each grid point. The result is an updated plausible population count for each grid point in each year. Future flood depth and land change information, generated separately in the 2017 Master Plan analysis, are then used to update composite index scores, bin assignment, and growth rate by grid point in each additional year.

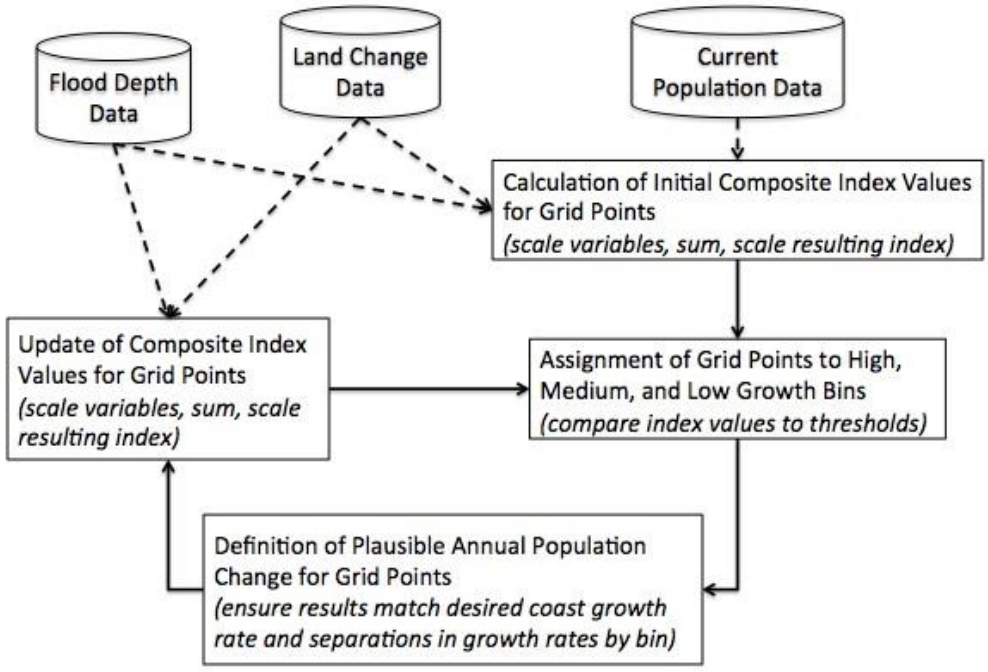

Figure 9-1: Flowchart Summary of the Population and Asset Scenario Methodology.

9.3.2 Constructing a Composite Index

CLARA produces estimates of flood depths that are a function of future environmental drivers of flood risk and risk reduction investments, including levees and other protection structures. CLARA can thus be used to generate dynamic flood depth data that changes over time as strategies and structures are implemented or built. Land loss data will also be produced by the Integrated Compartment Model (ICM) for the 2017 Coastal Master Plan, showing regions where high land loss rates are expected to be a problem in the future. The revised approach described here builds on these available inputs to construct scenarios of future population and asset distribution to define a composite growth index.

In this approach, CLARA flood depth outputs are used directly to represent the hazard posed by flooding. In the analysis presented in this report, median flood depths at the 100-year return period reflecting current (2015) conditions were adopted. However, as part of model production for the 2017 Coastal Master Plan, future projections of flood risk can be incorporated to

dynamically alter population and assets at risk growth rates over time. These changes could either yield lower growth rates (i.e., increasing depths due to sea level rise and subsidence lead to long-term emigration) or higher growth rates (i.e., new structural protection in a future with project leads to a net increase in assets for the newly protected area), thus modifying growth rates to track changing flood risk conditions.

Land change (loss or gain in m^2, by grid point polygon area) was incorporated into the final composite index input. This is based on the RAND team's expert judgment regarding the most likely drivers of current and future population change in areas of Louisiana facing high rates of loss. Land area change, like flood risk, is a primary decision metric that varies across environmental drivers and is specifically targeted by many proposed coastal restoration projects. Incorporating it into the growth index makes CLARA's asset growth model more dynamic and responsive to different future conditions and alternatives. As with the flood depth inputs, initial land change data for the preliminary analysis described below were adopted from 2012 Coastal Master Plan estimates of land change in the Less Optimistic future without action scenario.

Population density is the final variable incorporated into the composite index. As in the 2012 Master Plan analysis, the approach allows for differential growth rates in urban and rural areas. Here, the model is dynamic: population counts are used to estimate density, which is then used to estimate population growth, which in turn leads to revised population counts in the next year.

In summary, the proposed variables used to construct the composite index approach include flood depth, land change, and population density, summarized for each block group in the CLARA v2.0 domain.

Following an approach similar to the methods employed in the published research surveyed in Section 9.2, these data are next normalized and merged. The logarithms of flood depth and population density are computed, as these quantities are naturally non-negative. The variables are then transformed to z-scores that reflect how many standard deviations each individual observation differs from the mean of each transformed variable. For example, let $x_{PD}(a)$ be the population density observed at block group a. Across all the block groups, the average population density is $\overline{x_{PD}}$ and the standard deviation is σ_{PD}. Then the corresponding z-score $z_{HD}(a)$ for this variable at this location, would be:

$$z_{PD}(a) = \frac{x_{PD}(a) - \overline{x_{PD}}}{\sigma_{PD}} \quad (9\text{-}1)$$

The set of z-scores (one for each variable) observed at each block group are then combined in a simple additive model, with care taken to add the z-scores for population density and land change but to subtract the z-scores for flood depth. The simple addition of variables is based on an assumption of independence, which was assessed and confirmed using correlational analysis during methods development (not shown). The variables are added without any weights specified, because there is no reason to assume any one factor or variable is more or less important than another.

The resulting value is then itself re-centered and scaled so that the final results have some intuitive meaning. For example, if a particular block group has a score of -1, that means that its growth index value is 1 standard deviation below the average. The final calculation defines the composite index proposed for CLARA v2.0.

9.3.3 Population Change Based on Index Categorization

The output of the algorithm described above is an index quantifying the vulnerability of each census block in the study region. The vulnerability index is then combined with 2010 population data from the US Census to develop scenarios for population growth.

The first step uses the index to categorize block groups into one of three categories: low growth, medium growth, and high growth. The preliminary analysis presented here uses bins corresponding to normalized index values of 1) greater than 0.5, 2) -0.5 to 0.5, and 3) less than -0.5. Recall that the index values are centered and rescaled so that the growth index values in blocks labeled low growth are at least 0.5 standard deviations or more below average.

The model then incorporates the two scenario parameters. The first is the **coast wide annual growth rate**. An updated analysis of historical population growth rates in the study region during the postwar era suggests that values between 0.5 and 1.0% provide a useful plausible range. The average rate from 1990 to 2000 has been preliminarily identified as the nominal (mid-range) population growth rate, as in the 2012 analysis. However, the growth rate from 2000 to 2010 in Louisiana's coastal parishes dipped below zero, approximately -0.12%, due to the long-term effects of Hurricane Katrina and Hurricane Rita. Although these were exceptional and rare events, future coast wide population change may be influenced by large storms, which is why it is important to consider a wide of range of plausible coast wide growth rates. As a result, four points across this range were selected for the preliminary analysis: 0%, 0.5%, 0.67%, and 1.0%.

The second parameter, **rate difference between bins**, defines the differences in growth rates used for areas assigned to different categories. Setting this parameter to 0 would mean that the populations of all census blocks grow at the same annual rate. Setting this parameter to 1, alternately, results in growth rates for high growth areas 1 percentage point higher than growth rates in medium growth areas, and 2 points higher than growth rates in low growth areas. An initial range of 0.5 to 1.0 percentage points was identified for this parameter based on an initial tuning exercise, technical feedback received from CPRA and the Water Institute, and an examination of recent historical growth patterns by census tract.

For instance, Figure 9-2 shows a map of census tracts in the study area that have been color coded according their average annual population growth rates in the 2000-2010 time period. Note that growth rates in some census tracts are often a half or whole percentage point higher or lower than growth rates in neighboring tracts. A similar evaluation of average annual census tract growth rates, by decade, from 1970-2010 yields a standard deviation between tracts of 2 to 4 percentage points (not shown). This suggests that a difference in growth rates by bin of 0.5 to 1.0 percentage points is well within the observed historical range of variation between different locations across the coast.

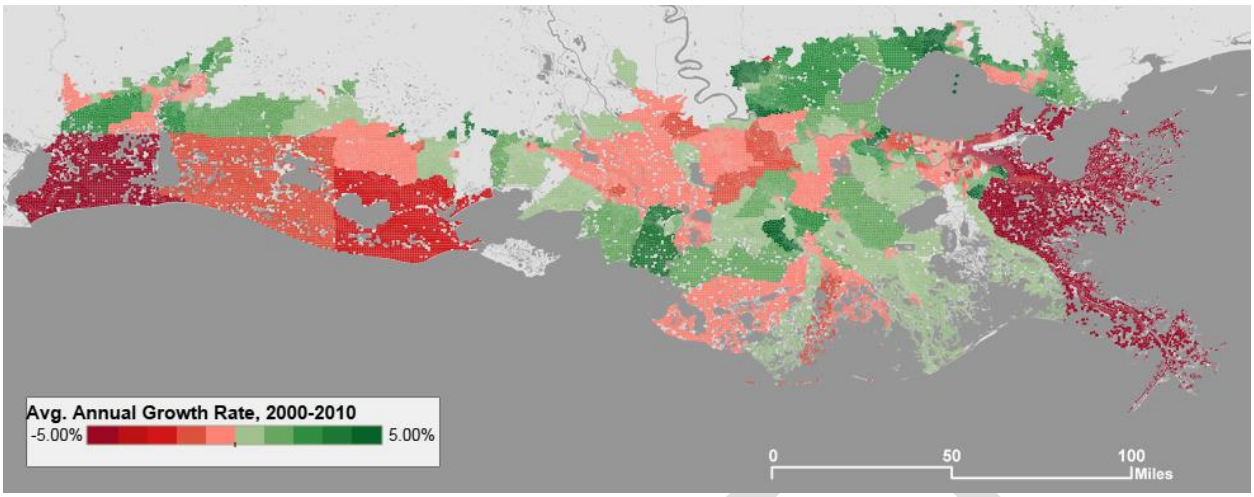

Note: Historical census tract population data derived from Minnesota Population Center (2011).

Figure 9-2: Average Annual Population Growth Rate by Census Tract, 2000-2010.

As noted earlier, fixing the two model parameters described above fully defines a scenario for future growth. There will be exactly one set of growth rates for each year for the three categories where the three rates are related in the manner specified by the second model parameter described above and, when applied to the 2015 population figures, yield a 2016 coast wide growth rate equal to the specified annual growth rate.

Defining this approach formally, assume the population currently living in the high, medium, and low growth areas are x_1, x_2, x_3 respectively. The annual coast-wide growth rate is set at *y*% and the growth rate in each area is z% higher than in an area that will experience less growth. One quantity of interest is the growth rate in high growth areas for the next year, *v*. If *v* is known, then the other growth rates for the next year are all determined by the value of z. Denoting the populations in each bin one year from now as $w_1, w_2, w_3, ,$ the following equation must be true:

$$w_1 + w_2 + w_3 = (1 + y)(x_1 + x_2 + x_3) \quad (9\text{-}2)$$

Furthermore, we can express w_i as a function of x_i and *v*. This yields the following:

$$x_1(1 + v) + x_2(1 + v - z) + x_3(1 + v - 2z) = (1 + y)(x_1 + x_2 + x_3) \quad (9\text{-}3)$$

All of the terms in the above equation are known except *v*, the growth rate in high growth areas. Solving for *v* yields

$$v = y + \frac{zx_2 + 2zx_3}{x_1 + x_2 + x_3} \quad (9\text{-}4)$$

Once *v* is set, the growth rates for all three categories for the next year are set. Simply subtract the parameter z from *v* to get the growth rate in medium growth areas and subtract the same value again to get the growth rate in low growth areas. Once the growth rates for each category have been determined, the growth rates for each census block group are set according to the category previously assigned to each census block group. Total population growth for the next year is then calculated using the growth rates in each block group. The process repeats to simulate population growth two or more years into the future. Note that the population of each bin will change and thus the annual growth rates of the bins will change

when going from year to year (although bin-specific growth rates will change not very much and the coast wide growth rate will, of course, remain constant).

9.3.4 Initial Parameter Assumptions

Once the method described in the previous section was finalized, an iterative process was used to explore the effect of different coastal growth rates and differential growth rates between bins.

Recall that the approach described here uses flood depth and land change data as an input to calculating localized population growth rates. If estimated flood depths or land loss rates change over time, for example as protection structures are built, the model would change over time. Using the approach described here with changing configurations of protection structures was not possible with the available test data, but the method allows for this during the 2017 analysis. Despite this, one goal of testing was to identify parameters that produce short-term growth in an initial timestep resembling growth over the past decade since Hurricanes Katrina and Rita.

Projected population growth was analyzed using visual inspection of mapped outputs to find parameter values consistent with activity such as the relocation of many lower Plaquemines Parish residents to Belle Chasse, the growth of North Shore communities, and redevelopment patterns within New Orleans. This assessment was also facilitated by comparing summary metrics such as total populations in each bin in Years 0 and 50, the implied growth rates for each bin under different overall growth scenarios, and the number of block groups assigned to each bin. Sensitivity testing results are included in the subsections below.

Although future growth is treated as a deep uncertainty, this initial calibration exercise was useful for eliminating model setups that would produce growth projections believed to be implausible. Based on this analysis, the next section describes results with the initial selection of model parameters that are recommended to be fixed, as well as the other parameters to be varied in the scenario analysis. These initial assumptions are easily modified as needed for the master plan analysis, however.

9.4 Sensitivity Testing Results

9.4.1 Block Group Composite Index Development and Bin Thresholds

The methodology as described above categorizes block groups by their composite index scores; low, medium, and high growth bins include areas that have scores that are more than 0.5 standard deviation below average, in the middle of the distribution, and more than 0.5 standard deviations above average, respectively.

The index definition and approach, using plus or minus 0.5 standard deviation cutoffs, yields a map of the Louisiana coast as shown in Figure 9-3. Areas in dark orange have the lowest index scores and would be included in the low growth bin, areas in green will grow faster, and areas in blue will grow at the highest rate. Note that this initial categorization assigns much of the geographic area of the coastline into the lowest growth category.

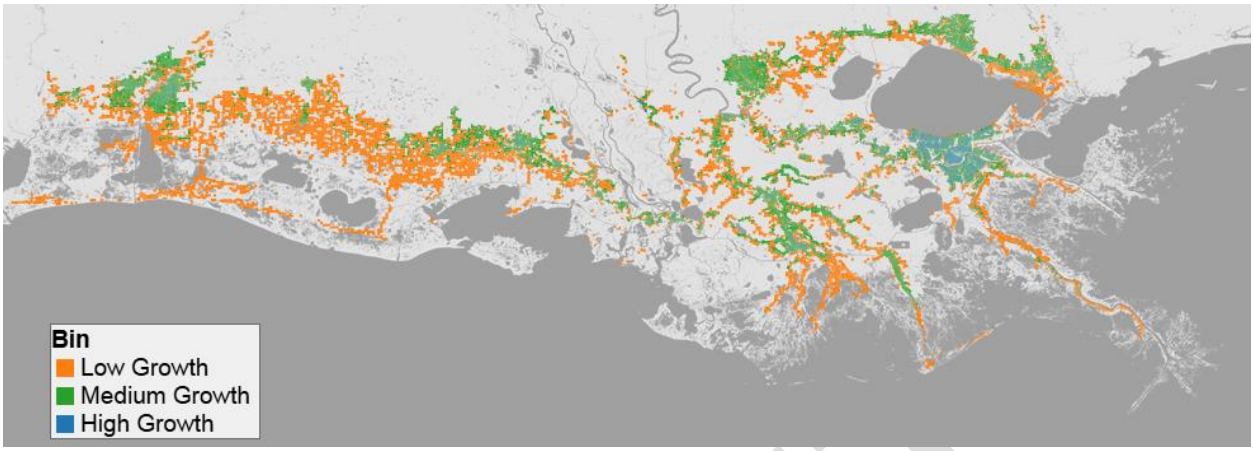

Figure 9-3: Initial Block Group Bin Assignment, Coast Wide.

Table 9-1 shows a sensitivity analysis of the index definitions to test whether population density, land change, and flood depth are all necessary to distinguish different areas of the coast. The table shows a count of census blocks and 2010 population using each alternate index definition, and shows how the assignment would change if any single variable is omitted. Total 2010 population in the study area is approximately 1.9 million persons.

Table 9-1: Counts of Block Groups and Starting Population by Bin Using Alternate Definitions.

Index Definition	Bin	Number of Grid Points	Population	Population Percent
Flood depth and land change	Low Growth	5,324	131,528	7%
	Medium Growth	42,952	1,775,221	93%
	High Growth	35	839	0%
Population density and flood depth	Low Growth	10,091	164,243	9%
	Medium Growth	19,206	642,766	34%
	High Growth	19,014	1,100,579	58%
Population density and land change	Low Growth	9,470	127,154	7%
	Medium Growth	22,106	769,582	40%
	High Growth	16,735	1,010,852	53%
Population density, flood depth, and land change	Low Growth	8,533	140,196	7%
	Medium Growth	24,226	814,263	43%
	High Growth	15,552	953,129	50%

Note: Starting population numbers from 2010 US Census estimates, by grid point.

The sensitivity results reveal that when population density is not used to define the composite index, the employed methodology will identify very few areas with high index values. This is because there are a great many areas that have no flooding or land loss. The index is unable to distinguish among these areas, and thus assigns them all to the medium growth bin. Dropping either flood depth or land change data from the index yields results that are relatively similar to the results obtained when all three variables are included, except that additional grid points and population are assigned to the high growth bin. The relative importance of population density also goes up if one of the other variables is omitted from the model, leading to urban areas being assigned, almost uniformly, to the high growth bin. This suggests that all three variables are

necessary to allow for growth rates to change with changing environmental conditions in both rural and urban areas.

Based on these results, the remainder of this discussion uses the composite index based on population density, land loss rates, and flood depth data alone with 0.5 standard deviation cutoffs. Looking more closely at Greater New Orleans and its immediate surroundings reveals areas spanning all three growth bins (Figure 9-4). Note that many of the most dense areas of the city are categorized as high-growth, while lower growth is noted in less dense areas and outside of the HSDRRS system. This is consistent with the idea that denser areas will grow faster, and the results here are driven both by density and anticipated flood depths. With this approach, the bin assignment for Greater New Orleans would change—moving more areas into lower-growth bins—in scenarios where 100-year flood depths in the city increase over time.

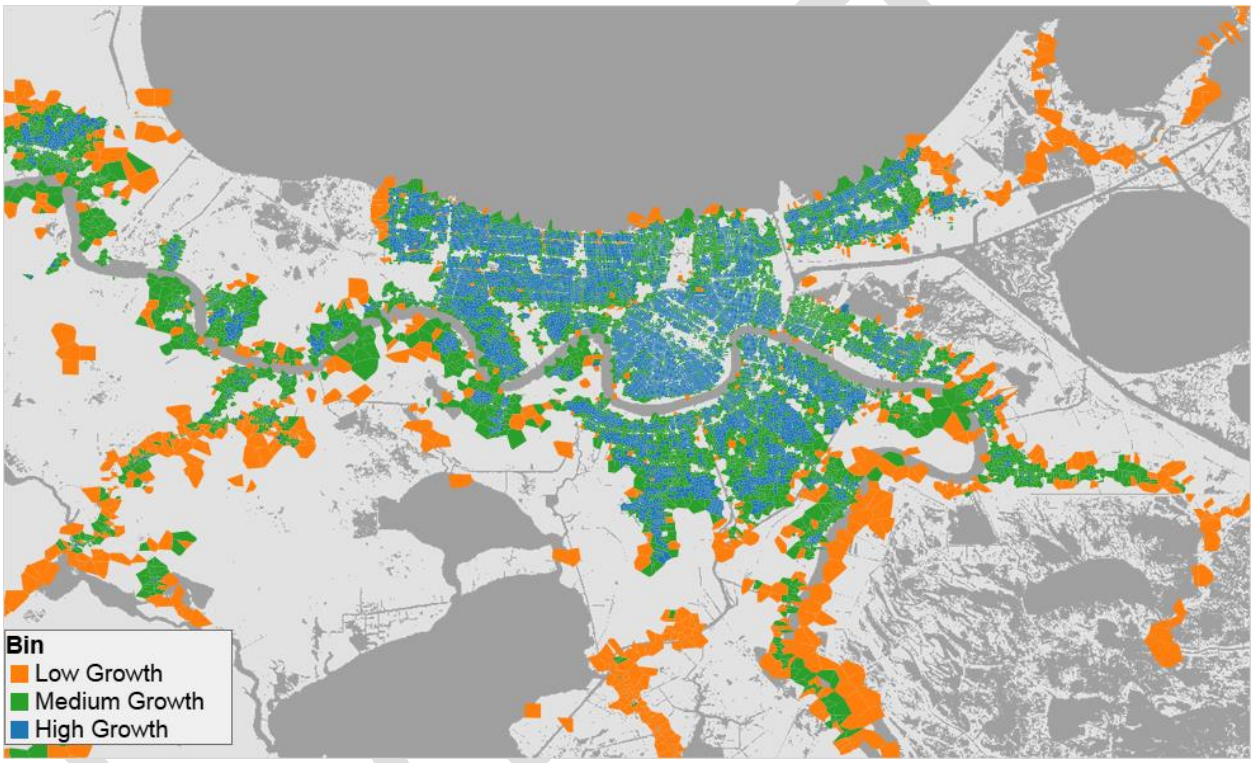

Figure 9-4: Initial Block Group Bin Assignment, Greater New Orleans.

9.4.2 Population Change with Different Parameter Assumptions

Recall that the overall growth rate and the difference in growth rates among areas in adjacent risk categories are treated as uncertain scenario parameters. The results of sensitivity testing across these parameters is shown here, demonstrating how altering these parameter values affects results.

Figure 9-5 details growth rates by bin as a function of model parameters. With 0% difference in the growth rates applied to the bins, each block group would have a constant growth rate that equals the coast wide annual growth rate (not shown). At the other extreme, assuming that the growth rate for the fastest growing areas is 1 percentage point higher than the growth rate for the slowest growing areas ensures a positive growth rate for some areas and a negative growth rate for others, regardless of the coast wide rate. In the most extreme preliminary scenario results,

block groups in the fastest growing areas grow rapidly relative to historical trends, while low growth areas lose population.

Coastwide Growth Rate	Separation Between Bins	Low Growth	Medium Growth	High Growth
0%	0.5%	-0.7%	-0.2%	0.3%
	1.0%	-1.4%	-0.4%	0.6%
0.50%	0.5%	-0.2%	0.3%	0.8%
	1.0%	-0.9%	0.1%	1.1%
0.67%	0.5%	0.0%	0.5%	1.0%
	1.0%	-0.7%	0.3%	1.3%
1.0%	0.5%	0.3%	0.8%	1.3%
	1.0%	-0.4%	0.6%	1.6%

Figure 9-5: Average Annual Population Growth Rate by Bin Under Alternate Scenario Parameter Assumptions, 2010-2011.

Under the more rapid growth scenarios, it is possible for all areas of the Louisiana coast to experience population growth. Consider the cases where the overall growth rate is relatively high, at 1% per year. This roughly corresponds to the growth rate observed in the study area in the decades following World War II. Using the assumption that differences among growth rates are set to 0.5%, the resulting change in population across the 50-year planning horizon[33] is shown in Figure 9-6. There is substantial population growth in more dense and upland grid points, with the population roughly doubling. The population in areas close to coast grows modestly, and areas further from the coast grow by roughly 50-100%.

[33] The results actually show a 55-year simulation, because a growth rate assumption is needed to bring the initial population data from 2010 to 2015, the base year of the master plan analysis.

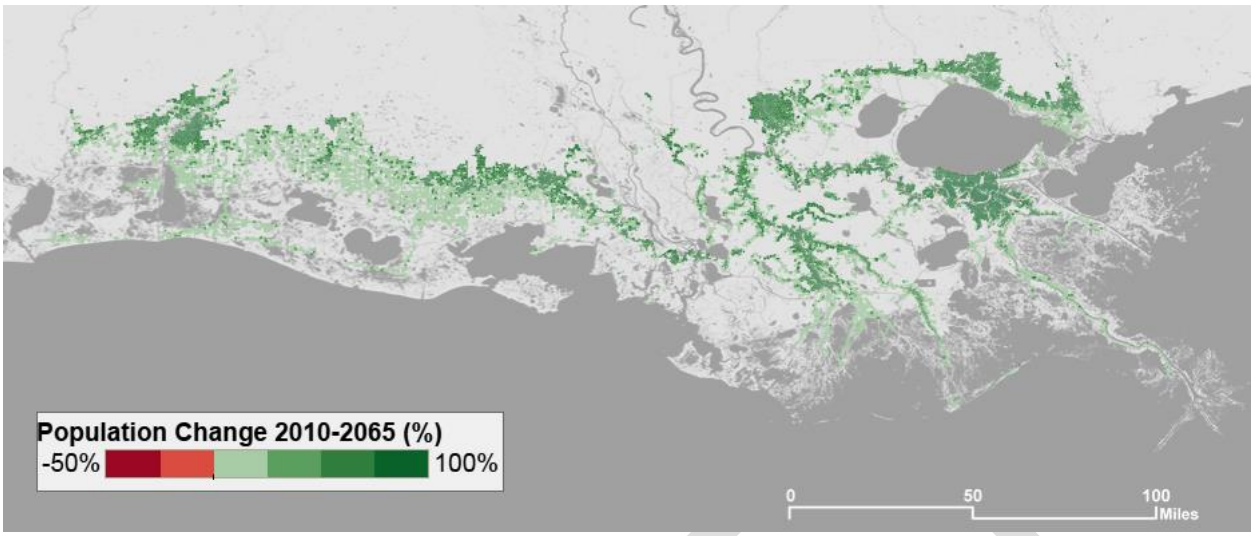

Note: Hypothetical Scenario Assumes 1.0 Percent Annual Coast Wide Growth and a 0.5 Percent Difference in Growth Rate Between Bins.

Figure 9-6: Population Change 2010-2065 by Grid Point Under a Higher-Growth Scenario.

Figure 9-7 shows the percent population change over the next 50 years by block group under a contrasting scenario. This scenario sets the scenario parameters to more pessimistic assumptions: the coast wide population grows more slowly, 0.67% per year over the next 50 years, with a 1.0 percent difference in annual growth rates between each growth bin. Enclosed urban areas continue to grow more rapidly, while areas further upland grow more slowly. In this scenario, however, areas facing higher flood depths and land loss rates lose about half of their population over 50 years, suggesting a pattern of slow transition away from the immediate coastline.

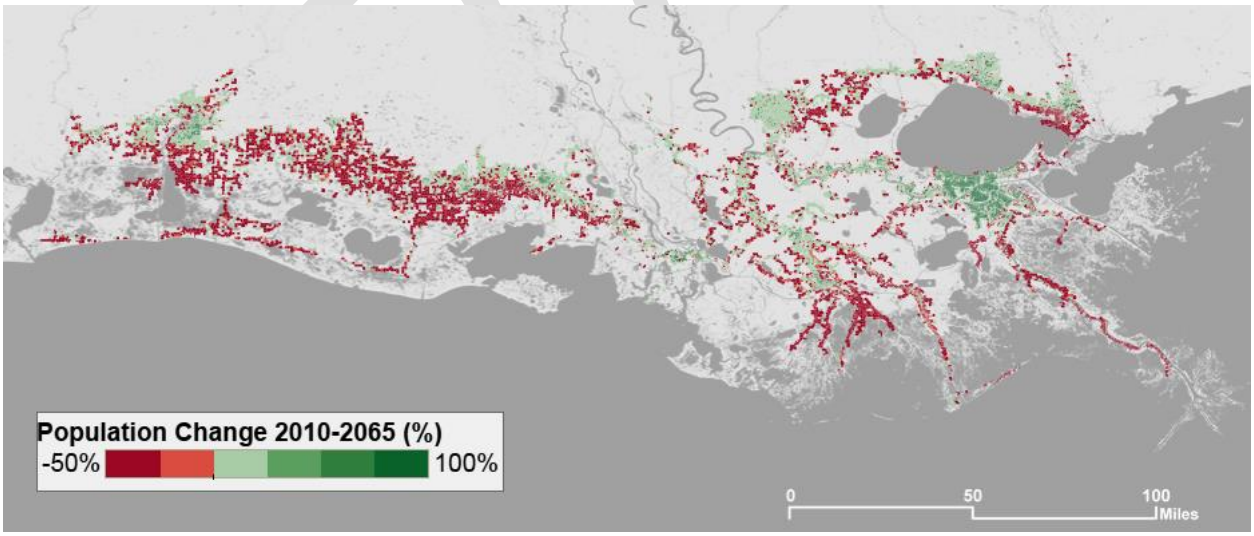

Note: Hypothetical Scenario Assumes 0.67 Percent Annual Coast Wide Growth and a 1.0 Percent Difference in Growth Rate Between Bins.

Figure 9-7: Population Change 2010-2065 by Grid Point Under a Lower-Growth Scenario.

Table 9-2 details population counts in 2065, by bin, for the initial scenario parameters considered during this investigation. The results of the sensitivity testing indicate that the plausible range for population in the highest growth bin ranges from 1.05 to nearly 2.1 million residents by 2065. Similarly, the population in the medium growth bin ranges from 688,000 to 1.19 million depending

on the assumptions. These are wide ranges, capturing the range of uncertainty present when considering the future coastal population and illustrating how sensitive population projections may be to assumptions regarding the extent to which flood risk and land loss shape development patterns.

Table 9-2: 2065 Population Projections by Bin Using Initial Scenario Parameters (Thousands of Persons).

			Bin			
Coastwide Growth Rate	**Separation Between Bins**	**Year**	**Low Growth**	**Medium Growth**	**High Growth**	**Grand Total**
0	0.5%	2040	139	729	1,046	1,914
		2065	127	688	1,104	1,919
	1.0%	2040	115	700	1,108	1,922
		2065	89	624	1,220	1,933
0.5%	0.5%	2040	162	848	1,214	2,224
		2065	167	907	1,450	2,523
	1.0%	2040	134	813	1,285	2,232
		2065	118	821	1,602	2,541
0.67%	0.5%	2040	170	892	1,277	2,339
		2065	183	996	1,590	2,770
	1.0%	2040	140	857	1,351	2,349
		2065	129	906	1,756	2,790
1.0%	0.5%	2040	187	985	1,408	2,579
		2065	218	1,194	1,901	3,313
	1.0%	2040	154	948	1,489	2,591
		2065	155	1,087	2,099	3,341

Note: Totals differ in the table due to rounding.

Table 9-3 details the projected populations of selected parishes in the two scenarios mentioned previously, as well as in a mid growth (nominal) scenario (0.67% coast wide annual growth rate and 0.5% separation between bins).

Table 9-3: Population Projections for Selected Parishes, Three Scenarios.

	Lower Growth			Mid Growth (Nominal)			Higher Growth		
	2010	2040	2065	2010	2040	2065	2010	2040	2065
Calcasieu Parish	170,750	167,875	166,716	170,750	195,097	219,354	170,750	201,226	232,953
Jefferson Parish	435,546	459,827	477,480	435,546	533,858	627,749	435,546	591,483	749,406
Orleans Parish	347,387	368,403	384,547	347,387	427,675	505,375	347,387	475,386	607,050
St. Tammany Parish	198,669	192,900	189,680	198,669	224,097	249,455	198,669	228,902	261,297

Figure 9-8 takes this further by showing how the population change translated to changes in future asset counts. The map illustrates the change over time in residential structures associated with the nominal growth scenario (0.67% annual growth rate, 0.5% bin separation). For each grid point, changes in residential structure counts are assumed to be in direct proportion to changes in population calculated at the grid point level. Non-residential structures are currently assumed to change in proportion to changes in population calculated at the census tract level.

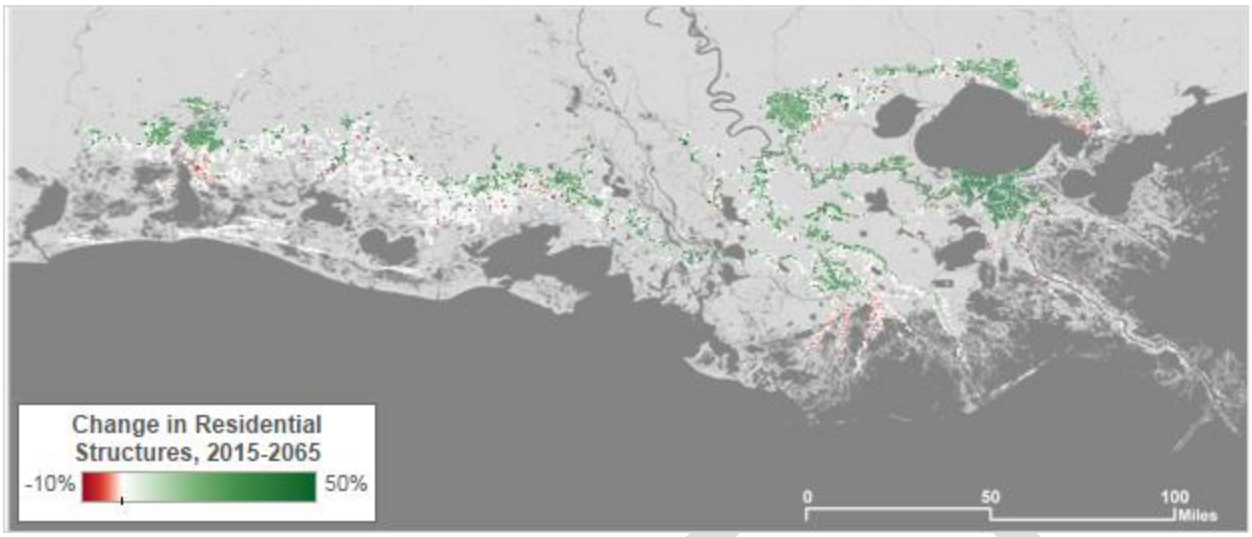

Figure 9-8. Change in Residential Structures, 2015-2065 (0.67% Annual Growth Rate, 0.5% Bin Separation).

Points with negative growth in residential structures are shown in red, and points with little or no change shown in white; points with positive growth are colored varying shades of green.

9.5 A Case Study: Terrebonne Parish

A case study application focusing on a single region, Terrebonne Parish, was also developed to demonstrate the ability of this scenario methodology to capture changes over time. This example includes both changes that would tend to lower growth rates due to increasing flood depths and/or land loss, as well the effect of a new levee alignment that would lower projected flood depths and thus potentially lead to higher growth (induced development). The case study considers two time periods and two future cases, one where the Morganza To The Gulf (MTTG) levee project is constructed and provides new protection for much of Terrebonne Parish, and one where the MTTG alignment is not constructed. This example uses a single set of population scenario assumptions: a 0.67% annual coast wide growth rate and 0.5% separation between bins, and the same test data on flood depths and land change as before. In this simplified example, 100-year flood depths are assumed to be zero for areas behind the MTTG alignment once constructed, and land loss rates are assumed to decline by half.

Table 9-4 summarizes the bin assignment and population in Terrebonne Parish in 2010 and 2065, with or without the MTTG alignment constructed during that time period. If no levee alignment is constructed (left pane), the grid points shift towards lower growth bins. High growth points decline from 535 to 267, for example, while low growth points increase from 641 to 826. If the MTTG system is built, however (lower-right), the lower land loss and flood depth estimates at many grid points results in a substantial increase in the number of grid points in the high growth bin. In turn, this increases the overall population in the parish, going from 146,071 in a future without action to 160,112 with the project implemented (roughly 10 percent greater).

Table 9-4: Bin Assignment and Population Change in Terrebonne Parish Example.

		MTTG Project Implemented			
		No		Yes	
Year	Bin	Grid Point Count	Population	Grid Point Count	Population
2010	Low Growth	641	23,011	641	23,011
	Medium Growth	1,249	55,466	1,249	55,466
	High Growth	535	35,744	535	35,744
	Total	2,425	114,221	2,425	114,221
2065	Low Growth	826	32,208	291	5,283
	Medium Growth	1,332	83,772	1,322	72,054
	High Growth	267	30,091	812	82,775
	Total	2,425	146,071	2,425	160,112

Figure 9-9 shows the same results graphically, showing where the points change bins in each of these cases. This clearly demonstrates how the methodology accounts for future change by adjusting to changes in future environmental conditions over time.

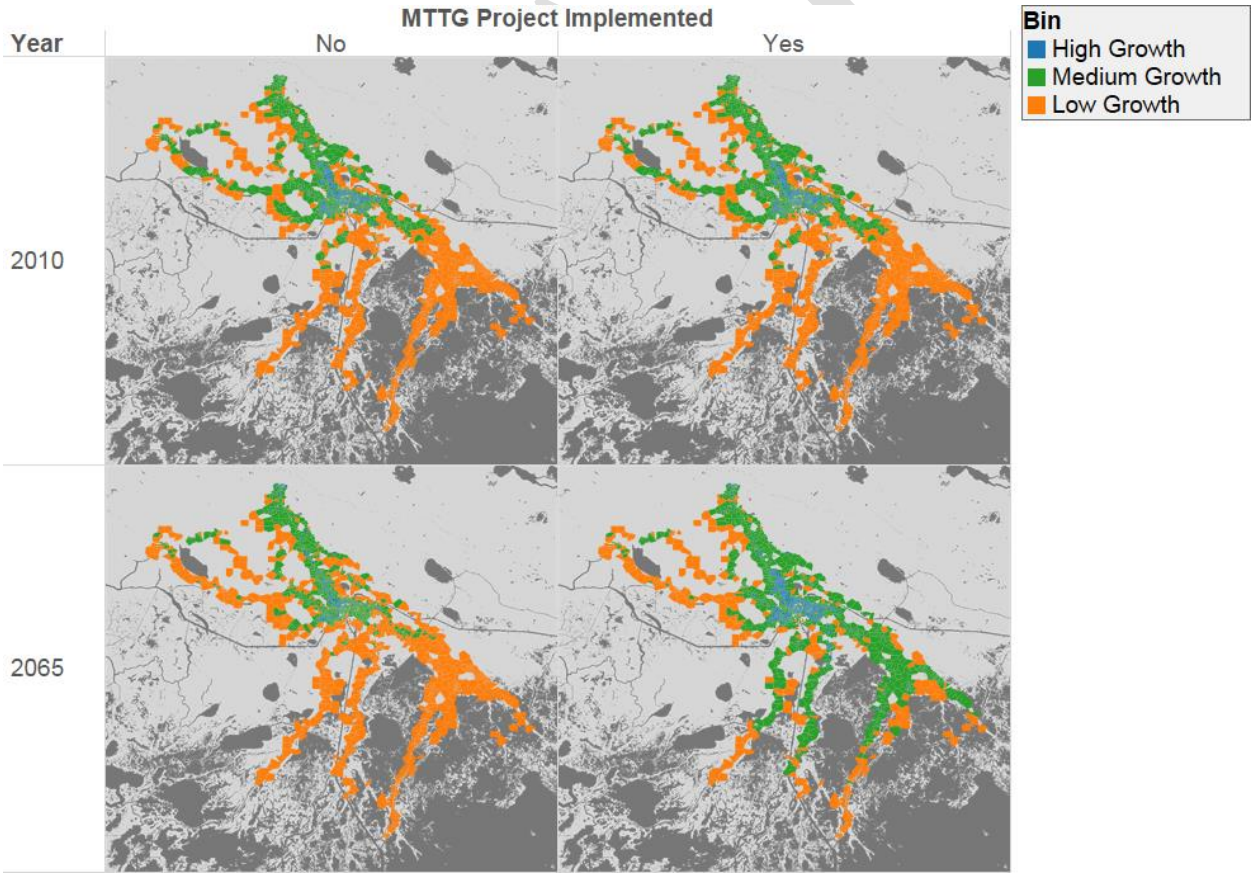

Figure 9-9: Map of Bin Assignment in Terrebonne Parish in 2010 and 2065, With and Without Project Implemented.

Figure 9-10 summarizes the total population change in Terrebonne Parish between 2010 and 2065 in the two cases considered. Without the MTTG project, many of the areas in Terrebonne Parish lose population. In the case where the project is constructed, conversely, the population of points behind the MTTG alignment grows more rapidly.

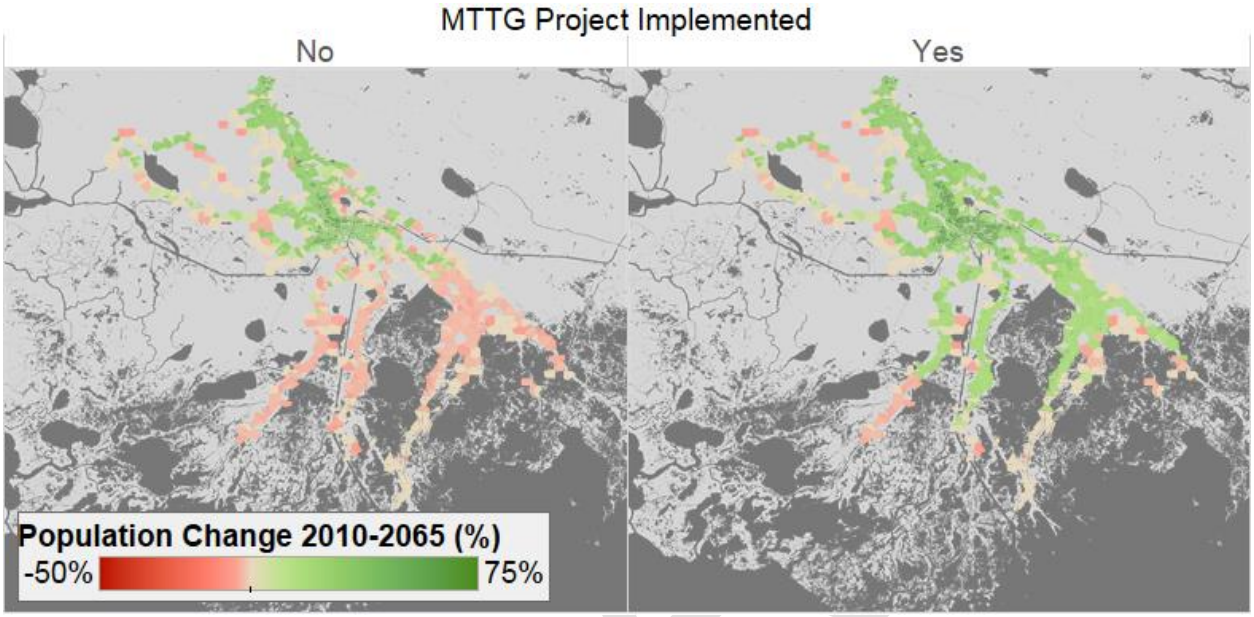

Figure 9-10: Population Change in Terrebonne Without and With Project Implemented.

9.6 Discussion

This section describes a survey of published results regarding migration patterns in response to environmental concerns and a description of a new model that provides plausible scenarios for population and asset growth in southern Louisiana. Sensitivity analysis showed that the developed model is sensitive to assumptions regarding the overall outlook for development in the area and how important flood risk and land loss will be in shaping development patterns.

The proposed approach builds on the 2012 analysis, but still rests on several key simplifying assumptions. Flood depth, land loss, and population density metrics can be dynamically updated to represent changing conditions. The approach outlined here, as was the case for the approach used in 2012, yields differing population estimates by location, but assumes that asset growth and distribution will directly track population change.

The preliminary scenario projections presented here result from a basic calibration and sensitivity testing exercise intended to divide the coastal region into categories broadly consistent with current development trends. The range of overall and differential growth rates modeled acknowledges that future growth could take many divergent pathways that produce contrasting distributions of assets. However, the choice of parameters for the composite index and ranges for the proposed scenario parameters are subject to change pending feedback from CPRA and the Model Decision Team.

10.0 Conclusion

10.1 Summary

This technical report described a series of improvements made to the Coastal Louisiana Risk Assessment model in preparation for the 2017 Coastal Master Plan analysis. The report also describes new analysis conducted using CLARA v2.0 designed to test the functionality of the model and its sensitivity to different modeling choices, as well as provide preliminary analysis results to CPRA for near-term planning purposes.

Key changes to the model included code adjustments to improve overall functionality and run efficiency, as well as a series of targeted steps that emerged from lessons learned discussions with CPRA after the 2012 Coastal Master Plan process was completed:

- expanding the model domain to account for a growing floodplain;
- creating a high resolution spatial unit with 1 km minimum resolution;
- updating and improving the inventory of coastal assets at risk;
- developing a new scenario approach for levee fragility to capture the range of different methods applied; and
- incorporating parametric uncertainty into estimates of flood depths, which in turns feeds into damage uncertainty estimates.

Additional analysis provided in this report included a comparison of flood depths and damage modeled in CLARA for an "Isaac-like" storm simulation with observed data from Hurricane Isaac in 2012 and a preliminary comparison of nonstructural project performance using the new model version and a refined decision analysis approach. In addition, the report described a new approach to develop scenarios of asset growth and distribution across the floodplain to support the 2017 analysis.

10.2 Current Limitations

The results presented in this report were produced primarily for the purpose of testing changes made to the CLARA model in preparation for the 2017 Coastal Master Plan production phase and for preliminary input to CPRA, and are based in part on legacy data from the 2012 analysis. Many key inputs that will be updated for the 2017 analysis and are likely to greatly influence modeled depth and damage results, including new scenario inputs for sea level rise and subsidence, revised estimates of future landscape change from the new Integrated Compartment Model, and updates to existing or proposed protection structure elevations, are not yet incorporated. In addition, this analysis considered only a single future scenario in a future without action condition and did not re-assess damage reduction benefits from the 2012 Coastal Master Plan. Except where noted, the results are intended primarily to illuminate the new methods and should be interpreted with caution.

Some tests were designed to investigate the impact of specific model changes, but CLARA v2.0 updates the methods and data used by nearly every submodule in the model, so the results here represent an entirely new iteration of the model. Comparisons to 2012 Coastal Master Plan outputs were made to verify the proper functioning of CLARA v2.0's new risk assessment

methods. These new results should not be interpreted as updates of or revisions to the 2012 results and conclusions.

The Less Optimistic landscape scenario only represents one possible future, and it does not reflect any updates to the scenario suite for 2017. Other pending changes include updates to the economic growth scenarios used in the damage module, which are discussed in Section 9 but not yet implemented in the test analysis described.

As most clearly explained in the model comparisons to the Hurricane Isaac experience (Section 7.0), the quality of economic damage estimates produced by CLARA is limited by the accuracy of the structural inventory data. Recognizing that an "out-of-the-box," Level 1 Hazus analysis is insufficient for modeling current risk in coastal Louisiana—even for high-level planning purposes—Sections 2 and 3 detail the many efforts made to better represent the physical quantity and location of exposed assets. Computational constraints have led to a number of design restrictions on the resolution and fidelity of economic data incorporated into CLARA, but parcel-level data from other coastal communities would further improve the quality of model results. To the extent possible, such data should also include secondary elements like foundation heights and square footage.

The economic results in this report also do not include damage to, or the loss of functionality from, critical infrastructure. As noted previously, critical infrastructure is treated differently by the model, which reports the number of assets inundated at each return period instead of damage. This portion of the analysis is intended to provide a high-level assessment of how individual critical infrastructure assets could be affected by flooding at different exceedance probabilities. It does not, however, address the functionality of critical infrastructure systems during storm events, and does not estimate supply chain impacts or broader effects on the regional and national economy.

Related to this, it is important to underscore that the confidence intervals reported for each case are only representative of the residual parametric uncertainty within a specified scenario. The deep uncertainties that define the Master Plan's scenarios, such as sea level rise and future changes in storm characteristics, can have a dramatic impact on risk, so it is important to view the parametric uncertainties in that context.

Confidence intervals also only reflect the particular uncertainties incorporated into the parametric framework. Critically, the parametric uncertainty approach currently focuses on the flood depth estimates. Some sources of uncertainty are not addressed by CLARA v2.0, particularly those emerging from the inventory of assets at risk, asset valuation methodology, or structure-specific damage calculations. For example, uncertainty in depth-damage relationships is excluded due to a lack of scientific consensus on appropriate methods for addressing it. In other cases, such as uncertainty in the baseline inventory of structures, sufficient data is unavailable or proper implementation would require analysis beyond the scope of this effort. Finally, the relatively small number of synthetic storms in the currently available JPM-OS storm library for coastal Louisiana also places limits on the model's new capabilities.

In other cases, the analyses described in this report have suggested further methodological adjustments, which could improve model performance. For example, the selection of representative variations (Section 5.2.3.2) could be adjusted to better ensure balance in the distribution of water from selected Markov chains into each BHU of a subsystem. This change could reduce the projected variation in flood depths in areas behind enclosed protection systems, and it may also reduce the number of samples required for each model case.

All of the model runs described in this report consist only of synthetic storms which have the characteristics of storms from the 446-storm set developed by previous studies. This contrasts with the approach used in 2012, which subdivided the storm parameter space into a total of 720 synthetic storms. This choice was made for computational expediency in testing: variation in storm velocity and track angle, along with the presence of intermediate "secondary" tracks, means that a partition of the parameter space (at similar resolution of that used in 2012) would consist of thousands of synthetic storms. The 446-storm set was designed for construction of surge and wave PDFs, ignoring threshold effects related to overtopping rates or levee failures. It thus forms a coarser partition that may not fully capture the thresholds at which point breaches begin to dominate interior flood dynamics. For production work, a larger set of synthetic storms, containing storms with parameter values in between those in the 446-storm set, can be used to further improve performance in enclosed areas. This will also make geospatial patterns of flooding more similar between different fragility curve scenarios.

11.0 References

Adelson, Jeff. (2012). Controlled breach of back levee begins in Plaquemines Parish to relieve Isaac's flooding. . *NOLA.com/Times-Picayune*. http://www.nola.com/hurricane/index.ssf/2012/08/controlled_breach_of_back_leve.html

Alexander-Bloch, Benjamin. (2013). Plaquemines Parish's main western thoroughfare, swamped by Hurricane Isaac floodwater, gets elevated. *NOLA.com/Times-Picayune*. http://www.nola.com/hurricane/index.ssf/2013/06/plaquemines_parishs_main_weste.html

Andersen, Christine F., Battjes, Jurjen A., Daniel, David E., Edge, Billy, Espey Jr, William, Gilbert, Robert B., . . . Traver, Robert. (2007). The New Orleans Hurricane Protection System: What Went Wrong and Why. Reston, VA: American Society of Civil Engineers Hurricane Katrina External Review Panel.

Assunção, Renato M, Neves, Marcos Corrêa, Câmara, Gilberto, & da Costa Freitas, Corina. (2006). Efficient regionalization techniques for socio- economic geographical units using minimum spanning trees. *International Journal of Geographical Information Science, 20*(7), 797-811.

Berg, Robbie. (2013). Tropical Cyclone Report: Hurricane Isaac (AL092012) 21 August – 1 September 2012: National Hurricane Center.

Black, Richard, Adger, W Neil, Arnell, Nigel W, Dercon, Stefan, Geddes, Andrew, & Thomas, David. (2011). The effect of environmental change on human migration. *Global Environmental Change, 21*, S3-S11.

Calthorpe Associates, & U.S. Army Corps of Engineers. (2008). Database of Structure Inventory and Characteristics.

Cao, Zechun, Wang, Sujing, Forestier, Germain, Puissant, Anne, & Eick, Christoph F. (2013). *Analyzing the composition of cities using spatial clustering*. Paper presented at the Proceedings of the 2nd ACM SIGKDD International Workshop on Urban Computing, Chicago, Illinois.

Chung, Kam- Hin, & Lee, Stephen. (2001). Optimal bootstrap sample size in construction of percentile confidence bounds. *Scandinavian journal of statistics, 28*(1), 225-239.

Cleveland, William S, & Devlin, Susan J. (1988). Locally weighted regression: an approach to regression analysis by local fitting. *Journal of the American Statistical Association, 83*(403), 596-610.

Coastal Protection and Restoration Authority of Louisiana. (2012a). *Louisiana's Comprehensive Master Plan for a Sustainable Coast*. Baton Rouge, La.: Coastal Protection and Restoration Authority of Louisiana.

Coastal Protection and Restoration Authority of Louisiana. (2012b). *Louisiana's Comprehensive Master Plan for a Sustainable Coast, Appendices A-J.* Baton Rouge, La.: Coastal Protection and Restoration Authority of Louisiana.

Cobell, Zachary (2013). [Personal Communication with ARCADIS].

Constable, A, Van Arsdol Jr, MD, Sherman, DJ, Wang, J, McMullin-Messier, PA, & Rollin, L. (1997). Demographic responses to sea level rise in California. *World Resources Review, 9*, 32-44.

Curtis, Katherine J, & Schneider, Annemarie. (2011). Understanding the demographic implications of climate change: estimates of localized population predictions under future scenarios of sea-level rise. *Population and Environment, 33*(1), 28-54.

Cutter, Susan L, Boruff, Bryan J, & Shirley, W Lynn. (2003). Social vulnerability to environmental hazards. *Social Science Quarterly, 84*(2), 242-261.

Dalbom, Christopher, Hemmerling, Scott A., & Joshua A. Lewis. (2014). Community Resettlement Prospects in Southeast Louisiana. New Orleans, LA: Tulane Institute on Water Resources Law & Policy.

Department of Commerce: Bureau of the Census. (2011). Urban Area Criteria for the 2010 Census; Notice. *Federal Register, 76*(164), Part II, 53032.

Department of the Army. (2010). Circular No. 1110-2-6067: USACE Process for the National Flood Insurance Program (NFIP) Levee System Evaluation. Washington, D.C.: U.S. Army Corps of Engineers.

Der Kiureghian, Armen , & Ditlevsen, Ove. (2009). Aleatory or epistemic? Does it matter? *Structural Safety, 31*(2), 105-112.

Efron, Bradley. (1979). Bootstrap methods: another look at the jackknife. *The Annals of Statistics, 7*(1), 1-26.

Federal Emergency Management Agency. (2005). *Multi-Hazard Loss Estimation Methodology, Flood Model: HAZUS®-MH MR2 Technical Manual* Washington, D.C.: Department of Homeland Security.

Federal Emergency Management Agency. (2011). *Hazus®-MH 2.0 Multi-hazard Loss Estimation Methodology Technical Manual: Flood Model*. Washington, D.C.: Department of Homeland Security.

Finch, Christina, Emrich, Christopher T, & Cutter, Susan L. (2010). Disaster disparities and differential recovery in New Orleans. *Population and Environment, 31*(4), 179-202.

Fischbach, Jordan R. (2010). *Managing New Orleans Flood Risk in an Uncertain Future Using Non-Structural Risk Mitigation*. Santa Monica, Calif.: RAND Corporation, RGSD-262.

Fischbach, Jordan R., Johnson, David R., Ortiz, David S., Bryant, Benjamin P., Hoover, Matthew, & Ostwald, Jordan. (2012a). *Coastal Louisiana Risk Assessment Model: Technical Description and 2012 Coastal Master Plan Analysis Results*. Santa Monica: RAND Corporation, TR-1259-CPRA.

Fischbach, Jordan R., Johnson, David R., Ortiz, David S., Bryant, Benjamin P., Hoover, Matthew, & Ostwald, Jordan (2012b). Appendix D-25: Risk Assessment (CLARA) Model Technical Report *Louisiana's Comprehensive Master Plan for a Sustainable Coast*. Baton Rouge, LA: Coastal Protection and Restoration Authority of Louisiana.

Frey, William H, & Singer, Audrey. (2006). *Katrina and Rita impacts on gulf coast populations: First census findings*: Brookings Institution, Metropolitan Policy Program.

Fussell, Elizabeth, Hunter, Lori M, & Gray, Clark L. (2014). Measuring the Environmental Dimensions of Human Migration: The Demographer's Toolkit. Boulder, CO: Population Center, Institute of Behavioral Science, University of Colorado.

Fussell, Elizabeth, Sastry, Narayan, & VanLandingham, Mark. (2010). Race, socioeconomic status, and return migration to New Orleans after Hurricane Katrina. *Population and Environment, 31*(1-3), 20-42.

Goldenberg, Stanley B, Landsea, Christopher W, Mestas-Nuñez, Alberto M, & Gray, William M. (2001). The recent increase in Atlantic hurricane activity: Causes and implications. *Science, 293*(5529), 474-479.

Governor's Office of Homeland Security and Emergency Preparedness. (2012, Sep 28). Hurricane Isaac Damaged almost 59,000 Residences in Louisiana. Retrieved January 22, 2015, from http://emergency.louisiana.gov/docs/IsaacHousingDamageRelease_final.pdf

Homeland Security Infrastructure Program. (2014). HSIP Gold [Geodatabase]: For Official Use Only.

Hunter, Lori M, White, Michael J, Little, Jani S, & Sutton, Jeannette. (2003). Environmental hazards, migration, and race. *Population and Environment, 25*(1), 23-39.

Hurricane Research Division. (2014, April). HURDAT (Hurricane Database). Retrieved August 15, 2014, from http://www.aoml.noaa.gov/hrd/hurdat/Data_Storm.html

Illinois Department of Commerce and Economic Opportunity. (2013). State of Illinois Disaster Recovery Substantial Action Plan Amendment: Disaster Relief Appropriations Act PL 113-2.

Interagency Performance Evaluation Taskforce. (2007). Performance Evaluation of the New Orleans and Southeast Louisiana Hurricane Protection System, Volume V – The Performance — Levees and Floodwalls: U.S. Army Corps of Engineers.

Interagency Performance Evaluation Taskforce. (2009). Performance Evaluation of the New Orleans and Southeast Louisiana Hurricane Protection System, Vol. VIII: Engineering and Operational Risk and Reliability Analysis: U.S. Army Corps of Engineers.

Jäger, J, Frühmann, J, Grünberger, S, & Vag, A. (2009). EACH-FOR-Environmental Change and Forced Migration Scenarios: Synthesis Report: EACH-FOR.

Johnson, David R., Fischbach, Jordan R., & Ortiz, David S. (2013). Estimating Surge-Based Flood Risk with the Coastal Louisiana Risk Assessment Model. *Journal of Coastal Research,* (Special Issue 67 - Louisiana2s 2012 Coastal Master Plan Technical Analysis), 109-126. doi: 10.2112/SI_67_8

Kniveton, Dominic, Schmidt-Verkerk, Kerstin, Smith, Christopher, & Black, Richard. (2008). Climate change and migration: improving methodologies to estimate flows.

Lempert, Robert J., Popper, Steven W., & Bankes, Steven C. (2003). *Shaping the Next One Hundred Years: New Methods for Quantitative, Long-Term Policy Analysis*. Santa Monica, Calif.: RAND Corporation, MR-1626-RPC.

Long, Larry. (1988). *Migration and residential mobility in the United States*: Russell Sage Foundation.

LSU AgCenter. (2013). 2013 State Totals. Retrieved January 22, 2015, from http://www.lsuagcenter.com/agsummary/archive/2013/-State-Totals/2013StateTotals.pdf

MARIS Technical Center. (2014, July 2014). Mississippi Automated Resource Information System: County Data. Retrieved August 15, 2014, from http://www.maris.state.ms.us/HTM/DownloadData/County.html

McCallum, BE, McGee, BE, Kimbrow, DR, Runner, MS, Painter, JA, Frantz, ER, & Gotvald, AJ. (2012). Monitoring Storm Tide and Flooding from Hurricane Isaac along the Gulf Coast of the United States, August 2012. *US Geological Survey Open-File Report 1263*. Retrieved January 22, 2015, from http://pubs.usgs.gov/of/2012/1263/

McLeman, Robert. (2013). Developments in modelling of climate change-related migration. *Climatic change, 117*(3), 599-611.

McLeman, Robert, & Smit, Barry. (2006). Migration as an adaptation to climate change. *Climatic change, 76*(1-2), 31-53.

Minnesota Population Center. (2011). National Historical Geographic Information System: Version 2.0. Minneapolis, MN: University of Minnesota.

Mitigation Assessment Team. (2013). Hurricane Isaac in Louisiana Building Performance Observations, Recommendations, and Technical Guidance: Federal Emergency Management Agency.

Molloy, Raven, Smith, Christopher L, & Wozniak, Abigail K. (2011). Internal migration in the United States: National Bureau of Economic Research.

Murtagh, Fionn. (1985). A survey of algorithms for contiguity-constrained clustering and related problems. *The Computer Journal, 28*(1), 82-88.

Myers, Candice A, Slack, Tim, & Singelmann, Joachim. (2008). Social vulnerability and migration in the wake of disaster: the case of Hurricanes Katrina and Rita. *Population and Environment, 29*(6), 271-291.

Oberkampf, William L., DeLand, Sharon M., Rutherford, Brian M., Diegert, Kathleen V., & Alvin, Kenneth F. (2002). Error and uncertainty in modeling and simulation. *Reliability Engineering & System Safety, 75*(3), 333-357. doi: http://dx.doi.org/10.1016/S0951-8320(01)00120-X

Ortiz, Elaine , & Plyer, Allison. (2011). Valassis Lists Data as an Indicator of Population Recovery in the New Orleans Area: Greater New Orleans Community Data Center.

Piguet, Etienne. (2010). Linking climate change, environmental degradation, and migration: a methodological overview. *Wiley Interdisciplinary Reviews: Climate Change, 1*(4), 517-524.

Piguet, Etienne, Pécoud, Antoine, & De Guchteneire, Paul. (2011). Migration and climate change: an overview. *Refugee Survey Quarterly*, hdr006.

Plaquemines Parish. (2013). Hurricane Isaac Community Development Block Grant (CDBG) Application, Recovery Proposal Form, Rev. 8-13. Retrieved January 21, 2015, from http://plaqueminesparish.com/uploads/Media/CDBG.pdf

Plyer, Allison, Bonaguro, Joy, & Hodges, Ken. (2010). Using administrative data to estimate population displacement and resettlement following a catastrophic U.S. disaster. *Population and Environment, 31*(1-3), 150-175. doi: 10.1007/s11111-009-0091-3

Resio, Donald T. (2007). White Paper on Estimating Hurricane Inundation Probabilities *Performance Evaluation of the New Orleans and Southeast Louisiana Hurricane Protection System, Vol. VIII: Engineering and Operational Risk and Reliability Analysis*. New Orleans: U.S. Army Corps of Engineers.

Seed, R. B., Bea, R. G., Abdelmalak, R. I., Athanasopoulos, A. G., Boutwell, G. P., Bray, J. D., . . . Yim, S. C. (2006). Investigation of the Performance of the New Orleans Flood Protection Systems in Hurricane Katrina on August 29, 2005: University of California, Berkeley.

Stringfield, Jonathan D. (2010). Higher ground: an exploratory analysis of characteristics affecting returning populations after Hurricane Katrina. *Population and Environment, 31*(1-3), 43-63.

Tate, Eric, Muñoz, Cristina, & Suchan, Jared. (2014). Uncertainty and Sensitivity Analysis of the HAZUS-MH Flood Model. *Natural Hazards Review*.

Thornton, Christopher , van der Meer, Jentsje, Scholl, Bryan, Hughes, Steven, & Abt, Steven. (2011, September). *Testing Levee Slope Resiliency at the New Colorado State University Wave Overtopping Test Facility*. Paper presented at the Coastal Structures 2011 Conference Yokohama, Japan.

U.S. Army Corps of Engineers. (2009a). Louisiana Coastal Protection and Restoration Technical Report. New Orleans, LA: U.S. Army Corps of Engineers.

U.S. Army Corps of Engineers. (2009b). Louisiana Coastal Protection and Restoration Technical Report: Economics Appendix. New Orleans, LA: U.S. Army Corps of Engineers.

U.S. Army Corps of Engineers. (2009c). Louisiana Coastal Protection and Restoration Technical Report: Hydraulics and Hydrology Appendix. New Orleans, LA: U.S. Army Corps of Engineers.

U.S. Army Corps of Engineers. (2009d). Mississippi Coastal Improvement Program: Socioeconomic database.

U.S. Army Corps of Engineers. (2013a). Draft Integrated Feasibility Report and Programmatic Environmental Impact Statement. Retrieved August 14, 2014, from http://www.mvn.usace.army.mil/Portals/56/docs/PD/Projects/SWCoastal/SouthwestCoastalDraftIntegratedProgrammaticFeasibilityReportandEIS.pdf

U.S. Army Corps of Engineers. (2013b). Final Post Authorization Change Report: Morganza to the Gulf of Mexico, Lousiana (pp. 122). New Orleans, LA: U.S. Army Corps of Engineers, Louisiana Coastal Protection and Restoration Authority Board, and Terrebonne Levee and Conservation District.

U.S. Army Corps of Engineers. (2013c, February). Hurricane Isaac with and without 2012 100-Year HSDRRS Evaluation. Retrieved January 21, 2015, from http://www.mvn.usace.army.mil/Portals/56/docs/PAO/20130208HurrIsaacW-WO2012HSDRRS.pdf

U.S. Army Corps of Engineers. (2013d). Larose to Golden Meadow Hurricane Protection Project Risk Based Benefit Cost Ratio HEC-FDA Analysis. New Orleans, LA.

U.S. Army Corps of Engineers. (2013e). West Shore-Lake Pontchartrain Study Integrated Feasibility Report/Environmental Impact Statement. Retrieved January 22, 2015, from http://www.mvn.usace.army.mil/Portals/56/docs/PD/Projects/WSLP/WSLPFINAL.pdf

U.S. Army Corps of Engineers: Task Force Hope. (2013, July 18). Greater New Orleans Hurricane and Storm Damage Risk Reduction System: HSDRRS Resiliency Brief [PDF document]. Retrieved August 8, 2014, from http://www.slfpae.com/presentations/2013 07 18 - USACE Resiliency.PDF

U.S. Census Bureau. (2010). Cartographic Boundary Shapefiles - Places (Incorporated Places and Census Designated Places). Retrieved January 22, 2015, from https://http://www.census.gov/geo/maps-data/data/cbf/cbf_place.html

U.S. Census Bureau. (2014, August 14, 2014). American Community Survey. Retrieved August 15, 2014, from http://www.census.gov/acs/www/

U.S. Department of Agriculture. (2013). National Agricultural Statistics Service. Retrieved August 15, 2014, from http://nassgeodata.gmu.edu/CropScape/index.jsp?state=LA

U.S. Department of Energy Oak Ridge National Laboratory. (2011). [Geodatabase] LandScan Retrieved August 15, 2014, from http://web.ornl.gov/sci/landscan/index.shtml

U.S. Small Business Administration. (2015). Home and Personal Property Loans. Retrieved January 22, 2015, from https://http://www.sba.gov/content/home-and-personal-property-loans

van der Meer, Jentsje. (2002). Technical Report Wave Run-up and Wave Overtopping at Dikes. Delft, The Netherlands: Technical Advisory Committee on Flood Defence.

van Heerden, Ivor L., Kemp, G. Paul, Mashriqui, Hassan, Sharma, Radhey, Prochaska, Billy, Capozzoli, Lou, . . . Boyd, Ezra. (2006). The Failure of the New Orleans Levee System during Hurricane Katrina. Baton Rouge, LA: Prepared for Louisiana Department of Transportation and Development.

Warner, Koko. (2011). Environmental change and migration: methodological considerations from ground-breaking global survey. *Population and Environment, 33*(1), 3-27.

Wolpert, Julian. (1966). Migration as an adjustment to environmental stress. *Journal of Social Issues, 22*(4), 92-102.

Zaninetti, Jean-Marc, & Colten, Craig E. (2012). Shrinking New Orleans: Post-Katrina population adjustments. *Urban Geography, 33*(5), 675-699.

Appendices

See Attachment C3-25.1 – Storm Surge and Risk Assessment Appendices for the following appendices:

- Appendix 1: ADCIRC+SWAN Model Updates and Validation
- Appendix 2: Synthetic Storm Suite Simulations
- Appendix 3: Raised Feature Elevation Interpolation Sensitivity Analysis
- Appendix 4: Sector-Based Wind Drag Analysis
- Appendix 5: Asymmetric Hurricane Literature Review
- Appendix 6: Initial Water Levels for Surge and Waves Simulations in the 2017 Louisiana Coastal Master Plan
- Appendix 7: River Stages for Production Simulations in the 2017 Louisiana Coastal Master Plan
- Appendix 8: Interpolation of Land Use Data for the 2017 Louisiana Coastal Master Plan